Investigation of stimuli-responsive nanogels as promising candidates to overcome multifaceted barriers: focus on mucosal delivery with related opportunities, issues, and challenges

Inaugural-Dissertation

to obtain the academic degree

Doctor rerum naturalium (Dr. rer. nat.)

Submitted to

The Department of Biology, Chemistry, Pharmacy

of Freie Universität Berlin, Germany

by

Rawan Charbaji

From Damascus, Syria

Berlin, 2021

The work presented in this thesis was carried out between October 2015 and June 2019
under guidance and supervision of
Prof. Dr. Sarah Hedtrich (née Küchler)
at the Institute of Pharmacy, department of Pharmacology and Toxicology,
Freie Universität Berlin, Germany

1st Reviewer: Univ.-Prof. Dr. Sarah Hedtrich (née Küchler)
Berlin Institute of Health at Charité
BIH Johanna Quandt Professorship for Translational Organ Models
Käthe-Beutler-Haus
Lindenberger Weg 80
13125 Berlin, Germany

2nd Reviewer: Prof. Dr. Daniel Klinger
Freie Universität Berlin
Institute of Pharmacy
Königin-Luise-Str. 2 – 4
14195 Berlin

Date of disputation: *21.02.2022*

"قف على ناصية الحلم... وقاتل!"

"Stand at the edge of the dream… and fight!"

-Mahmoud Darwish, Arabic poet, 1941 - 2008

ACKNOWLEDGEMENTS

Pursuing my doctoral studies in pharmacology in one of the leading countries in pharmaceutical sciences has always been a long-standing dream and great ambition of mine. I still recall that overwhelming day when I received her email to welcome me into her research group thus opening the door towards a future that I've always hoped for. For this and more, my utter and profound gratitude is entitled to my supervisor Prof. Dr. Sarah Hedtrich, whose devotion, efficiency, guidance, patience with me especially during writing, and her great unconditional support at all times and from any continent she was in, have captured my admiration and deepest appreciation.

Naturally, I couldn't have come this far, if it weren't for the financial support from the German academic exchange service (DAAD). Through their additional workshops, conventions, and empowerment programs for scholars, the DAAD made my studies in Germany a very enriching experience. Words cannot describe how thankful I am for the DAAD's longstanding support throughout my entire studies and even during the unprecedented lock-down due to the pandemic situation.

Working with an interdisciplinary project, I'd like to thank my collaborating partners and great chemists: Prof. Dr. Marcelo Calderon and his group members Loryn Theune and Mrityunjoy Kar, for the outstanding teamwork, very interesting discussions, and scientific exchange that widened my horizon and made me learn a lot. Here, I'd like to also thank Julián Bergueiro for his big help with the GPC studies and the insightful scientific discussions.

Another support that paved the way for this project was provided by the veterinarian physiology institute/ FU-Berlin. Here, a big „thank you" goes to Prof. Dr. Jorg Aschenbach and Dr. Friederike Stumpff including their research teams for providing the *ex vivo* intestinal tissue from sacrificed farm pigs and teaching me the proper handling and preservation techniques to maintain it. I am very grateful for their support, especially for welcoming me into their labs and allowing me to perform my studies on the *in vitro* intestinal models. Here, another "thank you" goes to Mrs. Susanne Trappe for her support in TEER measurements as well as to Mrs. Katharina Söllig for her aid in western blot studies.

Given the added value to the project by the important experiments they provided, the contributions of my colleagues: Anne Eichhorst for the penetration experiments on the lung models and Patrick Graff for the ETN release studies from the nanogels, are gratefully acknowledged.

Having come this far, I am also very thankful for Prof. Dr. Daniel Klinger for agreeing to be my second reviewer and taking the time to evaluate my work.

Indeed, I wouldn’t have made it without the love and support of my dear family and friends. I am very blessed to have such generous hearts and wise minds in my life. To my dearest late father, who taught me that a man is only as great as his ambition and his will to pursue it, I am forever grateful to you, and you are always with me and on my mind in every step of the way. To my dear mother, you have always been my beacon of hope and the light of my life, so thank you for your immeasurable love and I hope to make you proud always.

Another heartfelt “Thank you” to my sisters and brothers for motivating me and being the loving shoulder that I lean on in difficult times, especially my dear Nada, who made Berlin with her presence my second home. A warm “Thank you” goes to my little nieces and nephew: Hana, Mirna, and Neyar: your sweet laughter and loveliness have always lifted my spirit and made the world such a beautiful place, I love you with all my heart and wish you a future as sweet as you are.

To my great and true friends, Nawar, Maen, Caro, Stephanie, André, Anja, Ataa, Nemat, Heba, and Manal: Even at times of frustration and despair when I’ve almost given up on myself, you never seized to believe in me and my potential. You’ve strengthened me in times of weakness, opened my eyes to the light, supported me in every possible way, and kept me going on no matter what. So “THANK YOU” from the bottom of my heart.

STATEMENT OF AUTHORSHIP

I hereby declare that this presented thesis was solely written and composed by me, Rawan Charbaji, born in Damascus, without any unauthorized assistance or aid. All direct or indirect resources relevant to this work are cited and acknowledged as references.

I further confirm that this dissertation has not been previously published nor presented to any other examination board or prior academic degree.

Berlin, 12.11.2021

Rawan Charbaji

ABBREVIATIONS LIST

BSA	Bovine serum albumin
Caco-2	Colorectal adenocarcinoma epithelial cells
CD	Crohn's disease
CF	Cystic fibrosis
DMSO	Dimethyl sulfoxide
DSS	Dextran sulfate sodium
dPG	dendritic polyglycerol
Ect1/E6E7	Ectocervix epithelial cells
ED	Effective dose
EDTA	Ethylenediaminetetraacetic acid
EMA	European Medicines Agency
ETN	Etanercept
FDA	Food and Drug Administration
FITC	Fluorescein isothiocyanate
GI	Gastrointestinal
GPC	Gel permeation chromatography
GSH	Glutathione
H-bond	Hydrogen bond
i.v.	intravenous
IBD	Inflammatory bowel disease
IECs	Intestinal epithelial cells
IFN	Interferon
IL	Interleukin
KRB	Krebs-Ringer buffer
LCST	Lower critical solutiontemperature
mAbs	Monoclonal antibodies
MAPs	Mucoadhesive particles
MDCK	Madin-Darby Canine Kidney cell line
MFI	Mean fluorescence intensity
MPPs	Mucopenetrating particles
NIR	Near infrared
NP-based	Nanoparticulate-based
NPs	Nanoparticles
PBS	Phosphate buffered saline
PEG	Polyethylene glycol
PLGA	poly(lactic-co-glycolic acid)
PNIPAM	poly(N-isopropylacrylamide)
PNIPMAM	poly(N.isopropylmethacryl-amide)
PTS	Proline, threonine, serine
R&D	Research and Development
r.t.	room temperature
Rhd-B	Rhodamine B
s.c.	subcutaneous
SC	Stratum corneum
SDS	Sodium dodecyl sulfate
TEER	Trans electrical epithelial resistance
Th	T helper cells
TJs	Tight junctions
TNBS	2,4,6-trinitrobenzenesulfonic acid
TNF	Tumor necrosis factor
UC	Ulcerative colitis
UV	Ultraviolet
VE	Viable epidermis
VK2/E6E7	Vaginal epithelial cells
VPTT	Volume phase transition temperature
ZO-1	Zunola occludin-1

TABLE OF CONTENTS

1. INTRODUCTION

1.1 Nanoparticles as key tools for improved therapy

Nanoparticles (NPs) are ultrafine microscopic 3D structures with overall dimensions ranging from few hundreds to tens of nanometers. The first notion of nanoparticles genesis dates back to 1959, when the renowned physicist and noble laureate Richard P. Feynman proposed at his famous lecture *"there is plenty of room at the bottom"* a revolutionary approach to engineer materials within the nanoscale. At this scale, materials are reduced to the same sizescale of biological molecules and cellular components giving them advantage in medical applications. For this purpose, Feynman envisaged nanodevices that can enter the body and maneuver at a molecular level to leverage cellular repair and mediate treatment. His vision was further pursued and developed by many scientists and engineers starting with Drexler's popular writings between the 1980s and 1990s, and later with the writings of Freitas (1990s – 2000s), where the term "Nanomedicine" appeared for the first time marking a new era of modern medicine [1-3].

In the context of nanomedicine, the design and utilization of NPs have witnessed a massive growth over the past few decades. Outstanding features like the spherical shape providing large surface area compared to bigger particles of the same mass, the quantum properties, and functional surface and composition that enable conjugating, adsorbing, or encapsulating various active compounds (e.g., probes, drugs, and genes) made NPs attractive for a plethora of biomedical applications ranging from diagnostics to therapy as biosensors, imaging contrast agents, and drug delivery systems [4, 5].

NP-based drug delivery systems have become powerful key tools for potentiating pharmacological efficacy of existing drugs as well as creating new therapeutic approaches like gene delivery. Many conventional drugs and therapeutics (e.g., biomacromolecules) have serious issues that implicate their bioavailability and limit their efficacy, such as poor solubility, structural fragility, instability, unfavorable pharmacokinetics, cytotoxicity, and serious side effects due to non-specific interactions. Using NPs as delivery systems to stabilize these bioactives and transfer them to the intended cite of action allows to modify drug formulations significantly in a cost-effective manner and at low risk [6]. Furthermore, NPs can enhance the absorption of their associated therapeutics through impervious biological barriers like skin and mucosal membranes. Hence, drug administration can be facilitated through non-invasive easily accessible routes, which in turn improves patients' compliance and achieves localized and more specific treatments [7-10]. For example, the administration of therapeutic proteins like biologics can be shifted from i.v. and s.c. to topical or oral administration by means of suitable delivery systems thus enhancing their efficiency, minimizing potential immunogenicity, and avoiding toxicity [11, 12]. Just as the transport of biological molecules through different

barriers or to specific biological compartments is dictated by their, size, shape, and surface chemistry, controlling these features in engineered NPs enables to optimize their pharmacokinetics, biodistribution, and cargo release kinetics with respect to the characteristics of the targeted cite of action [13, 14].

Over the past few decades, numerous forms and types of NP-based delivery systems have entered the mainstream of pharmaceutical R&D and made substantial impact in the clinic, among which are mainly liposomes, micelles, polymeric NPs, dendrimers, and nanogels; composed of assembled lipids, amphiphiles, and dendritic polymers respectively, in addition to nanocrystals and inorganic NPs [15, 16]. Many of these NPs have made it to clinical trials and some were even able to reach the market gaining approval from the FDA or the EMA, starting with liposomal amphotericin-B for antifungal treatment in 1997 [17, 18] and continuing with the most recently licensed NP-based COVID-19 vaccines approved in Dec 2020, in which the NPs served as gene transporters and immune adjuvants [19-22].

NPs have indeed redefined modern medicine, yet despite current progress and advancements in nanomedicine, the rational design of efficient NP delivery systems remains to this day a prominent challenge and one of the greatest endeavors in pharmaceutical research. On one hand, nanocarriers must overcome critical hurdles pertaining to instability, off-target accumulation, inefficient delivery *in situ*, toxicity, and uncontrolled drug release [23, 24]. On the other hand, the design of NPs is still restricted to our limited understanding of the targeted biological barriers, especially those of complex nature and function i.e., mucous membranes [25, 26]. This, in turn, explains why most approved NP-based formulations are for parenteral administration, compared to very few for topical or local application [27].

Hence, fundamental aspects must be considered in tailoring appropriate NP-based delivery systems, including high biocompatibility, biodegradability, high drug-loading capacity, ability to solubilize and stabilize therapeutic cargo, ability to cross biological barriers in order to reach the target site and eventually release their payload in a controlled manner. Interestingly, nanogels favor such qualities and thus have recently attracted great scientific interest as promising drug delivery platform with tunable and adaptable properties to meet biological demands and impart pharmaceutical formulations with desirable merits [28]. Overall, efficient drug delivery is guided and optimized by understanding the nature of biological barriers and potential interplay between NPs and the encountered biological milieu [29, 30].

1.2 Nanogels: the next generation drug delivery systems

Nanogels are soft three-dimensional nanosized hydrogels made of crosslinked polymeric networks, able to swell in aqueous solutions by absorbing and trapping large amounts of water whilst maintaining an intact and stable structure. This water-swelling behavior endows nanogels with hydrophilicity as well as high loading capacity for drug solutions giving them excellent dispersion in biological fluids as well as high biocompatibility [31, 32]. Furthermore, nanogels provide flexible and adaptable platforms to conjugate, complex, or encapsulate a variety of guest molecules of different molecular weights and physicochemical properties into their matrix [33-35]. Additionally, nanogels can be designed to exhibit active release behavior of their cargo in response to specific environmental triggers at the target cite of action. Owing such unique properties, nanogels were propelled as “smart” nanodevices that allow to not only transfer payloads but also to control the delivery process and payload release kinetics [36-38]. Besides drug delivery, nanogels are widely utilized in various biomedical applications like imaging and diagnostics [39-41]. Such distinct features give nanogels many advantages over other nanocarrier systems and account for their designation as next generation drug delivery systems [42].

1.2.1 Polyglycerol-based nanogels

Basically, the physicochemical properties and characteristics of a nanogel system are determined by those of the polymers used in its fabrication, thus nanogels exhibit great variations depending on their comprising materials. Hence, careful selection of polymers for nanogels design is crucial to obtain the desired system properties. Polyglycerol polymer chains have gained considerable interest as highly advantageous and flexible scaffolds to produce versatile nanogel systems [43, 44].

A facile polymerization approach initiated by a traditional anionic or cationic ring-opening reaction of glycidol yields hyperbranched polyglycerol chains that radiate from a single central core in a globular dandelion-like configuration, known as dendritic polyglycerols (dPG) with diameters < 10 nm **(Figure 1.1)** [45, 46]. The multivalent hydroxyl-rich terminals in dPG architecture allow surface-functionalization with a variety of polymeric crosslinks whilst maintaining high water solubility [47, 48]. Owing its high water-swelling capacity, dPG behaves like macroscopic gels and thus confers a very suitable candidate to obtain nanogels with high loading capacity and controllable swelling by varying the dPG feed ratio in their composition. Moreover, the non-toxicity, compatibility for incorporating therapeutic proteins, and stealth properties (i.e., resistance to opsonization and to non-specific interactions with encountered biological molecules) add to dPG advantages as macro-crosslinker for designing smart

nanogels with stimuli-responsive functional moieties to achieve controlled drug delivery. [49-51].

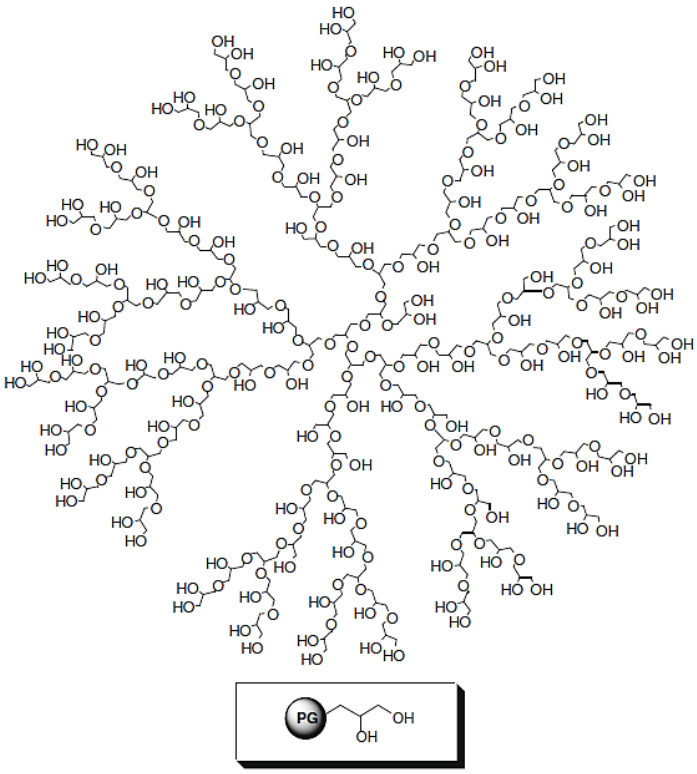

Figure 1.1 Schematic structure of hyperbranched polyglycerol exhibiting terminal, linear, and dendritic linkages, reprinted from [46] with Elsevier permission.

1.2.2 Nanogels functionalization for stimuli responsive behavior

Stimuli-responsiveness is one of the most effective strategies for targeted delivery. It enables a selective on-demand release of the active compound from nanocarriers at the targeted biological site in response to certain environmental cues, either of endogenous nature (e.g., changes in pH, enzyme levels, temperature, or redox status) or externally applied like magnetic fields, heat, or light irradiation. Once exposed to the environmental trigger, the nanogels undergo conformational alterations in the form of network swelling/deswelling, or degradation that eventually lead to cargo release [52, 53].

Introducing stimuli-responsive polymers/moieties to dPG as functional crosslinks yields smart nanogels [37]. According to the choice of those crosslinks, the nanogels response mechanism and release kinetics can be tuned with respect to the intended application [38, 54]. Whilst adding functional groups like carboxyl or tertiary amines induces reactivity to pH-stimulus by network swelling or collapse [55], crosslinking cleavable moieties like disulfide linkages renders them responsive to reductive environments. Upon encountering reducing enzymes like GSH, the disulfides get cleaved thus degrading the nanogels into smaller monomeric

fragments and releasing the encapsulated payload. This release process ensures clearance of the nanogels as an additional benefit [56, 57]. Owing GSH abundance in cytosol (1–10 mM), disulfide-containing nanogels enable intracellular triggered drug release [58]. In addition, reductive environments like cancer tissues or mucosal surfaces act on disulfide-containing nanocarriers as well, which makes them very interesting delivery targets [59].

Generally, cancer treatment has been the most researched application for disulfide-containing nanogels owing the elevated redox potential in tumor tissues and accumulation in cancer tissues [60-63]. In former work by the Haag group, disulfide linkages were introduced to dPG nanogels yielding delivery systems with pronounced cellular uptake and specific intracellular release of Doxorubicin via triggered degradation in 2D-cultured cell lines [64, 65]. Another study by Calderon and colleagues presented disulfide-containing dPG nanogels for gene therapeutics delivery to glioblastoma multiform GBM-bearing mice, showing EPR effect in tumor tissue and tumor growth inhibitory activity *in vivo* besides biocompatibility to healthy tissues [66].

Another interesting trigger is temperature. Polymer substitutes of N-alkyl poly(acryl amides), especially poly(N-isopropylacrylamide) PNIPAM and derivatives like poly-(N.isopropylmethacrylamide) PNIPMAM are common functional crosslinks to obtain thermoresponsive nanogels [67]. These polymers possess a so-called lower critical solution temperature (LCST) that controls the polymers hydration state. Heating the environment to temperatures ≥ LCST causes the thermoresponsive polymers to dehydrate and shrink. This behavior manifests in a volume phase transition of the nanogels in response to a critical temperature, defined as VPTT, above which the nanogels undergo drastic network deswelling (shrinkage) resulting in expulsion of their water content along with the entrapped payload [37, 68]. Whereas PNIPAM renders nanogels with a VPTT between 32 – 35 °C, the presence of the extra methyl group in PNIPMAM adds a steric rigidity that stabilizes the polymer's molecular network and promotes affinity towards H-bond formation with the surrounding water molecules, thus shifting the VPTT of PNIPMAM-based nanogels to 45 – 47 °C [69, 70].
Since the required release kinetics here can vary with respect to the intended application, the nanogels VPTT can be tuned accordingly by changing the feed ratio of dPG monomers and/or by co-polymerization of PNIPAM and PNIPMAM, which was reported to yield macro- or nanogels with excellent hydrodynamic properties and LCST-dependent phase transition behavior with transition temperatures between 34 – 47 °C depending on the ratio between the two polymers [70, 71].

Stimuli-responsive dPG nanogels present advantageous smart systems for controlled drug delivery. However, successful drug delivery is subject to NPs ability to overcome the

encountered biological barriers in order to reach the target site. The variation in properties and features among these barriers poses a challenge yet offers an opportunity to design tailor-made NPs for each of them. For this purpose, the responsive modalities of dPG nanogels can be respectively tuned and exploited to assist in crossing robust biological barriers like skin and mucus alongside their original function in triggering cargo release.

1.3 Dermal drug delivery

The topical dermal route is very attractive for drug administration owing the easy and painless application, absence of hepatic first-pass effect, and ability to increase therapeutic efficacy through localized treatment of skin conditions, which in turn minimizes side effects and helps avoiding systemic treatments that show only minor effect on skin. Nevertheless, skin is a very robust barrier that impedes drugs infiltration, especially therapeutic proteins, yet employing suitable NP delivery systems offers the chance to enhance drugs penetration into skin and achieve efficient local therapy.

1.3.1 The skin barrier

Skin is the body's largest and most accessible sensory organ. It serves as the first defense-line against foreign substances and pathogens, provides protection against UV radiation or mechanical injury, and regulates vital functions including the body's temperature and loss/resorption of water and salts [72, 73].

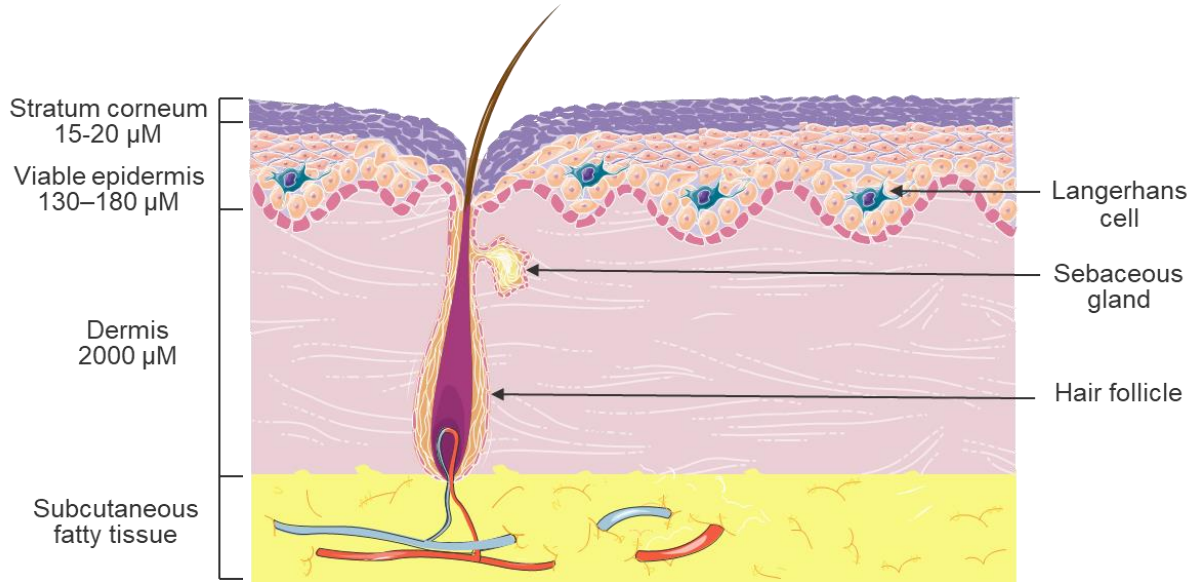

Figure 1.2 Schematic depiction of human skin barrier, showing the different layers, appendages, and blood vessels. Scheme was generated using Servier medical arts under creative commons license.

Starting from the surface and inward, human skin consists of three main layers: the epidermis, the dermis, and the subcutaneous fatty tissue **(Figure 1.2)**. The epidermis is essentially

responsible for skin regeneration and barrier properties; it is further subdivided into two distinct layers, the stratum corneum (SC), as interface with the outer world, and the viable epidermis (VE). Comprised of 15-20 layers of tightly stacked up fully cornified keratinocytes (corneocytes) embedded in an intercellular lipid matrix, the SC poses the primary absorptive as well as obstructive skin barrier with overall 10-15 µM thickness **(Figure 1.2)** [74, 75].

The entry of therapeutics, especially proteins, is restricted mainly by SC physical and size-filtering properties [76]. Basically, three main pathways for drugs entry into skin were identified: the intercellular route, through the extracellular lipid envelopes around corneocytes in the SC, which is mainly accessible by lipophilic compounds, the intracellular route, across corneocytes for hydrophilic compounds, and the third route is through the appendages (e.g., hair follicle and sweat glands), which is also suitable for hydrophilic compounds. Generally, compounds diffusion is determined by factors, including the absorbent size and extent of its hydrophilicity/hydrophobicity (i.e., partition coefficient). In addition, skin hydration, temperature, and pathology are crucial parameters affecting skin penetration [76-79].

1.3.2 Potential of thermoresponsive dPG nanogels in dermal drug delivery

dPG nanogels hold great potential for efficient dermal drug delivery. On one hand, they engulf large amounts of water, which act as a significant skin penetration enhancer. Upon their application, nanogels increase skin hydration allowing for water depots formation within the SC that disrupt its structure, leading to enhanced cargo penetration within the barrier [77, 80, 81]. On the other hand, the thermoresponsive modalities allow a “customized” drug release by tuning the VPTT of the nanogels with respect to skin natural thermal gradient (between 32 °C at the surface and gradually increasing to 37° C at the basal proliferative layer of the VE [82] or according to locally elevated temperature of hyperthermic dermal injuries caused by infections or inflammatory conditions [83]. PNIPAM-based nanogels have been in many instances applied on skin penetration studies owing their VPTT that is close to body temperature [84, 85]. Efficient thermoresponsive protein delivery into skin models was reported for PNIPAM-dPG nanogels with VPTT close to 35 °C. Here, successful penetration and intraepidermal release (93%) of encapsulated asparaginase and transglutaminase-1 were demonstrated in barrier-deficient skin [86, 87].

Another advantage of thermoresponsive nanogels is their compatibility for transdermal drug delivery approaches triggered by external hyperthermic stimulus like near infrared (NIR) light source, which significantly increases skin permeability and vascular perfusion and may promote percutaneous absorption of therapeutics with moderate hydrophobicity and low molecular weight [88, 89]. NIR light (700-950 nm) is generally tissue compatible and can achieve deep tissue penetration (up to 10 cm depending on light power) [90]. A proof-of-

concept study demonstrated deep skin penetration and successful cargo release of dPG nanogels consisting of poly(glycidyl methyl ether-co-ethyl glycidyl ether) upon localized NIR irradiation to 40 °C in excised human skin [91]. Another interesting application is photothermal therapy, in which thermoresponsive nanogels are embedded in tumor tissues to induce local tumor ablation in response to applied laser light [92, 93]. For these applications, nanogels VPTT must fall between 37 - 42 °C to maintain harmless local heating and avoid temperatures above 42 °C, by which protein denaturation and tissue damage may occur [94, 95].

1.4 Mucosal drug delivery

Besides skin, mucosal surfaces form the other interface with the external environment and present access-points to the body's internal milieu. They constitute multifunctional protective membranes that line various tissue cavities and organs in the body including the gastrointestinal tract, the respiratory tract, the urogenital tract, ocular surface, nasal, and oral cavities [96].

Drug delivery across mucosal surfaces entails various benefits by offering an alternative route of administration over other invasive techniques and is therefore generally associated with higher patients' compliance. It can also enable localized treatments, thereby improving drugs bioavailability at the target site, reducing the required effective dose (ED), and eradicating off-target side effects. Furthermore, systemic transmucosal delivery can also be promoted owing the high vascularization of many mucosal tissues [97]. However, efficient mucosal delivery is hampered by multiple challenges pertaining to the obstructive characteristics of the targeted mucosal tissue (e.g., limited accessibility, dynamic clearance mechanisms, enzymatic activity) on one hand, and to the poor stability of potential therapeutics (e.g., proteins and peptides) on the other. Although the utilization of NP-based delivery systems may offer protection to encapsulated therapeutics, NPs must overcome the highly challenging complex barrier overlining mucosal epithelia, namely the mucus barrier [98, 99].

1.4.1 Mucus barrier: structure, composition & properties

Mucus is a dynamic glycopeptide-based hydrogel that coats, lubricates, and protects the body's non-keratinized epithelial surfaces by forming an unstirred aqueous layer that is distally shed and replenished at a constant rate. It is mainly produced and secreted by specialized epithelial cells, known as goblet cells. In addition, subepithelial secretory glands contribute to mucus generation in certain tissues as well (e.g., airways and GI tract) [100, 101].

The gel-like properties of mucus are attributed to the main biopolymers forming its network: the mucins. Mucins are large glycoproteins (0.5 – 50 MDa) that consist of a protein backbone mainly built of numerous tandem repeats of three amino acids: proline, threonine, and serine,

referred to as PTS sequences. These amino acids are linked through their hydroxyl and amine groups to oligosaccharides, including galactose, fucose, sialic acid, N-acetylglucosamine (GleNAc), and N-acetyl galactosamine (GalNAc) to form the glycans mixture that densely coats mucins' protein backbone, thereby protecting it against endogenous proteases and providing massive water binding domains that confer the gel properties and impart mucins with a strong negative charge owing high content of sialic acid and sulfate groups **(Figure 1.3)** [102-104]. Meanwhile, the hydrophobic regions of mucins play an important role in mucins assembly and entanglement. Mucin monomers are interconnected through their cysteine-rich domains by disulfide bridges to form the mucus gel net-like structure **(Figure 1.3)** [104-106].

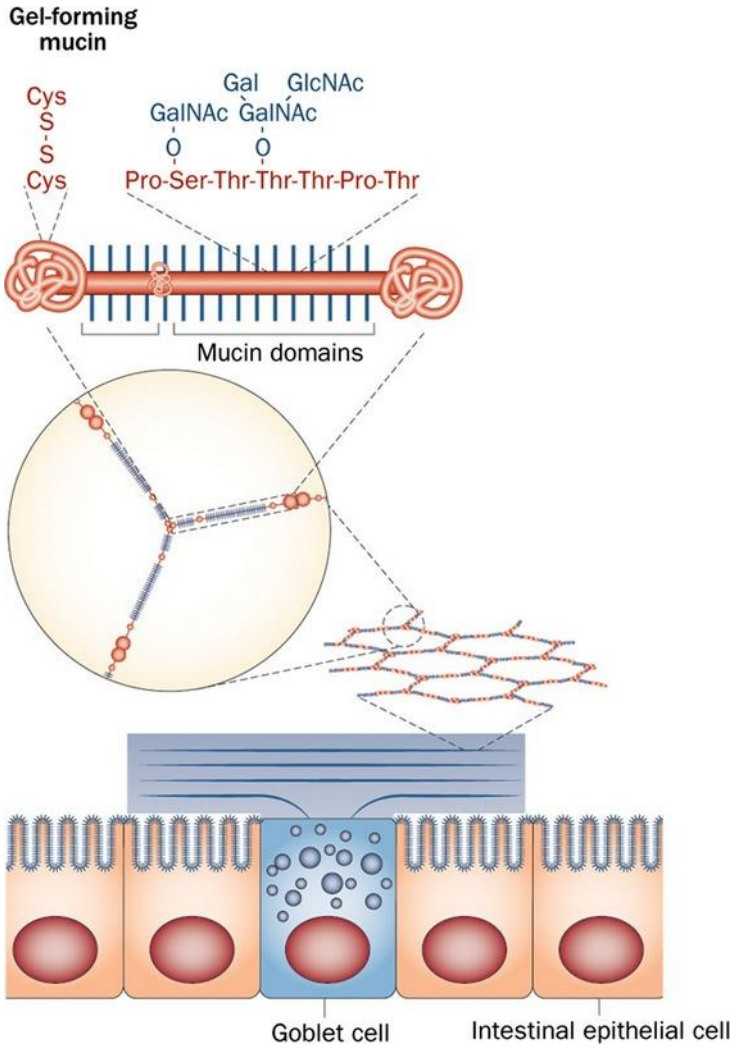

Figure 1.3 Schematic representation of secreted mucins that form the mucus gel barrier overlining mucosal surfaces like intestinal epithelium. Here, the structure of mucins is illustrated at different length scales down to the mucin monomers composition with the PTS (proline, serine, threonine) tandem repeats with O-linked oligosaccharides and the cysteine-rich domains "knots" that link mucin monomers together via disulfide bridges. Adapted and reprinted from [107] and [108] with permission from Nature and John Wiley and Sons publishing groups.

Mucins are diverse, namely 21 mucin genes (MUC) have been identified to this date that variate in glycosylation density, length and number of PTS tandem repeats, and molecular weight [109]. Multiple mucins can contribute to mucus composition and are classified as secreted loose mucins, or cell-bound firm mucins [110].

Overall, mucus presents a complex mixture of water (>90%), lipids, proteins, nucleic acids, and cell debris, and exhibits a mesh size ranging between 100 – 2000 nm that variates among the different mucosal tissues and even within the same site. Moreover, the thickness of mucus coating epithelia also varies among the different body sites, ranging from 0.2-1 µm in ocular surface and reaching 850 µm in large intestines [111, 112].

Within its functional capacity as a protective barrier against pathogens breach to underlying tissue, mucus acts as a selectively permeable membrane. It allows the diffusion of certain molecules like nutrients yet prohibits the passage of others, such as noxious substances and bacteria [113]. Despite the vital benefits of this selectivity, it presents a considerable hurdle for drug delivery to underlying epithelia and demands a specific design of efficient NP delivery systems [99, 100, 114].

Although the detailed molecular properties and events that direct and govern the mucus natural selectivity are still unravelled, physicochemical properties of mucus, including viscoelasticity, mesh size, pH, charge, and ionic strength are key factors that affect its permeability [115]. Based on the mucus biochemical properties, two critical mechanisms for particles filtering were identified: the size-dependant filtration (steric hindrance) and the interaction-dependent filtration [99, 116]. Basically, particles with sizes larger than the mucus cut-off are completely blocked and hindered from passage through mucus regardless of their surface chemistry **(Figure 1.4 A)**. Notably, the mucus mesh size is not necessarily uniform and follows the dynamic state of the gel [116, 117].

As for smaller-sized particles that fit through the mucus cut-off, their passage is restricted by the interactions between their surface chemistries and the mucus components. Particles demonstrating strong interactions with the mucus network are trapped and hindered, whilst particles displaying minimal interactions are allowed to pass [113, 116] **(Figure 1.4 B)**.
The main obstructive interactions with mucus include, hydrophobic, ionic, and electrostatic interactions (especially between cationic particles and the negatively charged mucins), in addition to covalent bonding and other specific interactions [118].

Noteworthy is that hydrogen bonding does not restrict particles diffusion through mucus but rather slow it, through contribution to binding interactions with mucus [119]. However, there is no direct correlation between hydrogen bonding and increased particles attachment to mucus,

since H-bond donor/acceptor groups in particles can paradoxically minimize binding to mucus by increasing mucus hydration and reducing its hydrophobicity, which in turn promotes mucus permeation. This effect seems rather predominant in polymers with H-bond acceptors in particular [120].

Plainly put, nanoscale sizes, hydrophilicity, neutral surface, and stealth properties are critical prerequisites for particles diffusion through mucus.

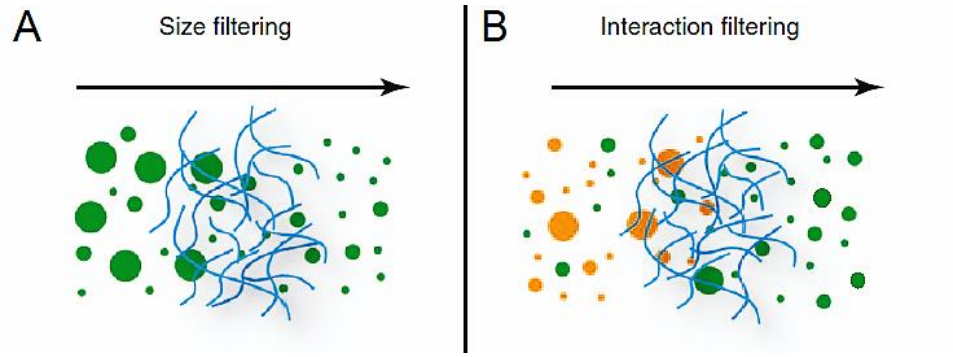

Figure 1.4 Schematic representation of mucus filtering mechanisms for permeation: (A) size-dependent filtration allows only particles smaller than mucus pore size to cross, while larger molecules are rejected. (B) interaction-dependent filtration allows particles selection with respect to surface properties: particles that strongly interact with mucus are immobilized and cleared (orange), whereas others avoid attachment to mucus and cross (green). Large particles are excluded anyways. Reprinted and adapted with Elsevier permission from [116].

Hence, nanoparticles intended for transmucosal drug delivery must accommodate the mucus selective properties in terms of size and surface chemistry, in order to penetrate it and deliver their therapeutics to the underlying epithelium [117, 121].
Still, the design of NP-based strategies for drug delivery to mucosal tissues depends on the intended application as well as the characteristics of the targeted mucosa, and whether a rapid or a prolonged diffusion through it may serve better the desired application. For example, some approaches take advantage of adhesion-interactions with the mucus to achieve sustained or extended drug release (e.g., topical buccal preparations), while others pursue rapid diffusion to overcome highly dynamic mucus regeneration and clearance (e.g., inhaled respiratory preparations) [122].

The following section outlines the most common strategies and NP-based systems for mucosal drug delivery.

1.4.2 Strategies and state-of-the-art systems for mucosal delivery

Various NP delivery systems were developed and tested for diverse mucosal applications. These systems can be mainly categorized as mucoadhesive or mucopenetrating particles:

Mucoadhesive particles (MAPs)

MAPs exploit the chemical interactions with mucus (e.g., hydrophobic interactions, ionic exchange reactions, covalent bonds formation, etc.) to increase their residence time in the mucus and, thus prolong drug absorption [119, 123, 124]. Mucoadhesive polymers include, chitosan, alginates, pectin, polyacrylates and cellulose derivatives. Chitosan is the most commonly used natural polysaccharide due to its biodegradability and intense cationic charge that forms electrostatic bonds with the negatively charged mucins [125-127]. To achieve polyvalent adhesion to mucus, two or more polymers can be combined together or with lipophilic nanomaterials (e.g., PLGA) to fabricate strongly adhesive NPs [128, 129]. Notably, mucoadhesion is particularly interesting to achieve extended release for drugs that are originally stable and naturally able to diffuse on their own through the mucus barrier [130-132]. Notably, such strategy is only efficient for tissues with slow mucus regeneration and shedding, whereas in mucosal tissues with continuous flow and dynamic turnover (e.g., intestines and lungs) mucoadhesion becomes impeding and causes NPs to be rapidly entrapped and eliminated **(Figure 1.5 A)** [106, 133, 134].

Mucopenetrating particles (MPPs)

In contrast to the above-mentioned particles, MPPs are designed to avoid attachment with the mucus gel in order to achieve rapid diffusion through it and reach underlying epithelium. According to the employed penetration strategy, MPPs can be subdivide into passive and active vehicles [122]. In the active approach, NPs are decorated with mucolytic proteases (e.g., papain, bromelain, or trypsin) that degrade mucin polymers and thus improve the particles transport by increasing the mesh spacing within the mucus gel network [135-137]. This confers an interesting strategy particularly for drug delivery across cystic fibrosis (CF) mucus, which is characterized by an abnormal densely compacted and stiffened dehydrated mucus matrix that inhibits drugs permeation [138, 139]. On the flip side, these particles may also cause temporary or permanent disruption in the mucus structure resulting in tissue injury, which makes their application questionable [122, 140].

As for the passive approach, it is based on avoiding trapping interactions with the mucus (e.g., electrostatic and hydrophobic interactions), either by mimicking the neutrally charged surface chemistry of viruses that are normally able to diffuse through mucus [141, 142], or by using the well-established strategy of coating hydrophobic NPs like liposomes, PLGA-, or polystyrene-based with hydrophilic muco-inert polymers, such as PEG, Pluronic® F-127, or other anti-

fouling agents to achieve free diffusion through mucus [143-146]. PEGylated NPs in particular have been widely studied in different mucosae, especially for the delivery of genes and small molecular weight drugs [147]. However, aside from few trials on PEGylated NPs for ocular application, none have reached the clinic as muco-penetrative yet [148].

Owing their ability to diffuse through mucous membranes of rapid turnover and dynamic mucus gel regeneration, MPPs present an effective strategy for most mucosal applications in general. Curiously, comparative studies between muco-inert MPPs and MAPs demonstrated a prolonged retention of MPPs in mucus, compared to MAPs. This is because MAPs attach to the outer layers of the mucus gel, which is turned over and cleared first, meanwhile MPPs, by avoiding interactions, can rapidly reach the inner layers of the mucus gel that are much slowly turned over, and so they are longer retained [133, 149-151]. Nevertheless, MPPs with uniform muco-inert surfaces come with eminent drawbacks like the possibility of reversed diffusion, and their limited epithelial absorption, which adversely affects their physiological efficacy **(Figure 1.5 B)** [122, 152, 153]. Conversely, the positive charge and hydrophobic nature of MAPs although limit their mucus permeation, yet they allow the particles to be anchored within mucus network and facilitate their cellular uptake [154, 155].

Interestingly, studies on particles-mucus interactions revealed that NPs that initially “slip in” and penetrate mucus, yet exhibit afterwards non-immobilizing interactions inside its network achieve higher partitioning within mucus, resulting in enhanced mucus permeation and epithelial absorption as well [156]. To address these competing interests in fabricating efficient mucosal delivery systems, NPs combining mucoadhesive and mucopenetrating qualities were developed as an optimized strategy **(Figure 1.5C)** [122, 157].

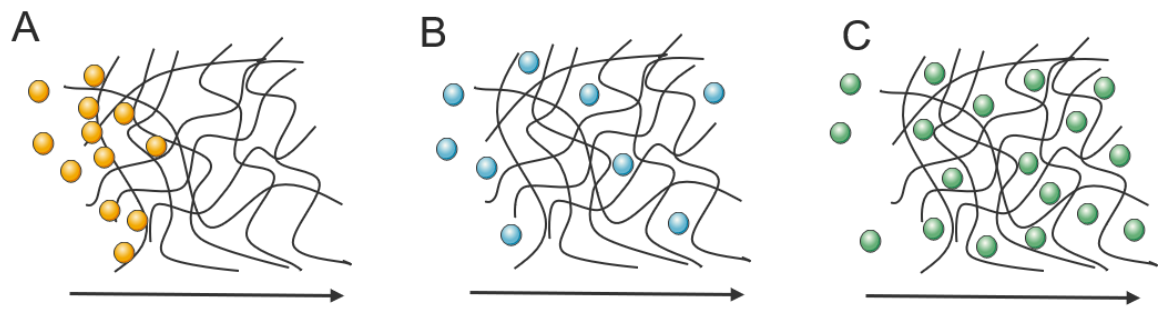

Figure 1.5. Effects of particles properties on their diffusion through mucus: (A) mucoadhesive particles bind to mucus and so their diffusion is impeded, (B) inert particles penetrate yet with low mucus-partitioning and limited epithelial absorption, (C) particles combining both features with neutral surface and weak adhesion interactions with mucus display increased mucus partitioning and subsequent penetration. Scheme is adapted from [113, 156] and includes features from Servier medical arts under creative commons license.

Muco-penetrating & -adhesive particles

Different NP-based approaches were proposed under this category as promising systems. For example, some approaches pursued a balance between hydrophobic and hydrophilic surface properties of the particles [157-159], or proposed NPs with dissociable hydrophilic coating and a positively charged chitosan-based core [160]. Others introduced zeta-potential converting NPs with negatively charged moieties cleavable by intestinal alkaline phosphatase leading to surface charge inversion from negative to positive during mucus permeation [161-163]. Additionally, nanogels based on thiolated poly acrylic acid (PAA) conjugated with mucolytic enzymes were also proposed to exert combined active mucopenetrating and mucoadhesive properties for oral administration. However, they were never investigated for drug delivery [164].

Polymers thiolation has been often employed to modify the properties of mucosal delivery systems [165, 166]. Prolonged mucus retention, improved hydrophilicity, enhanced permeation, increased cellular uptake, and efflux pump inhibitory activity are among the most reported advantages of thiolated particles [167-171]. Whereas the incorporation of free thiols into NPs structure can be disadvantageous for trans-mucus delivery, as it initiates strong mucoadhesion thus premature NPs elimination besides potential particles aggregation [172], conversely the integration of disulfide-linkages instead can avoid such issues and entail additional advantages, including improved mucopenetration and controlled redox-responsive degradation via disulfide-thiol exchange reactions with the mucins cysteine-rich domains **(Figure 1.3)** or with available reducing enzymes like glutathione (GSH) [173-175]. Hence, rationally designed disulfide-containing NPs confer a promising approach to tackle the contradictive demands for efficient mucus permeation and epithelial delivery.

1.4.3 Potential of dPG-nanogels in mucosal drug delivery

In terms of mucosal delivery, dPG falls into the same category as PEG in terms of biocompatibility, hydrophilicity, stability, and stealth effect, yet dPG offers additional benefits over PEG, including its multiple attachment capacity that allows conjugating responsive polymers and stabilizing macromolecular therapeutic proteins [51, 176, 177]. Furthermore, the abundant H-bond donor and acceptor substructures of dPG can enhance nanogels dispersion within the mucus network and assist in mucopenetration [51, 113].

Overall, dPG bears the qualities of a suitable scaffold for designing mucopenetrating nanogels, also the further equipment with disulfide-linkers as redox-sensitive moieties holds added potential for yielding biodegradable carriers with combined mucoadhesive and mucopenetrating features to overcome mucous membranes and transport labile therapeutics like biomacromolecules across mucosal barriers with dynamic turnover and enzyme active

lumen, such as the gastrointestinal mucosa [57, 178, 179]. So far, disulfide-containing dPG nanogels have not been tested for mucosal drug delivery. As a novel investigational concept, this falls within the scope of this thesis.

1.5 Biomacromolecules delivery across the intestinal mucous barrier

Since the FDA approval of recombinant human insulin as the first therapeutic protein in 1982, biomacromolecules like peptides and proteins have witnessed a remarkable uprise in pharmaceutical R&D and recently comprised over 50% of the newly approved drugs just within the past two years [180-182]. These biologics can modulate endogenous molecules and proteins that are involved in pathophysiological processes and disorders, and thus allow to restore biological function and treat diseases of complex mechanisms, such as cancer, infections, and autoimmune diseases.

Owing their high potency, low toxicity, and specificity, various biomacromolecules have entered the market and became indispensable therapeutics (e.g., peptide hormones, cytostatic agents, and biologics) [183-185]. However, despite the clinical benefits of therapeutic proteins, their application is greatly hampered by their labile structure and fragile nature as they are often prone to denaturation, enzymatic degradation, and aggregation, which can result in loss of their pharmacological activity or provoke an augmented specific immune response against them in the patient's system [186-188]. Moreover, their surface chemistry and large sizes (around 800 Da for peptides and up to 1000 kDa for proteins) further limit their mucosal penetration, therefore they are basically injected parenterally [186, 189].

NP-based approaches for non-invasive delivery of protein therapeutics offer an appealing alternative to overcome these issues and enable self-medication, which in turn shall increase patients' compliance through painless easy application, and eliminate systemic side effects due to the immunomodulatory behavior [190, 191]. The oral route has been by far the most preferable and convenient for drugs administration with over 60% of currently marketed drugs being orally administered [192]. Various NP-based formulations were proposed for oral delivery of therapeutic peptides and proteins, such as insulin or mAbs in order to promote localized treatment of GI tract-related disorders [154, 191, 193]. Nevertheless, the proposed NP-based formulations have yielded only limited success owing the complex and multi-resistant barrier characteristics of the intestinal mucosa.

1.5.1 Intestinal mucosa: composition and challenges for protein delivery

The intestinal tract is a fascinating organ. It presents the largest absorption surface in the body and harbors microbiota that outnumber the human body cells, yet it acts as a selective physicochemical and immunological barrier that restrains pathogens entry, controls molecules

trafficking (e.g., nutrients and enzymes), and regulates immune sensing and responses to maintain biological homeostasis and health. These outstanding barrier properties are mainly attributed to the luminal mucus blanket [107, 194].

The small intestine's barrier presents with an unstirred loosely adherent mucus layer coating the epithelial surface, whereas the large intestine's surface is coated by two mucus layers: inner cell-bound firm layer and outer loose layer [195]. The predominant mucin is MUC2, which has very large PTS domains (2300 amino acids) and is very densely glycosylated, which make it by far one of the few largest and most complex mucins in the human body [107]. Mucus thickness varies along the small intestine's segments (proximal to distal: duodenum, jejunum, and ileum) and was reported in rats between 120 – 500 µm [112]. This thickness is estimated to be higher in humans, however there are hardly reports on mucus thickness in human gut.

The underlying mucosa consists of a monolayer of polarized epithelial cells (IECs) manifesting into the lumen as crypts and finger-like projections, known as the villi, with apical microvilli protrusions that together give the small intestines its enormous surface area **(Figure 1.6)**. The absorptive enterocytes are the predominant epithelial cell type followed by the mucus secreting goblet cells and the transcytosis specialized M-cells [196]. IECs are interconnected through apical transmembrane tight junction (TJ) proteins, comprising claudins, occludin, and zunola occludins (ZO-1, ZO-2) as adaptor proteins. These tight junctions seal the interepithelial space to a great extent. Other junctional complexes, including adherens junctions (AJ) and desmosomes, also contribute to TJs assembly and function. Generally, the assembly/disassembly of TJs changes in health and disease as it is regulated by multiple signaling molecules, such as kinase enzymes and immune cytokines [194, 195].

Underneath the epithelium lies the connective tissue of the lamina propria, containing multiple cell populations like fibroblasts, pericytes, endothelial cells, neural cells, and immune cells (e.g., dendritic cells and macrophages) **(Figure 1.6)**. The lamina propria is separated from submucosa by a thin muscle lining, known as the muscularis mucosae [197].

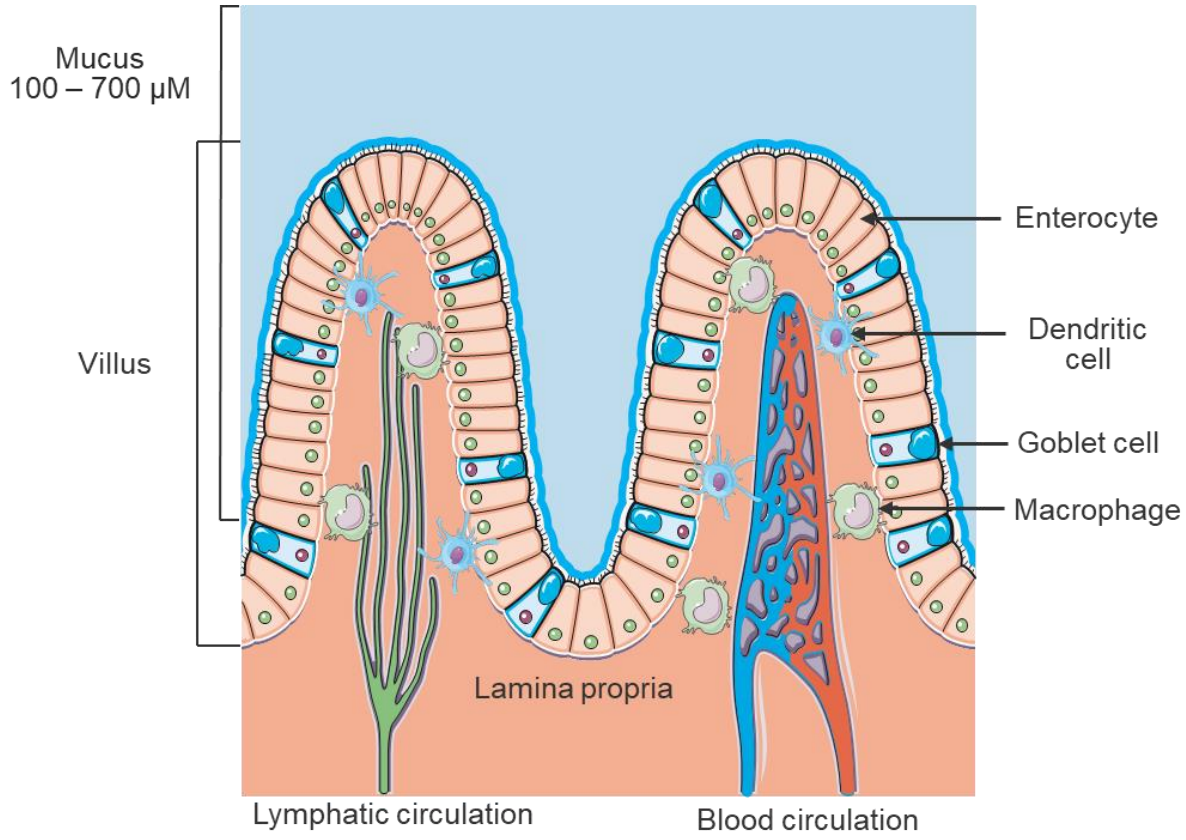

Figure 1.6 Simple schematic representation of the small intestine mucosa demonstrating the mucus blanket (loose mucus in light blue, membrane-bound in dark blue), the intestinal villi structure consisting of intestinal epithelial enterocytes, goblet cells, lymphatic and blood capillary networks, and immune components of the lamina propria that maintain and regulate barrier function. This Scheme is modified using Servier medical arts under creative commons license.

As the main absorption barrier for 90% of administered drugs (mostly through the oral route), the small intestine is the tissue of interest for drug delivery systems [192]. Typically, the intestinal epithelium offers two pathways for drugs diffusion, the paracellular route and the transcellular route. The latter is restricted by the cells' plasma membrane that is mainly accessible by moderately hydrophobic drugs of small molecular weight, meanwhile the former is restricted by TJs and is normally permeable to hydrophilic small drugs (≤ 600 Da), yet a leaky more permeable barrier is associated with some pathological conditions like inflammations, which allow enhanced drug absorption [198, 199]. Macromolecules typically pass via transcytosis through M-cells, assuming they survived the mucus barrier [196, 200]. Regardless of the epithelial absorption route, drugs must first overcome the luminal mucus barrier in order to reach the epithelium.

Intestinal mucus barrier, in particular, poses additional challenges for therapeutic proteins passage owing its enzymatic environment (e.g., GSH), the intestinal peristaltic dynamic motor activity of mucus distal flushing, and the heterogenous mesh spacing of mucus in intestines

[107, 108]. Still, biodegradable redox-sensitive nanogels are promising candidates in crossing the barrier if they exert controlled and adequate degradation while protecting their encapsulated therapeutic protein.

1.5.2 Experimental parameters in mucosal barrier function and permeability

The following parameters are often employed in established experimental techniques of mucosal drug delivery testing

Mucus rheology

As a highly viscoelastic polymeric hydrogel, mucus mechanical "rheological" properties are pivotal to its barrier characteristics and biological functions [201]. Unlike classic fluids, mucus exhibits a non-Newtonian shear-dependent viscoelasticity that is characterized by two components, the viscous (flow) modulus (G'') and the elastic (deformation resistant) modulus (G'). Rheology measurements indicate mucus as elastic dominant with G'>G'' at physiological shear rates [101, 201]. Mucus viscoelasticity is strongly dependent on the extent of mucins glycosylation, which variates among the different mucins, and it is also regulated by the covalent (e.g., thiol/disulfide exchange reactions), non-covalent, and physical entanglement interactions within its network. Hence, mucoadhesive interactions between particles and mucus result in a rheological synergism, which is proposed as an *in-vitro* parameter to assess particles-mucus interactions [132, 202].

Trans electrical epithelial resistance (TEER)

The epithelial barrier resistance to the transport of an electrical current is a critical and reliable indicator of its integrity and tightness. The higher the resistance is, the lower is the epithelial permeability and vice versa. TEER measurement is a sensitive method that quantifies resistance as a function of the barrier integrity (of both cells and tight junctions) and is expressed as a value of the measured surface area ($\Omega \times cm^2$). As a non-invasive *in vitro* technique, TEER is widely used to evaluate the barrier function of cell cultures and tissue models in normal and pathological conditions, especially for drug permeation studies [203].

1.5.3 Standard test models of the intestinal mucosa

To investigate mucus permeation and drug absorption into intestinal mucosa, various biological test systems are commonly employed, including animal models and in vitro cell culture models.

Animal models

Animals are essential subjects in preclinical research on GI relevant conditions. Excised intestinal segments from large animal models are used as resource for isolating native mucus

gel or as practical and cost-effective *ex vivo* tissue models for absorption and permeation studies in Ussing chambers or Franz diffusion cells [204, 205].

Pigs are particularly favored owing their outstanding anatomical and physiological similarities to humans. The GI tract in pigs closely resembles that of humans, especially the small intestines. Pigs and humans share the same ratio of intestinal length to body weight, same villi structure, similar epithelium composition (cell lineages, phenotypes, and expressed biomarkers), approximate immune system, similar colonizing microbiome, comparable mucus properties and composition, in addition to similar motility and mucosal transition. Based on these features, porcine models for intestines fulfill the FDA requirements for pharmaceutical testing and confer the most powerful analogues for humans in research [206, 207].

On the contrary, murine models do not exhibit such similarities, and thus are hardly comparable to humans due to major anatomical, physiological, immunological, and genetic differences of their GI tract that manifest in different intestinal permeability, absorption, metabolism, and absence of clinical hallmarks of human disease [208, 209]. Still the main reason behind their implementation is attributed to their law costs, ease of maintenance, and high reproduction rate [206]. In comparative permeation studies of marker proteins through intestinal explants from humans, pigs, and rats, Nejdfors et al. demonstrated similar rate and extent of intestinal permeability for human and porcine tissues, in contrast to rats that showed relatively higher tissue permeability, making their use for assessment of drugs permeability questionable [210]. Similar studies on NPs permeation have also confirmed the interspecies similarities between humans and adult pigs emphasizing the translational power of porcine models in intestinal permeability and absorption studies [211]. Respective TEER values of these animal models compared to human's are in line with these findings **(Table 1.1).**

Nevertheless, the use of large animal models for experimentation has fundamental issues pertaining to the fragility of the intestinal tissue, which requires careful handling and special conditions to maintain its viability before and during the very short experimentation period (up to max. 3 h) for drug absorption and permeation studies [212, 213]. Additionally, ethical concerns and approval requirement from the responsible regulatory authorities are further important considerations, along with the relatively high costs and difficulty in inducing human pathological disorders in pigs for *in vivo* studies [207]. Thus, reconstructed human-based microtissues confer attractive alternatives to animal testing that enable to simulate pathological processes of human diseases *in-vitro.*

In vitro human-based cell culture models

The intestinal barrier is one the most challenging tissues to mimic *in vitro* owing its complex polarized mucosa, the scarcity of primary human enterocytes, and short survival of intestinal

explant cultures *ex vivo*. Hence, the most commonly used *in vitro* intestine "equivalents" are based on cell lines, which do not resemble the small intestine's enterocytes as they are generated from colon or kidney tumor cells like Caco-2 and MDCK cells, respectively [214].

Caco-2 cell-based models have been extensively used for decades and are considered the gold standard for *in vitro* drug transport and absorption studies despite fundamental shortcomings that endow these models with unphysiological barrier properties. Notably, Caco-2 monolayers do not secrete mucus and are genuinely more resistant to particles permeation and less penetrable due to their densely packed cells through very tight paracellular junctions exhibiting up to 24 folds higher TEER values compared to human small intestine **(Table 1.1)** [215, 216]. To address these shortcomings, Caco-2 cells were co-cultured with the mucus-secreting cell line HT-29 derived of colon carcinoma to yield more in-vivo relevant intestinal models [217]. However, different mucins are expressed in cancer cells with altered structure and physicochemical characteristics leading to discrepancy between *in vitro* readout and the *in vivo* situation [218].

Moreover, such cell lines-based models also lack other important physiological features of the intestinal barrier. For example, they do not display crypt-villi-like structure, which is essential for ionic and water exchange across the epithelium, they lack efflux transporters and metabolic enzymes (e.g., CYP3A4), and display wide variations in the model properties according to the selected clone in the cell line generation and even upon using different passages of the same cells, which can yield unreproducible models [219]. Still, Caco-2 based models can be beneficial for toxicity screening tests or to investigate interplay and signaling between different co-cultured cell types [220]. However, they are rather infeasible for drug permeability and absorption studies. Disease modeling is another issue in cell lines usage, since changes in their culture conditions (e.g., cytokines stimulation) can result in irreversible genetic and phenotypic cellular alterations and induce development of different clonal populations within the same cell culture [221].

Despite recent progress in tissue engineering, only few small intestine models based on human primary cells were developed, including organoids and reconstructed microtissues [222]. Intestinal organoids are generated from primary stem cells isolated from the intestinal crypts and embedded in Matrigel matrix, where they differentiate and expand to spherical epithelial 3D cell clusters. Indeed, organoid cultures are important tools in studying intestinal physiology, but their culture setting is unsuitable for drug delivery studies [223, 224]. Conversely, reconstructed microtissues offer suitable drug delivery test systems, such as the commercially available *in vitro* 3D microtissue EpiIntestinal™ (MatTek, Ashland, MA) [225]. This primary cell-based model closely mimics the human small intestine's polarized nature and

structure, including, the barrier TEER, MUC2-secreting goblet cells, the crypt-villi axis, and the subepithelial fibroblasts-containing lamina propria [226]. Several studies demonstrated the structure related function of EpiIntestinal™ microtissues and presented them as reliable and reproducible *in vitro* test systems for drug absorption studies and disease modeling of pathological conditions like inflammatory bowel disease [225, 227, 228].

Table 1.1 List of conventional models for drug delivery studies to small intestines.

Experimental model	Source tissue	TEER (Ω × cm^2)	Mucus barrier	Reference
Human biopsies	Jejunum	~100	MUC2-based	[215]
Porcine biopsies	Jejunum	~100	MUC2-based	[229]
Rat biopsies	Jejunum	30 - 40	MUC2-based (less complex mucin structure than human's)	[230], [231]
Caco-2 monolayers	Human Colon adenocarcinoma	1400 – 2400 900	No mucus	[216, 232]
MDCK monolayers	Dog kidney	Type-I:1500 Type-II: 190 - 330	No mucus	[214]
Caco-2 & HT-29-MTX	Colon carcinoma	100 - 300	Altered mucus (MUC3-based)	[217]

1.5.4 Inflammatory bowel disease (IBD)

IBD is an autoimmune chronic condition of relapsing-remitting inflammation cycles in the GI tract that manifests in two disease forms: Crohn's disease (CD) and ulcerative colitis (UC). Both diseases arise from interplay between genetic and environmental factors (e.g., stress, smoking, unhealthy diet, high standards of hygiene), associated with intestinal innate immunity disorders in the sense of a mucosal barrier defect towards commensal microbiota leading to increased barrier permeability and pathogens influx into epithelium. However, the detailed etiology and initiating pathomechanism remain unravelled [233, 234]. CD and UC differ in the type of disease-driving immune response and the affected regions of the GI. Whereas UC manifests as a Th2-driven inflammation in the colon, CD occurs as Th1-mediated disorder with fistulas formation that is mainly localized in the ileum but can also affect any region along the

GI tract [235, 236]. Both diseases predispose patients to high risk of permanent GI damage or developing colorectal cancer (CRC) [237]. Epidemiological statistics indicate increased prevalence of IBD cases around the world with the highest yearly incidence alarmingly in Europe as 505/100,000 cases for UC and 322/100,000 for CD [238].

With no cure until now, IBD treatment aims to induce rapid remission and maintain it using oral and local non-specific anti-inflammatory drugs (e.g., 5-aminosalicylic acid and corticosteroids) in mild to moderate cases, or parenteral immunosuppressing agents like immunomodulators and anti-TNFα biologics in moderate to severe progression [239]. However, these therapeutic proteins exhibit limited efficacy in IBD treatment due to their low bioavailability and instability at the GI mucosa, in addition to their immunomodulation-related systemic side effects, including immunogenicity, toxicity, and increased propensity to opportunistic infections [240, 241].

NP-based formulations enable targeted delivery of biologics to optimize their therapeutic benefit while minimizing their adverse effects, especially since inflammation induces TJs reorganisation resulting in increased barrier permeability that can facilitate NPs penetration and biomacromolecules delivery [242]. Multiple *in vivo* studies in rodents with chemically induced IBD showed NPs selective accumulation in inflamed intestinal regions following oral or rectal administration just by the merit of their size (100 nm) and hydrophobic surfaces [243, 244]. Conversely, similar studies on human intestinal biopsies from actual IBD patients demonstrated quite the opposite with hydrophilic NPs, even of larger sizes, achieving high translocation and deposition in inflamed regions compared to hydrophobic or charged NPs showing no accumulation or translocation in diseased or healthy mucosa [245]. This discrepancy points out essential limitations of conventional *in vivo* rodent models of IBD, especially since most studies on drugs absorption and therapeutics delivery for IBD treatment are conducted using them.

IBD disease models

IBD does not naturally occur in rodents and is thus artificially induced employing either toxic chemicals or genetic engineering techniques. In the former approach, a severe chemical injury in the large intestine with inflammation (colitis) is typically induced in mice and rats by intrarectal injection of TNBS (2,4,6-trinitrobenzenesulfonic acid) or by spiking the rodents' drinking water with DSS (dextran sulfate sodium) over a week [246-248]. This approach, however, yields merely an acute chemical damage to the intestinal epithelial barrier with characteristics of a Th2-type response, yet very limited involvement of innate and adaptive immune processes, whose dysregulation actually plays an essential role in IBD pathogenesis and affects the response to administered therapeutics and drug delivery systems [249, 250].

To make this inflammation chronic, an approach based on repeated cycles of chemical toxins administration followed by chemicals-free rest periods was pursued over several months. This attempt, however, was time consuming and resulted in the death of many mice. Still, the surviving mice exhibited variable injuries and inflammatory responses eventually, making the test system unpredictable [246, 251].

Aiming to produce more human-relevant IBD characteristics in rodents, genetically modified mouse or rat models were developed. Here, target genes in IBD could be specifically modulated to induce inflammation [250, 252]. Although these models provide a helpful tool in understating the importance of certain molecules and proteins in IBD pathomechanism, they neglect the interspecies differences between humans and rodents with respect to the major variations in the immune system components and the complex signaling pathways and functions involved in the inflammatory response [253, 254]. For example, induced colitis in IL-10 deficient mouse models indicated the important role of this anti-inflammatory cytokine in reversing IBD, yet respective treatment with IL-10 yielded but little clinical effect in human subjects [255, 256].

Moreover, the commensal flora inhabiting rodents' gut is almost completely different to that in humans, thus making it more difficult to simulate characteristics of a disease that is markedly influenced by crosstalk and interplay between gut microbiota and the host immune system [257, 258]. To some extent, genetically modified murine models are much more beneficial than their chemically induced *in vivo* counterparts, yet they are less implemented in research due to their much higher costs [254]. Overall, it is only logical that human-based models can best reflect phenotypes and characteristics of autoimmune diseases that only occur in human beings by nature, such as IBD.

2. AIM OF THE THESIS

Within the scope of improving conventional pharmaceutical formulations through implementing nanoparticulate delivery systems, the goal of this project was the investigation of stimuli responsive nanogels for local and targeted delivery of biomacromolecules to skin and intestinal mucosa, with mucosal delivery as the main focus area of this thesis. Herein, this thesis emphasizes the pivotal role and challenging influence of the mucus barrier on drug delivery and highlights the potential of adapted stimuli responsive modalities of nanogels in facilitating the crossing of biological barriers besides controlling the drug release kinetics.

Hence, in collaboration with the Caldéron research group (FU Berlin), this thesis introduces two types of stimuli responsive systems based on innovative concepts with the following objectives:

1. Thermoresponsive dPG nanogels based on PNIPAM, PNIPMAM, and co-PNIPAM-PNIPMAM with different VPTTs, were investigated for controlled intraepidermal protein release into barrier-deficient human skin. Here, the protein release kinetics and yield were assessed and evaluated with respect to skin's natural thermal-trigger vs. an external trigger represented by NIR-lamp as a proof-of-concept.

2. Redox-sensitive dPG nanogels based on PNIPMAM tethered to disulfide linkers, developed to address the mucus barrier properties were characterized and thoroughly investigated as novel promising biodegradable systems for biomacromolecules delivery to intestinal mucosa. To unravel the nanogels behavior and mode of action, interactions with mucus as well as potential mucopenetrating properties were studied in isolated native mucus and freshly excised small intestine of pigs. Furthermore, the therapeutic efficacy of nanogels-based anti-TNFα treatment (etanercept as a model drug) was evaluated in human primary cell-based small intestine models emulating characteristics of IBD *in vitro* as a proof-of-concept.

3. PUBLICATIONS & RESULTS

3.1. Nanogel-based thermoresponsive protein delivery to skin

3.1.1 Publication

Online available under the following DOI-link: https://doi.org/10.1016/j.msec.2019.02.089

Title & authors

Critical parameters for the controlled synthesis of nanogels suitable for temperature-triggered protein delivery

Loryn E. Theune, **Rawan Charbaji**, Mrityunjoy Kar, Stefanie Wedepohl, Sarah Hedtrich, Marcelo Calderón

The following contributions were made to this publication:

Personal contribution

Planned, and conducted the temperature triggered skin protein delivery studies on excised human skin in two setups: under natural temperature trigger and under external trigger using an IR-lamp with subsequent data analysis. In addition, designed and conceived the experimental setup for the penetration studies using IR-lamp as an external trigger, all under supervision of Prof. Dr. Sarah Hedtrich. Also collected the tested human skin for these experiments from Behring hospital (Zehlendorf, Berlin) upon patients' informed consent. Reported the respective part into the manuscript and contributed to manuscript revision.

Co-author´s contribution

Loryn Theune synthesized and characterized the tested nanogels, conducted the respective experiments, and prepared the manuscript under supervision of Prof. Dr. Marcelo Calderon. Co-authors contributed to the study design, evaluation of the experiments, and manuscript revision.

Graphical abstract

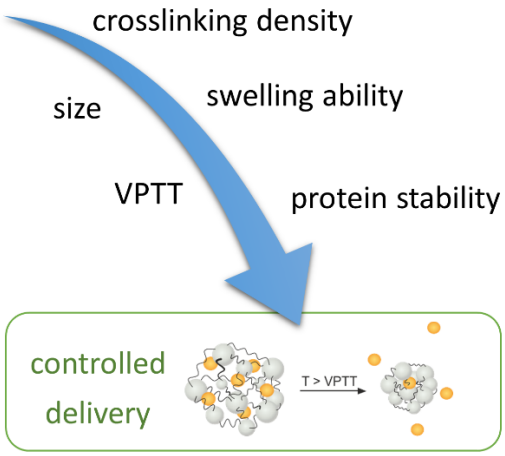

Abstract

Macromolecular bioactives, like proteins and peptides, emerged as highly efficient therapeutics. The main limitation for their clinical application is their instability and potential immunogenicity. Thus, controlled delivery systems able protect the proteins prior release are highly on demand. In the present study, we developed hydrophilic thermo-responsive nanogels with tunable volume phase transition temperatures (VPTTs) and suitable features for controlled protein delivery by the use of multifunctional, dendritic polyglycerol (dPG) as macromolecular cross-linker and temperature-sensitive polymers poly(N-isopropylacrylamide) (NIPAM) and poly(N-isopropylacrylmethacrylate) as linear counterpart. We comprehensively studied the impact of the initiator, monomers and cross-linker on the nanogel structure during the synthesis. Careful analysis of the polymerization process revealed importance of balanced reactions kinetics to form particles with diameters in the range 100-200 nm and low polydispersity. We can control the cross-linking density of the nanogels mainly by the dPG feed and its degree of acrylation. In addition, our screenings revealed that the hydrophilic character of dPG enables it to stabilize the growing particles during the polymerization and thereby reduces final particle size. Co-polymerization of NIPAM and NIPMAM allows precise tuning of the VPTT of the nanogels in the desired range of 34-47 °C. Our nanogels showed outstanding high protein encapsulation efficiency and triggered cargo release upon a temperature change. The delivery efficiency of these nanogels was investigated on excised human skin demonstrating efficient dermal penetration of encapsulated proteins dependent on a temperature triggered release mechanism.

1. Introduction

Nanogels are soft, polymeric gel particles in nanoscale size capable of holding large amounts of water within their cross-linked network and thus emerged as a hydrophilic platform to encapsulate a variety of guest molecules.[1-4] Nanogels found applications in diverse fields of nanomedicine ranging from biosensors,[5-7] diagnostic and imaging agents[8-10] to drug delivery systems.[2, 11, 12] In particular, stimuli-responsive "smart" nanogels have been studied extensively for drug delivery purposes as the release of an encapsulated cargo can be triggered and controlled by internal or external stimulus.[13] Physico-chemical properties and stimuli responsive behaviour of the nanogels depend on the polymeric characteristics of the materials used for the synthesis and therefore have to be carefully selected depending on the desired functions. For drug delivery approaches, temperature-responsive polymers like *poly*-(N-isopropyl acrylamide) (PNIPAM),[14-16] *poly*-oligo(ethylene glycol) (POEG),[17, 18] and *poly*-vinyl caprolactam (PVCL)[19, 20] are attractive materials, since nanogels formed from these materials are biocompatible and show a volume phase transition temperature (VPTT) close to body temperature. When exceeding the lower critical solution temperature (LCST) of the used thermo-responsive polymer, the crosslinked nanogel network collapses induced by the phase transition of the polymer chains leading to a shrinkage of the nanogels and an expulsion of inner water molecules.[13] Encapsulated molecules would thereby be released along with the expulsion of water. To use thermo-responsive nanogels as drug delivery systems, the VPTT as well as the range of temperature in which the collapse of the nanogels occurs are essential factors to prevent premature leakage of the encapsulated cargo.[21] Depending on the specific features and requirements of the respective bioactive that is to be delivered, the overall size and crosslinking density of the containing polymeric network must be accordingly tuned and optimized to achieve effective retention of the bioactive within the nanogels below the VPTT and a temperature dependent release.

To trigger the drug release from thermo-responsive materials, a local temperature change at the desired site of action is required. For systemic applications, a natural temperature elevation can appear, for example, due to an inflammation or infection.[22] However, in most cases, an external hyperthermic stimulus is needed.[21] Thereby, strictly localized heating of the targeted tissue is required. In addition, a VPTT of the nanogels in the range of 37-42 °C is needed to trigger the release of their cargo, yet prevent damage of surrounding tissue as at temperatures above 42 °C protein denaturation and disruption of anatomic structures are pending.[13, 23] For nanogels with VPTTs lower than 37 °C, topical applications are of great interest as the skin has a natural temperature gradient ranging from 32 °C on the skin surface up to 37 °C in deeper skin layers.[24, 25] Therefore, a temperature trigger will apply itself with increasing penetration depth of the drug carrier.[16, 26-30] Recent results indicate that besides the release of

the therapeutic also the expulsion of water molecules from the nanogels above their VPTT is crucial as this induces skin hydration and assists the therapeutics penetration into deeper skin layers.[27]

Moreover, nanogels emerged as a promising platform for the encapsulation and release of both, low molecular weight drugs[16, 28] and biomacromolecules like proteins, owing their potential to stabilize them, prevent their degradation by enzymes as well as suppress thermal denaturation.[1, 27, 29] Recently, we have developed the synthesis of thermo-responsive nanogels cross-linked with dendritic polyglycerol (dPG) and were able to demonstrate their excellent performance in dermal delivery of proteins using the natural temperature gradient of human skin.[15, 27, 29] As a hydrophilic, biocompatible, and multifunctional moiety, dPG allows easy functionalization and is known for its ability to stabilize proteins against degradation and denaturation.[31-33] Indeed, the use of dPG as macromolecular cross-linker of thermo-responsive polymers increased the stability of the nanogels themselves[34] as well as the encapsulated protein, efficiently protecting it and maintaining its biological function.[27, 29]

Although PNIPAM-based nanogels are great candidates for delivery of therapeutic actives into the skin, their VPTT below body temperature of 37 °C is unsuitable when it comes to systemic applications. One strategy to overcome this issue and increase the VPTT can be found in copolymerization with hydrophilic monomers like acrylic acid for example.[11, 35, 36] Doing so, the hydrophilic/hydrophobic balance in the polymer is shifted to higher hydrophilicity causing the nanogels to collapse at higher temperatures. One disadvantage of this strategy is that it often leads to broadening of the slope of the VPTT and charges may be added, which lead to pH dependency of the VPTT as well.[11, 36] On one hand, this pH dependency can be advantageous for specific applications,[11] yet on the other hand this can complicate the nanogels biological fate e.g. by enhancing the formation of a protein corona, which can lead to unexpected *in vivo* behaviour.[37, 38] Therefore, we were interested in the development of a tunable nanogel system without or with only minor changes in the physio-chemical properties. The structure of poly-N-isopropyl methacrylamide (PNIPMAM) is very close to PNIPAM containing only one more methyl group in its vinyl backbone (Fig.1). It is proposed that this methyl group induces a steric rigidity to the polymer weakening the intermolecular interactions between the amide groups and favouring hydrogen bonds with surrounding water molecules, thus, leading to a shift of the transition temperature to higher temperatures (40-45°C) despite similar hydrophobicity.[39-41] Macro- or nanogels from PNIPAM or PNIPMAM show similar hydrodynamic radii and spherical shape.[42] Studies of phase transition behaviour of linear PNIPAM-PNIPMAM copolymers showed ideal behaviour with a direct dependency of the lower critical solution temperature on the ratio of the two polymers.[40] Djopké and Vogt could demonstrate that the transition temperature of the randomly polymerized linear copolymers can be precisely fine-tuned

between 32.5 °C and 47 °C while the transition on molecular weight and concentration remains independent like for the homopolymers. These results motivated us to develop copolymeric nanogels based on PNIPAM-co-PNIPMAM crosslinked with macromolecular dPG optimized for a temperature-triggered protein delivery.

In the present study, we elucidate critical parameters to control the synthesis of thermoresponsive nanogels based on PNIPAM, PNIPMAM and dPG. In particular, factors affecting the nanogels in regard to their size, cross-linking density and swelling ability were determined. In addition, the conditions to generate copolymeric nanogels from PNIPAM and PNIPMAM in order to tune the VPTT without affecting other physicochemical properties were carefully analysed. The resulting nanogels were evaluated for their ability to encapsulate and release the model protein bovine serum albumin (BSA) into excised human skin in a temperature-controlled fashion whilst protecting the protein structure.

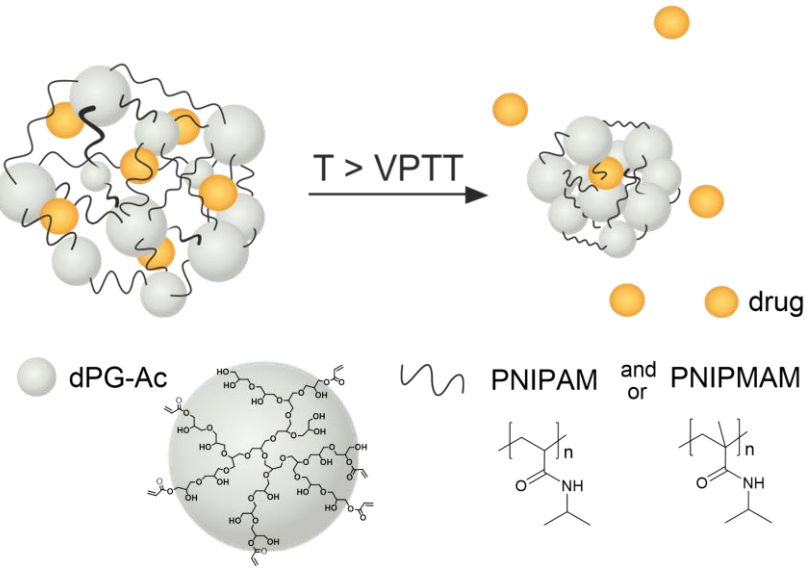

Fig. 1 Schematic representation of temperature triggered release of an encapsulated drug from thermo-responsive nanogels based on acrylated dendritic polyglycerol (dPG-Ac) and poly-N-isopropyl acrylamide (PNIPAM) and/or poly-N-isopropyl methacrylamide (PNIPMAM) and chemical structures of dPG, PNIPAM and PNIPMAM.

2. Materials and Methodes

2.1. Materials

The following chemicals were used as purchased: Acryloyl chloride (Ac-Cl, Aldrich, 97%), triethylamine (TEA, Acros, 99%), dry N,N-dimethylformamide (DMF, Acros, 99.8%), sodium dodecyl sulphate (SDS, Sigma, ≥98%), potassium persulfate (KPS, Merck, ≥99%), ammonium

persulfate (APS, Sigma, 98%). N-isopropylacrylamide (NIPAM, Sigma, 99%) and N-Isopropylmethacrylamide (NIPMAM, Sigma, 97%) were recrystallized in n-hexane prior use.

2.2. Methodes

2.2.1. Synthesis of acrylated dPG (PG-Ac)

Dendritic polyglycerol (dPG) was obtained from Nanopartica GmbH with an average M_w of 10 kDa (PDI 1.3) and was dried under high vacuum at 80 °C overnight prior use. In order to obtain different acrylation degrees in dPG, the desired mol% of available OH groups in dPG were set to 1 equivalent. The acrylation was achieved by adding Ac-Cl (1.3 eq.) dropwise to a cooled (0 °C) solution of dPG (1 eq.) and TEA (2 eq.) in dry DMF. The reaction was left stirring at r.t. for at least 4 h and the product was purified by dialysis (regenerated cellulose, molecular weight cut-off (MWCO) 1 kDa) in water for two days. The acrylated dPG was preferably used directly after purification. Otherwise, the product was stored at 6-8 °C in the presence of p-methoxyphenol and dialyzed before usage. Yield 85-90 %. ^{1}H-NMR (500 MHz, D2O), δ: 3.1-4.4 (m, 5 H, polyglycerol scaffold protons), 5.98–6.12 (m, 1 H, vinyl), 6.18–6.32 (m, 1 H, vinyl), 6.45–6.53 (m, 1 H, vinyl).

2.2.2. Synthesis of thermoresponsive nanogels

Thermoresponsive nanogels based on PNIPAM, PNIPMAM or their copolymers were synthesized according to previously reported methodologies with minor changes.[15] Different feeding ratios of acrylated dPG as well as different acrylation degrees have been screened for PNIPAM and PNIPMAM based nanogels. In addition, different ratios of NIPAM and NIPMAM feed have been investigated. In a typical reaction, 100 mg of monomers (dPG-Ac and NIPAM, NIPMAM or a mixture of NIPAM and NIPMAM) and SDS (1.8 mg) were dissolved in 4 mL distilled water. The reaction mixture was purged with Argon for at least 15 min before transferred to a hot bath at 70 °C. After 5 min, an aqueous solution of KPS (3.3 mg, 1 mL) was added quickly to initiate the polymerization. The mixture was left stirring at 70 °C for 3 h, followed by purification via dialysis (regenerated cellulose, MWCO 50 kDa) in water. After lyophilisation, the product was obtained as a white cotton-like solid. Yield 80-90 %.

FT-IR of PNIPAM-dPG nanogels: ν (cm^{-1}) = 3100-3500 (OH, dPG), 2971, 2931, 2874, 1732, 1643(C=O amide), 1540 (amide), 1458, 1387 (CH isopropyl group), 1366 (CH isopropyl group), 1226, 1172, 1129, 1074, 979, 927, 880, 839.

^{1}H-NMR of PNIPAM-dPG nanogels: (500 MHz, D2O), δ: 1.16 (s, 6 H, isopropyl groups of NIPAM), 1.57 (2 H, polymer backbone), 2.04 (1 H, polymer backbone), 3.35–4.10 (6 H, polyglycerol scaffold protons + 1 H NIPAM).

FT-IR of PNIPMAM-dPG nanogels: v (cm^{-1}) = 3100-3500 (OH, dPG), 2970, 2932, 2874, 1732, 1633(C=O amide), 1516 (amide), 1457, 1386 (CH isopropyl group), 1365 (CH isopropyl group), 1321, 1260, 1197, 1128, 1077, 962, 928, 883, 840.
^{1}H-NMR of PNIPMAM-dPG nanogels: (500 MHz, D2O), δ: 0.98 (s, 3 H, methyl group of NIPMAM), 1.15 (s, 6 H, isopropyl groups of NIPMAM), 1.78 (2 H, polymer backbone), 3.35-4.10 (6 H, polyglycerol scaffold protons + 1 H NIPMAM).

FT-IR of Co-dPG nanogels: v (cm^{-1}) = 3100-3500 (OH, dPG), 2971, 2931, 2874, 1732, 1645(C=O amide), 1526 (amide), 1458, 1386 (CH isopropyl group), 1366 (CH isopropyl group), 1220, 1173, 1129, 1077, 965, 927, 884, 840.
^{1}H-NMR of Co-dPG nanogels: (500 MHz, D2O), δ: 9.98 (s, 3 H, methyl group of NIPMAM), 1.16 (s, 6 H, isopropyl groups of NIPAM and NIPMAM), 1.57-2.15 (m, 3 H polymer backbone NIPAM + 2 H polymer backbone NIPMAM), 3.35–4.10 (7 H, polyglycerol scaffold protons + 1 H NIPAM + 1H NIPMAM).

2.2.3. Encapsulation and release studies

Protein encapsulation and release behaviour of the different NGs was studied using FITC conjugated bovine serum albumin (BSA-FITC, Sigma-Aldrich) as a model drug. To encapsulate BSA-FITC in the nanogels, dry nanogels were swollen in a solution of BSA-FITC (1 mg/mL, pH 7.4, PBS) for at least 24 h at 6-8 °C. The solutions were purified using Vivaspin 300 kDa centrifugal device (10 min at 6000 rpm; Sartorius AG, Göttingen, Germany). The concentration of encapsulated BSA-FITC was determined by absorbance at 492 nm. For the release, 10 mg of nanogels (10 mg/mL) with encapsulated BSA-FITC were placed in a Vivaspin 300 kDa device and diluted with acceptor medium (PBS, pH 7.4) to 10 mL. At certain time intervals, the samples were centrifuged (5 min, 5000 rpm) and the filtrate was taken for analysis (absorbance 492 nm) while fresh buffer was replaced.

2.2.4. MTT assay

Human dermal fibroblasts isolated from juvenile foreskin were isolated in accordance to local ethics and biosafety regulations (ethical approval EA1/345/14 by the Charité ethical committee). HeLa cells (#ACC-57) were obtained from Leibnitz Institute DSMZ- German collection of Microorganisms and Cell Cultures. To assess cell viability, 10000 cells per well were seeded into 96-well-plates (Sarstedt) in 100 µL/well Roswell Park Memorial Institute (RPMI) medium (for HeLa) or Dulbecco's Modified Eagle Medium (DMEM) (for fibroblasts) (Gibco, Thermo Fisher Scientific) containing 10% fetal bovine serum (FBS), (FBS Superior, Merck), 1% Penicillin/Streptomycin and 1% MEM non-essential amino acids (NEAA, RPMI only) (Thermo Fisher Scientific). The cells were incubated at 37 °C at 5% CO_2 overnight. Then,

medium was replaced with fresh medium containing various dilutions of the corresponding nanogel in duplicates and cells were incubated for 48 h at 37 °C and 5% CO_2. The cell culture supernatant was removed and cells were washed twice with PBS (200 µL/well). Then, 100 µL/well fresh full medium including 10 µL/well MTT (Sigma-Aldrich, 5 mg/mL in PBS) were added and incubated for another 4 h at 37 °C. After development of formazan crystals, the cell culture supernatant was removed and crystals were dissolved by addition of 100 µL/well of isopropanol containing 0.04 M HCl. Absorbance was read at 590 nm in a Tecan Infinite M200 Pro microplate reader. Relative viabilities were calculated by dividing average absorbance values of wells with treated cells by values of untreated cells (=100% viability). All tests were repeated 3 times independently and errors were expressed as SEM.

2.2.5. Skin penetration studies

To evaluate temperature-triggered delivery of encapsulated BSA into excised human skin, penetration studies were performed on barrier-impaired skin in two different setups: a) temperature ramp from 32-37 °C modelling the natural temperature gradient in the skin and b) increasing the skin surface temperature up 41 °C by local irradiation with an infrared (IR) lamp.

All experiments were conducted on excised abdominal skin from healthy male patients, who underwent plastic surgery and upon signed consent from each patient (ethical approval EA1/345/14 by the Charité ethical committee). Skin samples were obtained in accordance with the guidelines of Helsinki Declaration with ethical approval.

2.2.5.1. Temperature ramp experiments

Excised human skin (freshly obtained 3h after surgery or frozen for less than 6 months) was stretched on a metal block then tape stripped 50 times to disrupt the stratum corneum (SC) in order to mimic an impaired barrier integrity in diseased skin (e.g. skin inflammatory, infectious diseases). Skin punches of 15 mm diameter were taken and placed in 6-well inserts (Falcon® Cell Culture Inserts, 3 µm, HD, PET membrane). The inserts were placed in 6 well plates, each filled with 2 mL PBS. The explants were then treated with protein loaded nanogels to a final concentration of 20 µg/cm^2 of loaded BSA (6.8 mg/mL nanogels stock solution with a ~10wt% BSA-FITC loading). Afterwards the treated skin biopsies were incubated for 6 h applying a temperature ramp of 32 °C, 34 °C to 37 °C over the first three hours. Skin punches treated either with PBS or 20 µg/cm^2 BSA solution served as control.

2.2.5.2. IR irradiation experiments

The explants were tape-stripped and treated with thermoresponsive nanogels as described above. Here, the skin punches were incubated for one hour at room temperature in the dark,

followed by an irradiation with an IR lamp to increase the temperature of the skin surface to 41 °C (Efbe-Schott infrared lamp equipped with Philips pulp 150 W, Bad-Blankenburg, Germany). The IR lamp was fixed at a 40 cm distance from from the treated skin biopsies expressing a light intensity dose of 150 kJ/cm^2 measured by power density measuring device (HBM 1, Hydrosun GmbH, Mülheim, Germany). The irradiation persisted for 120 seconds until skin surface reached a maximum temperature of 41 ± 1 °C. Photos were taken before and after irradiation using a thermal IR camera (FLIR E4 camera, FLIR Systems GmbH, Frankfurt, Germany). After the irradiation, the skin punches were incubated for another 60 min with the nanogels. Control experiments of skin biopsies treated with nanogels at room temperature for 2 hours in the dark served for control.

2.2.6. Cryosectioning and microscopy imaging of skin punches

At the end of each experiment, skin punches were cleaned and subsequently embedded in freezing medium (Leica Biosystems, Nussloch, Germany). After 24 h at 80 °C, the tissues were cut at 6 µm thickness using a CM1510 S Cryotome (Leica Biosystems, Nussloch Germany). The mounted cryosections on the poly-l-lysine coated slides were then fixed with 4% paraformaldehyde (Roti® Histofix 4%, Carl Roth GmbH, Karlsruhe, Germany), rinsed with phosphate-buffered saline (PBS, pH 7.4) and stained with DAPI mounting solution (Roti®-Mount FluorCare DAPI, Carl Roth GmbH, Karlsruhe, Germany). Slides were then sealed with a cover slip and stored in the dark at 4 °C until. Cryosections were then subjected to fluorescence microscopy (BZ-8000, zoom 20×, Plan-Apo, DIC N2, Keyence, Neu-Isenburg, Germany, equipped with objective 20×/0.75, Nikon, Japan). Mean fluorescence intensity (MFI) of FITC-labeled BSA by its distribution area within epidermal layers was quantified using Image-J for at least three skin sections per sample. Experiments and subsequent analysis were repeated using skin from three different donors.

Analytical Methods

NMR spectra were recorded on a Jeol ECX 400 spectrometer operating at 400 MHz, Joel Eclipse spectrometer (500 MHz) and Bruker AVANCE III 700 (700MHz). Data was recorded in ppm and referenced to the mentioned solvents. For kinetic analysis of the polymerization, for each time step the integral of PNIPAM respectively PNIPMAM signal was set to 9 respectively 11 protons and ratio between integral of dPG signal and PNIP(M)AM signal was calculated.

The nanogels particle sizes, dispersity, VPTT, and ζ-Potential were measured at various temperatures by dynamic light scattering (DLS) using Malvern Zetasizer Nano-ZS 90 (Malvern Instruments) equipped with a red He-Ne laser (λ = 633 nm, 4.0 mW) or a green DPSS laser (λ = 532 nm, 50.0 mW) under a scattering angle of 173º. All samples were maintained for

stabilization at the desired temperature for 2-5 min before testing. Particle sizes and size distributions (PDI) are given as the average of 3 measurements from the intensity distribution curves. For determination of the VPTT, the sizes of the nanogels measured in a temperature range of 25 – 55 °C (step size 0.5 °C) was plotted against the temperature. The VPTT is defined as the temperature at the inflection point of the normalized size curve.

Swelling degree of the nanogels is defined by the ratio between particle volume in swollen state (25 °C) and collapsed state (55 °C).

FT-IR measurements were performed as a film on diamond on a *Nicolet Avatar 320 FT-IR* operating from 4000 - 400 cm^{-1}.

UV-VIS absorbance was measured in 96-well plates using a Tecan Infinite M200Pro microplate reader.

Transmission electron microscopy (TEM) samples were prepared on carbon-coated copper grids (300 mesh, Quantifoil). The nanogels were stained with uranyl acetate and visualized using the TEM mode of the Hitachi Scanning Electron Microscope (SU8030) (20 kV).

Circhular dichroism (CD) measurements for protein secondary structure determination were performed with a *Jasco J-810* spectropolarimeter. Protein solutions in the presence of nanogels are background corrected by corresponding nanogel solution. Temperature dependent measurements were conducted raising the temperature 1 °C/min.

3. Results and Discussion

3.1. Effects of the macromolecular cross-linker on nanogel structure and reaction kinetic analysis

In order to obtain thermoresponsive nanogels suitable for a broad band of applications like topical protein delivery as well as for systemic administration, we aimed to tune their VPTT in a range between 32-45 °C. Thus, we were interested in use of PNIPMAM beside PNIPAM as thermoresponsive polymer for the formation of nanogels. In a first approach, we aimed to synthesize thermoresponsive nanogels using our previously reported methodology[15] of the two homopolymers crosslinked with dPG as macromolecular crosslinker. Interestingly, we found that the initiator system APS/TEMED is working for PNIPAM based nanogels but yielding polydisperse aggregates for PNIPMAM. A screening of different initiator systems revealed that particles with low polydispersity for PNIPMAM could only be obtained using KPS or APS without TEMED (Table S1). We assumed that the reason for this might be evoked by different polymerization kinetics including different kinetics of the initiation as well as different polymerization rates of the used monomers. Therefore, we performed kinetic analysis of the

polymerization following size development and swelling ability of the particles via DLS, consumption of monomers by ^{1}H-NMR and reaction conversion by weight.

The comparison of different initiator systems for the nanogel synthesis revealed that initiation by KPS and APS is very similar, showing almost same increase in nanogels size in the beginning of the polymerization (Fig. 2). For both polymers, nanogels obtained by polymerization with KPS appear to be slightly smaller than their APS initiated analogues. In addition, for PNIPAM-dPG nanogels, additive TEMED accelerates the reaction and final particles size are reached quicker (Fig. 2). We found that the more TEMED is used, leading to faster initiation, the smaller the size of the final nanogels (Table S1). This is in good agreement with reported kinetics for acrylamides by Qiu et al., who demonstrated that TEMED accelerates the reaction and leads to fast conversion but at the same time yields linear polymer chains with lower molecular weight.[43] As the nanogels are a three-dimensional cross-linked network of polymer chains, the TEMED induced decrease in the polymeric chain length between the dPG-crosslinker appears in smaller nanogel sizes. However, for PNIPMAM-dPG, we observe the formation of polydisperse particles in the presence of TEMED regardless of the initiator used. Only using solely KPS or APS as initiator yielded nanogels with low polydispersity for both, PNIPAM and PNIPMAM. These results denote that the reaction rates between initiator and monomers have to be balanced out in order to induce a nanogel formation. Therefore, we performed kinetic studies of the monomer consumption via ^{1}H-NMR of NIPAM respectively NIPMAM and dPG during the polymerization. In good agreement with polymerization kinetics reported in the literature,[44, 45] we found that NIPAM reacts faster than NIPMAM with full conversion after 30 min (NIPAM) or 60 min (NIPMAM), respectively (Fig. 3A). For both systems, the consumption of dPG is faster than the formation of the temperature-responsive polymers yielding a high ratio of dPG to polymer in the beginning of the polymerization (Fig. 3B). This is much more pronounced for the slower forming PNIPMAM nanogels with convergence to the final ratio of dPG:polymer of 0.3 after 45-60 min (10-15 min for PNIPAM). These results indicate that probably APS/TEMED and KPS/TEMED initiation is so fast that mainly dPG reacts with itself and almost no or only very short PNIPMAM chains are getting crosslinked leading to the formation of linear PNIPMAM aggregates. In contrast, NIPAM reacts faster than NIPMAM and therefore nanogels are obtained with accelerated initiation getting smaller with higher TEMED amount due to shorter chain lengths between the dPG.

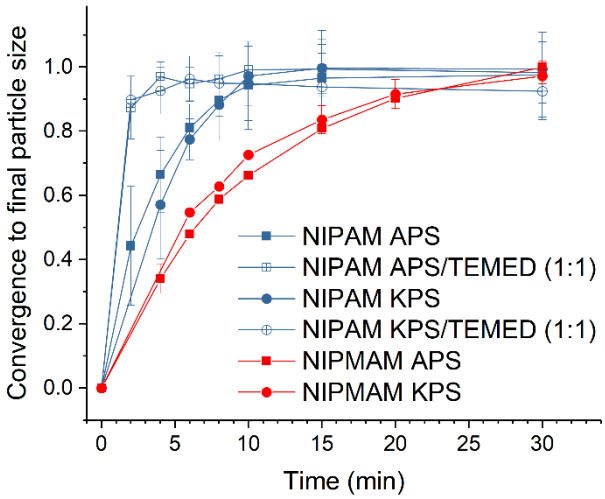

Fig.2. Normalized particles size development during polymerization with different initiator systems for NIPAM and NIPMAM based nanogels.

Another aspect coming to the field upon using dPG as crosslinker is its multi-functionality. In comparison to small molecular bi-functional BIS, each dPG molecule has several crosslinking points depending on the functionalization degree (e.g., 7 % acrylates correspond to 10 crosslinking units per dPG with a M_w of 10 kDa). This multi-functionality could explain our finding that the final size (Fig. 3C) of the nanogels is reached earlier than final weight Fig.3A) indicating that after consumption of the majority of cross-linker, further polymerization takes place mainly at the inside of the growing particles. We assume that once incorporated into the growing precursor particle, several other unreacted cross-linking points of the dPG are locally "trapped", facilitating the connection of remaining free crosslinking points in progress of the polymerization. This assumption is supported by the fact that the swelling ratio during the polymerization process first reaches a maximum contemporaneously with gaining final particle size and then drops to reach final swelling ratio by the time of full conversion (Fig. 3D). This effect is more pronounced for NIPAM based nanogels, probably due to the faster reaction rate.

In order to achieve a triggered release of encapsulated therapeutics from the nanogels gaining control over crosslinking density is crucial. Therefore, we screened the effect of the crosslinker on nanogels size and swelling ability. Due to its multi-functionality, dPG allows to tune the potential crosslinking degree in two ways: first, by varying the cross-linker feed and second, different functionalization degrees per macro-crosslinker. It is reported that using small, low molecular weight BIS, nanogel sizes increase with higher crosslinker feeds.[44, 47] In contrast, we observe for both, PNIPAM and PNIPMAM nanogels, a decrease in size with higher dPG feed (Fig. 4A,B). At the same time, the swelling ability decreases (Fig.4C) with higher dPG feeds showing an increase of rigidity indicating that the overall cross-linking density is increased with more cross-linker present. In addition, as discussed above, due to the

hydrophilicity of dPG we expect dPG to stabilize the nanogels during polymerization leading to smaller final particle sizes the higher the dPG content, similar to results reported for higher surfactant concentrations.[15, 45, 48] Caused by the slower reaction kinetics of NIPMAM, the size of PNIPMAM-dPG nanogels is for all dPG feeding ratios about 80-100 nm smaller than their PNIPAM-dPG analogues and show lower swelling abilities.

Remarkably, the impact of the functionalization degree of the dPG seems to be less prominent than the feeding ratio of crosslinking molecules. Nevertheless, both nanogel systems showed sensitivity against the acrylation degree with only a small window of functionalization percentage yielding in particles with a narrow polydispersity. Already for acrylation degrees larger than 13% (PNIPAM) or 10% (PNIPMAM) we obtained large aggregates probably due to the formation of crosslinks between single nanogel particles and decrease of the hydrophilicity of dPG. Interestingly, both nanogels show a minimum in their hydrodynamic radii for acrylation degrees in the range of 7% to 9% independent from the dPG feed (Fig 4A,B). Nevertheless, comparing swelling abilities of nanogels with same dPG feed but different acrylation percentages no major influence of the functionalization degree is observed (Fig. 4C). These results imply that within the suitable window of functionalization degree we found for nanogel formation, the additional cross-links due to higher functionalization do not significantly influence the rigidity of the network and main parameter to control the nanogels crosslinking density is the PG feed.

For a triggered release of bioactives from the nanogels, we aim for nanogels showing significant shrinkage upon temperature trigger but on same time dense enough to prevent premature cargo diffusion out of the network. In addition, for better comparability hydrodynamic radii of the nanogels should be as similar as possible. Therefore, we decided to continue to evaluate the features as a drug delivery system with the nanogels showing an intermediate swelling ratio of around 10 which we obtained from dPG with 7 % acrylation and a 30%-feed of the crosslinker.

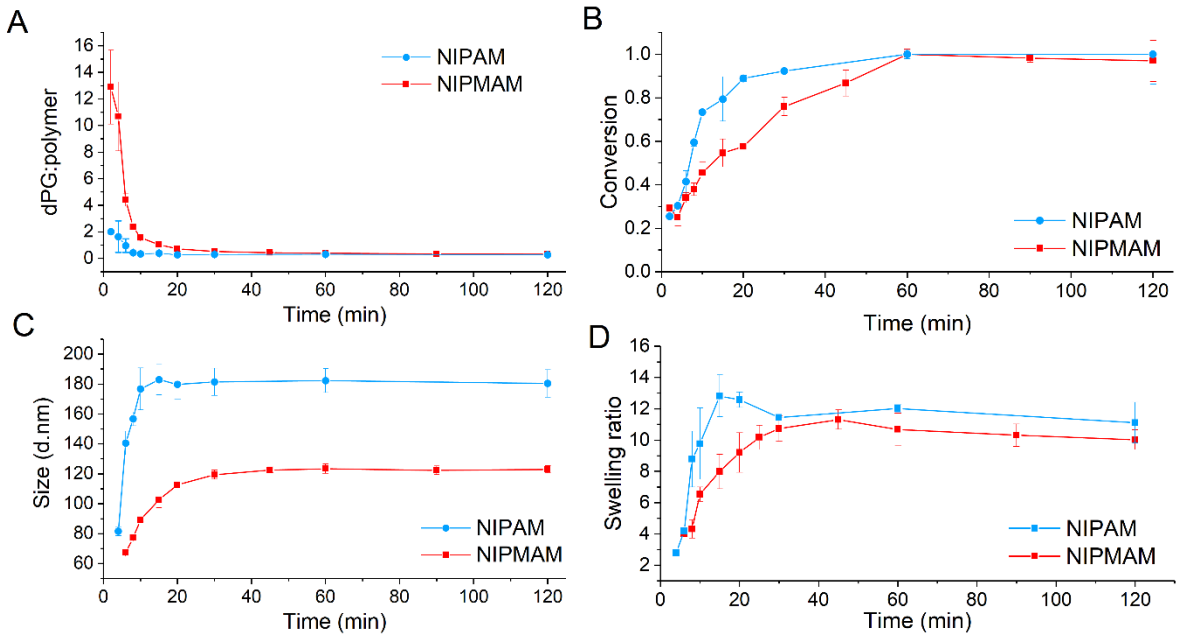

Fig. 3. (A) Consumption of NIPAM or NIPMAM and dPG during polymerization visualized by the ratio between dPG to PNIPAM or PNIPMAM obtained from ^{1}H-NMR analysis. (B) Time dependent conversion of the polymerization from NIPAM or NIPMAM with dPG by weight. (C) Hydrodynamic diameter of the nanogel particles dependent on reaction time. (D) Time evolution of the swelling ratio of the nanogels (defined as ratio between particle volumes in swollen (25°C) and collapsed state (55°C).

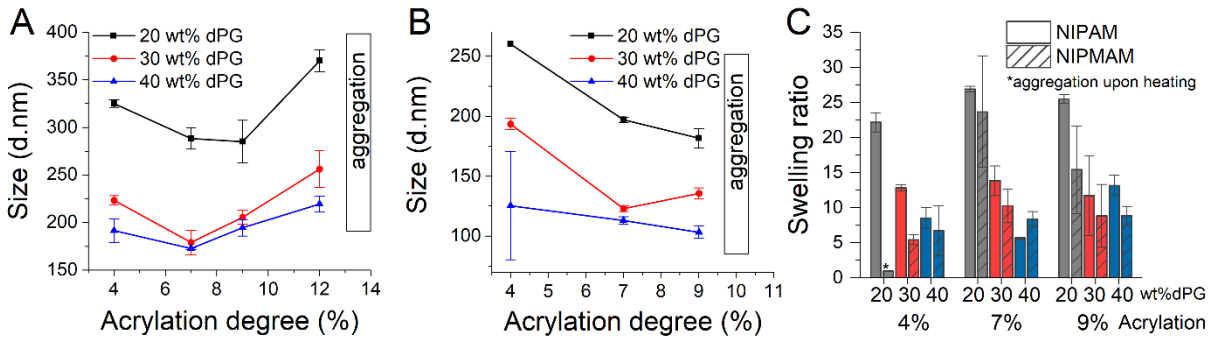

Fig. 4. The correlation of the hydrodynamic diameter of (A) PNIPAM-dPG and (B) PNIPMAM-dPG nanogels with dPG-Ac feed and acrylation degree. (C) Swelling ratio of the nanogels dependent on dPG feed in wt% and acrylation degree (% Ac).

3.2. Tuning the VPTT

Djopké and Vogt reported the phase transition behaviour of linear copolymers from NIPAM and NIPMAM showing a linear dependence of the transition temperature with the ratio between different monomer feeds.[40] These results motivated us to synthesize a range of copolymeric nanogels in order to find the conditions to fine tune the VPTT and find a suitable candidate for drug delivery in systemic applications. In fact, we obtain nanogels with VPTTs between 32 °C and 47 °C depending on the ratio between NIPAM and NIPMAM (Fig. 5A). The size of the

obtained nanogels correlate linearly to weight ratio between the two monomers. In addition, temperature dependent size measurements show a relatively sharp transition for all nanogels (Fig. 5B). Successful incorporation of both monomers was proven by ^{1}H-NMR even though a quantitative evaluation of the ratio between the monomers was not possible due to strong overlap of the signals (Fig. S1). TEM images (Fig. 5C) revealed that all nanogels show spherical shape with low polydispersity and a size around 70-100 nm, which is similar to the diameter obtained from DLS for nanogels in the shrunken state. Interestingly, in comparison to BIS cross-linked particles (Fig. S3), using dPG as cross-linker, in the TEM images the nanogel shape appears a bit “knobbly”, which may be attributed to the spherical shape of the dPG itself. As discussed above, we aimed to synthesize nanogels with higher VPTT without affecting other physico-chemical properties too much, in particular without affecting the surface charge of the nanogels. Therefore, measurements of the ζ-potential were performed with all nanogels. Indeed, we find neutral ζ-potentials for both homopolymeric as well as for all copolymeric nanogels below and above their transition temperature. Stability of the nanogels was evaluated using size measurements DLS showing no alterations in the hydrodynamic radii of all nanogels after redissolving and over a period of 2 months (Fig. S4).

For systemic applications with for example intravenous administration of the nanogels, a VPTT slightly higher than 37 °C body temperature is desirable. The (1:1)-copolymeric nanogel is therefore a suitable candidate, as it has a VPTT of 40 °C. At 37 °C it is still in a highly hydrophilic swollen state, but already from temperatures of 41 °C it is almost completely collapsed (Fig. 5B). In addition, knowing the good performance of PNIPAM-dPG as dermal delivery system and expecting the collapse of the nanogels crucial for this, the copolymeric nanogels are interesting candidates to evaluate the efficiency of an externally triggered topical delivery system.

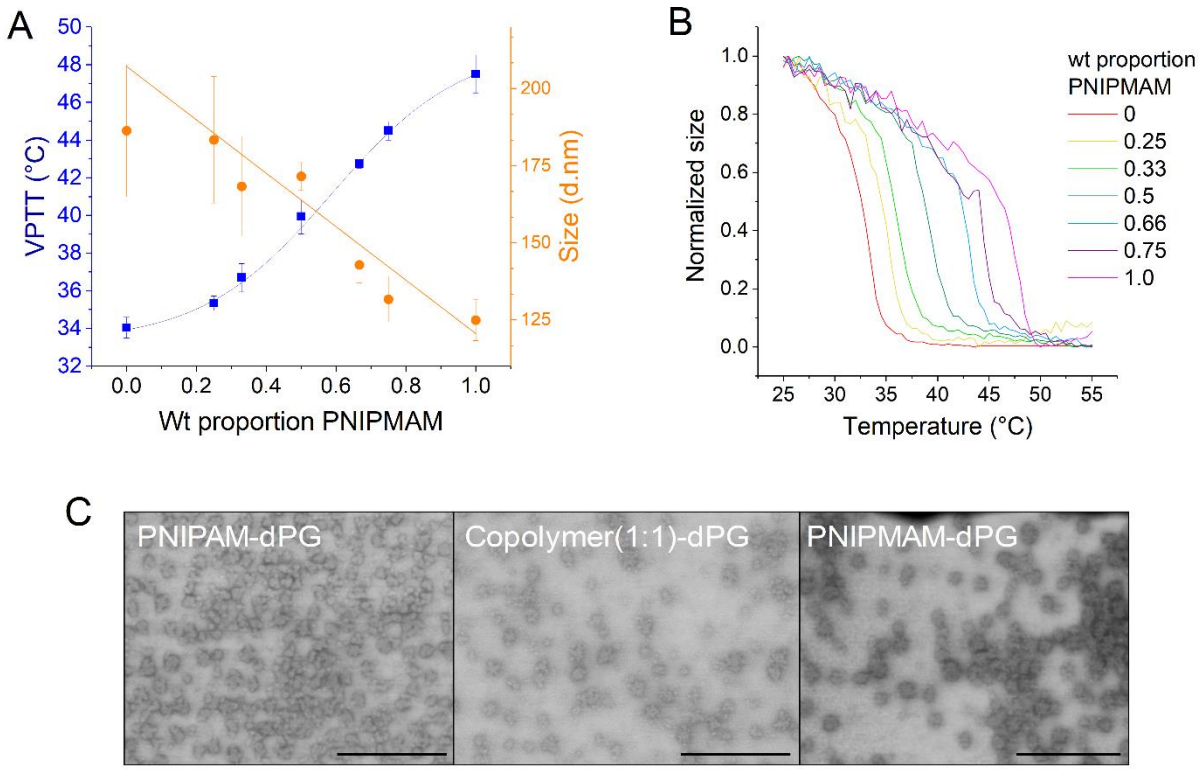

Fig. 5. (A) VPTT and hydrodynamic diameter for PNIPAM-co-PNIPMAM-dPG nanogels dependent on wt. proportion of PNIPMAM in monomer feed and (B) temperature dependent shrinkage of these nanogels. (C) TEM images for PNIPAM-dPG, PNIPAM-co-PNIPMAM (1:1)-dPG and PNIPMAM NGs. Scale bar = 500 nm.

3.3. Encapsulation and temperature triggered release of BSA-FITC

In order to evaluate the ability of the thermoresponsive nanogels to deliver therapeutic active agents in a controlled fashion, bovine serum albumin labelled with FITC (BSA-FITC) was loaded to the nanogels and its release profile dependent on a temperature stimulus was studied. Therefore, the nanogels were swollen in a solution of BSA-FITC to encapsulate the BSA into the nanogels. Three different ratios between nanogels and protein were tested. For the lowest ratio (10:1 nanogel:protein) loading efficiency was ≥ 86% BSA loaded to the nanogels. For PNIPAM-dPG and Co-(1:1)-dPG these high loading efficiencies were also observed with higher ratios of protein:nanogels (Fig. 6). Only for PNIPMAM-dPG nanogels there was a significant drop in the encapsulation efficiency from 80% (10:1 nanogel:BSA) to 50% with a 1:1 NG:BSA feeding ratio. In order to see if the different nanogel size is a reason for this efficiency loss, we performed encapsulation studies with surfactant free synthesized PNIPMAM nanogels which have a similar size to the PNIPAM and copolymeric ones with an average diameter of around 185 nm. Indeed, we observed a higher loading efficiency for these nanogels compared to the ones synthesized in presence of SDS (Fig. 6). Nevertheless, the encapsulation efficiency was reduced with higher PNIPMAM content of the nanogels.

These results emphasize the importance of the nanogels size for protein loading, but as well indicate that slightly higher hydrophobicity or sterical demand of PNIPMAM counteracts protein encapsulation. However, it is worth noticing that for all tested nanogels, protein encapsulation is outstandingly high.

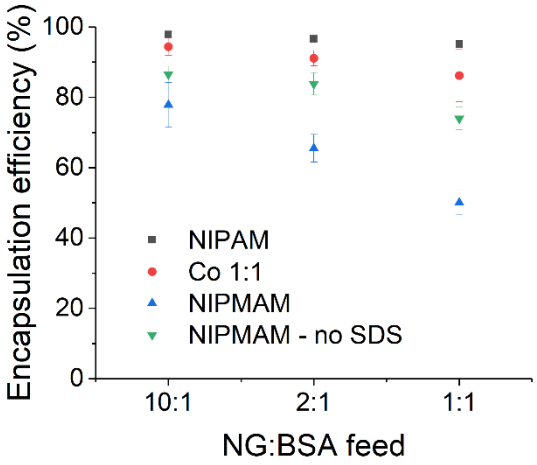

Fig. 6. Encapsulation efficiency of BSA-FITC into different thermo-responsive nanogels determined by UV-VIS spectroscopy.

To evaluate protein stability upon encapsulation and release, circular dichroism (CD) of encapsulated BSA was measured. As depicted in Fig. 7A, no significant spectra changes were observed for all nanogels indicating that the encapsulation process did not affect the secondary structure of the protein. As the nanogels are designed for the purpose of a temperature triggered release of their encapsulated cargo, stability of the used model protein BSA at different temperatures was analysed with and without nanogels present (Fig. 7B,C). As reported previously, we found that BSA is stable until temperatures of around 50 °C and starts to unfold at higher temperatures.[49-51] Apparently, presence of the nanogels do not alter this behaviour. These results indicate that in principle all three nanogels are feasible for the temperature-triggered release of BSA, as their VPTT is below the temperature at which the protein starts to unfold.

The release of BSA-FITC from all nanogels was studied at three different temperatures. For PNIPAM-dPG and Co(1:1)-dPG NGs a temperature triggered release could be observed showing a burst release of the encapsulated protein when the temperature is raised above the VPTT of the nanogels (Fig. 8). For NIPAM based nanogels, a significant increase of released BSA from 21% (29 °C) to 90-96% (37 °C or 42 °C) after 72 h could be observed. Similar results were obtained for the copolymer of NIPAM and NIPMAM where the release was accelerated to 72% after 72 h above its VPTT of 40 °C, whereas at 29 °C and 37 °C only minor release of less than 20% was determined. As a control for the temperature dependent release

mechanism, PNIPMAM-dPG nanogels were analysed as well, here all three tested temperatures were below the VPTT of the nanogels and we only expect minor release of encapsulated BSA. As the encapsulation efficiency was more similar to PNIPAM-dPG and Co(1:1)-dPG, the surfactant free synthesized nanogels was chosen for this study. Indeed, we observed only a minor release up to maximal 36% after 72 h for the NIPMAM-dPG nanogels. These results show that the release mechanism is indeed temperature triggered, in which the shrinkage of the nanogels lead to a burst release of encapsulated protein. We could also observe a contribution of diffusion processes to the overall release profile, as not all protein is released immediately and an accelerated temperature lead to increased release rates.

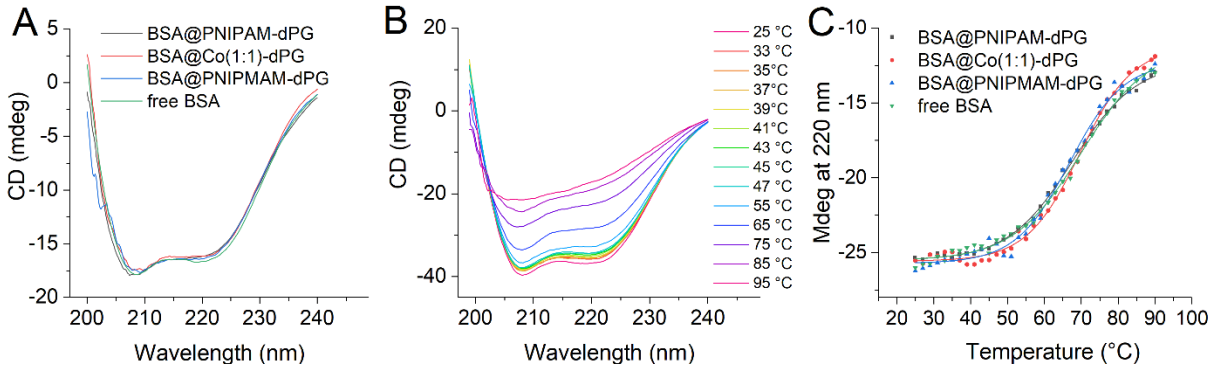

Fig. 7. Structural integrity of BSA during encapsulation and thermally triggered release. (A) CD spectra of encapsulated BSA in all three nanogels at 25 °C, (B) CD spectra of a BSA solution at different temperatures, (C) intensity values from CD spectra of BSA free and encapsulated in the nanogels at 220 nm plotted against the temperature.

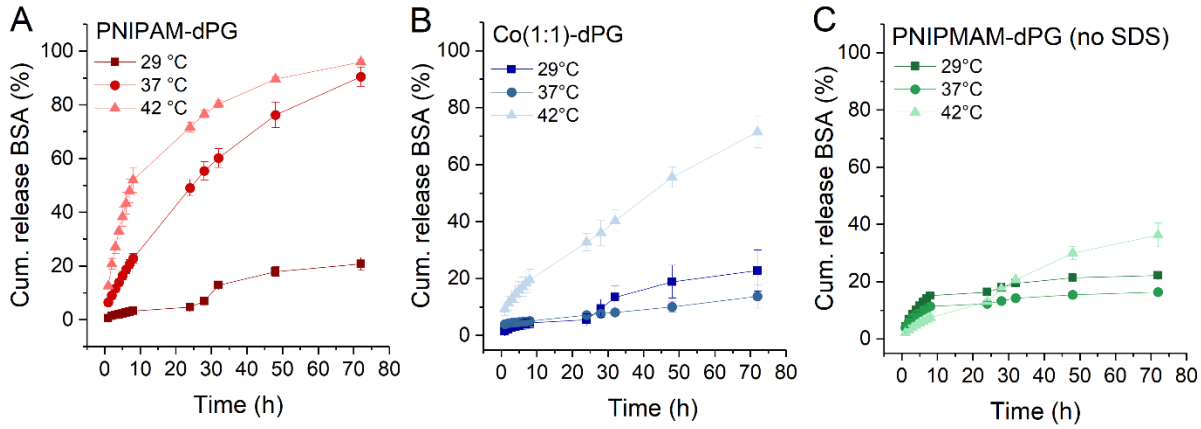

Fig. 8. Release profiles of BSA-FITC from (A) PNIPAM-dPG, (B) Co(1:1)-dPG and (C) PNIPMAM-dPG_no SDS at three different temperatures (29 °C, 37 °C, 42 °C).

3.4. Evaluation of cytocompatibility

Biocompatibility is an important issue for new materials for drug delivery applications. As a first indication thereof, we evaluated the cell compatibility of the bare thermo-responsive on primary

human dermal fibroblasts and HeLa cells using MTT assay. In both cell lines the three nanogels did not affect the cell viability in concentrations up to 0.1 mg/mL (Fig. 9). Increasing polymer concentration to 1.0 mg/mL resulted in reduced cell viabilities of 60% on HeLa cells and 50% in fibroblasts after 48 h incubation.

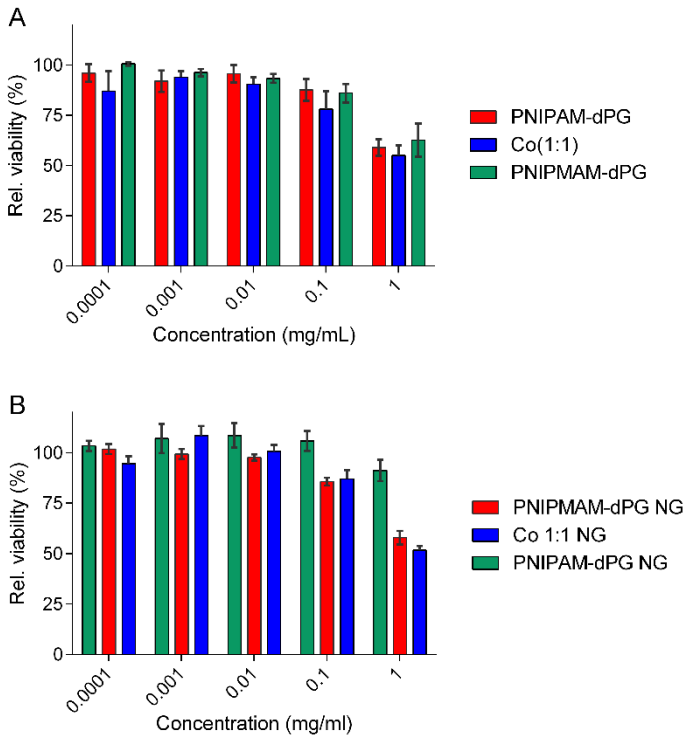

Fig. 9. Effect of bare thermoresponsive nanogels on cell viability analyzed by MTT assay on (A) HeLa cells and (B) fibroblast incubated with different nanogel concentrations of PNIPAM-dPG, Co(1:1)-dPG or PNIPMAM-dPG for 48 h.

In order to assess the suitability of our nanogels particularly designed for the delivery of therapeutic proteins, we have to consider the main factor that determines the concentration of nanogels that would be applied, the required dose of the chosen proteins to be delivered to achieve successful treatment. With over 130 proteins already approved for their clinical use, the variety of possible proteins and application modalities is quite high.[52] Doses for achieving efficient treatment are typically in the lower microgram range, but depend on the application, the selected protein and administration pathway. For the treatment of diseases that impair the skin barrier, the protein Etanercept for example is typically administered by subcutaneous injections.[53-55] Pharmacokinetics studies upon a 25 mg injection show an average maximum concentration of Etanercept in serum of 1.65 µg/mL.[56] Recent results from our group demonstrated efficient transdermal delivery of Etanercept from hydrophilic nanogels and anti-inflammatory activity with 35 µg/cm2 topically applied.[27] Another example for a therapeutic protein delivery in dermal applications is the protein Transglutaminase 1. It is reported to

achieve successful mitigation on deficient skin barrier functions by supplementing the lacking proteins caused by genetic congenital ichthyosis disease.[29, 57] Here, protein concentrations of 5-10 µg/cm^{-2} delivered to the skin with the help of hydrophilic nanogels sufficiently improved the skin barrier function. Taking the high encapsulation efficiencies of more than 80 % into account, here the tested concentrations of the nanogels, which showed cytotoxic effects are 100-1000-fold higher than what is expected to be required for potential applications.

3.5. Temperature dependent protein delivery to the skin

Recent results of our group demonstrate the good performance of nanogels with a VPTT of around 32–34 °C as dermal drug delivery system using the natural temperature gradient in human skin [27, 29] In addition, the results indicate a correlation between collapse of nanogel and dermal penetration enhancement of encapsulated cargos. With the copolymeric nanogels, we now have the opportunity to evaluate temperature-dependent dermal delivery using an external trigger and compare the delivery profile to nanogels using the internal trigger caused by the temperature gradient in human skin. Therefore, we evaluated the temperature dependent release from NIPAM-dPG and Co-(1:1)-dPG nanogels on ex vivo skin. In order to see the temperature dependency of the release and the effect of the external trigger, we used two different setups: first, a temperature ramp from 32 to 37 °C modelling the natural temperature gradient on skin and second, increasing the temperature for a maximum of 2 min up to 41 °C by irradiation with an IR lamp. As a control, we also tested the delivery of BSA-FITC from PNIPMAM-dPG nanogels, which show a high VPTT and do not collapse under both conditions.

In the temperature gradient setup, only NIPAM based nanogels show significant enhancement of the BSA penetration into viable skin layers (Fig. 10A,B). Topical application of BSA solution as well as BSA encapsulated in Co(1:1)-dPG and PNIPMAM-dPG nanogels resulted in no significant BSA penetration into the viable epidermis (VE) (Fig.10 B). These findings can be related to the fact that PNIPAM-dPG nanogels show a VPTT of 34 °C and are therefore the only nanogels in the tested setup, which VPTT is crossed. This shows that the release mechanism found in the *in vitro* studies could be successfully transferred to the intended application on skin. In a second setup, we used a medical IR lamp to increase the temperature to maximally 41 °C for a short time period of max-120 s. As anticipated, a significantly increased intradermal delivery of BSA to the VE was observed for both nanogels of which we cross the VPTT, PNIPAM-dPG and Co(1:1)-dPG, with PNIPAM-dPG showing superior penetration enhancement (Fig. 10C,D). This is concordance with the *in vitro* release study, in which we observed a steeper release profile at 42 °C for PNIPAM-dPG than for the copolymeric nanogels (Fig. 8). This could be attributed to the fact that, at temperature of 41 °C the copolymeric nanogels are still not completely collapsed (85% of total size change),

whereas the transition of PNIPAM based nanogels is occurring already earlier. PNIPMAM-dPG nanogels at 41 °C are still in a swollen state and therefore do not release their loaded BSA into the VE resulting in MFI values non-significantly different to the free BSA control. Anyhow, application of the IR-irradiation results for all nanogels to an enhanced MFI in the SC in comparison to the free BSA solution as well as to the non-irradiated controls (Fig. 10D). These results might indicate an increased penetration of the nanogels themselves upon IR irradiation similar to our findings for other thermo-responsive nanogels.[26]

Interestingly, the comparison between MFI values from the temperature gradient setup and the external triggered release reveals that for the PNIPAM-dPG nanogels the penetration to the VE is slightly higher using the IR lamp regardless of the relatively short exposure period. Furthermore, MFI of BSA delivered upon IR irradiation by copolymeric nanogels reaches similar values like achieved with PNIPAM-dPG in the temperature gradient setup. These results highlight the effectiveness of an external trigger showing similar or even pronounced penetration enhancement despite only a single and relatively short exposure time. In addition, with the copolymeric nanogels an effective delivery system was generated that, besides the triggered delivery, allows for a local control of the release through a defined area of irradiation.

Bringing the results from the two different setups together, we can conclude that the release of the BSA from the nanogels is following a temperature trigger, which is in concordance with *in vitro* data showing shrinkage/expulsion of water of the nanogels above their VPTT and temperature dependent release profiles. In addition, the comparison of external and internal trigger revealed that with the external trigger a similar or even increased penetration enhancement can be achieved. In addition, with a system showing a higher VPTT than 37 °C like the copolymeric nanogel, the delivery of encapsulated cargos can be local and temporal controlled through application of the external trigger.

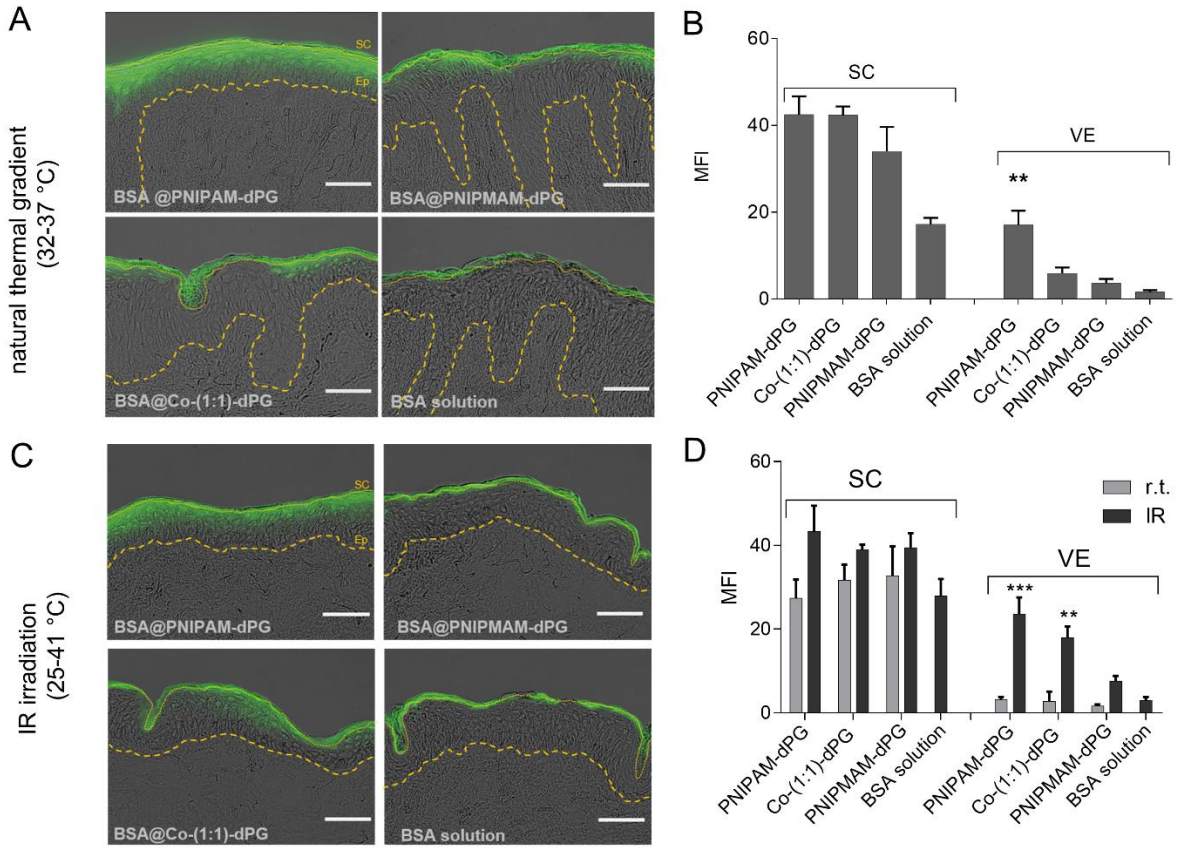

Fig. 2. Intradermal delivery of BSA using the temperature gradient approach or IR-irradiation following topical application of PNIPAM-dPG, Co(1:1)-dPG and PNIPMAM-dPG. (A) Representative fluorescence images of skin explants following topical application of BSA-loaded nanogels for 6 h and by applying a temperature ramp from 32-37 °C. Images show fluorescence of the FITC-labeled BSA. Scale bars = 50 µm. (B) Analysis of mean fluorescence intensity (MFI) by area in stratum corneum (SC) and viable epidermis (VE) of skin punches from temperature gradient setup. N=3. Mean values were normalized to the untreated control (PBS, PH=7.4). (C) Representative fluorescence microscopy images of skin explants topically treated with BSA-loaded nanogels after 1 h incubation at r.t in the dark, followed by IR-irradiation for 120 s and another hour incubation at r.t. Images show fluorescence intensity of the FITC-labeled BSA. Scale bars = 50 µm. (D) Mean fluorescence analysis of SC and VE of skin punches treated with FITC-BSA loaded nanogels following irradiation with an IR lamp for 120 seconds. N=3. Mean values were normalized to the untreated control (PBS, PH=7.4). Statistical significance for figures (B) and (D) was determined by one-way analysis of variance deploying Bonferroni's post-test to compare the differences between all values in VE and SC separately, with *P≤0.05 as significant, **P≤0,01 as very significant, and ***P≤0,001 as highly significant. All depicted values are mean ± standard error of the mean (SEM).

4. Conclusion

Herein, we presented the elucidation of the critical synthetic parameters that lead to control over the desired features of thermo-responsive tunable nanogels using PNIPAM and PNIPMAM as temperature responsive polymers cross-linked with macromolecular acrylated

dPG. The influence of the monomers and hydrophilic and macromolecular nature of the cross-linker on nanogels formation and architecture was analysed, showing that dPG is able to stabilize the growing particles during the polymerization and thereby has, together with the reaction rates, a strong impact on the final particle size. In addition, we could observe a “trapping” effect of crosslinking points due to the multi-functionality of dPG visualized by the swelling ability of the forming nanogels. By co-polymerization of NIPAM and NIPMAM we obtained nanogels with tunable VPTTs in the range of 34-47 °C. All nanogels show high encapsulation efficiencies for the model protein BSA rendering them promising candidates to deliver therapeutic active bio-macromolecules. Nanogels with VPTTs below 37 °C are well working dermal delivery systems as they promote the penetration of encapsulated cargos using the natural temperature gradient from the skin. For nanogels with higher VPTTs, we could demonstrate that efficient dermal penetration enhancement can be achieved by application of an external heat source like an IR-lamp offering local and temporal control over the delivery of therapeutic proteins. In addition, with the knowledge of the synthetic parameters that enable precise tuning of the VPTT, thermally responsive nanogels suitable for systemic applications can be generated.

Conflict of interest

There are no conflicts to declare.

Acknowledgements

We gratefully acknowledge financial support from Bundesministerium für Bildung und Forschung (BMBF) through the NanoMatFutur award (13N12561). We thank Dr. Anke Hoppensack and Johanna Scholz for the isolation of dermal fibroblasts. We would also like to acknowledge Dr. Maria Molina for helpful preliminary work and Nicolas Guillaume for practical support. In addition, we gratefully thank the German Academic Exchange Service (DAAD) for providing a PhD scholarship for R. Charbaji through funding program (57129429).

References

1. K. S. Soni, S. S. Desale and T. K. Bronich, *J. Controlled Release*, 2016, **240**, 109-126.
2. A. J. Sivaram, P. Rajitha, S. Maya, R. Jayakumar and M. Sabitha, *WIREs Nanomed Nanobiotechnol*, 2015, **7**, 509-533.
3. A. V. Kabanov and S. V. Vinogradov, *Angew. Chem. Int. Ed. Engl.*, 2009, **48**, 5418-5429.
4. M. Molina, M. Asadian-Birjand, J. Balach, J. Bergueiro, E. Miceli and M. Calderon, *Chem. Soc. Rev.*, 2015, **44**, 6161-6186.

5. W. Wu, N. Mitra, E. C. Yan and S. Zhou, *ACS Nano*, 2010, **4**, 4831-4839.

6. A. Ghimire, O. Zore, V. Thilakarathne, V. Briand, P. Lenehan, Y. Lei, R. Kasi and C. Kumar, *Sensors*, 2015, **15**, 23868-23885.

7. T. Hoare and R. Pelton, *Biomacromolecules*, 2008, **9**, 733-740.

8. A. Soleimani, F. Martinez, V. Economopoulos, P. J. Foster, T. J. Scholl and E. R. Gillies, *J. Mater. Chem. B*, 2013, **1**, 1027-1034.

9. H. Wang, F. Ke, A. Mararenko, Z. Wei, P. Banerjee and S. Zhou, *Nanoscale*, 2014, **6**, 7443-7452.

10. X. Qian, J. Li and S. Nie, *J. Am. Chem. Soc.*, 2009, **131**, 7540-7541.

11. J. C. Cuggino, M. Molina, S. Wedepohl, C. I. A. Igarzabal, M. Calderón and L. M. Gugliotta, *Eur. Polym. J.*, 2016, **78**, 14-24.

12. F. Sultana, Manirujjaman, M. Imran-Ul-Haque, M. Arafat and S. Sharmin, *J. Appl. Pharm. Sci.*, 2013, **3**, 95-105.

13. E. Fleige, M. A. Quadir and R. Haag, *Adv. Drug Delivery Rev.*, 2012, **64**, 866-884.

14. R. H. Pelton and P. Chibante, *Colloids Surf.*, 1986, **20**, 247-256.

15. J. C. Cuggino, C. I. Alvarez I, M. C. Strumia, P. Welker, K. Licha, D. Steinhilber, R.-C. Mutihac and M. Calderon, *Soft Matter*, 2011, **7**, 11259-11266.

16. G. S. Singka, N. A. Samah, M. H. Zulfakar, A. Yurdasiper and C. M. Heard, *European journal of pharmaceutics and biopharmaceutics : official journal of Arbeitsgemeinschaft fur Pharmazeutische Verfahrenstechnik e.V*, 2010, **76**, 275-281.

17. Y. Tian, S. Bian and W. Yang, *Polym. Chem.*, 2016, **7**, 1913-1921.

18. M. Asadian-Birjand, J. Bergueiro, F. Rancan, J. C. Cuggino, R. C. Mutihac, K. Achazi, J. Dernedde, U. Blume-Peytayi, A. Vogt and M. Calderon, *Polym. Chem.*, 2015, **6**, 5827-5831.

19. A. Melle, A. Balaceanu, M. Kather, Y. Wu, E. Gau, W. Sun, X. Huang, X. Shi, M. Karperien and A. Pich, *J. Mater. Chem. B*, 2016, **4**, 5127-5137.

20. K. Madhusudana Rao, B. Mallikarjuna, K. S. V. Krishna Rao, S. Siraj, K. Chowdoji Rao and M. C. S. Subha, *Colloids Surf., B*, 2013, **102**, 891-897.

21. L. Zha, B. Banik and F. Alexis, *Soft Matter*, 2011, **7**, 5908-5916.

22. A. Chanmugam, D. Langemo, K. Thomason, J. Haan, E. A. Altenburger, A. Tippett, L. Henderson and T. A. Zortman, *Advances in Skin & Wound Care*, 2017, **30**, 406-414.

23. M. Kar, L. Fechner, G. Nagel, E. Glitscher, G. Noe Rimondino and M. Calderon, in *Nanogels for Biomedical Applications*, The Royal Society of Chemistry, 2018, DOI: 10.1039/9781788010481-00210, pp. 210-260.

24. F. G. Benedict, W. R. Miles and A. Johnson, *PNAS*, 1919, **5**, 218-222.

25. S. Aizawa and M. Cabanac, *J. Therm. Biol.*, 2000, **25**, 313-316.

26. F. Rancan, M. Giulbudagian, J. Jurisch, U. Blume-Peytavi, M. Calderón and A. Vogt, *Eur. J. Pharm. Biopharm.*, 2017, **116**, 4-11.

27. Y. G. Giulbudagian M, Hönzke S, Edlich A, Geisendörfer B, Kleuser B, Hedtrich S, Calderón M., *Theranostics*, 2018, **8**, 450-463.

28. M. Giulbudagian, S. Honzke, J. Bergueiro, D. Isk, F. Schumacher, S. Saeidpour, S. B. Lohan, M. C. Meinke, C. Teutloff, M. Schafer-Korting, G. Yealland, B. Kleuser, S. Hedtrich and M. Calderon, *Nanoscale*, 2018, **10**, 469-479.

29. M. Witting, M. Molina, K. Obst, R. Plank, K. M. Eckl, H. C. Hennies, M. Calderón, W. Frieß and S. Hedtrich, *Nanomed. Nanotechnol. Biol. Med.*, 2015, **11**, 1179-1187.

30. O. Zavgorodnya, C. A. Carmona-Moran, V. Kozlovskaya, F. Liu, T. M. Wick and E. Kharlampieva, *J. Colloid Interface Sci.*, 2017, **506**, 589-602.

31. S. Abbina, S. Vappala, P. Kumar, E. M. J. Siren, C. C. La, U. Abbasi, D. E. Brooks and J. N. Kizhakkedathu, *J. Mater. Chem. B*, 2017, **5**, 9249-9277.

32. D. Steinhilber, M. Witting, X. Zhang, M. Staegemann, F. Paulus, W. Friess, S. Küchler and R. Haag, *J. Controlled Release*, 2013, **169**, 289-295.

33. J. Khandare, M. Calderon, N. M. Dagia and R. Haag, *Chem. Soc. Rev.*, 2012, **41**, 2824-2848.

34. E. Miceli, B. Kuropka, C. Rosenauer, E. R. O. Blanco, L. E. Theune, M. Kar, C. Weise, S. Morsbach, C. Freund and M. Calderón, *Nanomedicine*, 2018, **13**, 2657-2668.

35. H. Yang, Q. Wang, S. Huang, A. Xiao, F. Li, L. Gan and X. Yang, *ACS Appl Mater Interfaces*, 2016, **8**, 7729-7738.

36. G. N. Rimondino, E. Miceli, M. Molina, S. Wedepohl, S. Thierbach, E. Rühl, M. Strumia, M. Martinelli and M. Calderón, *J. Mater. Chem. B*, 2017, **5**, 866-874.

37. M. Lundqvist, J. Stigler, G. Elia, I. Lynch, T. Cedervall and K. A. Dawson, *PNAS*, 2008, **105**, 14265-14270.

38. J. Lazarovits, Y. Y. Chen, E. A. Sykes and W. C. W. Chan, *Chem. Commun.*, 2015, **51**, 2756-2767.

39. J. Dybal, M. Trchová and P. Schmidt, *Vib. Spectrosc*, 2009, **51**, 44-51.

40. E. Djokpé and W. Vogt, *Macromol. Chem. Phys.*, 2001, **202**, 750-757.

41. S. Fujishige, K. Kubota and I. Ando, *J. Phys. Chem.*, 1989, **93**, 3311-3313.

42. B. Wedel, Y. Hertle, O. Wrede, J. Bookhold and T. Hellweg, *Polymers*, 2016, **8**.

43. X. D. Feng, X. Q. Guo and K. Y. Qiu, *Die Makromolekulare Chemie*, 1988, **189**, 77-83.

44. D. Duracher, A. Elaïssari and C. Pichot, *J. Polym. Sci., Part A: Polym. Chem.*, 1999, **37**, 1823-1837.

45. X. Wu, R. H. Pelton, A. E. Hamielec, D. R. Woods and W. McPhee, *Colloid. Polym. Sci.*, 1994, **272**, 467-477.

46. M. H. Smith, E. S. Herman and L. A. Lyon, *J. Phys. Chem. B*, 2011, **115**, 3761-3764.

47. O. L. J. Virtanen, M. Brugnoni, M. Kather, A. Pich and W. Richtering, *Polym. Chem.*, 2016, **7**, 5123-5131.

48. W. McPhee, K. C. Tam and R. Pelton, *J. Colloid Interface Sci.*, 1993, **156**, 24-30.

49. A. Michnik, K. Michalik and Z. Drzazga, *J. Therm. Anal. Calorim.*, 2005, **80**, 399-406.

50. A. Michnik, *J. Therm. Anal. Calorim.*, 2003, **71**, 509-519.

51. C. Giancola, C. De Sena, D. Fessas, G. Graziano and G. Barone, *Int. J. Biol. Macromol.*, 1997, **20**, 193-204.

52. B. Leader, Q. J. Baca and D. E. Golan, *Nature Reviews Drug Discovery*, 2008, **7**, 21.

53. P. J. Mease, B. S. Goffe, J. Metz, A. VanderStoep, B. Finck and D. J. Burge, *The Lancet*, 2000, **356**, 385-390.

54. L. W. Moreland, M. H. Schiff, S. W. Baumgartner, E. A. Tindall, R. M. Fleischmann, K. J. Bulpitt, A. L. Weaver, E. C. Keystone, D. E. Furst, P. J. Mease, E. M. Ruderman, D. A. Horwitz, D. G. Arkfeld, L. Garrison, D. J. Burge, C. M. Blosch, M. L. M. Lange, N. D. McDonnell and M. E. Weinblatt, *Annals of Internal Medicine*, 1999, **130**, 478-486.

55. P. Geborek, M. Crnkic, I. F. Petersson, T. Saxne and G. South Swedish Arthritis Treatment, *Ann. Rheum. Dis.*, 2002, **61**, 793-798.

56. *Journal*, https://www.pfizermed.de/fileadmin/produktdatenbank/pdf/011927_freigabe.pdf.

57. R. Plank, G. Yealland, E. Miceli, D. Lima Cunha, P. Graff, S. Thomforde, R. Gruber, V. Moosbrugger-Martinz, K. Eckl, M. Calderón, H. C. Hennies and S. Hedtrich, *Journal of Investigative Dermatology*, 2018, DOI: https://doi.org/10.1016/j.jid.2018.11.002.

3.1.2 Supplementary Information

Table S1. Characterization of PNIPAM-dPG and PNIPMAM-dPG nanogels synthesized with varied initiator systems and concentrations and PNIPAM-BIS and PNIPMAM-BIS nanogels.

Nanogel system	initiator system	[init] (µmol) /100mg monomers	[init]/[TEMED]	Size (d.nm) at 25° C	PDI
PNIPAM-dPG	APS	12.2	-	200	0.088
	APS/TEMED	12.2	0.1	191	0.128
	APS/TEMED	12.2	0.5	169	0.125
	APS/TEMED	12.2	1	152	0.201
	KPS	12.2	-	186	0.137
	KPS/TEMED	12.2	0.1	165	0.122
	KPS/TEMED	12.2	0.5	151	0.165
	KPS/TEMED	12.2	1	135	0.195
PNIPMAM-dPG	APS	12.2	-	141	0.183
	APS/TEMED	12.2	0.1-1	polydisp.	>0.5
	KPS	12.2	-	123	0.205
	KPS/TEMED	12.2	0.1-1	polydisp.	>0.5

Table S2. Characterization of surfactant free PNIPAM-dPG and PNIPMAM-dPG nanogels. Given values of sizes are intensity values of DLS measurement. Swelling ratio is determined by ratio between volumes in swollen (25 °C) and shrunken state (55 °C).

Nanogel	Size (d.nm) at 25 °C (PDI)	Size (d.nm) at 50 °C (PDI)	swelling ratio	VPTT
PNIPAM-dPG	348 (0.124)	171 (0.109)	8.4	33 °C
PNIPMAM-dPG	187 (0,223)	88 (0.086)	9.8	45.5 °C

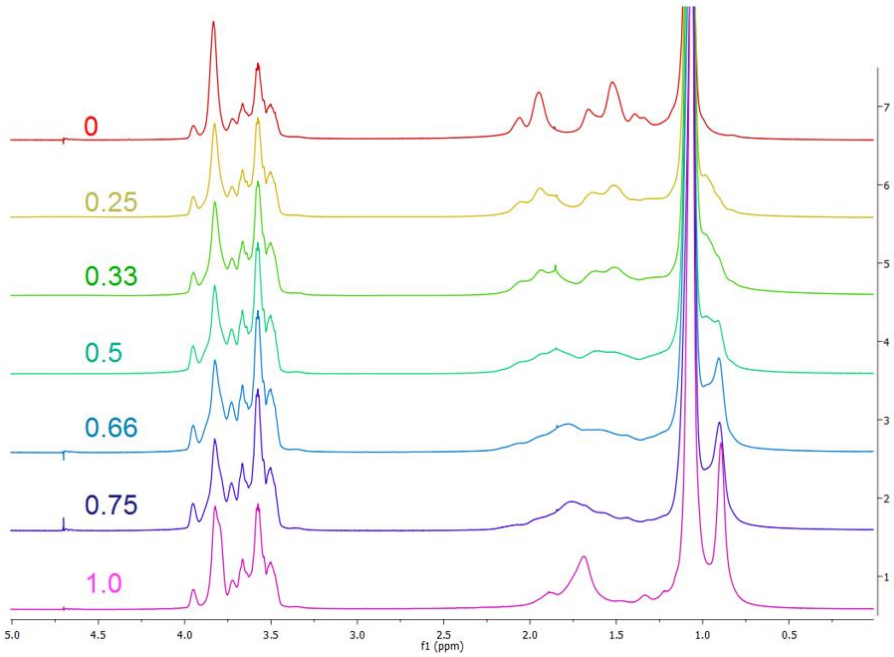

Fig. S1. ^{1}H-NMR spectra of PNIPAM-co-PNIPMAM and both homopolymeric nanogels with increasing ratio of PNIPMAM (top to bottom). Numbers indicate the amount of NIPMAM feed of the total weight.

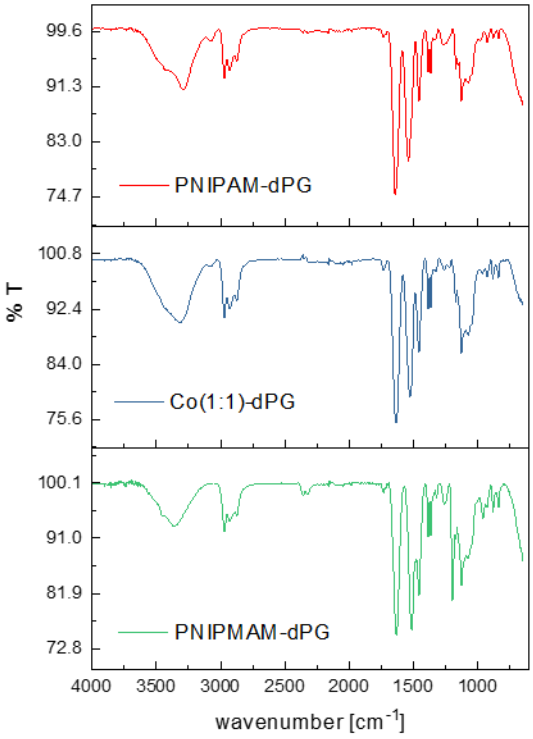

Fig. S2. FTIR spectra of NIPAM, NIPMAM and copolymeric nanogels.

Table S3. Characterization of NIPAM, NIPMAM and copolymeric nanogels: sizes values obtained from DLS measurement (Intensity), Zeta-Potentials and VPTTs (DLS).

Thermoresponsive monomers (wt%)						
NIPAM	**NIPMAM**	**Size (d.nm) at 25 °C (PDI)**	**Size (d.nm) at 50 °C (PDI)**	**ζ at 25 °C**	**ζ at 50 °C**	**VPTT (°C)**
100	0	186 (0.137)	87 (0.093)	-1.13	-3.66	34.1
75	25	183 (0.170)	75 (0.067)	-1.2	-2.74	35.4
67	33	168 (0.153)	72 (0.066)	-1.0	-2.83	36.7
50	50	172 (0.146)	86 (0.088)	-0.54	-2.00	39.9
33	67	143 (0.193)	75 (0.162)	-2.74	-4.42	42.7
25	75	132 (0.209)	81 (0.157)	-2.64	-3.07	44.5
0	100	131 (0.205)	61 (0.058)	-2.23	-2.15	47.5

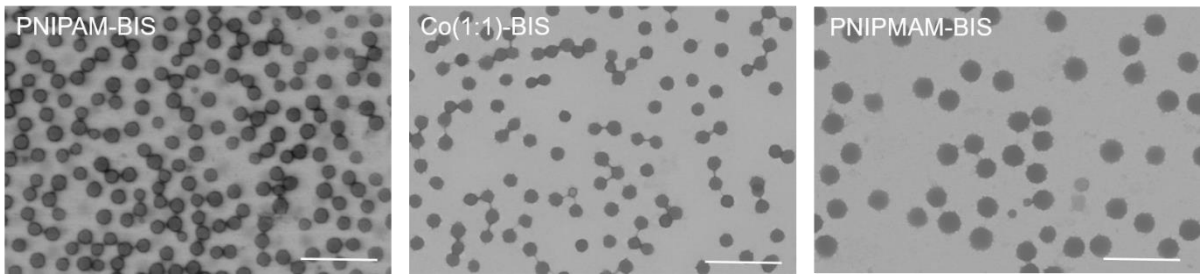

Fig. S1: TEM picture of NIPAM-BIS nanogels. Scale bar = 1 µm.

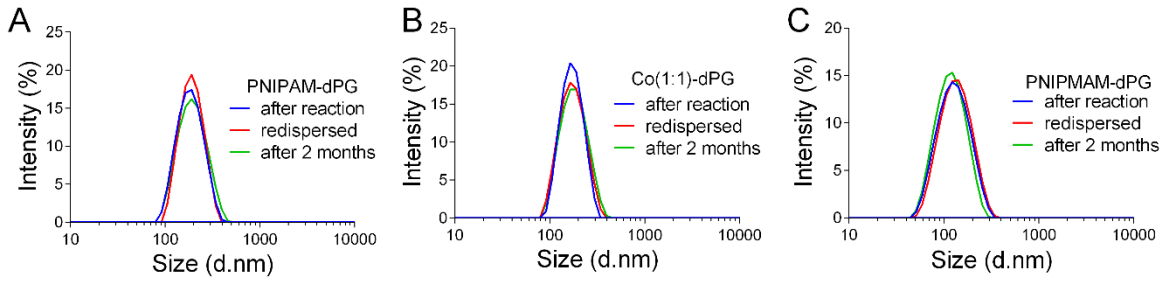

Fig. S2. Stability of nanogels determined by DLS measurements after redispersing and after 2 months.

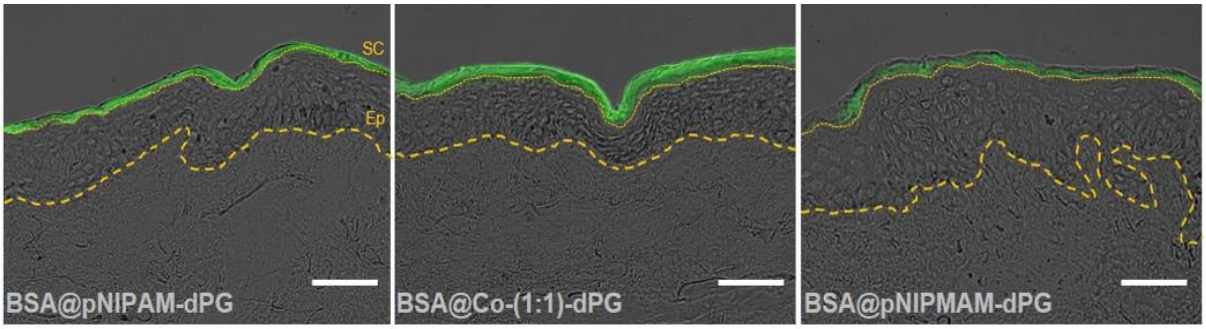

Fig. S5. Control experiment of non-triggered skin penetration of fluorescently labeled BSA delivered by nanogels. Representative fluorescence microscopy images of skin explants topically treated with BSA-loaded nanogels incubated 2h at r.t in the dark. Images show fluorescence intensity of the FITC-labeled BSA. Scale bar = 50 µm.

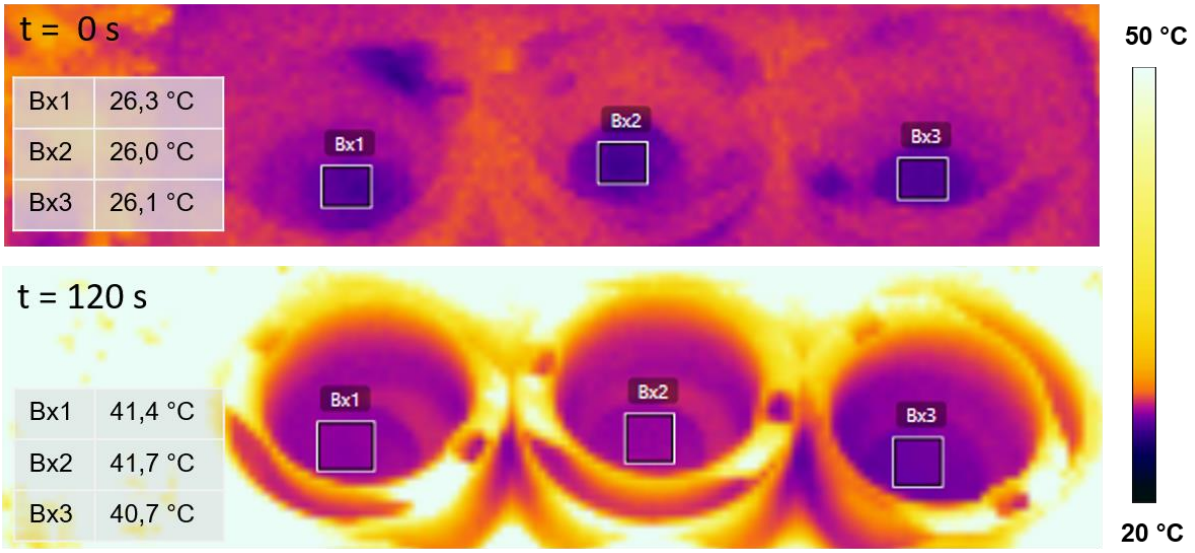

Fig. S6. IR-camera pictures taken from skin punches before (top) and after 120 s (bottom) irradiation with IR lamp and measured maximum temperatures within the shown boxes for skin punches with PNIPAM-dPG (Bx1), Co(1:1)-dPG (Bx2) and PNIPMAM-dPG (Bx3) nanogels applied on top.

3.2. Nanogel-based redox-sensitive protein delivery across the mucous membrane

3.2.1 Publication

The following section has been published as a peer-reviewed research article at the Journal of *Small*, 2021, Vol. 17, No. 23, and appears in this thesis as the accepted peer reviewed version with *John Wiley & Sons* permission.

Online available under the following DOI-link: https://doi.org/10.1002/smll.202007963

Supplementary data are also online available under: smll202007963-sup-0001-SuppMat.pdf

Title & authors

Design and testing of efficient mucus-penetrating nanogels – pitfalls of preclinical testing and lessons learned

Rawan Charbaji, Mrityunjoy Kar, Loryn E. Theune, Julián Bergueiro, Anne Eichhorst, Lucila Navarro, Patrick Graff, Friederike Stumpff, Marcelo Calderón, Sarah Hedtrich

The following contributions were made to this publication:

Personal contribution

Designed, conceived, and performed the biological testing of the nanogels. Isolated native mucus from sacrificed farm pigs and conducted rheological studies, GPC degradation studies. Also obtained freshly excised porcine small intestines and conducted mucopenetration and absorption studies. Performed cytocompatibility studies on different cell lines. Cultivated primary macrophages from monocytes upon isolation from human whole blood for subsequent cytotoxicity and uptake studies. Investigated ETN (etanercept) TNFα-binding capacity after encapsulation onto the nanogels via enzyme-linked immunosorbent assay (ELISA), induced IBD-like inflammation in commercially available human-based small intestines models

(EpiIntestinal-FT, MatTek, USA) and investigated delivery and therapeutic efficiency of encapsulated ETN employing trans-electrical epithelial resistance measurements (TEER), cytokines quantification via enzyme-linked immunosorbent assay (ELISA), western blot protein analysis (WB), immunofluorescence staining (IF) and histological evaluation (H&E, Alcian blue), wrote and prepared the manuscript under supervision of Prof. Dr. Sarah Hedtrich.

Co-author´s contribution

Mrityunjoy Kar designed the disulfide-containing nanogels and characterized them together with Loryn E. Theune (H-NMR, FT-IR, Raman, DLS) under supervision of Prof. Dr. Marcelo Calderón. Loryn E. Theune additionally synthesized the tested disulfide-containing and control nanogels, encapsulated ETN, conducted circular dichroism measurements, and reported the respective parts into the manuscript. Julián Bergueiro supported in the GPC study. Anne Eichhorst cultivated the human bronchial epithelium *in-vitro* models and performed mucopenetration and ETN delivery studies on them. Lucila Navarro & Patrick Graff performed ETN release study from the nanogels, nanogels' zeta-potential measurements, and TEM analysis of the nanogels w/ & w/o GSH. All done under supervision of Prof. Dr. Marcelo Calderón & Prof. Dr. Sarah Hedtrich. Co-authors contributed to the study design, evaluation of the experiments, and manuscript revision.

Graphical abstract (as table of content figure)

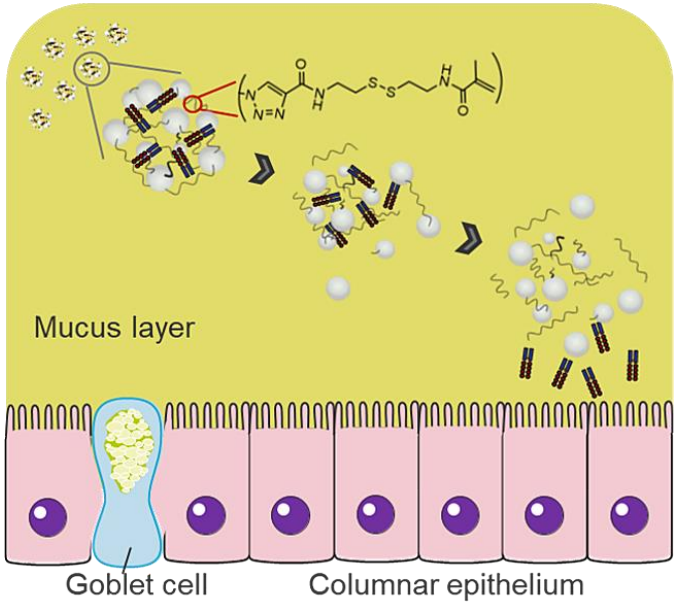

Abstract

Mucosal surfaces pose a challenging environment for efficient drug delivery. Various delivery strategies such as nanoparticles have been employed so far; yet, still yielding limited success. To address the need of efficient transmucosal drug delivery, we report on the synthesis of novel disulfide-containing dendritic polyglycerol (dPG)-based nanogels and their preclinical testing. A bifunctional disulfide-containing linker was coupled to dPG to act as a macromolecular cross-linker for poly-N-isopropylacrylamide (PNIPAM) and poly-N-isopropylmethacrylamide (PNIPMAM), in a precipitation polymerization process. A systematic analysis of the polymerization revealed the importance of a careful polymer choice to yield mucus-degradable nanogels with diameters between 100-200 nm, low polydispersity and intact disulfide-linkers.

Absorption studies in porcine intestinal tissue and human bronchial epithelial models demonstrated that disulfide-containing nanogels are highly efficient in overcoming mucosal barriers. The nanogels efficiently degraded and delivered the anti-inflammatory biomacromolecule etanercept into epithelial tissues yielding local anti-inflammatory effects. Over the course of this work, several problems were encountered due to a limited availability of valid test systems for mucosal drug-delivery systems. Hence, this study also emphasizes how critical a combined and multifaceted approach is for the preclinical testing of mucosal drug-delivery systems, discusses potential pitfalls and provides suggestions for solutions.

Keywords: Mucosal drug delivery, mucopenetrating, local drug delivery, polyglycerol-based nanogels, inflammation

1. Introduction

Mucosal surfaces of human epithelia, like those in the lung or gastrointestinal (GI) tract, pose a challenging first line of defence for therapeutics.[1] Successful transmucosal delivery, however, offers great therapeutic opportunities for the treatment of various diseases including chronic conditions like inflammatory bowel disease (IBD) or diseases of the respiratory tract. Mucus is a tenacious hydrogel (97% water) comprising a porous network of cross-linked, entangled, glycosylated mucin polymers (mucins) filled with sloughed cells, bacteria, proteins and cellular debris. Through their cysteine moieties, mucins are cross-linked in a complex network by disulfide bridges that form the mucus backbone.[2] The basic structure of mucus is similar in all mucosal surfaces despite distinct local differences.

Nanoparticles (NP) that aim to overcome the mucosal barrier must tackle the complex nature of the mucus gel to reach the underlying epithelium.[3] Features of the mucosal barrier that must be addressed include: its dynamic motion due to continuous secretion and shedding; steric obstruction, owing to the size filtration properties of the mucus;[4] and its heterogenic composition and greatly varying thickness.[5] In recent decades, several different mucosal delivery particle systems were proposed that can be categorized as either mucoadhering or mucopenetrating particles;[6] the latter may be further subcategorized by type of penetration which may be active or passive. For passive penetration, particles are designed to minimize any mucosal interaction yielding rapid diffusion through the mucus.[7] Passive penetration is facilitated either by mimicking viral surface features[8] or by particle functionalization with inert polymers like polyethylene glycol (PEG). For active penetration, peptide bonds in the mucin protein backbone of the mucus gel are cleaved by mucolytic enzymes (e.g., papain) that are attached to the NP surface.[9, 10] In contrast, muco-adhering NPs deploy chemical interactions (i.e., hydrogen and covalent bond formations) with the mucus to increase their residence time and, thus, enhance drug absorption.[11]

The target tissue determines the approach of mucosal drug delivery. For example, mucoadhesive NPs are preferred for buccal drug delivery[12] whereas mucopenetrating NPs more efficiently overcome the mucus in the nasal tract.[13] Intestinal mucus, in particular, poses the toughest mucosal barrier due to its thickness and to continuous mucus flushing.[14] Mucoadhesive and mucopenetrating NPs were tested for intestinal drug delivery and both demonstrated limitations. Strong mucoadhesion promotes mucus entrapment and subsequent rapid particle elimination[15] or causes drastic alterations to the physicochemical properties of the mucus.[16] Mucopenetrating NPs showed limited diffusion because of the hydrophobicity and rigidity of its building blocks.[17, 18] Interestingly, implementation of disulfide bonds as permeation enhancers rendered both mucopenetrating and mucoadhesive properties, yielding

improved drug delivery.[19-21] This finding suggests that mucopenetrating NPs that slip through the mucus network can, through gradual degradation within the mucus, display weak mucoadhesive properties that enable a certain degree of mucus entanglement. As a result, mucopenetrating NPs can achieve improved distribution and enhanced penetration through the mucus and, thus, may be the most effective approach for overcoming the intestinal barrier.

Polymeric nanogels emerged as a tuneable platform that efficiently encapsulates a variety of guest molecules.[22-28] Nanogels are three-dimensional cross-linked gel particles that can swell in water. They can be finetuned through adaptation or combination of materials to control the release of their loaded cargo in response to stimuli such as temperature,[29-31] pH,[32, 33] or redox-potential.[25] We used a novel nanogel design because we endeavored to achieve a highly efficient transmucosal delivery. The following components were combined to generate the novel nanogel. First, dendritic polyglycerol (dPG) – a biocompatible hydrophilic scaffold bearing a high number of hydroxyl groups on its surface that leverage mucopenetration and slight mucoadhesion due to stealth properties, hydrophilicity, and hydrogen bonds formation with the mucus domains.[34, 35] Second, poly-N-isopropylacrylamide (PNIPAM) and poly-N-isopropylmethacrylamide (PNIPMAM) – biocompatible building blocks with neutral zeta-potential that show excellent performance for delivery of sensitive proteins.[29, 31] Finally, disulfide units, which act as mucosal permeation enhancers[19-21] and render the nanogels biodegradable through their reduction to thiols by glutathione (GSH),[36-38] for example, which is ubiquitously expressed in mucus. Nanogel biodegradability may facilitate cargo release[39-42] and reduce toxicological concerns as smaller polymeric fragments ensure fast clearance from the body.[43-46]

In this study, we report the development of novel, disulfide-containing dendritic polyglycerol (dPG)-based nanogels as transmucosal drug delivery systems. We hypothesize that the hydrophilicity of this nanogel system will facilitate mucus entanglement along with disulfide bond reduction by mucosal GSH, which will result in degradation enabling efficient mucus-penetration.[47, 48] We designed a bifunctional disulfide-containing linker for facilitating coupling to dPG through a copper-catalyzed click reaction and concurrent translation of dPG to a macromolecular cross-linker for poly-N-isopropylacrylamide (PNIPAM) and poly-N-isopropylmethacrylamide (PNIPMAM).

Systematic analysis of our nanogel polymerization process revealed the importance of careful polymer choice to form particles with diameters in the 100-200 nm range that yield low polydispersity and intact disulfide-bonds. Nanogel interactions with the mucus and potential mucopenetrating properties were tested in gastrointestinal mucus of freshly excised porcine small intestines and in reconstructed human-based models of bronchial epithelium. The

nanogels observed were loaded with etanercept (ETN) as a model drug for anti-tumour necrosis factor alpha (anti-TNFα) treatment of inflammatory diseases of the GI tract. The efficacy of the ETN-loaded nanogels was then assessed in three-dimensional human intestinal models which emulate characteristics of IBD.

2. Results

2.1 Synthesis of disulfide-containing linker and nanogel preparation

Since the introduction of disulfide moieties seems highly promising to enhance mucus-penetrating properties of nanogels,[19, 21, 49, 50][166, 167, 259, 260] a cystamine based, heterogenous end-functionalized linker design was employed to modify the cross-linker dPG. This approach allowed to generate a variety of nanogels using different monomers and to apply the knowledge gained about the key parameters in the synthesis of nanogels using precipitation polymerization.[30] The degradable linker was synthesized in a 4-step procedure using a slightly modified approach as previously reported (Scheme S1, Supporting Information).[51] In brief, cystamine was used as starting material which was initially mono-tert-butyl oxycarbonyl (BOC) protected using BOC anhydride in the presence of a base. This allowed the carbodiimide-promoted amide coupling of an alkyne bearing propionic acid via the formation of an activated ester in the second step. After deprotection of BOC in acidic conditions, the resulting free amine reacted with methacryloyl chloride to yield the degradable linker.

The linker was then coupled to azide-functionalized dPG using copper promoted azide-alkyne cycloaddition (Figure 1A). Successful coupling was verified by ^{1}H-NMR analysis of the purified conjugate showing the signals of both, dPG backbone (Figure S1, peak h, Supporting Information) and the linker (peaks b, d, a) as well as a shift of the signal from the alkyne (g) to lower field due to the formation of the triazole upon the alkyne azide cycloaddition. In addition, FT-IR analysis of the conjugate showed complete reduction of the signature peak of the azide at 2100 cm^{-1} proving successful reaction (Figure S2, Supporting Information). As the copper catalysed coupling reaction worked quantitatively, the grafting density of degradable linkers per dPG could be tuned between 4-8% directly by percentage of azide functionalization of total OH-groups available on the dPG.

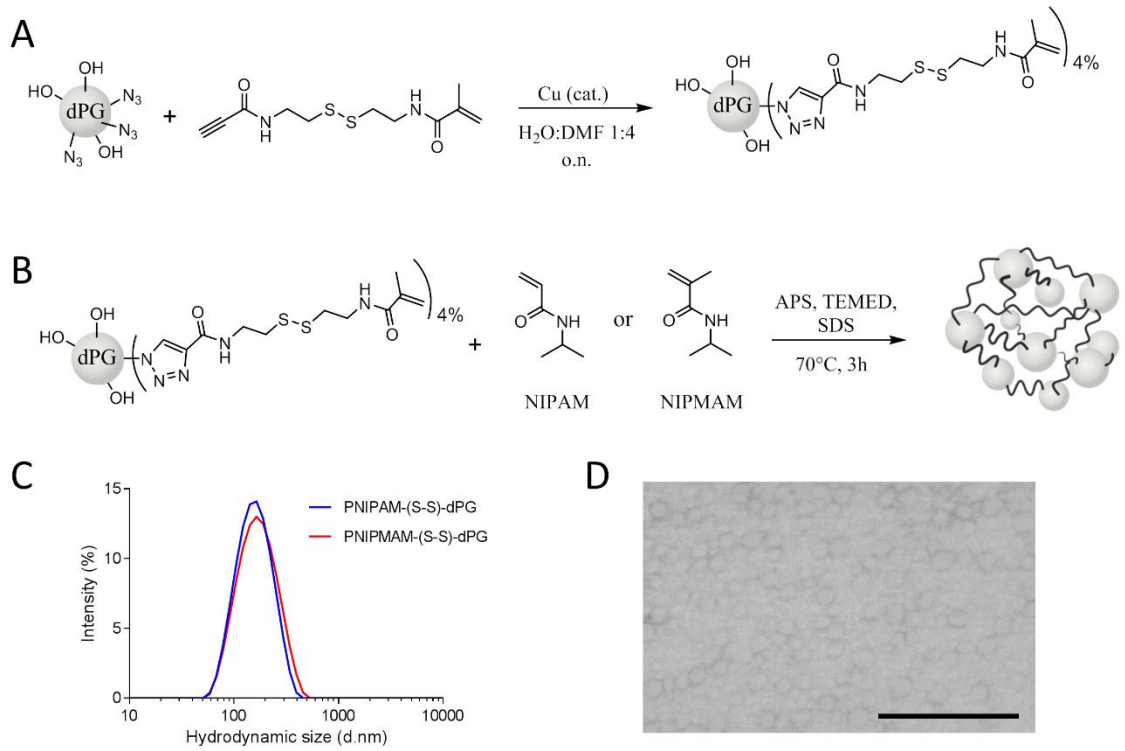

Figure 1. (A) Conjugation of degradable linker to dPG-azide via copper promoted cycloaddition and (B) synthesis of degradable nanogels. (C) Size distribution of PNIPAM-(S-S)-dPG and PNIPMAM-(S-S)-dPG nanogels obtained by dynamic light scattering (DLS). (D) TEM image of PNIPMAM-(S-S)-dPG. Scale bar 200 nm.

Table 1. Hydrodynamic sizes (d.nm) and PDI of degradable nanogels with different composition determined by DLS (intensity) at 25 °C.

Monomer	wt% monomer	wt% dPG	Size (d.nm) at 25 °C	PDI at 25 °C
NIPMAM	90	10	166	0.218
	80	20	97	0.241
	70	30	80	0.433
	60	40	46	0.396
NIPAM	90	10	250	0.132
	80	20	185	0.116
	70	30	159	0.144
	60	40	100	0.172

Using this degradable cross-linker, the nanogel synthesis was performed by precipitation polymerization with NIPAM and NIPMAM as monomers (Figure 1B). By varying the dPG and monomer feeding ratio, the size of the nanogels was tuned to values of 100–250 nm (PNIPAM-(S-S)-dPG) or 45–170 nm (PNIPMAM-(S-S)-dPG) (Table 1). For PNIPMAM based nanogels, polydispersity index (PDI) value was found to increase with the dPG feed ratio. Therefore, nanogels synthesized with a monomer:dPG ratio of (90:10) gave the lowest PDI for an average

size of 166 nm and were selected as best candidates for further studies. With NIPAM as monomer, nanogels with a *PDI* ≤ 0.2 were obtained in all tested conditions. Thus, the PNIPAM nanogels with a similar hydrodynamic size of 160 nm (70:30 monomer:dPG) were chosen for the evaluation of the degradation profiles and the interaction with mucus (Figure 1C). Further analysis of nanogels' morphology by transmission electron microscopy (TEM) revealed spherical shape and low polydispersity in concordance with the dynamic light scattering (DLS) data (Figure 2B). Moreover, the zeta-potential indicates a neutral surface charge for both nanogels (Table S2, Supporting Information).

2.1.1 Monomer used for nanogel synthesis impacts the disulfides present in the network

To proof the presence of the disulfides in the nanogels network, their degradation in a reductive environment (Figure 2A) facilitating the cleavage of disulfides to free thiols, was initially investigated by TEM (Figure 2B, C). Upon incubation of PNIPMAM-(S-S)-dPG with 5 mM GSH for 24 h, their degradation to smaller fragments was observed (Figure 2C). Subsequently, time and concentration dependent changes of the nanogel sizes were monitored in more detail by DLS. For PNIPMAM-(S-S)-dPG, a fast degradation at high GSH concentrations (2×10^{-3} and 5×10^{-3} M) resulting in an almost complete disulfide cleavage was observed within 4 h (Figure 2E, F). Incubation with (5×10^{-3} M) GSH up to (12 h) resulted in a broad signal which is indicative for the formation of aggregates. At lower GSH concentrations (0.5×10^{-3} M, Figure 2D), no size decrease of the nanogels was observed.

In contrast, PNIPAM-(S-S)-dPG nanogels as well as control nanogels without a disulfide linker were nondegradable even at high GSH concentrations (Figure 2G,H). For PNIPAM-(S-S)- dPG nanogels only a slight decrease in intensity and broadening of the signal was observed suggesting premature degradation of the disulfides during the nanogel synthesis (Figure 2G). To confirm the lack of disulfides in PNIPAM-(S-S)-dPG nanogels, Raman spectroscopy was performed. The comparison of PNIPMAM-(S-S)-dPG and PNIPAM-(S-S)-dPG (Figure 2I) clearly shows the disulfide signal at 400 cm^{-1} for PNIPMAM based nanogels but no signal for PNIPAM-(S-S)-dPG.

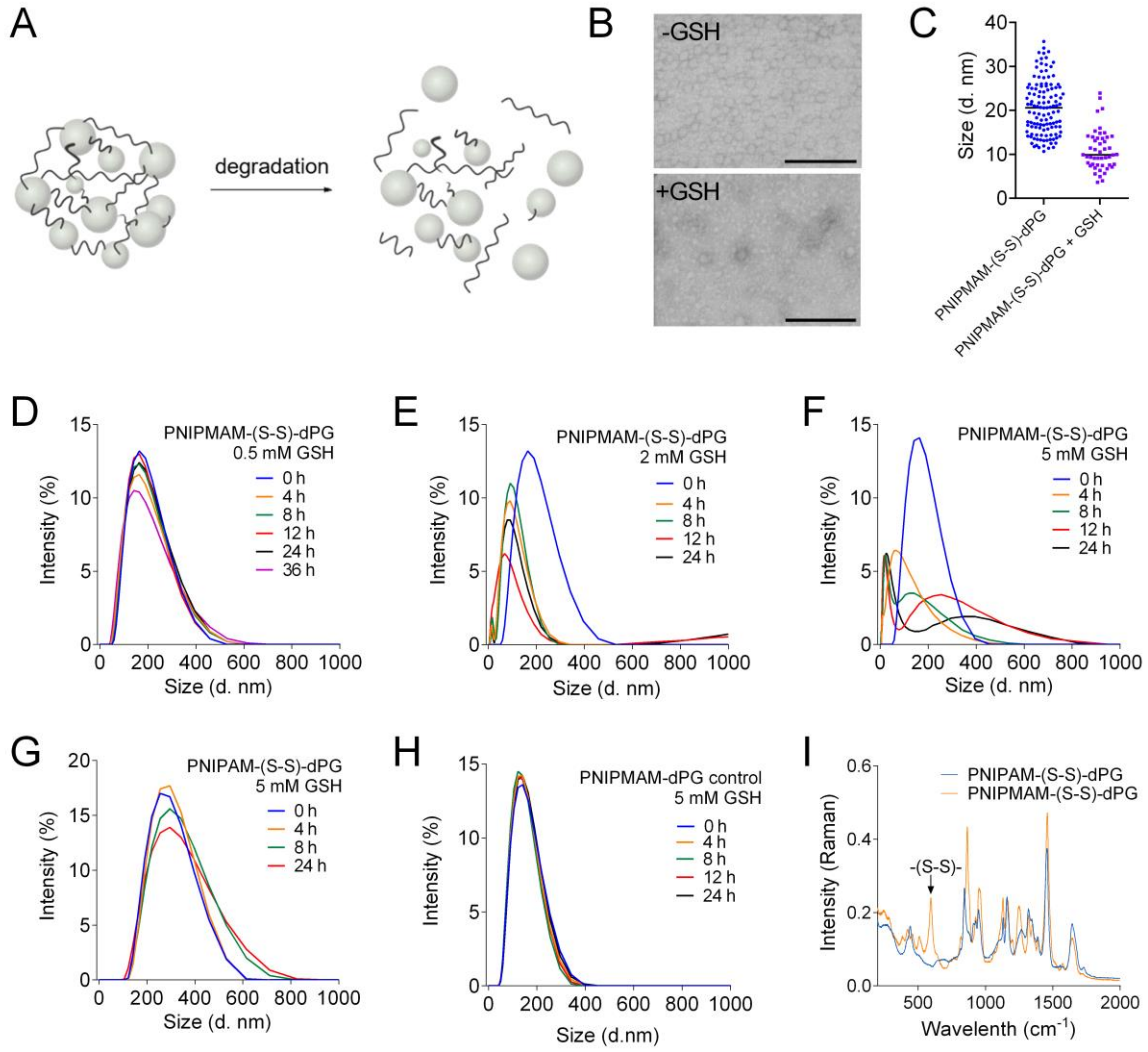

Figure 2. A) GSH induced cleavage of nanogels through reduction of disulfides to thiols. B) TEM images of PNIPMAM-(S-S)-dPG before and after incubation with 5×10^{-3} M GSH for 24 h. Scale bar = 200 nm. C) Distribution of particle diameter semi-quantified using the TEM images. Degradation profiles monitored by DLS of D) PNIPMAM-(S-S)-dPG nanogels in (0.5×10^{-3} M) GSH solution, E) (2×10^{-3} M) GSH, and F) (5×10^{-3} M) GSH, G) degradation study of PNIPAM-(S-S)-dPG and H) nondegradable PNIPMAM-dPG control nanogels in (5×10^{-3} M) GSH. I) Raman spectra of PNIPAM-(S-S)-dPG and PNIPMAM-(S-S)-dPG nanogels.

Importantly, for PNIPAM-(S-S)-dPG hydrogels synthesized at r.t., full degradation upon incubation with GSH (5×10^{-3} M) was observed (Figure S3, Supporting Information). Since the main difference between the reaction conditions of the nano- gels and macro hydrogels was the reaction temperature, we then evaluated the impact of the reaction temperature on the stability of the disulfides. Therefore, the nanogel formation was screened increasing the reaction temperature stepwise to 50 °C. Nanogels with low PDI and sizes around 130–160 nm

were obtained, but none of them was degrading in the presence of GSH (Table S1, Supporting Information).

For the degradation behavior of copolymeric nanogels with different PNIPAM and PNIPMAM ratios, it was found that with increasing NIPMAM content, the broadening of the DLS signal gets more prominent until fragmentation into smaller particles occurs from ratios of NIPMAM:NIPAM of 3:1 onwards (Figure S4A–C, Supporting Information). Based on those findings, all following investigations have been exclusively performed with PNIPMAM-based nanogels, whereby PNIPMAM-(S-S)-dPG are the biodegradable and PNIPMAM-dPG the nonbiodegradable (= control) nanogels.

2.2 Nanogel-Mucus Interactions

2.2.1 Disulfide-containing nanogels fully degrade upon incubation with mucus and show stability over a wide pH range

To investigate the interactions of the nanogels with mucus, we first studied the ability of the nanogels to be degraded by Cys, which is bound to the mucin in the mucus backbone. As expected, and in line with the GSH data, a time and concentration dependent size reduction was found for PNIPMAM-(S-S)-dPG nanogels after incubation with Cys (Figure 3A; Figure S4G,H, Supporting Information). In addition, stability of the nanogels at different pH values was tested (Figure S4D–F, Supporting Information). Time dependent size measurement showed that the nanogels are stable over 96 h in acidic and neutral conditions while in basic pH, the nanogels slowly degrade over time.

Second, direct interaction of the nanogels with mucus was determined. Here, porcine intestinal mucus was incubated with the nanogels at 37 °C. Retention profiles were then assessed using gel permeation chromatography (GPC) combined with ultraviolet-visible (UV-vis) absorbance measurements of Rhod-B labeled nanogels to clearly identify the nanogels among the complex mucus components. To assess the degradation profile of the disulfide-containing nanogels in GPC, they were initially incubated with GSH resulting in prolonged retention over time (Figure S5A, the Supporting Information). The fast degradation of PNIPMAM-(S-S)-dPG to dPG following GSH exposure was in line with the degradation profiles obtained by DLS (Figure 2B–D). Concordantly, the incubation with the mucus also demonstrated prolonged retention times for the disulfide-containing nanogels PNIPMAM-(S-S)-dPG indicating their gradual breakdown (Figure 3B). Full nanogel degradation (≈98%) was observed within 12 h. In contrast, the retention time of PNIPMAM-dPG control nanogels did not change after incubation with GSH nor mucus (Figure S5B, Supporting Information; Figure 3C). It should be noted that no release of free Rhod-B was observed, evidencing that the

longer retention times peaks in the GPC measurements correspond to fragmentation of the nanogels upon reductive activity of the mucus.

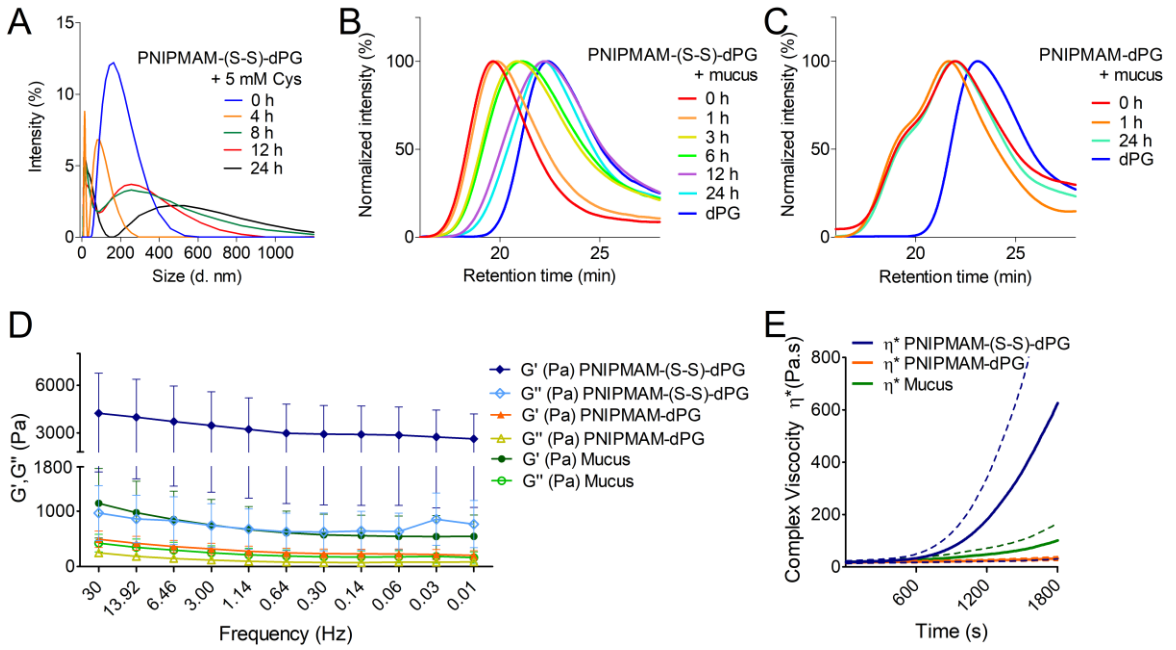

Figure 3. A) Degradation of PNIPMAM-(S-S)-dPG nanogels in presence of (5×10^{-3} M) l-cysteine (Cys), monitored by DLS. Degradation profiles monitored by GPC upon incubation with native mucus of Rhod-B labeled B) PNIPMAM-(S-S)-dPG and C) control PNIPMAM-dPG nanogels, the dPG moiety of each nanogel served as a reference. Rheological behavior of isolated mucus with and without the nanogels: D) Frequency sweep (30–0.01 Hz) strain controlled (0.5%). G′, G″ elastic and viscous moduli, respectively. E) Viscoelasticity of mucus presented as complex viscosity η* over 30 min time sweep. Mucus diluted with (20 µL) PBS served as a reference. n = 3, mean = SEM. Statistical significance was not achieved due to high SEM values.

2.3.2 Disulfide-containing nanogels demonstrate mucoadhesive properties

Since previous work indicated that thiolation facilitates mucoadhesion,[52] which in turn affects the mucus rheological properties, we next investigated the viscoelastic behavior of isolated intestinal mucus upon exposure to the nanogels. Incubation of the PNIPMAM-(S-S)-dPG nanogels with mucus increased the elastic and viscous moduli *G'* and *G''* over the tested frequencies, whereas no change was observed after incubation with the control (PNIPMAM-dPG) nanogels **(Figure 3D)**. This was also consistent with a distinct increase in bulk viscosity *η** over 30 min in the presence of the disulfide-containing nanogels, compared to no change in viscoelasticity after incubation with the control nanogels **(Figure 3E)**.

2.3.3 Disulfide-containing nanogels exert distinct mucopenetrating properties in both ex vivo and in vitro tissue models and demonstrate high biocompatibility with 2D epithelial and immune cells

To assess the mucopenetrating properties of the disulfide-containing (PNIPMAM-(S-S)-dPG) and control (PNIPMAM-dPG) nanogels, Rhodamine B (Rhod-B) labeled nanogels were applied onto freshly excised porcine jejunum (Figure 4A-D) and tissue models of the bronchial epithelium (Figure 4E, F). Fluorescence-based analysis of tissue sections showed efficient mucus penetration for the disulfide-containing nanogels in intestinal (Figure 4A, C) and bronchial tissues (Figure 4E). In contrast, no mucopenetration was observed for the control PNIPMAM-dPG nanogels (Figure 4B, D) even after incubation for 6 h with the bronchial epithelial models (Figure 4F).

MTT assays showed very good cytocompatibility for the disulfide-containing and the control nanogels even at high concentrations (Figure 4G). In addition, incubation with primary human macrophages for ≤ 24 h did not trigger any apoptosis or necrosis as derived from flow cytometry (Figure 4H). Cellular internalization studies with the macrophages also showed an active and efficient particle uptake within 3 h. Interestingly, the PNIPMAM-(S-S)-dPG nanogels were taken up more efficiently than their non-thiolated analogues (Figure 4I).

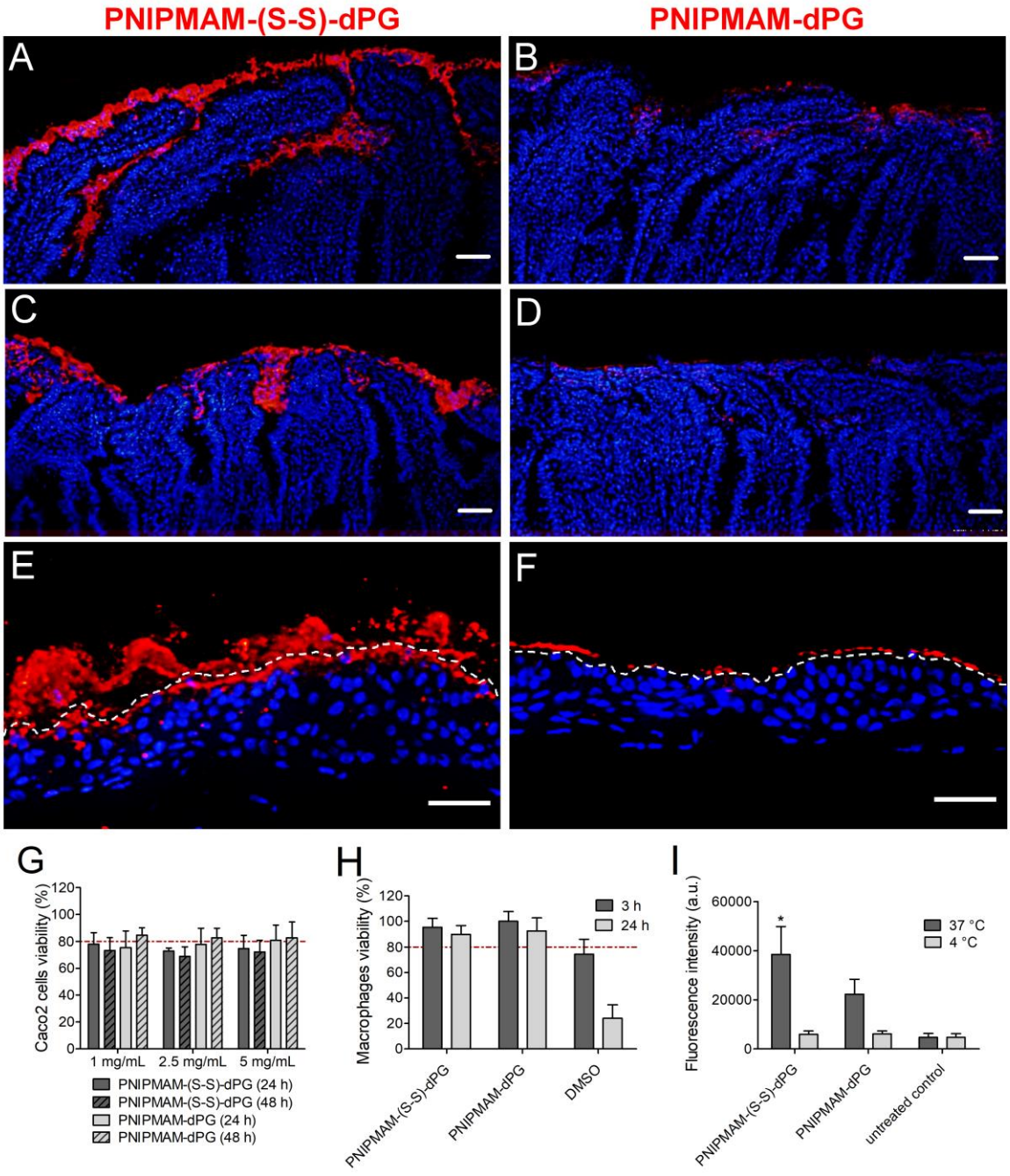

Figure 4. Representative microscopy images of cryosections from excised porcine jejunum after application of Rhod-B labeled (red) PNIPMAM-(S-S)- dPG nanogels and control PNIPMAM-dPG nanogels after 1 h (A,B, respectively) and 3 h (C,D, respectively) exposure, n = 3. Representative cryo-sections of *in vitro* bronchial epithelial models following 3 h incubation with E) PNIPMAM-(S-S)-dPG nanogels and F) control PNIPMAM-dPG nanogels, epithelial boarder of the bronchial models is illustrated by a dashed line, n = 2. Nuclei were counterstained with DAPI. Scale bar 50 µm. Interactions of nanogels with 2D cell cultures: G) Cell viability of Caco-2 cells after 24 and 48 h exposure to the nanogels at different concentrations. H) Viability of macrophages after incubation with Rhod-B labeled nanogels (1 mg mL^{-1}) for 3 and 24 h. The red dotted line indicates the cell viability limit of 80%. I)

nanogels internalization into macrophages at 37 and 4 °C determined by fluorescence activated cell sorting (FACS) analysis. n = 3, mean = SEM.

2.4 Assessment of the Nanogel Delivery Efficiency and Efficacy of ETN in Inflammatory Intestinal Models

2.4.1 Structural and Functional Integrity of Encapsulated ETN in the Nanogels

The encapsulation of ETN was achieved by swelling dry nanogels yielding an encapsulation efficiency of 79 ± 3.8% (8 wt%; PNIPMAM-(S-S)-dPG) and 88 ± 2.5% (9 wt%; PNIPMAM-dPG). For both nanogels, the stability of the encapsulated and released ETN was determined using circular dichroism (CD) measurements. No major changes in the CD spectra were observed between free, encapsulated and released ETN and the secondary structure of ETN seems to be unaffected after loading and release from the nanogels (Figure 5A ─ C).

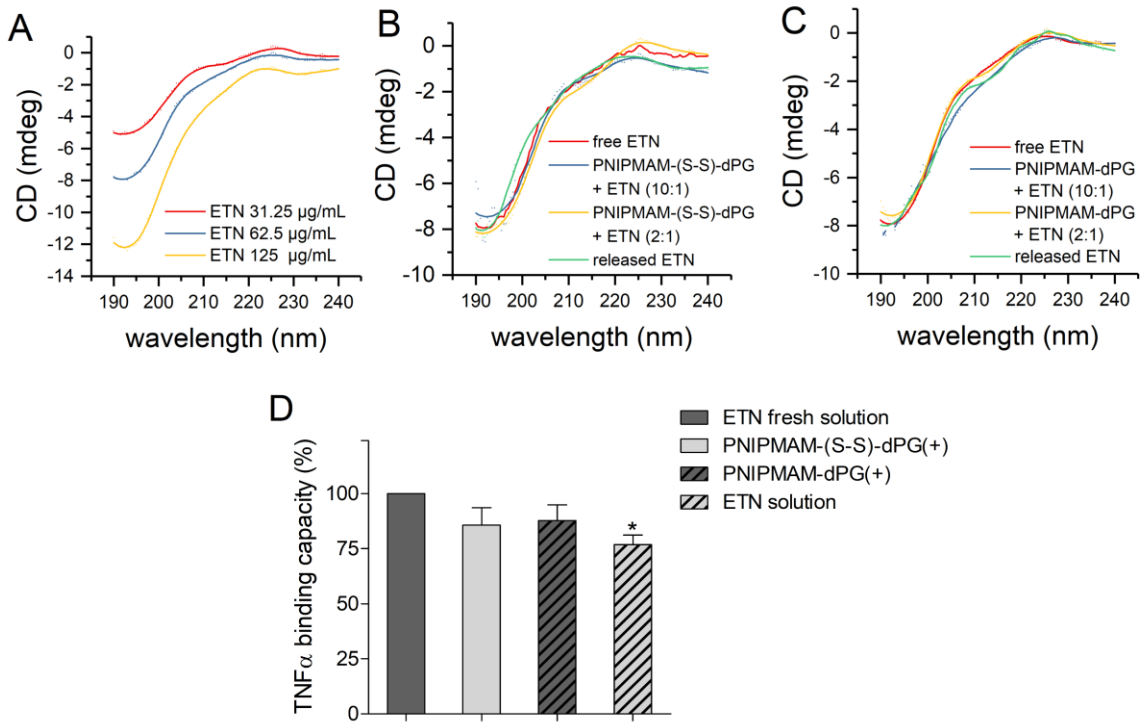

Figure 5. CD spectra of ETN A) in solution (PBS, pH 7.4), encapsulated and released from B) PNIPMAM-(S-S)-dPG and C) PNIPMAM-dPG nanogels, respectively. D) ETN binding capacity to TNF-α two weeks after loading onto disulfide-containing (PNIPMAM-S-S-dPG) and control (PNIPMAM-dPG) nanogels and storage at 4 °C. ETN in solution served as a control. All data were normalized to the TNF-α binding capacity of a fresh ETN solution (100%). All values are expressed as mean ± SEM obtained from three independent experiments using three different nanogel batches. * indicates statistically significant differences to fresh ETN solution values before normalization; (*p < 0.05).

Additionally, the TNFα binding capacity of ETN after loading and release from the nanogels was determined (Figure 5D). ETN loaded onto the nanogels retained > 85% binding affinity to

TNFα after storage at (4 °C) over 14 days and demonstrated a significantly higher TNFα binding capacity compared to ETN in solution. These results are also in line with previous findings from our labs showing that nanogels protects protein cargo from degradation.[29]

2.3.2 In vitro ETN Release and Activity after Release

To monitor ETN release and activity (ability to bind TNF- α) after release, PNIPMAM-(S-S)-dPG nanogels loaded with ETN were incubated with (0.5×10^{-3}, 2×10^{-3} M) GSH solutions, or phosphate buffered saline (PBS) over 24 h. Nondegradable PNIPMAM-dPG nanogels incubated at (2×10^{-3} M) GSH served as control (Figure 6A). As expected, the degradable PNIPMAM-(S-S)-dPG nanogels showed a continuous ETN release over time in the reductive environment. The release was faster in the presence of (2×10^{-3} M) GSH concentration compared to the lower, yet physiologically relevant GSH concentration (0.5×10^{-3} M). Interestingly, incubation in both GSH concentrations (0.5×10^{-3} and 2×10^{-3} M) only yielded ≈40% of active ETN over 24 h despite a faster release at (2×10^{-3} M) GSH. To unravel the reason for this finding, we ran a Bradford protein quantification assay, which provides information about the total amount of released ETN but does not convey any information about the active portion. The Bradford assay showed that in the presence of (2×10^{-3} M) GSH ≈ 80% total ETN is released from PNIPMAM-(S-S)-dPG after 24 h compared to 40% in the presence of (0.5×10^{-3} M) (Figure 6B). This indicates that at (2×10^{-3} M) about 50% of the released ETN is inactivated, which is not the case at the physiologically relevant GSH concentra- tion (0.5×10^{-3} M). No significant ETN release was observed following incubation with PBS or when incubating the non- degradable PNIPMAM-dPG nanogels with (2×10^{-3} M) GSH.

A) ETN ELISA

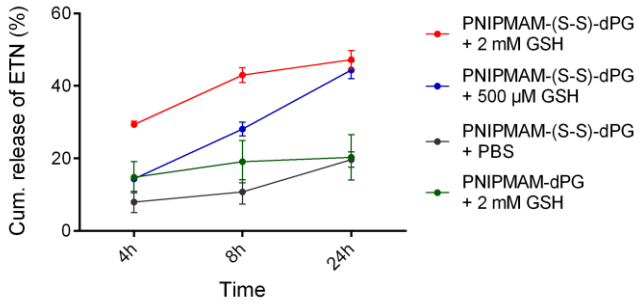

B) Bradford Assay

	4h	8h	24h
2 mM	46 ±11%	65 ±9%	84 ±9%
0.5 mM	13 ±0.8%	24 ±0.2%	42 ±2%

Figure 6. Cumulative release of active ETN over 24 h from the nanogels in reductive environment (0.5 mM or 2 mM GSH) or PBS determined by ELISA (A) or overall released ETN (active and inactive) by Bradford assay (B).

2.3.3 Topical Application of ETN Improves the Intestinal Barrier and Efficiently Suppresses Pro-Inflammatory Cytokine Release

To assess the therapeutic efficiency of topically applied ETN delivered by the nanogels, characteristics of IBD were induced by cytokine supplementation of human intestinal models. TEER values were continuously recorded to monitor changes in the barrier integrity of the models after triggering the inflammation. Untreated intestinal models had an average TEER value of 120 ± 14 Ω*cm2, which is in line with reference TEER values of human intestinal tissue.[53] After the addition of TNF-α and IFN-γ, the relative TEER values dropped from 100% to 74 ± 1% (mean ± SD) indicating a successful induction of inflammation (Figure 7). At this point, ETN treatment was started. Within 48 h after the first ETN treatment, the TEER values of the models recovered to 90 ± 12% after treatment with ETN loaded to PNIPMAM-(S-S)-dPG, to 82 ± 11% after treatment with ETN loaded to PNIPMAM- dPG nanogel, and 68 ± 9% after treatment with ETN solution (Figure 7A). Treatment with unloaded nanogels did not improve the barrier integrity (Figure 7B). Although a clear trend toward a superiority of ETN loaded onto PNIPMAM- (S-S)-dPG nanogels has been observed, statistical significance was not achieved due to the high standard deviations. Additionally, in response to inflammation intestinal epithelial and laminal cells produce excessive amounts of cytokines, which further promote inflammatory processes. Therefore, increased IL-6 and IL-8 levels were measured in the culture medium of the inflamed intestinal models, which once again confirmed the successful induction of inflammation in the intestinal models (Figure 7C,D). As expected, the topical application of ETN loaded nanogels or ETN solution then significantly inhibited IL-6 and IL-8 secretion (Figure 7C,D). Unexpectedly, no superiority of the ETN loaded nanogels was observed. To confirm the effects of the anti-inflammatory treatment, we also assessed the expression of the intestinal tight junction (TJ) proteins occludin, zonula occludens-1 (ZO-1), and claudin-2 which is indicative for the barrier function of intestinal tissue.[54,55] As expected, stimulation with TNF-α and IFN-γ triggered a downregulation of occludin and ZO-1 and an upregulation of claudin-2 (Figure S7, Supporting Information; Figure 8A).[56] Following treatment with ETN, the expression of occludin and ZO-1 increased, and that of claudin-2 decreased indicating a recovery of the intestinal barrier as determined by immunofluorescence (IF) (Figure S7, Supporting Information) and western blot (Figure 8A). However, again no superiority of the nanogel formulations was observed in this setting. Due to these unexpected findings, we had a closer look at the actual mucus production of the intestinal models which turned out to be unphysiologically low with hardly any mucus being secreted at all (Figure S7 A,B, Supporting Information). We then assessed the ETN delivery efficiency in the home-made bronchial epithelial models (Figure S7 C,D, Supporting Information) where mucus is continuously secreted in physiologically relevant amounts. Here, the PNIPMAM-(S-S)-dPG

nanogels efficiently delivered the ETN through the mucus into the epithelial layer and outperformed the PNIPMAM-dPG nanogels and ETN solution where no ETN delivery was observed (Figure 8B).

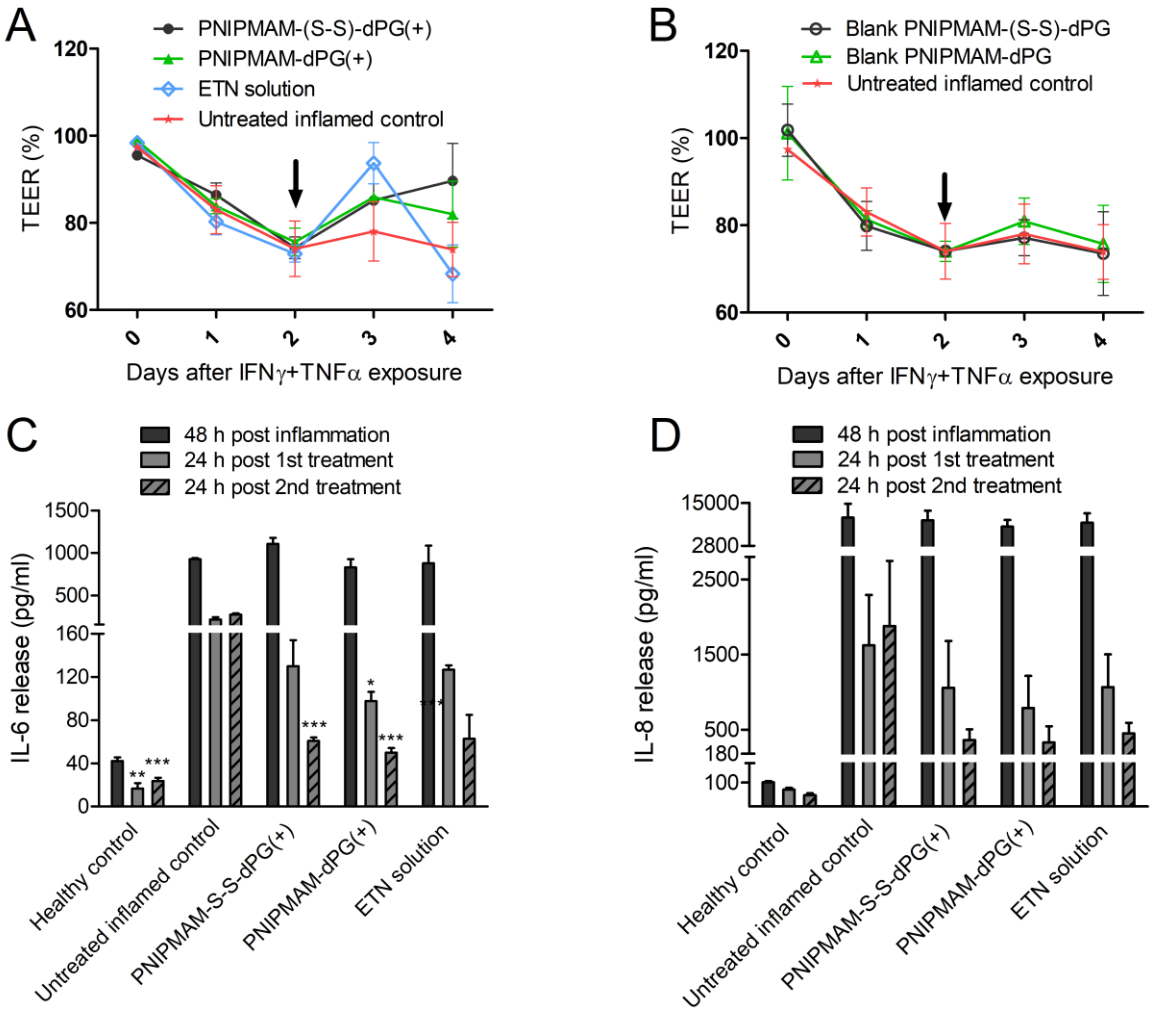

Figure 7. TEER values of EpiIntestinal™ models over 4 days following the induction of inflammation with TNFα and INFɣ. TEER values were normalized to the untreated, healthy control. ETN treatment started 2 days after the induction of inflammation (arrow). A) Relative TEER values before and after topical treatment with ETN in solution (ETN solution) and loaded (+) onto PNIPMAM-(S-S)-dPG or control PNIPMAM-dPG nanogels. B) Unloaded nanogels (blank) did not affect TEER values. Mean ± SEM, n=3. Concentrations of cytokines C) IL-6 and D) IL-8 released from EpiIntestinal-FT™ models after the induction of inflammation and following topical treatment with ETN loaded (+) onto PNIPMAM-(S-S)-dPG, control PNIPMAM-dPG nanogels or ETN solution. * indicates statistical significance over the untreated inflamed model. *p ≤ 0.05, **p ≤ 0.01, ***p ≤ 0.001; n = 3.

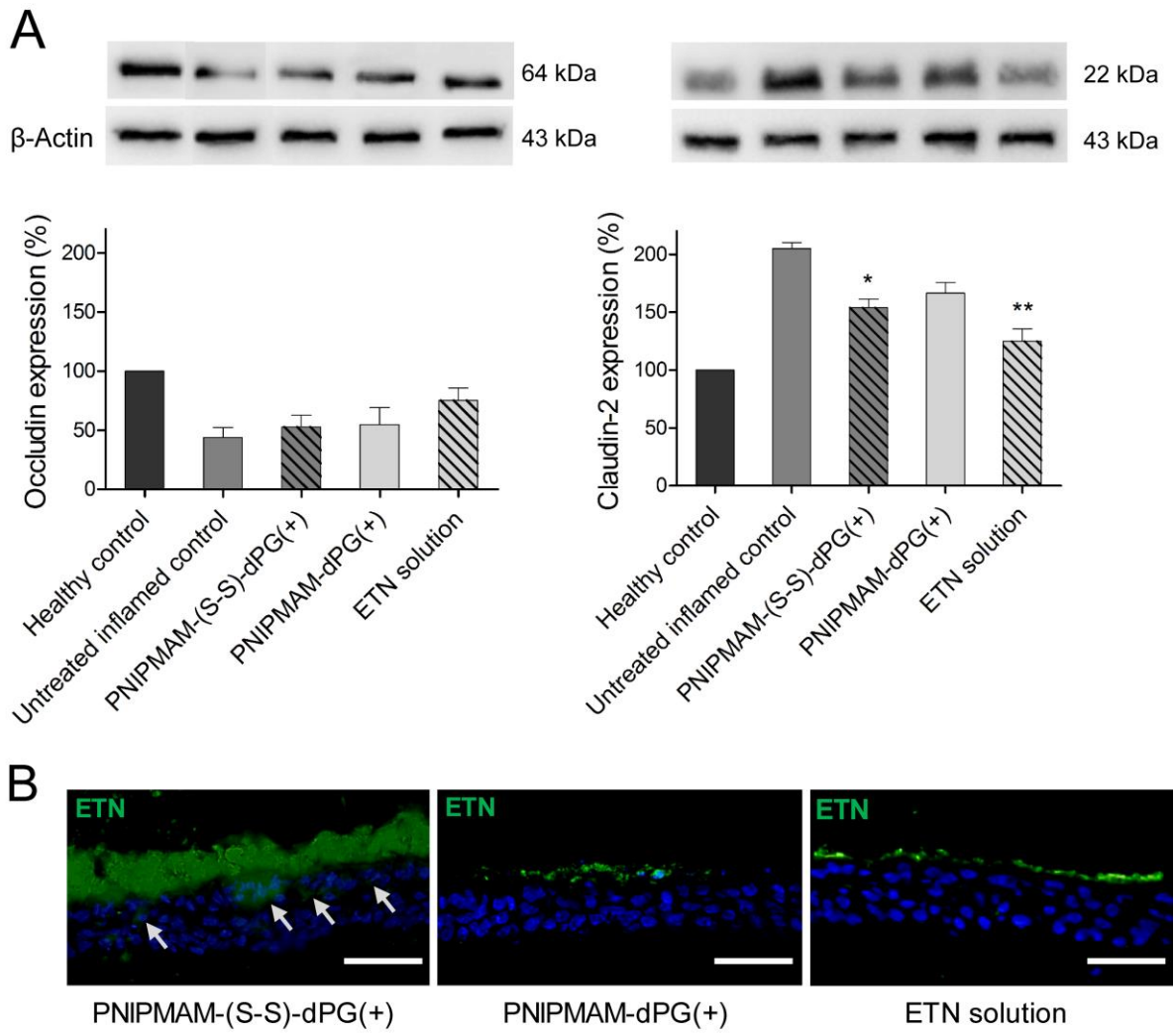

Figure 8. A) Western blot data of occludin (64 kDa) and claudin-2 (22 kDa) expression in inflamed EpiIntestinal-FT™ models before and after topical treatment with ETN loaded (+) onto PNIPMAM-(S-S)-dPG and control PNIPMAM-dPG nanogels or in solution. Blots were normalized to β-actin expression and the bars are depicted as percentages relative to the healthy control ± SEM, * indicates statistical significance over the inflamed control. *$p \leq 0.05$; **$p \leq 0.01$. (B) Representative immunofluorescence staining of etanercept (ETN) after topical application of PNIPMAM-(S-S)-dPG, PNIPMAM-dPG nanogels and ETN solution in human bronchial epithelial models after 6 h incubation. Cell nuclei were counterstained with DAPI, n = 3, sections thickness (5 µm). Scale bar (50 µm).

3. Discussion

Successful mucosal drug delivery is very difficult to achieve, and currently available delivery strategies have various short- comings, especially those intended for intestinal administration.[14] Therefore, novel approaches and more efficient mucosal delivery systems are of high interest. According to a previous proposal, improved mucus penetration can be achieved by

nanocarrier thiolation[19,21] combined with use of hydrophilic neutral polymers.[48] We built on this proposal to develop a novel mucosal delivery system based on dPG-based nanogels that contain disulfide units in their network. As a linear coun- terpart for dPG, we also tested the thermo-responsive polymers PNIPAM and PNIPMAM which facilitate controlled generation of biocompatible nanogels by precipitation polymerization.[30]

A bi-functional disulfide-containing linker design was used for conjugation with dPG through a copper-catalyzed cycloaddition. The linker conjugation carried a methacrylate group on one end and translated dPG into a crosslinker suitable for radical polymerization, allowing nanogel synthesis through a precipitation polymerization technique with the monomers NIPAM and NIPMAM (Table 1). By monitoring nanogel degradation in reductive environments, we found that intact disulfides were only present in PNIPMAM-(S-S)-dPG nanogels (Figure 2B–H). However, the nanogels were nondegradable with NIPAM use, as indicated by only slight broadening of the DLS signal. Raman spectroscopy (Figure 2I) confirmed that the presence of NIPAM during polymerization induced premature cleavage of most disulfides. We assume that the broadening of the DLS signal for PNIPAM-based nanogels is related to cleavage of the few existing disulfide bonds under reductive conditions, leading to partial loosening of the network structure and, thus, slight swelling of the nanogels (Figure 2G). This observation aligns with the behavior of periodate-sensitive microgels[57] and macro-sized disulfide-based hydrogels[58] which equally showed gel swelling before full disintegration.

We prepared macro-hydrogels with the same materials used to construct our nanogels to better understand the impact of NIPAM on the lack of degradability of the network. Interestingly, we found that the hydrogel disintegrated completely after incubation with (5×10^{-3} M) GSH (Figure S3, Supporting Information). The hydrogels were synthesized at r.t., but precipitation polymerization for nanogel formation was

performed at (70 °C). Thus, we believe that the reaction temperature could be one possible reason for the absence of disulfides in the nanogels. Nevertheless, the precipitation polymerization technique requires temperatures above the transition temperature of the thermoresponsive polymer. The approximate transition temperature for PNIPAM is (32–34 °C), making nanogel formation at r.t. impossible. Therefore, we gauged the nanogel formation by decreasing the reaction temperature stepwise down to (50 °C). However, none of the resulting nanogels degraded in the presence of GSH (Table S1, Supporting Information).

Copolymerization of NIPAM and NIPMAM confirmed that the presence of NIPAM is likely responsible for the premature cleavage of disulfides observed, yielding only partially degradable nanogels (Figure S4 A–C, Supporting Information). Degradability increased with decreased PNIPAM content in copolymeric nanogels. So far, the reason for such drastic effect

of NIPAM on disulfide stability is unclear. We believe that varying reactivities of the radicals formed from acrylate and methacrylate combined with high reaction temperatures is a possible explanation. Since PNIPAM-based nanogels lacked disulfide bonds, we focused on PNIPMAM-based nanogels for further characterization.

We determined whether disulfide-containing nanogels interact with mucus, and specifically with cysteines in the mucus, by first incubating the nanogels with a cysteine solution and then measuring the nanogel sizes. As seen in the GSH studies, we observed a time- and concentration-dependent degradation profile for PNIPMAM-(S-S)-dPG, indicating gradual breakdown of the nanogels through disulfide reduction (Figure 3A, Figure S4G,H, Supporting Information). Additionally, we assessed the stability of PNIPMAM-(S-S)-dPG nanogels at varying pHs and observed acceptable stability, especially in neutral and acidic conditions (Figure S4D–F, Supporting Information). Zeta-measurements confirmed the neutral surface charge of the nanogels (Table S2, Supporting Information) which is a prerequisite for efficient mucopenetration.[59,60]

Moreover, we further investigated the interactions of the disulfide-containing nanogels with native, freshly isolated mucus by performing GPC, and this also revealed a time- dependent degradation of the disulfide-containing nanogels into smaller fragments, which may yield improved mucopenetrating properties. This degradation resulted from the presence of the disulfide linker as the control nanogels PNIPMAM- dPG, which lacked the disulfide linker, showed no degradation (Figure 3B,C). Interestingly, the nanogel degradation studies (Figure 2) and incubation with fresh mucus samples and tissue models (Figure 4, Figure 8) resulted in comparable degradation kinetics, although the actual mucosal GSH concentration is lower (around 0.2–0.6 $\times$ 10^{-3} M[61,62]) than the GSH concentrations used in the degradation studies. This is likely due to other components of the mucus that also contribute to nanogel degradation such as cysteine residues and reducing enzymes. Accordingly, drug release studies showed continuous ETN release in the presence of (0.5 $\times$ 10^{-3} and 2$\times$$10^{-3}$ M) GSH while the ETN activity was only retained at physiologically relevant GSH concentrations (Figure 6A).

We also performed rheological and mucopenetration studies to characterize the effects of disulfide-containing and control nanogels on mucus gel. Rheological synergism is a previously proposed phenomenon for assessing potential mucoadhesive effects of nanogels in vitro.[63,64] The results of rheological measurements of our nanogels indicated an increase in the viscous (G″) and elastic (G′) behavior of the mucus in the presence of the PNIPMAM-(S-S)-dPG nanogels (Figure 3D,E) in contrast to the control PNIPMAM-dPG nanogels (Figure 3D,E). These observations align with previously published data on thiolated particles.[65]

For further studies of our nanogels in models that closely resemble human tissue, we attempted to investigate the mucus- penetrating properties of our nanogels using excised porcine jejunum and human-based bronchial epithelium (Figure 4A–F). Porcine jejunum is considered the best animal model of the human intestinal tract,[66,67] but rapid necrosis of this tissue[68] prevents ex vivo maintenance for longer than 4 h and, thus, limits the duration of penetration experiments. Ex vivo experiments on intact bronchial epithelia are even more difficult to perform.

Therefore, and since a major goal of the current study was to facilitate mucosal drug delivery in general, and not specifically intestinal delivery, we used reconstructed bronchial epithelial models that express critical features of the bronchial epithelium like ciliated cells and continuous mucus secretion. Our PNIPMAM-(S-S)-dPG nanogels efficiently penetrated the mucus of the intestinal and bronchial tissues while control PNIPMAM-dPG nanogels stayed on top of the mucus layer (Figure 4A–F). Moreover, a test of cytotoxicity in Caco-2 cells and primary macrophages demonstrated that the nanogels were not cytotoxic (Figure 4G,H) even at very high concentrations. Similar findings were obtained with cells of other mucosal epithelia (ectocervical Ect1, and vaginal cells VK2) (Figure S6, Supporting Information). Interestingly, cell uptake studies indicated more efficient uptake of disulfide-containing nanogels by macrophages (Figure 4I), which may be leveraged by interactions with specific phagocytic surface receptors.[69] This, however, is speculative and requires further investigation.

We assessed the applicability of our nanogels for mucosal drug delivery by loading model cargo, ETN, onto the nanogels. ETN (150 kDa) is a very potent tumor necrosis factor (TNF-α) inhibitor that is approved for treating several inflammatory conditions. In the clinic, it must be systemically administered due to unfavorable physicochemical properties, but systemic administration of ETN may trigger serious side effects.[70,71] Hence, a topical application seems more favorable for some patients, also previous work from our lab demonstrated nanogel capability for efficient topical delivery of biomacromolecules.[29] ETN encapsulation into the nanogels and exposure to physiological GSH concentrations for up to 24 h did not affect its structural or functional integrity (Figures 5 and 6; Figure S9, Supporting Information), aligning well with previous work.[29,31] Nevertheless, when moving from this proof-of-concept study to more translational work, other enzymes in the gut that may inactivate proteins such proteases need to be considered, too. To prevent an inactivation, the nanogels could be covered with gastric resistant coatings, but this is beyond the scope of this study.

The predictive value of IBD animal models is a controversial matter[72,73] as IBD does not naturally occur in rodents. Thus, a disease-like phenotype must be induced by highly artificial means such as gene modulation or exposure to highly toxic chemicals;[74,75] yet these models

fail to truly emulate IBD.[72,76] Therefore, we specifically avoided the use of IBD animal models in this study and opted for an inflammatory model of the human intestine which emulates IBD characteristics in vitro. TNF-α and IFN-γ are key players in IBD pathophysiology[77,78] and thus were used to induce an IBD phenotype in vitro.

After successful induction of inflammation, we treated the intestinal models topically with ETN that was either loaded onto the nanogels or dissolved in culture solution. Topical application of ETN inhibited inflammation and yielded recovery of the intestinal barrier, but the PNIPMAM-(S-S)-dPG nanogels showed superior effect only for the TEER values at the beginning of the treatment (Figure 7A). Notably, the ETN solution did not result in a significant recovery of the TEER values likely due to the lack of prolonged ETN release (Figure 6). In contrast, all ETN formulations ameliorated the inflammation similarly, as indicated by suppression of proinflammatory cytokines and normalization of tight junction protein expression (Figures 7C,D and 8A; Figure S7, Supporting Information). One potential reason for these unexpected findings may be structural limitations of the intestinal model, thus, we investigated the structure of the intestinal model.

Alcian blue staining indicated very low amounts of mucus on the intestinal models (≤ 4 µm; Figure S8A,B, Supporting Information)[79] compared to (100–700 µm) thick mucus layers reported for animal and human ex vivo explants.[80] Consequently, the lack of an adequate, mucus-rich environment may explain why the disulfide-containing nanogels did not outperform the control nanogels or the ETN solution in this setting. This hypothesis is supported by the degradation profile of the nanogels in mucus-rich environments and/or after exposure to 0.5×10^{-3} M GSH (within the physiologic range) and higher (Figure 2, Figure 4, Figure 6). We therefore validated this explanation and verified the superior transmucosal delivery capacity of the PNIPMAM-(S-S)-dPG nanogels by assessing ETN delivery with nanogels in human-based bronchial epithelial models that continuously secrete mucus and, thus, express a physiological mucus layer (Figure S8C,D, Supporting Information). Immunofluorescence staining confirmed the highly efficient penetration of ETN after topical application of PNIPMAM-(S-S)-dPG nanogels (Figure 8B), but ETN did not overcome the mucus layer when applied as a solution or when encapsulated in the control (nondegradable) PNIPMAM-dPG nanogels (Figure 8B).

4. Conclusion

We investigated a novel means of transmucosal drug delivery by developing and characterizing biodegradable, disulfide-containing dPG-based nanogels. Precipitation polymerization was used to yield nanogels with controlled size and functionality, circumventing limitations related to reactivity of the monomers. Mucosal penetration and adhesion of the nanogels was enhanced by incorporating disulfide bonds into the hydrophilic nanogel network,

yielding nanogel degradation triggered by the environment and, thus, controlled drug release. We corroborated our hypothesis that building nanocarrier systems with bio-inert components using disulfide linkages results in efficient mucosal penetration of the polymeric building blocks and large hydrophilic cargoes like proteins.

Our findings strongly emphasize the crucial significance of choosing the correct model and experimental setup for investigations of nanoparticle delivery and highlight the shortcomings of currently available test systems for mucosal delivery. As mentioned above, the translational value of in vivo IBD models is controversial. Tissue models constructed based on human mechanisms, such as intestinal inflammation models, are apparently promising alternatives. Nevertheless, these models still lack the complexity of a living organism and have "physiological shortcomings" such as insufficient mucus production.

An alternative to reconstructed tissue models may be tissue explants like porcine intestinal tissue, but this tissue decomposes rapidly, thus, special handling and transportation are required, and experimentation time is significantly limited. For example, deterioration of intestinal tissue resulting in complete damage of the villi was observed within 20 min post animal death when the tissue had not been properly handled or treated.[81] Another even simpler model for investigating mucosal delivery systems is commercially available mucus. However, this model differs significantly from its native pendant in constitutive components. Furthermore, important steric and viscoelastic gel properties may be lost due to mucus purification steps and protease treatment.[5]

Overall, it appears that none of the currently available models (in vivo and in vitro) can be recommended without reservation. Therefore, the best strategy for enabling valid and rigorous assessment of novel mucosal delivery systems appears to be a combined approach comprising complementary methods that assess the effects of the delivery systems from different angles.

5. Experimental Section

5.1 Analysis methods

5.1.1 NMR spectroscopy

All 1H-NMR spectra were recorded on Joel ECX 500 spectrometer operating at indicated frequencies. Typically, (10-30 mg) of compound dissolved in suitable deuterated solvents were used as standardized procedure. All spectra were recorded at room temperature and were analyzed with MestReNova software.

5.1.2 Dynamic light scattering (DLS)

For size analysis, DLS (scattering angle 173°) technique was used operated on Zetasizer Nano-ZS90 machine equipped with a He–Ne laser (λ = 633 nm) (Malvern Instruments, Herrenberg, Germany). For a typical measurement, samples of (1 mg/mL) concentration were used.

5.1.3 UV-VIS absorbance and fluorescence spectroscopy

Spectra were measured in 96-well plates using a Tecan Infinite M200Pro microplate reader.

5.1.4 FT-IR spectroscopy

Spectra were recorded as a film on diamond on a Nicolet Avatar 320 FT-IR operating from 4000 to 400 cm-1.

5.1.5 Transmission electron microscopy (TEM)

Samples for TEM were prepared on carbon-coated copper grids (300 mesh, Quantifoil). The nanogels were stained with uranyl acetate for better contrast. Visualization was performed using the TEM mode of the Hitachi Scanning Electron Microscope (SU8030) (20 kV). For an initial assessment of GSH-triggered degradation, nanogels were incubated for 24 h with 5×10^{-3} m GSH solution (in DI water, adjusted to pH 7.4).

5.1.6 Raman spectroscopy

Measurements were performed on the dry nanogels by using a modified OLYMPUSBX 41 microscope with a 100 standard (MPLN) objective. Raman excitation was carried out using a (532 nm) CW laser (Millennia, Spectra Physics). Detection is accomplished by a fibre-coupled (80 cm) DILOR XY800 spectrometer (HORIBA-JOBIN YVON, Bensheim, Germany) using three (1800 l mm-1) gratings in the subtractive mode along with a Synapse Si CCD-detector cooled to (-66 °C). The laser power was limited to (12 mW) to avoid laser-induced degradation of the samples. The spectral resolution of the Raman spectra was of the order of cm-1, using a 0.2 mm entrance slit.

5.2 Synthetic protocols

5.2.1 Materials

Cystamine dihydrochloride (96%), di-tert-butyl dicarbonate (98%), propiolic acid (95%), dicyclohexylcarbodiimide (99%), trifluoroacetic acid (TFA) (99%), methacryloyl chloride (97%, contains ~200 ppm monomethyl ether hydroquinone as stabilizer), methane sulfonyl chloride (99.7%), 2,2′-bipyridyl (99%), sodium L-ascorbate (98%), copper sulfate pentahydrate (98%),

aminoguanidine hydrochloride (98%), ammonium persulfate (APS) (98%), N,N,N',N' tetramethyl ethylenediamine (TEMED) (99%), N-isopropylacrylamide (NIPAM) (99%), N-ispropylmethacrylamide (NIPMAM) (97%), reduced glutathione (98%), L-cysteine (97%) and sodium dodecyl sulphate (SDS) (98%) were obtained from Sigma Aldrich, Germany. All organic solvents were purchased from Merck, Germany. Extra dry dimethylformamide (DMF, 99.8 %), triethylamine (TEA) (99%), and Rhodamine B (Rhod-B) (98%) were obtained from Fisher Scientific GmbH, Schwerte, Germany. Sephadex G-25 fine was obtained from GE healthcare, Germany. Dendritic polyglycerol (dPG) was obtained from Nanopartica GmbH, Germany. Dialysis membranes were obtained from Carl Roth, Germany. Etanercept (ETN) was purchased from Shanghai TheraMabs Biotechnology co., Ltd, China.

5.2.2 Synthesis of degradable linker (N-methacryloyl N'-propargyoxylcystamine, D)

The degradable linker was synthesized in 4 steps by using following synthetic procedures modifying synthetic method reported by Takeuchi and co-workers for the synthesis of a bifunctional cystamine based linker (Scheme S1).[51] Synthetic details for each step are given in supporting information (SI).

5.2.3 Synthesis of dPG-(RhodB)-azide

Azide functionalization of dPG was performed in two steps as described in Scheme S2 following reported methodology (details see SI).[82] Rhod-B labelled dPG-azide was synthesized through EDCI promoted coupling of Rhod-B to dPG-azide (details see SI).

5.2.4 Synthesis of degradable dPG-(S-S)-methacrylate using Cu(I) mediated alkyne-azide cycloaddition

The synthesis procedure (Figure 1A) was adopted from earlier reported literature.[83] dPG azide or Rhod-B-dPG azide (375 mg, 0.405 mmol N3 groups) was dissolved in (1 mL) milli-Q water followed by addition of copper sulfate (12.9 mg, 0.081 mmol, 0.2 eq.) and aminoguanidine hydrochloride (30 g, 0.405 mmol, 1 eq.) and slowly mixed with (4 mL) DMF solution of the degradable linker (125 mg, 0.486 mmol, 1.2 eq.) and 2,2' bipyridyl (25.3 mg, 0.162 mmol, 0.4 eq.). The reaction mixture was purged with argon for 30 min followed by addition of sodium ascorbate (32 mg, 0.162 mmol, 0.4 eq.). The reaction mixture changed the color to dark brown due to Cu(I) formation. The reaction was stirred at room temperature overnight followed by column purification using G-25 fine. Yield (260 mg). 1H-NMR (500 MHz, CDCl3), δ : 8.44 (b, 1H, triazole), 5.69 (s, 1H,C sephadex =CH2), 5.43 (s, 1H,C=CH2), 3.3-4.1 (m, dPG backbone, 5 H), 2.93 (b, 4H, NHCH2), 1.90 (s, 3H, CH3).

5.2.5 Synthesis of disulfide-containing nanogels

The synthesis of degradable nanogels was carried out by using precipitation polymerization [30, 31]. Briefly, (100 mg) of monomers (NIPAM and /or NIPMAM), dPG-(S-S)-methacrylate, SDS (1.8 mg, 6.2 µM), and APS (2.8 mg, 12.3 µM) were dissolved in (5 mL) of distilled water. Argon was bubbled into the reaction mixture for 30 min. Then, the reaction mixture was transferred into a hot bath at 70 °C and after 5 min polymerization was activated by addition of a catalytic amount of TEMED (0.75 µL, 0.582 mg, 5.01 µM). The mixture was stirred at 300 rpm for 3 h. The products were purified by dialysis (regenerated cellulose, molecular-weight cut-off 50 kDa) in water for 48 h and then lyophilized to yield the nanogels. Alternatively, nanogels with Rhod-B label were synthesized in similar manner as described above using Rhod-B labelled PG-(S-S)-methacrylate as cross-linker. Non-degradable analogues for each nanogel were synthesized as described previously.[30]

1H-NMR of PNIPAM-(S-S)-dPG nanogels: (400 MHz, D2O), (δ: 1.13), (s, 6H, isopropyl groups of NIPAM), 1.57 (2 H, polymer backbone), 2.00 (1 H, polymer backbone), 3.35-4.10 (6 H, polyglycerol scaffold protons + 1H NIPAM).

1H-NMR of PNIPAM-co-PNIPAM-(S-S)-dPG (Co-(S-S)-dPG) nanogels: (400 MHz, D2O), δ: 0.98 (s, 3 H, methyl group of NIPMAM), 1.15 (s, 6 H, isopropyl groups of NIPMAM), 1.78 (2 H, polymer backbone), 3.35 4.10 (6 H, polyglycerol scaffold protons + 1 H NIPMAM).

1H-NMR PNIPMAM-(S-S)-dPG nanogels: (400 MHz, D2O), δ: 1.13 (s, 6H, isopropyl groups of NIPAM), 1.57 (2 H, polymer backbone), 2.00 (1 H, polymer backbone), 3.35-4.10 (6 H, polyglycerol scaffold protons + 1H NIPAM).

5.2.6 Hydrogels

Hydrogels were synthesized at r.t. using same constituents as the corresponding nanogels but increasing overall monomer concentration to (100 mg/ml).

5.3 Particle characterization and assessment of particle – mucus interactions

5.3.1 Redox-mediated degradation study by DLS

Degradation profiles of the nanogels (at 1 mg/mL concentration) were assayed using time dependent size measurements by DLS post incubation with different reducing solutions and buffers of different pH. A Zetasizer Nano-ZS90 device equipped with a He–Ne laser (λ = 633 nm) (Malvern Instruments, Herrenberg, Germany) was used for these measurements.

5.3.2 Nanogel – mucus interaction

To investigate mucus-nanogel interactions, ex vivo studies were conducted on small intestines obtained from 4 - 6 months old male farm pigs sacrificed for research purposes (ethics votes: T 0264/15, T 0297/17). To harvest the native loose mucus layer, the jejunum was sectioned into 25 cm pieces, opened longitudinally and carefully rinsed with ice-cold PBS (pH 7.4) to remove food residues. The mucus was then gently scraped off and stored at -20 °C until further usage.[84]

5.3.3 Rheological studies

The isolated mucus (2 g) was incubated with (1 mg) of disulfide-containing or non-degradable control nanogels, solubilized in (20 µL) PBS. Mucus incubated with (20 µL) PBS served as reference. Dynamic oscillation tests were performed on a Kinexus lab+ rotational rheometer (Malvern instruments Ltd, UK) using parallel upper plate geometry of 40 mm diameter and a gap width set to (0.4 mm at 25 °C). Initially, an amplitude sweep was carried out to determine the viscoelastic linear region for the reference mucus sample. Shear strain was applied in a range of (0.01-10%) at (1 Hz). Directly after mucus exposure to the nanogels, the frequency sweep for each sample was carried out from (30 - 0.01 Hz) controlled by auto shear strain value within the viscoelastic range. The viscous (G″) and elastic (G′) moduli were recorded. The changes on both elastic and viscous behavior of the mucus gel were determined before and after treatment with the NPs according to previous publications.[85] Additionally, a time dependent measurement was performed at a constant frequency and strain (1 Hz, 0.5%) to monitor the changes in the viscoelastic behavior of the mucus gel with and without NPs within the shear independent plateau. Here, changes in complex modulus (G*) and phase angle (δ*) were recorded upon mixing the nanogels with the mucus (every 5 seconds over 30 min) and complex viscosity (η*) was obtained. Each measurement was performed at least three times using each time mucus gel from a different animal.

5.3.4 Mucus-related biodegradation assessed by GPC

The Rhod-B labeled nanogels PNIPMAM-(S-S)-dPG and PNIPMAM-dPG were incubated (5 mg of each) with (100 mg) isolated mucus in a total volume of (1 mL) PBS solution (pH 7.4) for up to 24 h at 37 C, followed by ultracentrifugation at (16,100 × g) for (30 min). Supernatants were then collected, shock-frozen in liquid nitrogen and lyophilized at (-80 °C) with (0.1 mbar). GPC studies were conducted on a Shimadzu Prominenze-i LC-2030 liquid chromatography system (Shimadzu, Japan). The lyophilized samples were dissolved in (1 mL) mobile phase (PBS, pH 7.4), filtered through (0.45 µm) filters (Minisart® with polyethersulfone (PES) membrane, Satorius GmbH, Germany) before (50 µL) were injected and analyzed with a flow rate of (1 mL/min). Shodex OHpak SB-806M HQ column was used with OHpak SB-G 6B as guard pre-column. The columns were operated at r.t. with the UV-visible detector at a

wavelength of (567 nm). Pure mucus and labeled nanogels served for control. In parallel, a GSH related degradation profile was determined for both nanogels at different GSH concentrations (5 – 100 mM) and incubation time points (up to 48 h).

5.3.5 Mucopenetration studies

Mucopenetration of the nanogels was investigated using a Franz cell setup.[86] Upon the animals' sacrifice, the freshly excised jejunum was cut-open, rinsed and immediately transferred to the lab using ice-cold oxygenated KRB (pH 7.4).[87, 88] Intestinal punches (diameter: 15-16 mm) were then placed onto the acceptor chamber, which was filled with (12 mL) oxygenated KRB. After 10 min equilibration at 37 °C, (50 µL) of (10 mg/mL) Rhod-B labelled nanogels were applied onto the intestinal punches topically. After 1 h and 3 h, the biopsies were removed, and their surface was gently rinsed with PBS. The punches were then snap frozen in liquid nitrogen. Untreated tissue punches served as control. cryo-sections of (5 µm) thickness were obtained using a CM1510 S Cryotome (Leica Biosystems, Nussloch Germany). Afterwards, the tissue sections were fixed with (4%) paraformaldehyde (Roti® Histofix 4%, Carl Roth GmbH, Karlsruhe, Germany), mounted with DAPI mounting solution (Roti®-Mount FluorCare DAPI, Carl Roth GmbH, Karlsruhe, Germany), and visualized using a BZ-8000 fluorescence microscope (Keyence, Germany) with an objective (20×/0.75), zoom 10×, Plan-Apo, DIC N2 lens (Nikon, Japan).

Additionally, the mucopenetrating properties of the nanogels were determined in human-based models of the bronchial epithelium. For model generation, (6.3 × 105) primary human lung fibroblasts (Lonza, Switzerland) were embedded in bovine collagen-I mimicking the bronchial epithelial matrix. Subsequently, (6.3 × 105) primary human bronchial epithelial cells were seeded on top. 24 h later, the 12 well-constructs were lifted to the air-liquid interface and further cultivated for 21 days. Subsequently, (13 µL) nanogels (10 mg/mL) were topically applied. After 3 and 6 h, the models were harvested and cryo-preserved as previously explained for subsequent histological and immunofluorescence analyses.

5.4 Cytocompatibility of the nanogels

5.4.1 Cytotoxicity assays

Colorectal epithelial Caco2 cells (ATCC® HTB37™, ATCC, USA), vaginal epithelial VK2 cells (ATCC CRL-2616, ATTC, USA), and ectocervical epithelial Ect1 cells (ATCC CRL-2614, ATCC, USA) were used to assess the cytotoxicity of the nanogels by MTT assay.[89] Caco2 cells were cultured in minimum essential medium (Gibco/ Fisher Scientific GmbH, Germany) supplemented with 20% fetal bovine serum (FBS) (Biochrom, Germany), 1% MEM non-essential amino acids solution 100x (Sigma Aldrich, Germany) and 1% sodium pyruvate

(Gibco/ Fisher Scientific GmbH, Germany). Whereas keratinocyte-serum free medium (K-SFM) (Gibco/ Thermo Fisher Scientific, USA) supplemented with (0.1 ng/mL) human recombinant epidermal growth factor (EGF) and (0.05 mg/mL) bovine pituitary extract served as a culture medium for VK2 and Ect1 cells. Cells were seeded into 96 well-plates (1×104 cells/well). The nanogels were then added 24 h later at final concentrations of (1, 2.5, 5 mg/mL). Following 24 h and 48 h, respectively, MTT stock solution (5 mg/mL) was diluted in the cell medium (1:10) and the plates were further incubated at 37 °C for 4 h. Afterwards, the supernatant was discarded, and the formed formazan salt was solubilized in (50 µL/well) dimethyl sulfoxide (DMSO). Optical density (OD) was measured at 570 nm with FLUOstar plate-reader (OPTIMA BMG LABTECH GmbH, Germany). Cells treated with (0.005%) SDS served as positive control.

In addition, human buffy coats from healthy donors (German red-cross blood donation center: Deutsches Rotes Kreuz, Germany; ethical approval EA1/227/14) were centrifuged with a NycoPrep 1.077™ sugar density gradient (Axis-Shield PoC AS, Norway) to separate peripheral blood mononuclear cells (PBMCs). Monocytes were selected from PBMCs by semi-adherence and were then differentiated into macrophages over 6 days in RPMI 1640 supplemented with 10% heat-inactivated FBS, (2 mM) L-glutamine, (1%) penicillin/streptomycin, and (20 ng/mL) macrophage-colony stimulating factor (M-CSF) (Miltenyi Biotech, Germany). Subsequently, necrosis and apoptosis of primary macrophages before and after 24 h exposure to (1 mg/mL) nanogels was assessed by double staining against Annexin V-FITC/ propidium iodide (PI). Apoptotic and necrotic cells were identified by CytoFLEX flow cytometry (Beckman Coulter GmbH, Germany). Macrophages treated with (5% DMSO) for 3 h and 24 h respectively served as positive controls.

5.4.2 Cellular uptake

Nanogel uptake by primary human macrophages was investigated by flow cytometry. Here, Rhod-B labeled nanogels were at (1 mg/ml) final concentration incubated with (1 × 105) macrophages for 3 h at 37 °C and at 4 °C in parallel to inhibit active endocytosis processes. Afterwards, the cells were collected and transferred to FACs tubes (BD Falcon™, Germany) then rinsed repeatedly (3 × ice cold PBS-EDTA) to eliminate remaining fluorescent particles. The cells were then resuspended in FACs buffer (PBS-EDTA + 0.5% BSA) and fluorescence intensity of the cells was then measured (10,000 cells/sample) by CytoFLEX flow cytometer (Beckman Coulter GmbH, Germany). Untreated cells served as negative control.

5.5 ETN encapsulation, protein integrity and release studies

5.5.1 Encapsulation of Etanercept

Protein encapsulation was studied using etanercept (ETN; Shanghai TheraMabs Biotechnology, China). To encapsulate ETN in the nanogels, dry nanogels were swollen in a solution of ETN (1 mg/mL, pH 7.4, PBS) for at least 24 h at 6 - 8 °C. The solutions were purified by centrifugation (10 min at 6000 rpm: Sartorius AG, Germany) using vivaspin (300 kDa cut-off). The concentration of encapsulated ETN was determined by Bradford assay according to standard procedure.[90]

Encapsulation efficiency is calculated using following equation:

$$EE[\%] = \frac{m\,(ETN_{init.}) - m\left(ETN_{free}\right)}{m\,(ETN_{init}\,)} * 100$$

5.5.2 Protein stability after encapsulation and release from the nanogels

The secondary structure of ETN was analyzed by circular dichroism measurements as surrogate parameter for ETN stability after encapsulation and release from the nanogels. Protein solutions containing nanogels were background corrected by the corresponding nanogel solution without proteins. To verify ETN activity after loading and release, its ability to bind to TNFα was tested using Etanercept ELISA kit (Tani Medicals, Turkey). ETN was tested at a concentration of (150 ng/mL) in a TNFα pre-coated 96-well plate. The assay was conducted according to manufacturer's instructions. The obtained values were normalized to the TNFα binding capacity of a freshly prepared ETN solution.

5.5.3 ETN Release and Activity

PNIPMAM-(S-S)-dPG and PNIPMAM-dPG nanogels were loaded with ETN as described above. Afterwards, they were incubated with (0.5 mM, 2 mM) GSH solutions, or PBS for up to 24 h. After 4 h, 8 h, and 24 h, the released ETN was separated from the nanogels using vivaspin devices (cut-off 300kDa, centrifugation 10 min at 6,000 rpm) allowing ETN to go through while holding back the nanogels. Quantification of active ETN was performed using the Etanercept ELISA IG-AA102 (ImmunoGuide, Ankara, Turkey) according to the manufacturer's instructions. Overall protein release was quantified using Bradford assay according to standard protocols.[90]

5.6 Anti-inflammatory efficacy of ETN loaded nanogels in inflammatory intestinal models

EpiIntestinal-FT™ tissue models (MatTek, USA) were used to mimic characteristics of IBD in vitro. To induce the inflammation, (40 ng/mL) recombinant TNFα and (5 ng/mL) IFNɣ were added to the culture medium of the intestinal models over seven days. Subsequently, the

models were topically treated with either ETN solution (in PBS, 20 µg/cm2) or ETN loaded onto disulfide-containing and control nanogels (20 µg/cm2 in 200 µg/cm2 nanogels) at day 2 and 4 after the induction of the inflammation. Normal intestinal models and untreated inflammation models served as control.

Aiming to monitor the epithelial barrier integrity of the intestinal models, the transepithelial electrical resistance (TEER) was determined every 24 h for 4 days after the induction of inflammation using a Millicell-ERS (Electrical Resistance System; Millipore GmbH, Schwalbach, Germany).

5.6.1 ELISA.

Medium samples of (200 µL) were collected from the wells of the intestinal models and replaced with fresh medium following 24 h of each medium change (every 48 h) over seven days. Subsequently, the secretion of IL-6 and IL-8 were assessed using Human IL-6 ELISA kit, and Human IL-8 ELISA kit according to the manufacturer's instructions (Invitrogen™, Germany).

5.6.2 Immunohistochemistry (IHC)

For IF analysis, paraffine blocks were sectioned using a microtome (Zeiss HYRAX M40, MICROM GmbH, Germany). The dry tissue sections were deparaffinized in Roti®-Histol (Carl Roth GmbH, Germany) and rehydrated with PBS. For antigen retrieval, a buffer of citraconic anhydride (0.05%) with pH 7.4 was freshly prepared and heated for 45 min with the slides at 95-98 °C. Afterwards, sections were permeabilized with 0.5% (v/v) Triton X-100, rinsed again in 1% BSA in PBST, blocked with goat serum and incubated overnight at 4 °C with primary monoclonal antibodies against occludin and claudin-2. Subsequently, the secondary antibody was added for 1 h at r.t. Sections only stained with the secondary antibody served as negative controls. Slides were then rinsed, mounted using antifading DAPI mounting solution (Roti®-Mount FluorCare DAPI, Carl Roth GmbH, Germany) and stored in the dark at 4 °C until visualization. Fluorescence images were captured using BZ-8000 fluorescence microscopy (Keyence, Germany) equipped with a special oil lens to visualize the tight junctions in EpiIntestinal-FT™ models (Objective 60×/1.40 Oil, zoom 30×, Plan-Apo, VC, Nikon, Japan). For histological analysis, H&E and Alcian Blue staining were performed according to standard protocols.

5.6.3 Western blot.

To quantify the protein expression in the intestinal model, the tissues were lysed in tris-based radioimmunoprecipitation assay buffer (pH 7.4) for 15 min on ice, followed by centrifugation

(12,000×g, 15 min, 4 °C). The total protein content was determined using a bicinchoninic acid (BCA) protein assay kit (Thermo Fisher Scientific, USA). Samples were heated in SDS-page loading buffer supplemented with (100 mM) DTT at (95 °C, 5 min). Protein sample of (10 µg) were then loaded into 10% polyacrylamide gel and separated by electrophoresis (60 min at 150 V). After preparing the sandwich and proteins transfer to the PVDF membranes (Bio-Rad, USA), 5% skimmed milk powder (Carl Roth GmbH, Germany) in TBST was used to block the membranes before further incubation with the primary antibody (1:1,000) over night at 4 °C. Subsequently, the membranes were incubated with anti-mouse horseradish peroxidase conjugated secondary antibodies for 1 h at r.t. Chemiluminescence signals were detected by a ChemiDoc device (Bio-Rad, USA). Quantification was done by the Image Lab Software (Bio-Rad, USA). Data were normalized to β-actin as the standard protein. (Table 2) lists the primary and secondary antibodies used here.

Table 2. Antibodies for Western blot analysis

Antibodies	Type	Dilution	Company
Mouse anti-occludin	Primary, monoclonal	1:1,000	Thermo Fisher Scientific
Mouse anti-claudin-2	Primary, monoclonal	1:1,000	Thermo Fisher Scientific
Mouse-anti β-actin	Primary, monoclonal	1:5,000	Sigma Aldrich
HRP anti-mouse IgG	Secondary	1:2,000	Thermo Fisher Scientific

5.7 Anti-inflammatory efficacy of ETN loaded nanogels in bronchial epithelial models

Human bronchial 3D models were cultivated as previously mentioned above for 21 days. Three days before applying the ETN loaded nanogels, the models were rinsed by PBS to imitate the mucocilliary clearance of shed cells and induce new mucus secretion. Afterwards, (17 µl) of loaded nanogels were applied to each model as (10 mg/ml) NGs-solution containing (0,7mg/ml) ETN. Models treated with (17 µl nanogels of 0.7 mg/ml ETN) and ETN solution (0.7 mg/ml) as a control. Following 6 hours, all models were removed from culture and cryo-preserved as previously explained for subsequent immunofluorescence analyses. Cryosections of (5 µm) were obtained as beforehand mentioned. To visualize Etanercept (ETN) the sections were incubated overnight at 4 °C with the primary monoclonal antibody against IgG1_FC part in ETN (ab1927, Abcam, UK), dilution (1:500). Thereafter, the Alexa Fluor®-488 conjugated secondary antibody of goat Anti-mouse IgG H&L (ab150113, Abcam, UK), dilution (1:1,000) was applied 1 h in the dark at r.t. and the slides were eventually mounted with DAPI mounting solution (Roti®-Mount FluorCare DAPI, Carl Roth GmbH, Germany),

sealed and left to dry at 4° C in the dark. Visualisation deployed BZ-8000 fluorescence microscopy (Keyence, Germany) equipped with a suitable lens (objective 20×/0.75, zoom 20×, Plan-Apo, DIC N2, Nikon, Japan).

5.8 Statistics

Data are depicted as mean ± SEM. Statistical analysis was performed by one-way analysis of variance (ANOVA) with Bonferroni-Holm post-test. Differences were considered statistically significant at (*$p \leq 0.05$, **$p \leq 0.01$ and ***$p \leq 0.001$). Cytotoxicity experiments were repeated three times with quadruplicates for each test sample. Data was normalized against the untreated control. Macrophage experiments were repeated three times including relevant negative controls for each condition. GPC measurements were performed using freshly isolated mucus from 4 different healthy farm pigs (normal nutrition, no special diet). Mucopenetration studies were performed in duplicates using the jejunum from 3 different healthy animals and 2 different donors of human-based bronchial epithelial models. Two batches of EpiIntestinal-FT™ tissue models and 3 of human-based bronchial epithelial models were tested for etanercept (ETN) delivery using duplicates for each test condition.

Supporting Information

Supporting Information is available from the authors.

Acknowledgements

We gratefully acknowledge the financial support of the German academic exchange service (DAAD) for the PhD scholarship for R. Charbaji (funding program 57129429) as well as financial support of the MINECO project RTI2018-099227-B-I00 and the NanoMedicines Innovation Network (NMIN), Vancouver, Canada and the Mitacs Accelerate Grant (IT19059, S. Hedtrich). We also thank S. Thierbach for the help with Raman spectroscopy, E. O. Blanco for support with DLS measurements, as well as professor J. R. Aschenbach and the research teams at the Veterinarian Physiology of the Freie Universität Berlin for their support on this project. A special thanks goes to the technical assistants Mrs. S. Trappe and Mrs. K. Söllig for their support during TEER measurements and western blot.

Conflict of Interests

The authors declare no conflict of interests.

References

1. R.A. Cone, Adv Drug Deliv Rev 2009, 61(2): p. 75.

2. S.K. Lai, Y.-Y. Wang, D. Wirtz, and J. Hanes, Adv Drug Deliv Rev 2009, 61(2): p. 86.

3. M. Krukemeyer, V. Krenn, F. Huebner, W. Wagner, and R. Resch, J Nanomed & Nanotech 2015, 6(1).

4. H.M. Yildiz, C.A. McKelvey, P.J. Marsac, and R.L. Carrier, J Drug Target 2015, 23(78): p. 768.

5. M. Boegh and H.M. Nielsen, Basic Clin Pharmacol Toxicol 2015, 116(3): p. 179.

6. K. Netsomboon and A. Bernkop-Schnurch, Eur J Pharm Biopharm 2016, 98: p. 76.

7. F. Laffleur, F. Hintzen, G. Shahnaz, D. Rahmat, K. Leithner, and A. Bernkop-Schnürch, Nanomedicine 2014, 9(3): p. 387.

8. S.S. Olmsted, J.L. Padgett, A.I. Yudin, K.J. Whaley, T.R. Moench, and R.A. Cone, Biophys J 2001, 81(4): p. 1930.

9. I. Pereira de Sousa, B. Cattoz, M.D. Wilcox, P.C. Griffiths, R. Dalgliesh, S. Rogers, and A. Bernkop-Schnurch, Eur J Pharm Biopharm 2015, 97(Pt A): p. 257.

10. C. Muller, G. Perera, V. Konig, and A. Bernkop-Schnurch, Eur J Pharm Biopharm 2014, 87(1): p. 125.

11. B.M. Boddupalli, Z.N. Mohammed, R.A. Nath, and D. Banji, J Adv Pharm Technol Res 2010, 1(4): p. 381.

12. S.K. Ramineni, T.D. Dziubla, L.L. Cunningham, and D.A. Puleo, Oral Surg. Oral Med. Oral Pathol. Oral Radiol 2014, 118(6): p. 665.

13. M.S. Ali and J.P. Pearson, Laryngoscope 2007, 117(5): p. 932.

14. M.E. Johansson, H. Sjovall, and G.C. Hansson, Nat Rev Gastroenterol Hepatol 2013, 10(6): p. 352.

15. S.K. Lai, Y.-Y. Wang, and J. Hanes, Adv Drug Deliv Rev 2009, 61(2): p. 158.

16. Y.-Y. Wang, S.K. Lai, C. So, C. Schneider, R. Cone, and J. Hanes, PLoS One 2011, 6(6): p. e21547.

17. O. Lunov, T. Syrovets, C. Loos, J. Beil, M. Delacher, K. Tron, G.U. Nienhaus, A. Musyanovych, V. Mailander, and K. Landfester, ACS Nano 2011, 5(3): p. 1657.

18. D.L. Sellers, T.H. Kim, C.W. Mount, S.H. Pun, and P.J. Horner, Biomaterials 2014, 35(31): p. 8895.

19. S. Oh and S. Borros, Colloids Surf B Biointerfaces 2016, 147: p. 434.

20. G. Shahnaz, A. Vetter, J. Barthelmes, D. Rahmat, F. Laffleur, J. Iqbal, G. Perera, W. Schlocker, S. Dunnhaput, P. Augustijns, and A. Bernkop-Schnurch, Int J Pharm 2012, 428(1-2): p. 164.

21. L. Yin, J. Ding, C. He, L. Cui, C. Tang, and C. Yin, Biomaterials 2009, 30(29): p. 5691.

22. J.C. Cuggino, E.R.O. Blanco, L.M. Gugliotta, C.I. Alvarez Igarzabal, and M. Calderon, J Control Release 2019, 307: p. 221.

23. E. Fleige, M.A. Quadir, and R. Haag, Adv Drug Deliv Rev 2012, 64(9): p. 866.

24. A.V. Kabanov and S.V. Vinogradov, Angew Chem Int Ed Engl 2009, 48(30): p. 5418.

25. M. Molina, M. Asadian-Birjand, J. Balach, J. Bergueiro, E. Miceli, and M. Calderon, Chem Soc Rev 2015, 44(17): p. 6161.

26. S. Mura, J. Nicolas, and P. Couvreur, Nat Mater 2013, 12(11): p. 991.

27. A.J. Sivaram, P. Rajitha, S. Maya, R. Jayakumar, and M. Sabitha, WIREs Nanomed Nanobiotechnol 2015, 7(4): p. 509.

28. K.S. Soni, S.S. Desale, and T.K. Bronich, J Control Release 2016, 240: p. 109.

29. M. Giulbudagian, G. Yealland, S. Honzke, A. Edlich, B. Geisendorfer, B. Kleuser, S. Hedtrich, and M. Calderon, Theranostics 2018, 8(2): p. 450.

30. L.E. Theune, R. Charbaji, M. Kar, S. Wedepohl, S. Hedtrich, and M. Calderon, Mater Sci Eng C Mater Biol Appl 2019, 100: p. 141.

31. M. Witting, M. Molina, K. Obst, R. Plank, K.M. Eckl, H.C. Hennies, M. Calderon, W. Friess, and S. Hedtrich, Nanomedicine 2015, 11(5): p. 1179.

32. M. Molina, S. Wedepohl, E. Miceli, and M. Calderón, Nanomedicine 2017, 12(2): p. 117.

33. G.N. Rimondino, E. Miceli, M. Molina, S. Wedepohl, S. Thierbach, E. Ruhl, M. Strumia, M. Martinelli, and M. Calderon, J Mater Chem B 2017, 5(4): p. 866.

34. M. Calderon, M.A. Quadir, S.K. Sharma, and R. Haag, Adv Mater 2010, 22(2): p. 190.

35. B. Chatterjee, N. Amalina, P. Sengupta, and U.K. Mandal, J App Pharm Sci 2017, 7(5): p. 195.

36. F. Hatahet, V.D. Nguyen, K.E. Salo, and L.W. Ruddock, Microb Cell Fact 2010, 9: p. 67.

37. A. Meister and M.E. Anderson, Ann. Rev. Biochem 1983, 52(1): p. 711.

38. S. Singh, F. Topuz, K. Hahn, K. Albrecht, and J. Groll, Angew Chem Int Ed Engl 2013, 52(10): p. 3000.

39. Y. Li, D. Maciel, J. Rodrigues, X. Shi, and H. Tomas, Chem Rev 2015, 115(16): p. 8564.

40. Z. Shatsberg, X. Zhang, P. Ofek, S. Malhotra, A. Krivitsky, A. Scomparin, G. Tiram, M. Calderon, R. Haag, and R. Satchi-Fainaro, J Control Release 2016, 239: p. 159.

41. D. Steinhilber, A.L. Sisson, D. Mangoldt, P. Welker, K. Licha, and R. Haag, Adv Funct Mater 2010, 20(23): p. 4133.

42. H.Q. Wu and C.C. Wang, Langmuir 2016, 32(25): p. 6211.

43. M. Kar, L. Fechner, G. Nagel, E. Glitscher, G. Noe Rimondino, and M. Calderón, in Nanogels for Biomedical Applications. 10.1039/9781788010481-00210, The Royal Society of Chemistry 2018, Ch. 12.

44. S. Li, J. Zhang, C. Deng, F. Meng, L. Yu, and Z. Zhong, ACS Appl Mater Interfaces 2016, 8(33): p. 21155.

45. Y. Tian, S. Bian, and W. Yang, Polym Chem 2016, 7(10): p. 1913.

46. Y. Tian, Y. Wang, S. Shen, X. Jiang, Y. Wang, and W. Yang, Part Part Syst Charact 2015, 32(12): p. 1092.

47. M.L. Circu and T.Y. Aw, Free Radic Res 2011, 45(11-12): p. 1245.

48. M. Liu, J. Zhang, W. Shan, and Y. Huang, Asian Journal of Pharmaceutical Sciences 2015, 10(4): p. 275.

49. P.I. Chater, M.D. Wilcox, and J.P. Pearson, Adv Drug Deliv Rev 2018, 124: p. 184.

50. X. Murgia, B. Loretz, O. Hartwig, M. Hittinger, and C.M. Lehr, Adv Drug Deliv Rev 2018, 124: p. 82.

51. Y. Suga, H. Sunayama, T. Ooya, and T. Takeuchi, Chem Commun (Camb) 2013, 49(76): p. 8450.

52. S. Duggan, W. Cummins, O.D. O, H. Hughes, and E. Owens, Eur J Pharm Sci 2017, 100: p. 64.

53. B. Srinivasan, A.R. Kolli, M.B. Esch, H.E. Abaci, M.L. Shuler, and J.J. Hickman, J Lab Autom 2015, 20(2): p. 107.

54. C.T. Capaldo, A.E. Farkas, R.S. Hilgarth, S.M. Krug, M.F. Wolf, J.K. Benedik, M. Fromm, M. Koval, C. Parkos, and A. Nusrat, Mol Biol Cell 2014, 25(18): p. 2710.

55. J. Konig, J. Wells, P.D. Cani, C.L. Garcia-Rodenas, T. MacDonald, A. Mercenier, J. Whyte, F. Troost, and R.J. Brummer, Clin Transl Gastroenterol 2016, 7(10): p. e196.

56. A.M. Marchiando, L. Shen, W.V. Graham, C.R. Weber, B.T. Schwarz, J.R. Austin, 2nd, D.R. Raleigh, Y. Guan, A.J. Watson, M.H. Montrose, and J.R. Turner, J Cell Biol 2010, 189(1): p. 111.

57. M.H. Smith, E.S. Herman, and L.A. Lyon, J Phys Chem B 2011, 115(14): p. 3761.

58. M. Kar, Y.R. Vernon Shih, D.O. Velez, P. Cabrales, and S. Varghese, Biomaterials 2016, 77: p. 186.

59. G.A. Duncan, J. Jung, J. Hanes, and J.S. Suk, Mol Ther 2016, 24(12): p. 2043.

60. J. Witten, T. Samad, and K. Ribbeck, Curr Opin Biotechnol 2018, 52: p. 124.

61. T.M. Hagen, G.T. Wierzbicka, B.B. Bowman, T. Aw, and D.P. Jones, Ameri J Physio 1990, 259(4): p. G530.

62. P.S. Samiec, L.J. Dahm, and D.P. Jones, Toxicol Sci 2000, 54(1): p. 52.

63. E.E. Hassan and J.M. Gallo, Pharm Research 1990, 7(5): p. 491.

64. S. Rossi, F. Ferrari, M.C. Bonferoni, and C. Caramella, Eur J Pharm Sci 2001, 12(4): p. 479.

65. J. Barthelmes, S. Dünnhaupt, S. Unterhofer, G. Perera, W. Schlocker, and A. Bernkop-Schnürch, Nanomedicine 2013, 8(1): p. 65.

66. P. Nejdfors, M. Ekelund, B. Jeppsson, and B.R. Westrom, Scand J Gastroenterol 2000, 35(5): p. 501.

67. A. Ziegler, L. Gonzalez, and A. Blikslager, Cell Mol Gastroenterol Hepatol 2016, 2(6): p. 716.

68. R. Nunes, C. Silva, and L. Chaves, in Concepts and Models for Drug Permeability Studies, Eds. B. Sarmento, Woodhead Publishing, UK 2016, Ch. 4.2.

69. H.H. Gustafson, D. Holt-Casper, D.W. Grainger, and H. Ghandehari, Nano Today 2015, 10(4): p. 487.

70. S.O. Adegbola, K. Sahnan, J. Warusavitarne, A. Hart, and P. Tozer, Int J Mol Sci 2018, 19(8).

71. N. Scheinfeld, J Dermatolog Treat 2004, 15(5): p. 280.

72. M. Barnett and A. Fraser, in Ulcerative Colitis–Treatments, Special Populations and the Future, Vol. 2, Eds. M. O'connor, InTech: Rijeka, Croatia 2011, Ch. 10.

73. G. Kolios, C.O. Gastroenter 2016, 32(4): p. 251.

74. J.A. Jiminez, T.C. Uwiera, G. Douglas Inglis, and R.R. Uwiera, Gut Pathog 2015, 7: p. 29.

75. H. Laroui, S.A. Ingersoll, H.C. Liu, M.T. Baker, S. Ayyadurai, M.A. Charania, F. Laroui, Y. Yan, S.V. Sitaraman, and D. Merlin, PloS one 2012, 7(3).

76. T.L. Nguyen, S. Vieira-Silva, A. Liston, and J. Raes, Dis Model Mech 2015, 8(1): p. 1.

77. A. Geremia, P. Biancheri, P. Allan, G.R. Corazza, and A. Di Sabatino, Autoimmunity Rev 2014, 13(1): p. 3.

78. J. Mankertz and J.-D. Schulzke, C.O. Gastroenter 2007, 23(4): p. 379.

79. Y. Chen, Y. Lin, K.M. Davis, Q. Wang, J. Rnjak-Kovacina, C. Li, R.R. Isberg, C.A. Kumamoto, J. Mecsas, and D.L. Kaplan, Sci Rep 2015, 5: p. 13708.

80. J.K. Gustafsson, A. Ermund, M.E. Johansson, A. Schutte, G.C. Hansson, and H. Sjovall, Am J Physiol Gastrointest Liver Physiol 2012, 302(4): p. G430.

81. P. Pietzonka, E. Walter, S. Duda-Johner, P. Langguth, and H.P. Merkle, Eur J Pharm Sci 2002, 15(1): p. 39.

82. S. Roller, H. Zhou, and R. Haag, Mol Divers 2005, 9(4): p. 305.

83. M. Kar, N. Tiwari, M. Tiwari, M. Lahiri, and S.S. Gupta, Part Part Syst Charact 2013, 30(2): p. 166.

84. J. Rohrer, A. Partenhauser, S. Hauptstein, C.M. Gallati, B. Matuszczak, M. Abdulkarim, M. Gumbleton, and A. Bernkop-Schnurch, Eur J Pharm Biopharm 2016, 98: p. 90.

85. C. Taylor, A. Allen, P.W. Dettmar, and J.P. Pearson, Biochim Biophys Acta 2004, 1674(2): p. 131.

86. A.B. Dezani, T.M. Pereira, A.M. Caffaro, J.M. Reis, and C.H. Serra, J Pharmacol Toxicol Methods 2013, 67(3): p. 194.

87. P. Annaert, J. Brouwers, A. Bijnens, F. Lammert, J. Tack, and P. Augustijns, Eur J Pharm Sci 2010, 39(1-3): p. 15.

88. L.L. Clarke, Am J Physiol Gastrointest Liver Physiol 2009, 296(6): p. G1151.

89. T. Mosmann, J Immunol Methods 1983, 65(1): p. 55.

90. M.M. Bradford, Analytical Biochemistry 1976, 72(1–2): p. 248.

3.2.2 Supporting Information

Synthesis of disulfide-containing linker (D) in four steps according to Scheme S1.

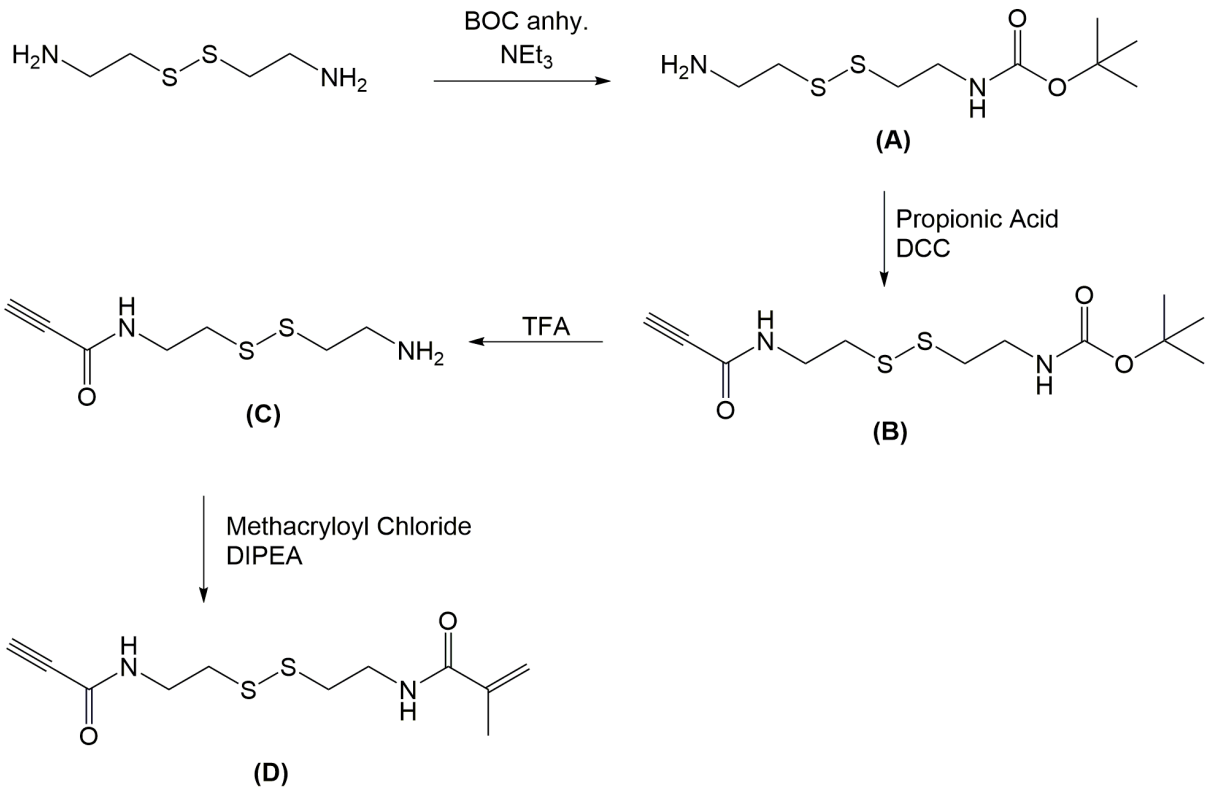

Scheme S1. Synthetic procedure of the degradable cystamine based linker end-functionalized with methacryl and alkyne group.

Synthesis of N-tert-butoxycarbonyl cystamine (A). The synthetic procedure followed an earlier published report.[51] Briefly, cystamine dihydrochloride (5 g, 22.2 mmol) and triethylamine (9.3 mL, 66.6 mmol) were dissolved in methanol (50 mL) and cooled in an ice bath. Into the reaction mixture ice cold methanolic solution (20 mL) of di-tert-butyl dicarbonate (2.42 g, 11.1 mmol) was added. The reaction mixture was then stirred for 6 h at 0 °C, after which the solution was dried under reduced pressure. (1 M) sodium dihydrogen phosphate was added to the white residue and the solution was washed with diethyl ether (20 mL, 3 times) to remove N,N'-di-tert-butoxycarbonyl-cystamine. The aqueous solution was adjusted to pH 9 by addition of (5 M) NaOH while stirring, followed by extraction with ethyl acetate (20 mL, 3 times). To the combined organic phases, (5 g) anhydrous sodium sulfate was added and the solution was dried under reduced pressure. The resulting yellow oil was dried overnight in vacuum to yield N-tert- butoxycarbonyl cystamine (A). Yield: (2.1 g) (37.5%). TLC: Rf 0.35 (MeOH).

1H-NMR (400 MHz, CDCl3): δ = 5.04 (b, 1H, NH-Boc), 3.41 (q, 2H, C(=O)-NHCH2), 2.98 (t, 2H, CH2NH2), 2.75 (q, 4H, CH2SSCH2), 1.41 (s, 9H, CH3).

Synthesis of N'-propargyoxylcystamine (C). N'-propargyoxylcystamine was synthesized by following previously reported literature.[51] To a stirred solution of dicyclohexylcarbodiimide (1.8 g, 8.72 mmol) in 20 mL of anhydrous dichloromethane, under argon, at 0 °C, propiolic acid (0.51 mL, 8.32 mmol) was added. After 10 min, N-tert-butyloxycarbonyl cystamine (A) (2 g, 7.92 mmol) dissolved in (20 mL) of anhydrous dichloromethane (DCM) was added dropwise and the resulting mixture stirred for 1 h at 0 °C and for 1 h at r.t.

The mixture was then filtered, and the solution was evaporated under reduced pressure. The crude product was purified by flash chromatography on silica gel using as eluent ethyl acetate/hexane (1:1). The obtained pure compound (B) (2.1 g, yield 87%) was concentrated in reduced pressure and used immediately for the next step without further characterization. The compound (B) was dissolved in 20 mL of DCM and cooled to 0 °C. TFA (10 mL) was added and the mixture was stirred until only a single spot was obtained on TLC. Upon completion, the reaction mixture was dried using vacuum, mixed with Milli-Q water (10 mL, 3 times) and dried over vacuum to remove the residual TFA from the obtained compound N'-propargyoxylcystamine (C) as trifluoroacetate salt in high purity. The obtained compound was immediately used for next step without any characterizations.

Synthesis of N-methacryloyl N'-propargyoxylcystamine (D). N'-propargyoxylcystamine (C) (1 g, 3.14 mmol) and N,N'-diisopropylethylamine (1 mL, 6.28 mmol) were dissolved in anhydrous DCM (20 mL), cooled on ice and followed by addition of methacryloyl chloride (0.399 mL, 4.08 mmol) solution in anhydrous DCM (10 mL). The reaction mixture was stirred for 24 h at 0°C, after which the reaction solution was washed with brine. The organic phase was evaporated and purified by silica gel column chromatography using ethyl acetate/hexane (1:1). Purified compound (D) was concentrated under reduced pressure and dried overnight under high vacuum yielding a yellow solid (0.76 g, 89.5%). TLC: Rf 0.4 (ethyl acetate: hexane = 1:1). 1H- NMR (400 MHz, CDCl3): δ = 6.93 (b, 1H, C(=O)-NH), 6.39 (C(=O)-NH), 5.75 (s, 1H,C=CH2), 5.37 (s, 1H,C=CH2), 3.64 (t, 4H, CH2S-S-CH2), 2.87 (t, 4H, NHCH2), 2.81 (s, 1H, HC≡C), 1.97 (s, 3H, CH3).

Synthesis of mesylated dPG (E). Mesylated dPG was obtained by dissolving dry dPG (1 g, 13.5 mmol OH groups, 10% OH's groups = 1 eq.) and TEA (374 µl, 2.7 mmol, 2 eq.) in anhydrous DMF (20 mL). The reaction mixture was cooled on ice followed by addition of methanesulfonyl chloride (115 µl, 1.49 mmol, 1.1 eq.). The reaction mixture was stirred for 5 h at r.t. and then dried using reduced pressure. Purification was done by dialysis in methanol using 1 kDa molecular weight cut off (MWCO) membrane for 1 day. The dialyzed solution was

dried under vacuum to obtain mesylated dPG. 1H-NMR (400 MHz, CD3OD): δ = 3.3-4.1 (m, dPG backbone, 5 H), 3.1 (s, mesyl-CH3, 3H).

Synthesis of dPG-azide (F). Mesylated dPG (3.0 g, 8.1 mmol mesyl groups) and sodium azide (2.11 g, 32.4 mmol, 4 eq.) were added in (100 mL) anhydrous DMF. The reaction mixture was stirred at 90 °C for 24 h and then another 72 h at 60 °C. The reaction mixture then cooled down to room temperature and filtered using celite. DMF was evaporated under reduced pressure and the product was dialyzed (RC, MWCO 1 kDa) for 72 h. The dialyzed solution was dried under vacuum to obtain dPG-azide. FT-IR: N3-peak at 2100 cm -1. 1H-NMR (400 MHz, CD3OD): δ = 3.3-4.1 (m, dPG backbone, 5 H).

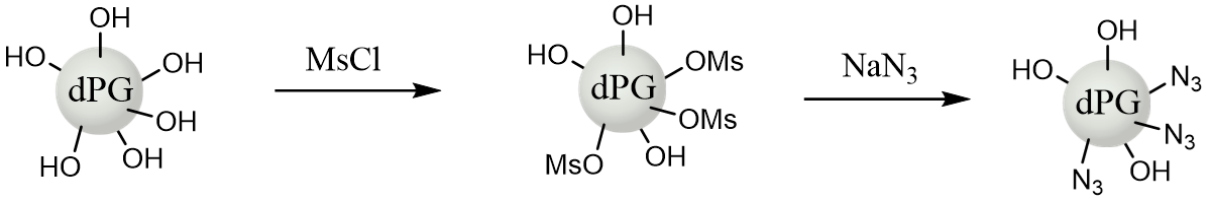

Scheme S2. Synthesis of dPG azide in two steps via mesylation and azidation.

Synthesis of RhodB labelled dPG-azide. Anhydrous dPG-azide (479.0 mg, 0.048 mmol, 1 eq.), RhodB (91.0 mg, 0.192 mmol, 4 eq.), EDCI (20.2 mg, 0.105 mmol, 2.2 eq.) and DMAP (1 mg, 8 µmol, cat.) were added in anhydrous DMF in presence of argon and stirred at room temperature for 24 h. Then, the reaction mixture was dialyzed against methanol for 2 days (RC, 1kDa MWCO). The dialyzed solution was concentrated under reduced pressure and purified using sephadex G-25 fine. The coloured Rhod-B-grafted dPG-Azide was collected and dried under vacuum and used for conjugation of the degradable linker.

Table S1. Variation of conditions for the synthesis of PNIPAM-(S-S)-dPG nanogels. No size changes upon incubation of the nanogels with (5 mM GSH) solution for 24 h (measured by DLS) is defined as 'no degradability'.

T (°C)	Initiator	Size at 25°C (d.nm)	PDI at 25°C	Degradability
70	APS/T	159	0.144	no
60	APS/T	136	0.090	no
55	APS/T	132	0.122	no
50	APS/T	141	0.090	no

Figures:

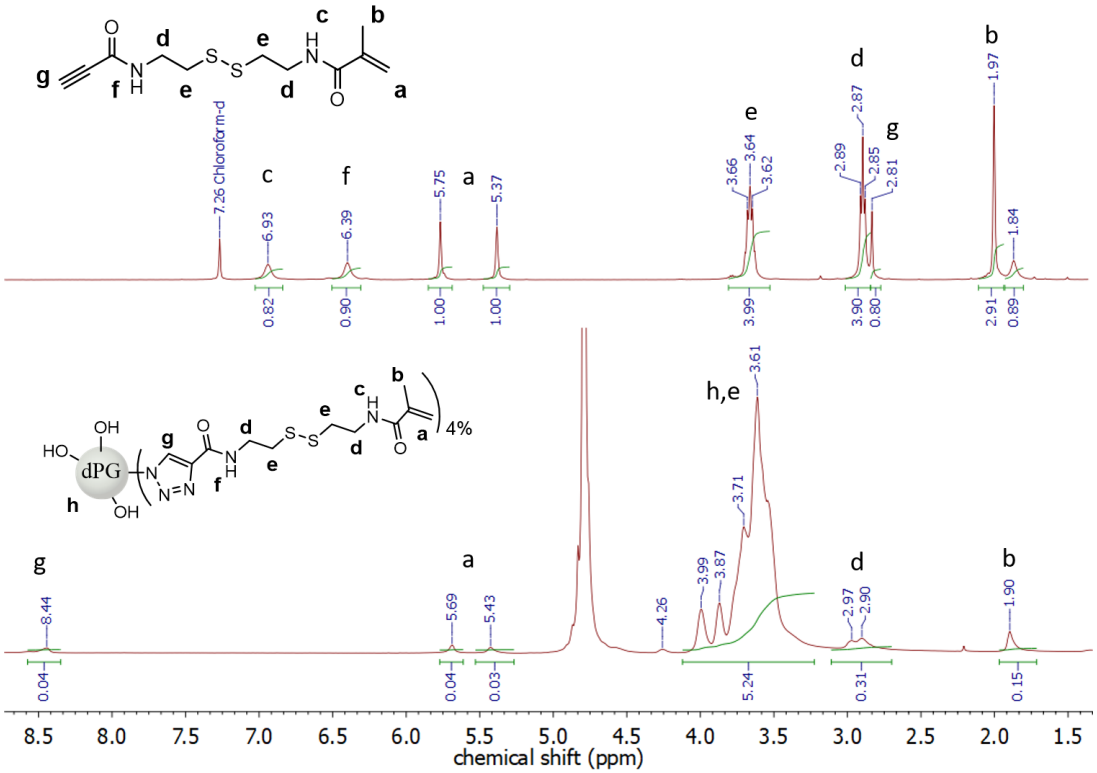

Figure S1. 1H-NMR spectra of the degradable, disulfide containing linker and the corresponding dPG conjugate (grafting density 4% per dPG) proving successful coupling.

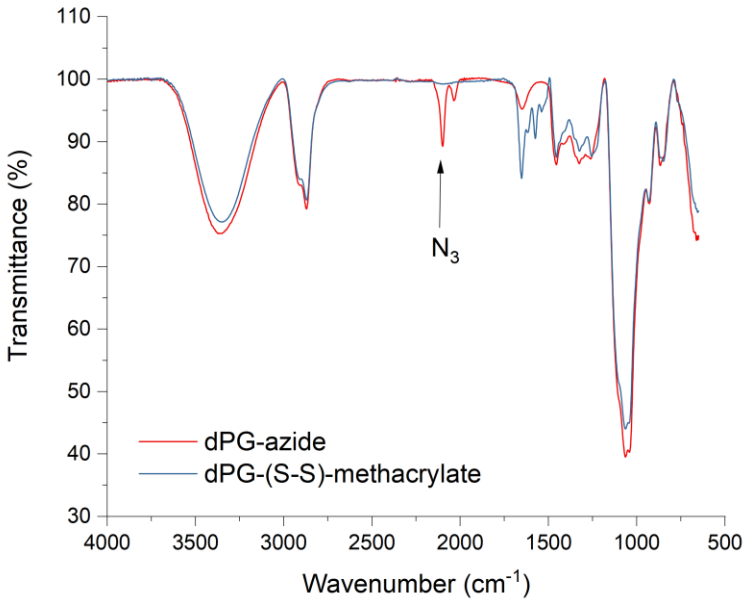

Figure S2. FT-IR spectra of dPG-azide and dPG conjugated with the degradable linker (dPG-(S- S)-methacrylate) showing complete removal of azide signal at 2100 cm-1 proving successful coupling.

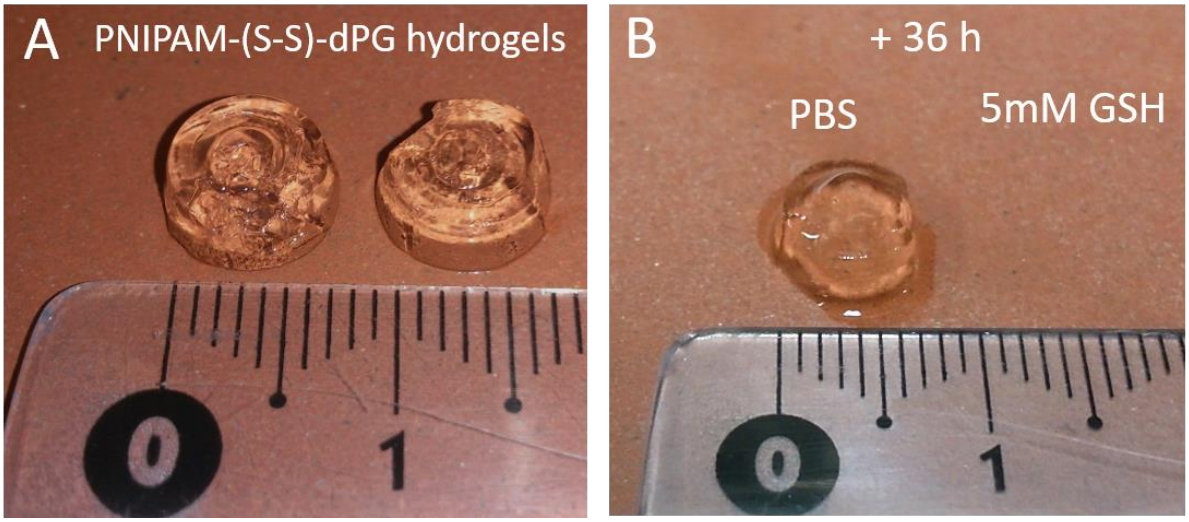

Figure S3. Hydrogel of PNIPAM-(S-S)-dPG (A) before and (B) after incubation with (5 mM) GSH or PBS solution.

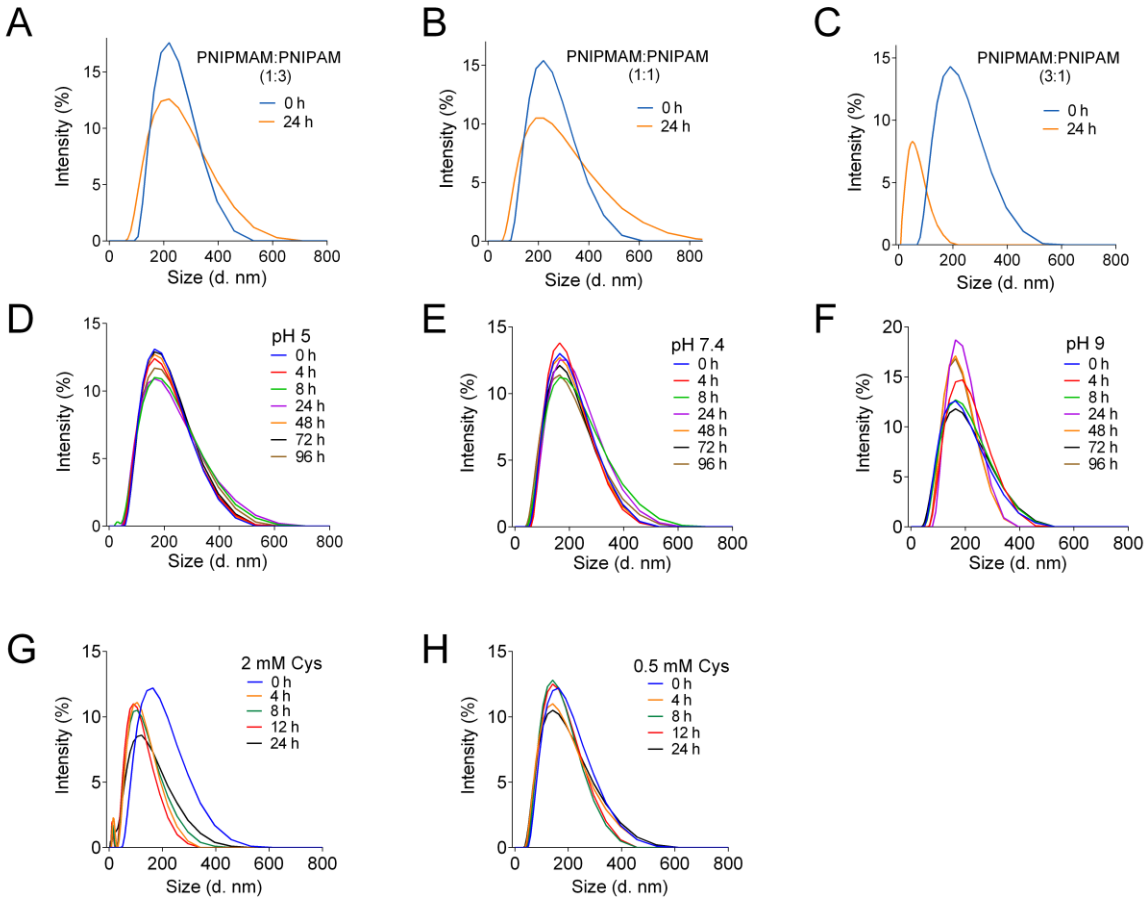

Figure S4. Degradation profiles of copolymeric nanogels in GSH solution (5 mM) with different PNIPMAM:PNIPAM ratios: (A) 1:3, (B) 1:1, and (C) 3:1. Stability of PNIPMAM-(S-S)-dPG nanogels at different pH values: (D) pH 5, (E) pH 7.4 and (F) pH 9. Degradation of PNIPMAM- (S-S)-dPG nanogels in presence of L-cysteine (Cys) (G) 2 mM or (H) 0.5 mM monitored by DLS.

Table S2. Zeta-potential of degradable nanogels and non-degradable analogues.

Nanogels	PNIPMAM-(S-S)-dPG	PNIPMAM-dPG
Zeta-Potential	0.230 mV	-0.516 mV

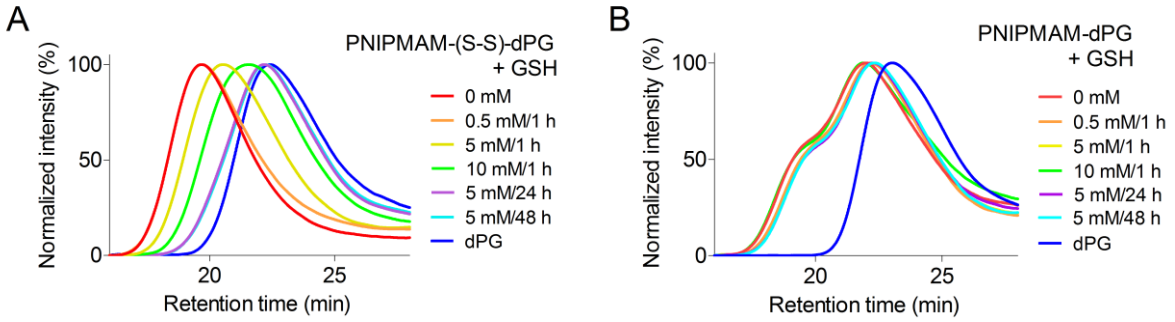

Figure S5. Degradation profiles monitored by GPC upon incubation with GSH of (A) PNIPMAM-(S-S)-dPG and (B) control PNIPMAM-dPG nanogels.

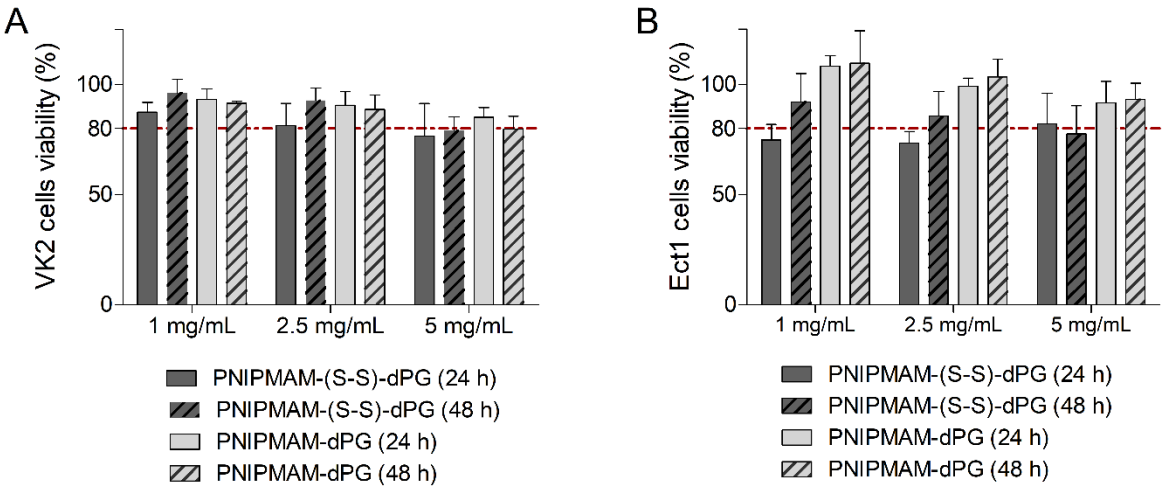

Figure S6. Cell viability of (A) vaginal epithelial cell line (VK2/E6E7) and (B) human ectocervix epithelial cell line (Ect1/E6E7) after 24 h and 48 h exposure to the nanogels at different concentrations. n = 3, mean ± SEM.

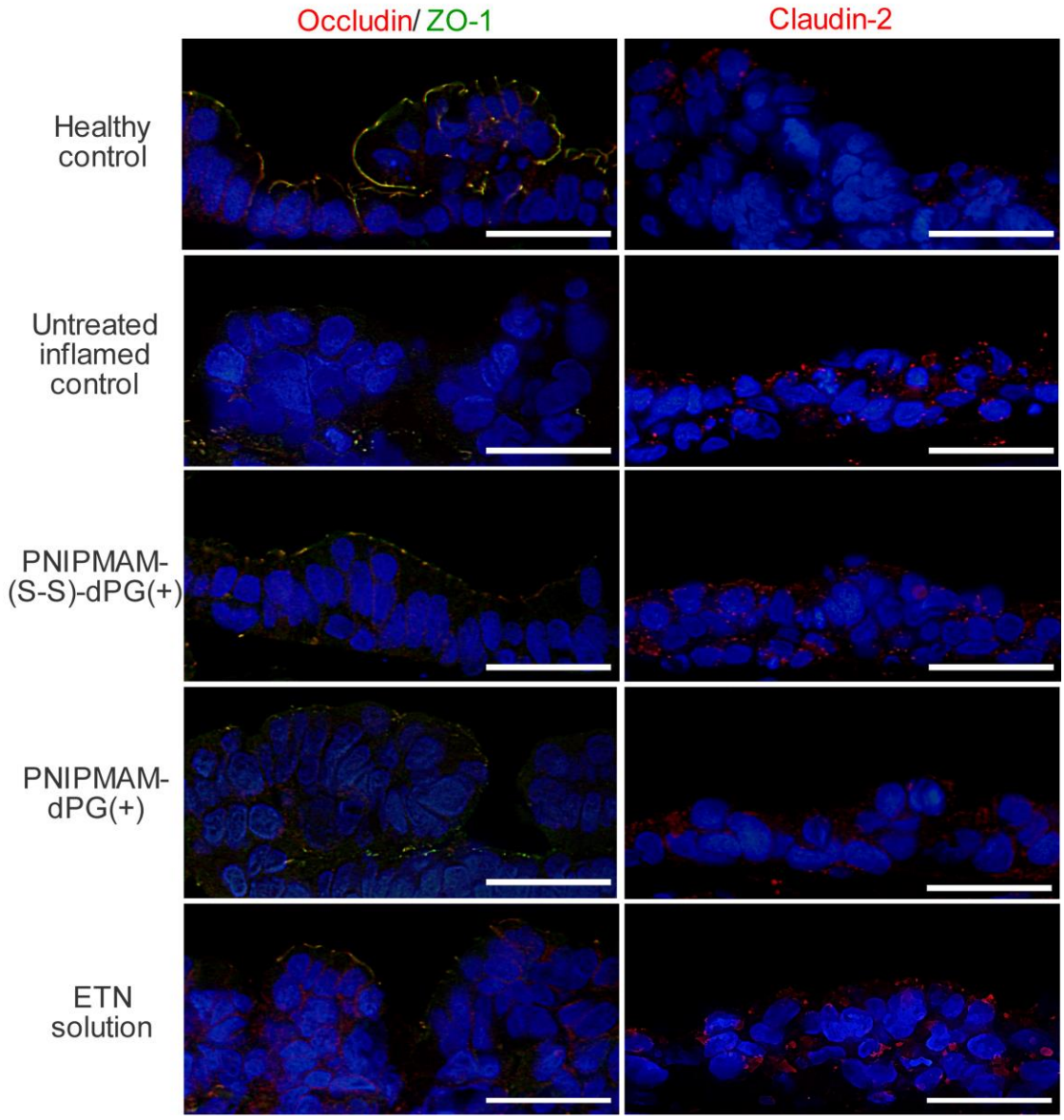

Figure S7. Representative immunofluorescence staining of the tight junction proteins occludin, ZO-1 and claudin-2 in EpiIntestinal-FT™ models after the induction of inflammation and topical treatment with ETN loaded (+) onto disulfide-containing (PNIPMAM-(S-S)-dPG), control (PNIPMAM-dPG) nanogels or in solution (ETN solution). Magnification 60x30x (1800x); n = 2.

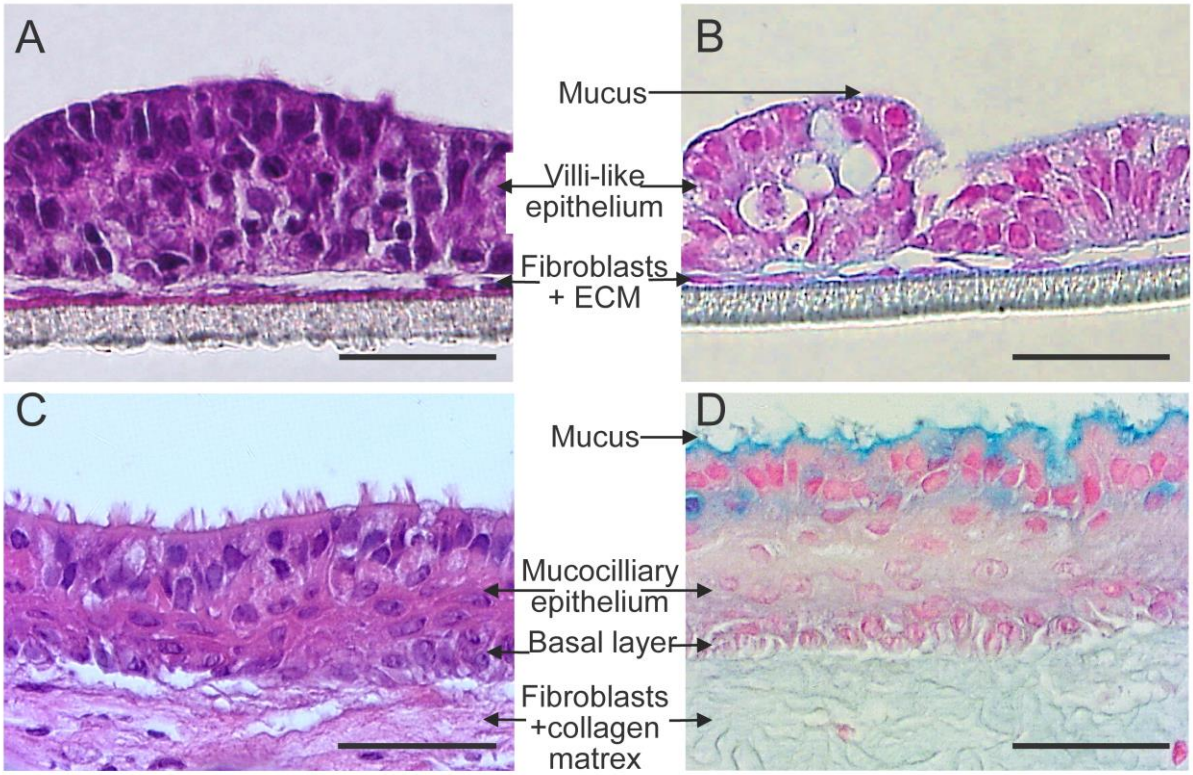

Figure S8. Histological H&E staining of EpiIntestinal-FT™ models (A) and bronchial epithelial models (C) showing the expression of all relevant epithelial tissue layers. (B, D) show the Alcian blue staining of the intestinal (B) and bronchial epithelial models (D). Blue staining on top of the tissues is indicative for the presence of a mucus layer. Scale bar = 50µm.

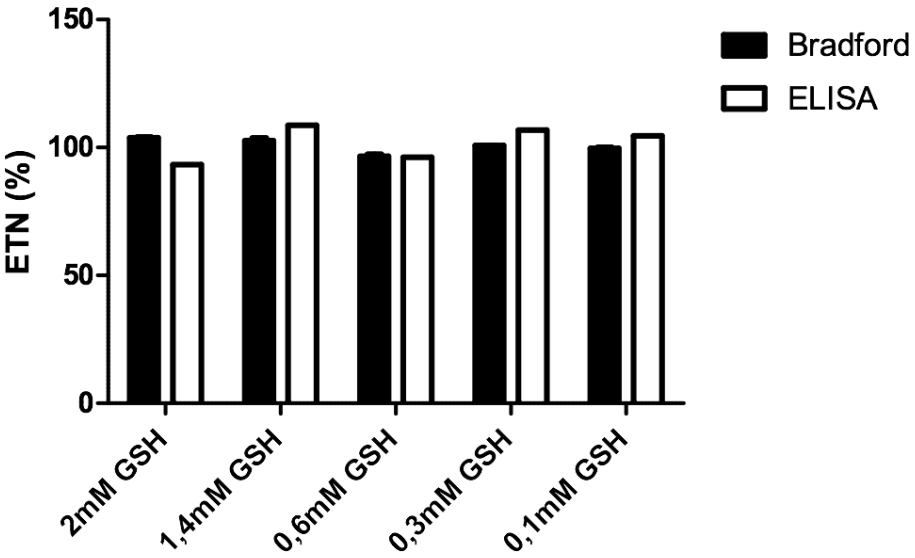

Fig. S9. Stability/activity of etanercept loaded onto PNIPMAM-(S-S)-dPG nanogels after incubation with varying GSH concentrations for 4 h.

3.2.3 Complementary unpublished results

Histological analysis of excised porcine jejunum

Experimental procedure:

Freshly excised jejunum from sacrificed 6 months old male farm pigs was cut-open, rinsed and immediately transferred to the lab using ice-cold oxygenated Krebs-Ringer buffer (KRB) (pH 7.4) [204]. Intestinal punches (diameter: 15-16 mm) were then placed onto Punches of freshly excised pig's jejunum were embedded in freezing medium, snap frozen in liquid nitrogen and preserved at -80°C freezing chamber. Cryo-sections of 5 µm thickness were cut using a CM1510 S Cryotom (Leica Biosystems, Germany). Sections were then preserved at -80°C for further staining. Afterwards, the segments were fixed with 4% paraformaldehyde (Roti® Histofix 4%, Carl Roth GmbH, Karlsruhe, Germany) and subsequently stained with Alcian blue solution and nuclear fast red (Sigma-Aldrich GmbH, Germany) according to a previously reported standard method [261]. Light microscopy images were captured using BZ-8000 microscope (Keyence, Germany) equipped with a suitable lens (objective 20×/0.75, zoom 20×, Plan-Apo, DIC N2, Nikon, Japan).

Results

Light microscopy visualization of vertical sections from excised intestinal jejunum demonstrated the tissue's intact viable architecture shoeing the finger-like villi structures constituting the absorptive surface and overlined with mucus gel (blue). The epithelial monolayer of the villi shows enteric cells (pink) and the abundant mucus-secreting goblet cells (blue) (Figure 3.1).

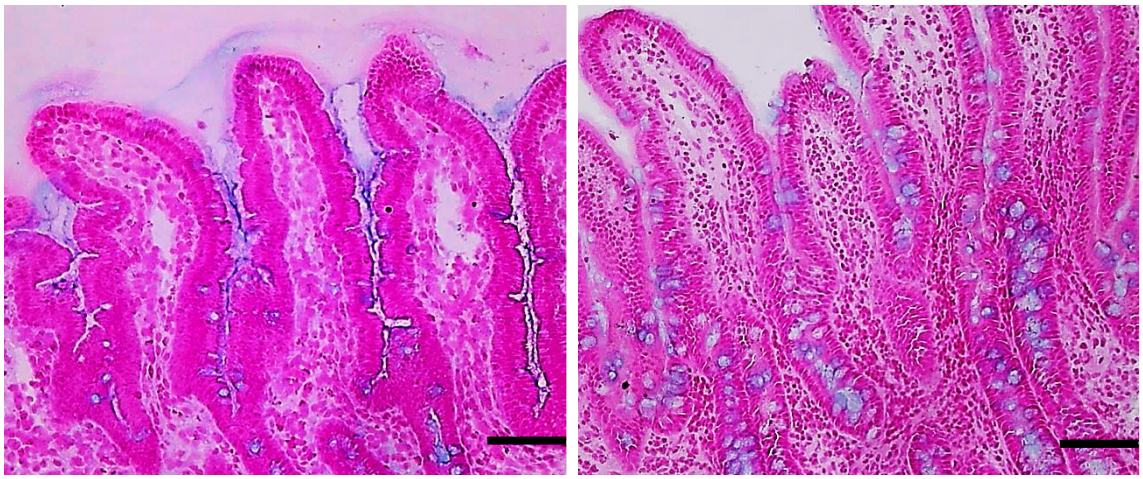

Figure 3.1. Alcian Blue stained cryosection from freshly excised and rinsed porcine jejunum showing the mucus with goblet cells (blue), nuclei (red) and cellular structures (pink) through contra staining with nuclear fast red. Scale bar = 100µm.

4. Discussion & Prospects

Given the current exponential growth in the number of therapeutic proteins entering the pipeline or being approved for diverse indications, improved drug formulations of these biopharmaceuticals are becoming more and more crucial to shift their administration from parenteral to non-invasive in order to increase therapeutic efficiency and overcome detrimental issues limiting their clinical application, such as loss of efficacy, serious side effects, and poor patients' compliance [262, 263]. As main routes for non-invasive drug administration, skin and mucosal surfaces comprise very challenging barriers to drug delivery, especially of labile biomacromolecules [264, 265]. For many years now, NPs have been recognized as sophisticated carrier systems capable of entirely altering drugs pharmacokinetics and bioavailability without compromising the barriers' physiological structure and functions [12, 266]. Modifying NPs synthesis parameters and physicochemical properties allows to control how they interact with biological barriers [31, 36]. As next generation drug delivery systems, dPG nanogels offer protein-friendly vehicles and smart systems that can be adapted to address the biological barrier properties in order to enable efficient localized delivery of biomacromolecules [51, 177].

Working with responsive dPG nanogels, this project investigates the role of different responsive modalities in facilitating dermal and mucosal protein delivery.

4.1. Thermoresponsive protein delivery to skin.

For dermal applications, thermoresponsive nanogels confer promising candidates to overcome the barrier and promote interpenetration of their payload within viable skin layers [92, 267]. For this purpose, the careful tuning of the nanogels' VPTT is pivotal to prompt a thermally controlled drug release into skin [68]. Nanogels with VPTT < 37 °C rely on the natural thermal gradient of the human skin (ranging between 32 – 37 °C from SC surface to deep VE), meanwhile nanogels with VPTT that exceeds the normal body temperature of 37 °C allow employing an external hyperthermic trigger that can exert a controlled local and temporal payload release [82, 268]. In fact, the latter type of nanogels is interesting for therapeutic applications in conditions associated with local hyperthermia, such as infections (~38 °C), or tumor photothermal therapy, which employs localized tissue heating processes reaching 41 °C [89, 269].

As thermoresponsive units, PNIPAM and PNIPMAM were employed as feasible and widely used scaffolds for nanogels synthesis using previously reported method [84]. Whilst PNIPAM produced nanogels with VPTT around 33 – 35 °C, PNIPMAM-dPG nanogels displayed VPTT at 45 – 47 °C, which can be attributed to the hydrophobic input by the extra methyl group in PNIPMAM. To obtain nanogels with attenuated VPTT between 38 – 42 °C that allows

harmless local heating and rational application, a co-polymerization procedure of PNIPAM and PNIPMAM was pursued as previously proposed [69, 270], yielding Co-(1:1)-dPG nanogels with VPTT between 39 – 40 °C as suitable candidates. Here, critical synthesis parameters were considered to tune the VPTT in the desired range without altering the nanogels physicochemical properties, such as dPG feed, functionalization ratio of dPG : polymer, the crosslinking density, and swelling degree (see chapter 3.1; Theune et al. 2019, for detailed synthesis procedure and VPTT tuning).

For temperature-dependent dermal protein release, the Co-(1:1)-dPG nanogels were evaluated next to the nanogels based on the homopolymers; namely PNIPAM-dPG and PNIPMAM-dPG. Overall, these nanogels displayed comparable physicochemical properties in terms of spherical shape, size, low polydispersity, and most importantly neutral zeta potential (Fig. 1-5; Theune et al.2019).

As a model protein cargo, fluorescently labeled bovine serum albumin BSA-FITC was successfully loaded onto all three nanogels at 10:1 nanogel to BSA ratio, demonstrating outstanding loading efficiencies above 80% (Fig. 6; Theune et al. 2019). Structural integrity of encapsulated BSA was confirmed in all nanogels via circular dichroism measurements (Fig. 7A; Theune et al. 2019). In addition, BSA thermal stability was explored over a series of increasing temperatures to verify its compatibility to a thermally triggered release. In line with previous findings [271-274], this analysis for both encapsulated and free BSA confirmed structural integrity at temperatures up to 50 – 55 °C, above which the protein undergoes unfolding process (Fig. 7B,C; Theune et al. 2019). Notably, the presence of nanogels did not seem to influence the thermodynamic stability of BSA. Overall, these results favor BSA as a suitable stable payload within the VPTTs range of the tested nanogels and the investigated temperature conditions.

Dermal protein release studies were carried out *ex vivo* in barrier disrupted human abdominal skin. Here, the nanogels performance with respect to different thermal triggers was investigated in two different setups: first, a temperature ramp of 32 – 37 °C over 6 h exposure period simulating the natural thermal gradient of human skin *in-vivo* and second, under a brief irradiation (max. 120 sec) with a medical NIR lamp prompting localized elevated temperature up to 41 °C during only 2 h exposure period at r.t. in order to avoid thermally-induced tissue damage or increased tissue permeability by higher temperatures and longer exposure [90, 94]. Generally, the applied NIR source is tissue compatible and allows a local and temporal irradiation to defined tissue areas with high precision [90].

In the first setup, BSA penetration into the VE was observed only for PNIPAM-dPG nanogels with very significant MFI of FITC-labeled BSA compared to the control BSA solution, which

hardly showed any penetration. Conversely, Co-(1:1)-dPG and PNIPMAM-dPG nanogels showed minimal traces of BSA within VE (Fig. 10 A,B; Theune et al. 2019). These findings are merely attributed to the VPTT of PNIPAM-dPG nanogels (~35 °C), which falls within the natural dermal temperature gradient, starting with 32 °C at the SC surface and steadily increasing to 37 °C in VE [88, 275]. Hence, PNIPAM-dPG are the only nanogels in this setup, whose VPTT was exceeded. These results are in accordance with previous work from our group demonstrating efficient temperature-dependent cutaneous protein delivery for PNIPAM-dPG nanogels within similar conditions [276, 277].

Moving on to the second setup, NIR irradiation resulted in pronounced BSA penetration into the VE for both Co-(1:1)-dPG and PNIPAM-dPG nanogels, as expected, since the irradiation triggered the VPTTs for both nanogels (Fig. 10 C,D; Theune et al. 2019). In contrast, the non-irradiated control samples kept at r.t. showed barely any signs of BSA within the VE (Fig. S5, Theune et al. 2019). This confirms that BSA release from the nanogels and subsequent penetration follows a temperature trigger.

Interestingly, upon NIR irradiation PNIPAM-dPG outperformed Co-(1:1)-dPG by exhibiting a pronounced BSA release with highly significant MFI values compared to Co-(1:1)-dPG showing very significant MFI with respect to the irradiated control BSA solution (Fig. 10 C,D; Theune et al. 2019). This can be explained by the temperature dependent behavior of these nanogels; as the payload release begins at the nanogel VPTT, it is boosted as the temperature further increases until reaching the point, by which the entire cargo is released and the nanogel is completely collapsed [68]. This behavior was evident in the *in vitro* release study showing at 42 °C an accelerated and boosted temporal BSA release from PNIPAM-dPG (96 %), compared to (72%) for Co-(1:1)-dPG (Fig. 8; Theune et al. 2019). Hence, PNIPAM-dPG nanogels superiority is likely due to their total collapse by 41 °C since their transition occurs already by 35 °C, compared to a partial collapse for Co-(1:1)-dPG nanogels since the irradiation temperature of 41 °C is very close to their VPTT (~40 °C).

Reviewing the data altogether, a temperature responsive behavior for the nanogels was demonstrated, substantiating a proportional relationship between nanogels collapse and enhanced intraepidermal penetration of their protein cargo, which is in good alignment with previous work [86, 87, 277]. Moreover, comparing both setups, the results emphasize the efficiency of the NIR external stimulus in promoting a comparable or even stronger dermal protein penetration than the natural thermal trigger setup, despite much shorter experimental period and very brief irradiation. Whilst previous work using the natural thermal gradient confirmed that the nanogels remain retained at the SC [86, 278], studies using IR irradiation attributed the supremacy of the IR setup to an increased penetration of the nanogels

themselves into VE alongside their cargo upon irradiation [91]. This assumption, however, requires further investigations. Concerning the nanogels behavior in enhancing protein penetration, the mechanism of action remains unclear. Given the uncharged neutral surface of the nanogels, a surface charge-induced cell adhesion can be ruled out [279, 280]. A plausible suggestion would be an improved penetration through interactions between the collapsing hydrophobic moieties of the nanogels and the SC lipophilic components [281, 282]. Moreover, the water expulsion associated with nanogels deswelling can create water depots that perturb the SC and untighten its stiff structure thus improving the SC hydration and facilitating the payload interpenetration [80].

Overall, the data show good correlation between *ex vivo* and *in vitro* data demonstrating the nanogels VPTT dependent release profile associated with conformational change, size reduction, and increased hydrophobicity [92]. Furthermore, they endorse thermoresponsive nanogels with VPTT > 37 °C as compatible smart systems for controlled local and temporal drug delivery, either by applying an external trigger to achieve a specific drug delivery (e.g., tumor ablation via photothermal therapy) or by utilizing their ability to sense pathological hyperthermia and trigger a selective drug release in diseased regions without affecting intact healthy tissues.

Finally, these findings stand proof for dPG nanogels agility and resilience as tunable smart devices for further development of tailor-made drug delivery systems.

4.2. Redox-sensitive mucosal protein delivery

The major concern of this project was to implement nanogel carrier systems that address the requirements for mucosal drug delivery and are able to overcome the mucus barrier. Given the previously reported advantages of NPs thiolation in enhancing mucus permeation and improving subsequent drug delivery [167, 168, 171], disulfide-containing nanogels based on dPG and PNIPMAM were synthesized via precipitation polymerization. A time and concentration-dependent degradation in GSH solutions validated the redox-sensitive behavior of the obtained PNIPMAM-(S-S)-dPG nanogels in contrast to PNIPMAM-dPG nanogels (See sections 2.1, 2.2; Charbaji et al. 2021, for details on nanogels synthesis and disulfides characterization).

To substantiate the merit of the incorporated disulfide units in mucosal delivery, PNIPMAM-dPG nanogels without the disulfide linker served as a negative control.

4.2.1 Physicochemical properties of PNIPMAM-(S-S)-dPG nanogels render them suitable candidates for efficient mucosal delivery

Despite being an amphiphilic polymer, PNIPMAM maintains a hydrophilic state at temperatures below its transition temperature of ~45 ºC. Hence, using it beside dPG ensures an increased hydrophilicity of the nanogels for local mucosal as well as systemic applications (*T* ~37°C) [270]. Moreover, dPG has a huge impact, as a macro-crosslinker, on the stability and inertness of the nanogels in different physiological media as demonstrated in previous work from our group [283]. In addition, initial characterization of the obtained nanogels demonstrated very law poly dispersity and an average size of 166 nm for PNIPMAM-(S-S)-dPG (Table 1; Charbaji et al. 2021). Furthermore, zeta-potential measurements demonstrated a neutral surface charge for PNIPMAM and dPG based nanogels with and without the disulfide linker (Table S2; Charbaji et al. 2021) [284].

Taken together, these properties in addition to thiolation meet the essential prerequisites for mucus permeation and put forth PNIPMAM-(S-S)-dPG nanogels as promising mucosal delivery candidates [99, 113, 165, 169].

4.2.2 Disulfides-containing nanogels undergo temporal degradation in native mucus whilst remaining stable in different pH conditions

Intestinal mucosa displays luminal pH ranging from 5.5 to 7.5 between proximal small intestine and distal ileum [285]. Monitoring the nanogels in different pH environments demonstrated good stability of the nanogels, especially in acidic and neutral conditions (Fig. S4 D - F; Charbaji et al. 2021). This makes the nanogels suitable for applications in intestinal mucosa as well as other mucosal surfaces like bronchial mucosa, for which a slight acidic pH is reported [286].

The disulfide units in the nanogels allow exchange interactions with thiol groups of reducing enzymes present in mucus or cysteine-rich domains of the mucins glycoproteins, thus subsequent biodegradation of the carrier system in mucus is anticipated [287]. Predominantly, GSH is abundant in small intestine lumen at concentrations that variate along the different intestinal segments ranging between 0.1 – 0.6 mM for rodents [288-290]. These levels for GSH, as well as those for other intestinal redox enzymes, are dependent on food intake and can greatly vary with diet [291]. Based on this and due to the lack of equivalent measurements of GSH levels for human intestinal luminal mucus, a wide range of GSH concentrations was investigated for redox-sensitive degradation studies as the complexity of the *in-vivo* scenario cannot be modelled by a single GSH concentration. The results obtained from GPC

measurements confirmed a gradual degradation of the PNIPMAM-(S-S)-dPG nanogels in a concentration- and time-dependent manner (Fig. S5; Charbaji et al. 2021).

To substantiate these findings in native mucus, the nanogels were incubated with isolated porcine intestinal mucus. GPC analysis revealed a temporal mucus-dependent break down for the PNIPMAM-(S-S)-dPG nanogels reaching full degradation (~ 98%) by 12 h incubation (Fig. 3 B; Charbaji et al. 2021). This biodegradation can only be attributed to disulfides cleavage since the control PNIPMAM-dPG nanogels demonstrated no degradation at the same conditions (Fig. 3 C; Charbaji et al. 2021). This gradual biodegradation of the nanogels brings additional benefits as it could further assist in mucopenetration and allows a rapid non-toxic clearance of the degraded small fragments [292]. Interestingly, the consistency of the nanogels GPC degradation profiles between mucus (Fig. 3 B, C; Charbaji et al. 2021) and GSH solution (Fig. S5; Charbaji et al. 2021) despite scaling up the tested GSH concentrations to unphysiological levels (5 mM) [288, 289] indicates that multiple reductive entities present at native GI mucus are likely contributing to the nanogels cleavage at the same time (e.g., Cys residues, GSH, thioredoxin, etc.) [293].

4.2.3 The presence of disulfides imparts dPG nanogels with mucoadhesive and mucopenetrating qualities

Previous studies could demonstrate that adhesive interactions between polymeric NPs and the mucus gel manifested in increased bulk viscoelasticity of the NPs ─ mucus mixture compared to that of the independent mucus gel, therefore a so-called rheological synergism was defined as a parameter to determine mucoadhesion of polymeric particles to mucus [294, 295]. Monitoring the rheological profile of the native mucus following incubation with PNIPMAM-(S-S)-dPG nanogels revealed pronounced elastic (G') and viscous (G'') gel properties with a time-dependent increase in the viscoelastic behavior, as opposed to the control PNIPMAM-dPG nanogels, for which such effect did not occur (Fig. 3 D, E; Charbaji et al. 2021). These observations indicate a rheological synergism induced by the presence of the disulfides linker. The Bernkop-Schnürch group previously atributed similar findings to mucoadhesion via disulfide bonds formation between thiolated NPs and the free thiols at the Cys-rich domains of mucin glycoproteins [296-298]. On the other hand, since the mucins in the GPC analysis were fully precipitated via ultracentrifugation of the nanogels ─ mucus incubates and the nanogels were found and measured in the supernatants, it means they did not adhere to the pelleted mucins. Considering this, it seems quite plausible that the mucoadhesion demonstrated in these rheological measurements may be attributed to disulfides formation yet between the nanogels' degraded fragments bearing thiol groups and the mucins [297]. However, given the heterogenous composition of the native intestinal mucus and the fact that

rheology analysis does not provide direct information on the nature of the interactions taking place, such assumption is rather speculative and requires further investigations of the nanogels ─ mucus interactions on the micromolecular level [101, 295].

Concerning mucopenetration studies of the nanogels, freshly excised porcine jejunum was employed as a well-known reliable *ex vivo* model that closely mimics the human intestinal tract (Fig. 3.1) [299, 300]. Following the Rhod-B labeled nanogels after 1 and 3 h incubation with viable intestinal jejunum demonstrated that the PNIPMAM-(S-S)-dPG nanogels were able to efficiently penetrate and move upstream against the flow of continuously secreted mucus from goblet cells, and thus reach underlying epithelium (Fig. 4A, C; Charbaji et al.2021). In contrast, the control PNIPMAM-dPG nanogels distributed faintly over the mucus layer within the first hour and were almost completely cleared out by the mucus dynamic flow after 3 h (Fig. 4B, D; Charbaji et al. 2021). These results clearly demonstrate that the presence of disulfides rendered the nanogels mucopenetrating most likely through mucus-dependent gradual degradation to smaller particles that accommodate the dynamic heterogeneous mesh spacing of the intestinal mucus allowing the nanogels to infiltrate the mucus barrier network and overcome distal clearance mechanism [108].

One of the main drawbacks of excised intestinal tissue is its high fragility and short viability lasting up to max. 4 h *ex vivo* [213], afterwards the tissue undergoes fast necrotic deterioration process. This clearly detrimentally limits the duration of penetration/permeation studies even when special equipment are used to preserve the tissue, such as the Ussing chambers, continuous tissue supply with oxygen-gas, and adjustment to body temperature [301].

To be able to evaluate the nanogels' mucopenetrating properties over an extended time and in a different yet comparable mucosal tissue, bronchial epithelia was of interest. In terms of structure related function, bronchial and intestinal mucosae bear various similarities and share common features, including the same gel comprising mucins (MUC2, MUC5AC, MUC5B) [114], the loose mucus gel barrier with dynamic mucus regeneration and heterogenous mesh size [114, 260], the availability of redox enzymes in both mucosal lumens [302], and the same epithelial arrangement in both that is based on columnar epithelium mainly comprised of absorptive epithelial cells and goblet cells interconnected with tight junctions [98]. Hence, reconstructed *in vitro* bronchial epithelial microtissues were used. These "home-made" microtissues were generated from primary human lung cells and as fully cultured 3D microtissues, they express critical markers of the human bronchial epithelium such as ciliated epithelial cells, goblet cells, and continuous mucus secretion [303]. Similar to the intestinal mucopenetration findings *ex vivo*, incubating the bronchial microtissues with the nanogels for up to 6 h reproduced the very same outcome (Fig. 4E, F; Charbaji et al. 2021).

Taken together, these findings emphasize the essential role of the disulfide-linkers in facilitating mucus entanglement and subsequent interpenetration through gradual degradation yet rule out immobilizing interactions of the PNIPMAM-(S-S)-dPG with the mucus. They also indicate the added value of the incorporated disulfide linker in promoting mucus penetration of the nanogels, besides the standard requirements of hydrophilicity, inertness, and nanoscale size, which seemed on their own insufficient after all to enable the particles to effectively circumvent the dynamic obstructive mechanisms of mucus in both bronchial and intestinal mucosae.

4.2.4 Nanogels demonstrate compatibility to mucosal epithelial cells and the disulfides facilitate cellular internalization

Generally, dPG based nanogels are well known for their high biocompatibility and safety to biological milieu [47, 85, 304]. As newly optimized systems for mucosal delivery, the safety of the disulfides-containing nanogels was examined on mucosal epithelial cells. As the gold standard cell lines for intestinal epithelium, monolayers of Caco-2 cells were tested for potential cytotoxic effects [305]. Both disulfides-containing and control nanogels exhibited good biocompatibility with Caco-2 cells despite testing relatively high concentrations (up to 5 mg/mL) (Fig. 4 G; Charbaji et al. 2021). Similar results on cell viability were also obtained from further toxicological data using cells from other mucosal surfaces, namely vaginal epithelial cell line (VK2/E6E7) and human ectocervix epithelial cell line (Ect1/E6E7) (Fig. S6; Charbaji et al. 2021). Interestingly, the control nanogels were still better tolerated by the cell lines than the disulfide-containing nanogels. This is likely because cancer cells, in particular, are more susceptible to disulfides-containing nanoparticles [306].

Given the important role of intestinal macrophages as key players in disease progression as well as mucosal healing [307], it was critical to evaluate their interactions with the nanogels. In terms of safety, both nanogels demonstrated outstanding cytocompatibility to primary human macrophages with a viability > 90%. Here, the nanogels induced almost neither necrotic nor apoptotic cell death in primary macrophages even after prolonged direct exposure (24h). Conversely, over 80% of the macrophages underwent apoptotic and/or necrotic death when exposed to 5 % DMSO solution (Fig. 4 H; Charbaji et al. 2021). This is in good agreement with previous findings for dPG nanogels from our lab [304].

Furthermore, uptake studies were also carried out to evaluate the nanogels internalization into macrophages. Successful active internalization was demonstrated for both nanogels into primary macrophages. Interestingly, the active uptake of disulfides-containing nanogels was more pronounced indicating promising characteristics for potential drug delivery to immune cells (Fig. 4 I; Charbaji et al. 2021) [308]. These uptake results align with previous proposal by

the Bernkop-Schnürch group suggesting enhanced uptake of thiolated NPs into macrophages [168], which was attributed to thiol-disulfide exchange interaction between the NPs and the cysteine rich domains present in the scavenger surface receptors of macrophages [309, 310]. This provides a plausible explanation, when projected onto the data obtained for the disulfides-containing nanogels and macrophages, especially since the enhanced uptake can only be attributed to the presence of the disulfide linker, as the control nanogels showed only mediocre uptake (Fig. 4 I; Charbaji et al. 2021). It is also reasonable that the disulfides-containing nanogels were thus able to trigger several internalization and phagocytosis mechanisms in macrophages leading to more internalized particles [311]. However, this remains rather speculative and requires further studies to clarify the exact uptake mechanisms and identify interactions with macrophages receptors [312, 313].

4.2.5 Disulfides-containing nanogels enable efficient intramucosal delivery of biologics to human based IBD-like models and lung models

The use of tumor necrosis factor blockers (anti-TNFα) made a quantum leap in the treatment of various chronic inflammatory conditions [314]. In IBD treatment, the potency of anti-TNFα biologics surpassed that of classic treatments by promoting mucosal heeling and clinical remission besides minimizing surgical interventions or hospitalization [315-317]. Nevertheless, the loss of biological efficacy has been a major concern limiting the clinical application of these biologics as it occurs in over one third of IBD patients and is mainly attributed to their physicochemical instability and systemic immunogenic effects [318, 319]. Nanogel-based oral administration of anti-TNFα biologics holds great potential to tackle these issues by stabilizing these sensitive protein drugs and facilitating a non-invasive localized IBD treatment through oral or rectal route [11, 320, 321].

As a model protein drug, the anti-TNFα biologic etanercept (ETN; 150 kDa) was loaded into PNIPMAM-(S-S)-dPG and PNIPMAM-dPG nanogels achieving excellent encapsulation efficiencies (> 80%) for both nanogels. Moreover, ETN encapsulation did not affect its structural or functional integrity even after two weeks of storage (Fig. 5; Charbaji et al. 2021), which was in line with previous work from our lab demonstrating the nanogels' stabilizing and shielding effect on encapsulated biomacromolecules over longer storage durations (up to 4 weeks) [86, 277]. Since the nanogels undergo gradual degradation in mucus, an intact delivery of ETN through mucus is essential. Hence, the release profile for ETN was monitored in physiologically relevant GSH concentrations confirming ETN retention in the nanogels for 4 h and a slow-release profile over 24 h, during which ETN maintained its structural and functional integrity (Fig. 6, Fig S9; Charbaji et al. 2021). Interestingly, even when applying increased unphysiological GSH concentrations (> 0.6 mM) ETN remained intact (Fig. 6, Fig S9; Charbaji

et al. 2021), which further emphasizes the nanogels stability and suitability for the intact protein transfer to mucosae with variating redox potential [59, 322].

Next, the therapeutic efficiency of ETN-loaded nanogels was investigated in IBD-like models. For this purpose, IBD animal models were precluded from these studies due to their questionable predictive value as they lack the ability to emulate human-relevant IBD characteristics and are thus rather unreliable for evaluating the tissue response to anti-inflammatory drugs [323-325]. Instead, the commercially available small intestines microtissues based on reconstructed human primary cells (EpiIntestinal™) were employed as suitable candidates previously reported to enable modulating inflammation and studying drugs permeation [225-227]. As key players in IBD pathophysiology and mediators of the inflammatory process, TNFα and IFNɣ were supplemented to normal intestinal microtissues to stimulate IBD phenotype *in vitro* [326, 327].

IBD pathophysiological changes are mainly characterized *in vivo* by barrier deficiency due to reorganization of tight junctions towards increased permeability, increased release of proinflammatory cytokines (e.g., IL-6, IL-8), and increased mucus production [242, 328-330]. Hence, these characteristics can serve as parameters to evaluate the disease status and assess the anti-inflammatory efficiency of ETN formulations.

After the successful induction of intestinal inflammation over 48 h, the intestinal models were topically treated with ETN-loaded nanogels as well as ETN solution as a control. Monitoring the pathophysiological changes over the course of inflammation and ETN treatment, all the applied ETN formulations seemed to similarly reverse the intestinal inflammation and exhibit anti-inflammatory therapeutic effect. Notably, only TEER measurements indicated a rather pronounced effect for the disulfides-containing nanogels in inducing barrier recovery in the first 2 days of treatment, in contrast to the ETN solution that showed TEER improvement only on the first day of treatment (Fig. 7A, B; Charbaji et al. 2021). This can be explained by the nanogels ability to retain ETN thus prolonging its release as opposed to ETN solution that lacks this quality; such effect for NPs was also observed for TEER in similar studies [331]. However, in terms of suppressing the pro-inflammatory cytokines IL-6 and IL-8 and TJs restitution demonstrated by protein expression (occludin upregulation and claudin-2 down regulation) by the end of ETN treatment, the disulfides-containing nanogels did not outperform the other formulations as anticipated based on their superior penetration *ex vivo* (Fig. 7C, D, Fig 8A, Fig. S7; Charbaji et al. 2021). As these unexpected findings indicate a non-selective permeation of all ETN formulations through the mucus barrier despite its obstructive filtering properties, a structural limitation in the intestinal models was suspected.

Histological examination of the healthy models using Alcian-blue, to visualize the mucus layer, revealed very poor mucus production (≤ 4 µm) and scarcity in goblet cells (Fig. S8 A, B; Charbaji et al. 2021). With respect to the intestinal mucus layer thickness of 100-700 µm in *ex vivo* explants [332], the mucus layer in the intestinal models is considered unphysiologically relevant and inadequate for drug permeation studies [333]. Moreover, such lack in mucus even counteracts the disease manifestation in IBD models, since an overproduction of mucus in small intestines was evident for CD patients due to goblet cells hyperplasia and enhanced mucins secretion under TNFα and IFNɣ stimulation [334]. This strongly suggests that the tested ETN formulations were able to directly reach the inflamed epithelium in the *in vitro* setting due to the lack of mucus and not based on their mucopenetrating merit, which in turn explains why the disulfide-containing nanogels did not outperform the control nanogels or the ETN solution in this setting and elucidates the discrepancy from the *ex vivo* findings, which demonstrated the superior mucopenetrating performance of the disulfides-containing nanogels at physiological conditions.

To validate this hypothesis, ETN delivery was investigated in the bronchial epithelial *in-vitro* models. Given the accordance in mucopenetration findings between these *in-vitro* models and the *ex-vivo* intestinal mucosa (Fig. 4 A–F; Charbaji et al. 2021) that is likely attributed to the abundance of mucus-secreting goblet cells imparting these models with an adequate mucus layer (Fig. S7 C, D; Charbaji et al. 2021), the merit of PNIPMAM-(S-S)-dPG nanogels in mucus permeation can be verified. Following topical administration of ETN formulations, a pronounced efficient penetration of ETN into underlying epithelium was confirmed in PNIPMAM-(S-S)-dPG treated models via immunofluorescence staining (Fig. 8B; Charbaji et al. 2021). In contrast, ETN from the other formulations could not penetrate the mucus layer, whether applied as a solution or loaded onto the control PNIPMAM-dPG nanogels. Here, only small amounts of ETN were detected, indicating poor release from the control nanogels in mucus (Fig. 8B; Charbaji et al. 2021), which is in line with the mucus-related degradation data (Fig. 3B, C; Charbaji et al. 2021).

These findings underline critical shortcomings in the currently available *in vitro* intestinal models and highlight the major impact of the mucus barrier on NP-based drug absorption studies as inadequate mucus production is capable of entirely altering the experimental readout. Reviewing widely used mucosal test models, Lock et al. outlined liabilities in terms of mucus production and emulation of a physiologically relevant mucus thickness, which questions their reliability for NP-based drug delivery studies [335]. Despite considerable advances in tissue engineering, mimicking the human small intestines *in vitro* has been a problematic issue owing its fragile, complex, and highly regenerative structural components, and thus, certain physiological limitations in the used model must always be considered [336].

Overall, it is crucial to understand the limitations of the implemented biological test models and employ complementary systems to reflect the physiological characteristics of the investigated barrier in order to achieve rational assessment and yield reliable data. Given the continuous progress in biomaterial science and the rising need for efficient and non-invasive NP-based drug formulations, the lack of adequate biological test models for drug delivery poses indeed a considerable challenge towards translational approaches, and thus explains the large gap between the huge number of pre-clinically investigated NPs and the very few reaching the clinic.

4.3 Prospects

Although we could demonstrate the nanogels efficiency in localized delivery of sensitive biomacromolecules, further studies are still needed.

In terms of thermoresponsive dermal drug delivery, the therapeutic efficiency of the nanogels in response to an external thermal trigger needs to be investigated. With a VPTT of ~40 °C that exceeds the normal temperature of healthy biological milieu, the Co-(1:1)-dPG nanogels confer suitable candidates for localized and selective photothermal therapy employing NIR-laser as an external trigger. Here, equipping these nanogels with a photothermal transducing moiety (e.g., polypyrrole) to convert the laser light into heat, and encapsulating them with a chemotherapeutic render them very promising for combined photothermal-chemotherapy of tumor tissues, which can be investigated in terms of efficient responsive release *in vitro* and therapeutic efficiency on tumor microtissue models *in vitro* and tumor-bearing rodents *in vivo* [337-339].

Concerning the redox-sensitive mucosal drug delivery, further investigations on the disulfides-containing nanogels are still needed to complete the picture for interactions with the mucus as well as the underlying cells. For starters, investigations of nanogels ─ mucus interactions on the micro-molecular level are needed to unravel the mechanism by which the nanogels degraded in mucus and increased the bulk viscoelasticity of the mucus gel. These micro-rheological studies can be conducted using several precision techniques, such as multiple particle-tracking analysis (MPT) technique, which provide in-depth information on the interactions between the nanogels and mucin fibers [101, 340, 341]. In addition, the microfluidic chamber mucus-on-a-chip can serve as a useful new tool to determine the time-dependent mucopenetrating and mucoadhesive profile for the nanogels and monitor exchange interaction between the nanogels and mucins on different time and length scales [342].

In terms of the therapeutic efficiency testing, the deficiency in mucus secretion of *in-vitro* intestinal models can be compensated by applying biosimilar mucus to epithelium of cultured models [343]. Unlike the commercial gastric mucus solutions that lost its viscoelastic gel-like properties owing proteolytic processing [344], biosimilar mucus closely simulates its native intestinal pendant in terms of rheological and gel-like properties [343, 345]. However, one disadvantage of this mucus that it is based on purified mucins, which reduces the donner-related biological variability, thus compromising experimental reproducibility. In addition, It excludes the dynamic flow of secreted mucus and potential interactions between the nanogels and the mucus heterogenic components like enzymatic reactions or protein corona formation [283, 322].

Since mucus exhibits altered physicochemical properties in pathological conditions, analyzing the nanogels interactions with isolated mucus and excised mucosa from IBD patients who underwent surgical intervention would provide valuable insights into the nanogels penetration and drug delivery capability to diseased tissues [334].

With regards to IBD modeling, immune competent microtissues can better reflect the *in-vivo* disease characteristics. Incorporating dendritic cells and macrophages into the intestinal models would provide a more comprehensive evaluation and elicit the nanogels therapeutic efficiency, owing the paradoxical bilateral role of these immune cells in driving the inflammatory response via IFNγ (from DCs) and TNFα (from macrophages) production, yet also in mediating the anti-inflammatory response and promoting mucosal heeling upon treatment with anti-TNFα biologics [346-349].

Finally, although our studies confirmed the nanogels stability and slow degradation in physiologically relevant levels of the intestinal reducing enzymes, protease enzymes are also available in the gastrointestinal lumen and can compromise the nanogels structure and may even diffuse through their network, given their small size, and degrade the protein payload [350]. Hence, the nanogels can be administered in enteric coating to stabilize them for oral delivery. For example, using Eudragit L-30/D-55 coating protects the nanogels from proteolytic enzymes and the stomach acidic environment, thus promoting their release in the small intestinal mucosa (pH > 5.5) as the desired site of action [351].

5. SUMMARY

Efficient pharmacotherapy is mainly dependent on the effective localized delivery of therapeutic agents to the targeted biological site. Many potent therapeutics exhibit detrimental effects owing their systemic administration and off-target interactions. Hence, local drug formulations have become a necessity to optimize current treatments. Such formulations, however, must address, the unsuited physicochemical properties of drug molecules on one hand, and the obstructive nature of the targeted biological barrier on the other. In this context, nanosized drug delivery systems have literally taken modern medicine to a new dimension by providing adaptable vehicles able to transfer and stabilize therapeutics. Responsive nanogels, in particular, offer biocompatible and versatile tools that can be tuned to suit the targeted barrier requirements in order to facilitate smart delivery and controlled release of the payload.

Aiming to overcome the highly challenging dermal and mucus barriers and provide respectively efficient non-invasive formulations of labile biomacromolecules, the goal of this project was the rational investigation of polyglycerol based nanogels exerting two different response mechanisms as promising vehicles for dermal and mucosal applications.

In the dermal delivery approach, thermoresponsive dPG nanogels were modified to exhibit different volume phase transition temperatures (VPTTs) ranging between 33 – 47 °C using PNIPAM and PNIPMAM thermoresponsive polymers. All nanogels demonstrated high protein encapsulation efficiency (>80%), maintained integrity of protein cargo, and exhibited dermal penetration and subsequent VPTT-dependent protein release and delivery to the viable epidermis in excised human skin. Here, the equal co-polymerization of PNIPAM and PNIPMAM yielded nanogels with VPTT ~40 °C, which enabled to expand dermal applications to include using an external thermal trigger like NIR lamp resulting in pronounced protein delivery in a controlled local and temporal manner.

As for the mucosal delivery approach, for the first time redox-responsive dPG nanogels based on PNIPMAM conjugated to a bifunctional disulfide linker were developed and comprehensively investigated for protein delivery across the mucus barrier. Addressing essential prerequisites for mucus permeation, the nanogels physicochemical properties were fine-tuned to yield hydrophilic nanogels with size range between 100 – 200 nm, inert surface, and intact disulfide linkages. Monitoring the interactions between the nanogels and native intestinal mucus, a gradual disulfides-dependent degradation of the nanogels in mucus was confirmed. Furthermore, rheological measurements indicated mucoadhesive interactions between the mucus gel and the disulfides-containing nanogels, meanwhile absorption studies in excised porcine jejunum revealed outstanding mucopenetration of the disulfides-containing nanogels and demonstrated the disulfides merit in facilitating efficient circumvention of the mucus filtering and clearance mechanisms. Similar findings were also confirmed in

reconstructed human bronchial epithelial *in vitro* models following longer exposure period to the nanogels. In addition, the cytocompatibility of the nanogels was also demonstrated in various mucosal epithelial cell types and primary macrophages as well. Next, the therapeutic efficiency of the nanogels in delivering the biological protein-drug etanercept (ETN; 150 kDa) was examined. Here, high loading efficiency along with structural and functional stability of encapsulated ETN were observed. Moreover, *in vitro* release studies in mucus-relevant redox conditions confirmed ETN retention in the nanogels for several hours and its sustained intact release upon nanogels degradation, which demonstrate the great potential of disulfides-containing nanogels for biomacromolecules delivery. Finally, topical application of ETN-loaded nanogels to human-based *in vitro* models of small intestinal tissue simulating IBD phenotype and bronchial epithelial tissue demonstrated efficient intraepithelial ETN delivery and subsequent anti-inflammatory effect. Throughout this investigation, serious issues pertaining to structural limitations in the available biological test systems for intestinal mucosa were revealed. Since these shortcomings significantly hamper drug absorption studies, multiple mucosal test systems were employed to validate the findings and allow a comprehensive and reliable assessment.

Overall, this thesis introduces novel stimuli responsive nanogels as versatile and resilient tools for efficient local delivery of biomacromolecules to dermal and mucosal surfaces. It also demonstrates the role of the responsive modalities in facilitating the crossing of impervious biological barriers besides prompting a controlled release of the therapeutic payload. In addition, this work highlights critical problems in currently implemented test systems for predicting mucosal drug delivery and outlines present challenges in translating experimental approaches into tangible clinical success.

6. ZUSAMMENFASSUNG

Eine effiziente Pharmakotherapie hängt hauptsächlich davon ab, dass die therapeutischen Wirkstoffe effektiv an den biologischen Zielort gelangen. Viele potente Therapeutika weisen aufgrund ihrer systemischen Verabreichung und Off-Target Wechselwirkungen nachteilige und sogar schädliche Auswirkungen auf. Daher sind lokale Arzneimittelformulierungen zu einer Notwendigkeit geworden, um die derzeitigen Behandlungen zu optimieren. Solche Formulierungen müssen jedoch berücksichtigen die ungeeigneten physikochemischen Eigenschaften der Wirkstoffmoleküle einerseits, sowie die obstruktiven Eigenschaften der biologischen Zielbarriere andererseits. In diesem Zusammenhang haben Wirkstofftransportsysteme in Nanometer-Größe die moderne Medizin tatsächlich zu einer neuen Dimension gebracht, indem sie sich als flexible Vehikel, die die Therapeutika übertragen und stabilisieren herausgestellt haben. Vor allem responsive Nanogele bieten biokompatible und vielfältige Werkzeuge, die gemäß spezifischen Anforderungen der Zielbarriere angepasst werden können, um eine so genannte „smarte“ Verabreichung und kontrollierte Freisetzung des beladenen Mittels zu ermöglichen.

Mit dem Ziel, die besonders anspruchsvollen Haut- und Schleimhautbarrieren zu überwinden und jeweils effiziente, nicht-invasive pharmazeutische Formulierungen für labilen Biomakromolekülen bereitzustellen, beruht sich der Schwerpunkt dieses Projekts auf die rationale Untersuchung von responsive Nanogele basierend auf Polyglycerin, die zwei unterschiedliche Response-Mechanismen aufweisen, als vielversprechende Transport-systeme für dermale und mukosale Anwendungen.

Für den dermalen Ansatz wurden thermoresponsive Nanogele so modifiziert, dass sie unterschiedliche Volumenphasenübergangstemperaturen (VPTT) zwischen 33 und 47 °C aufweisen, wobei die thermoresponsiven Polymere PNIPAM und PNIPMAM verwendet wurden. Alle Nanogele zeigten eine hohe Protein-Verkapselungseffizienz (>80 %), bewahrten die Integrität des verkapselten Proteins, und konnten eine dermale Penetration mit VPTT-bedingter Freisetzung des Proteins und anschließender Abgabe in die lebensfähige Epidermis in exzidierter menschlicher Haut nachweisen. Durch die gleichmäßige Co-Polymerisation von Poly-N-Isopropylacrylamid (PNIPAM) und Poly-N-isopropylmethacrylamid (PNIPMAM) führte zu Nanogelen mit einer VPTT von ca. ~40 °C, was eine Erweiterung der dermalen Anwendungen ermöglichte, indem eine Verwendung externer Wärmequellen, wie einer Nahinfrarot-Lampe löst eine ausgeprägte Abgabe von Proteinen in die Haut auf kontrollierte lokale und zeitliche Weise aus.

Was den Schleimhaut Ansatz betrifft, wurden zum ersten Mal Redox-responsive Nanogele aus PNIPMAM Polymer mit bifunktionellen Disulfid-Vernetzer entwickelt und für die Verabreichung von Proteinen über die Schleimbarriere umfassend untersucht. Mit Blick auf die wesentlichen

Voraussetzungen für effiziente Mukus-Permeation, wurden die physikochemischen Eigenschaften der Nanogelen feinjustiert, um hydrophile Nanogelen mit einer Größe zwischen 100 und 200 nm, einer inerten Oberfläche, sowie intakten Disulfid-Bindungen zu erhalten. Die Überwachung von Wechselwirkungen zwischen den Nanogelen und nativem Darmschleim bestätigte einen allmählichen Disulfid-abhängigen Abbau der Nanogele in Mukus. Außerdem deuteten rheologische Messungen auf mucoadhäsive Wechselwirkung zwischen Mukus und Disulfid-haltigen Nanogelen hin. Zugleich zeigten Absorptionsstudien in frisch exzidiertem Schweine-Jejunum eine hervorragende Mukopenetration der Disulfid-haltigen Nanogelen und belegten die Vorzüge von Disulfiden in Bezug auf eine effiziente Überwindung der Mukus-korrelierten Filter- und Clearance-Mechanismen. Ähnliche Ergebnisse wurden auch in rekonstruierten menschlichen bronchialen Epithelmodellen *in vitro* nach längerer Expositionsdauer zu den Nanogelen bestätigt. Zudem wurde die Zytokompatibilität der Nanogelen auch in verschiedenen Schleimhautepithelzelltypen sowie primären Makrophagen nachgewiesen.

Als Nächstes wurde die therapeutische Effizienz der Nanogelen bei der Verabreichung vom Biologikum-Protein Etanercept (ETN; 150 kDa) untersucht. Dabei wurden eine hohe Verkapslungs-effizienz sowie eine strukturelle und funktionelle Stabilität des verkapselten ETN festgestellt. Zudem ergaben *in vitro* Freisetzungsstudien unter Mukus-relevanten Redox-Bedingungen, dass ETN mehrere Stunden lang in den Nanogelen aufbewahrt geblieben ist und weiterhin schrittweise unversehrt freigesetzt wurde beim Abbau der Nanogelen, was das große Potenzial von Disulfid-haltigen Nanogelen für die Verabreichung von Biomakromolekülen belegte. Die topische Anwendung von ETN-beladenen Nanogelen auf humane *in vitro* Modelle des Dünndarmgewebes, die das Krankheitsbild der chronisch-entzündlichen Darmerkrankung (IBD) simulieren, und auf bronchiales Epithelgewebe zeigten schließlich eine effiziente intraepitheliale ETN Verabreichung und entsprechende entzündungshemmende Wirkung. Im Laufe dieser Untersuchung wurden ernste Probleme in Bezug auf strukturelle Einschränkungen in den verfügbaren biologischen Testsystemen für die Darmschleimhaut festgestellt. Da solche Mängel die Studien zur Arzneimittelabsorption erheblich beeinträchtigen, wurden mehrere Schleimhaut-Testsysteme hierzu eingesetzt, um die Ergebnisse zu validieren und eine umfassende und zuverlässige Bewertung zu ermöglichen.

Insgesamt sind in dieser Arbeit neue responsive Nanogele als vielseitige und flexible Werkzeuge für die effiziente lokale Abgabe von Biomakromolekülen an die Haut- und Schleimhautoberflächen dargestellt. Weiterhin wird die Rolle der responsiven Modalitäten bei der Durchquerung von den robusten biologischen Barrieren neben der kontrollierten Freisetzung der therapeutischen Fracht demonstriert. Außerdem wurden kritische Probleme

bei den bestehenden Testsystemen zur Voraussage von Medikamenten-Verabreichung über die Schleimhäute hervorgehoben und die aktuellen Herausforderungen erläutert, um den entsprechenden experimentellen Verfahren in greifbaren klinischen Erfolg umzusetzen.

7. REFERENCES

1. Freitas Jr, R.A., *What is nanomedicine?* Nanomedicine: Nanotechnology, Biology and Medicine, **2005**. 1(1): p. 2-9.
2. Kim, B.Y., Rutka, J.T., and Chan, W.C., *Nanomedicine.* New England Journal of Medicine, **2010**. 363(25): p. 2434-2443.
3. Clyvedon, P. *The royal society & the royal academy of engineering*. in *Nanoscience and Nanotechnologies, workshop, Science Policy Section*. **2004**.
4. Murthy, S.K., *Nanoparticles in modern medicine: state of the art and future challenges.* International journal of nanomedicine, **2007**. 2(2): p. 129.
5. Krukemeyer, M., Krenn, V., Huebner, F., Wagner, W., and Resch, R., *History and possible uses of nanomedicine based on nanoparticles and nanotechnological progress.* Journal of Nanomedicine & Nanotechnology, **2015**. 6(1).
6. Fenton, O.S., Olafson, K.N., Pillai, P.S., Mitchell, M.J., and Langer, R., *Advances in Biomaterials for Drug Delivery.* Adv Mater, **2018**. 10.1002/adma.201705328: p. e1705328.
7. Meng, S., Chen, Z., Yang, L., Zhang, W., Liu, D., Guo, J., Guan, Y., and Li, J., *Enhanced transdermal bioavailability of testosterone propionate via surfactant-modified ethosomes.* International journal of nanomedicine, **2013**. 8: p. 3051.
8. Nochi, T., Yuki, Y., Takahashi, H., Sawada, S.-i., Mejima, M., Kohda, T., Harada, N., Kong, I.G., Sato, A., and Kataoka, N., *Nanogel antigenic protein-delivery system for adjuvant-free intranasal vaccines.* Nature materials, **2010**. 9(7): p. 572-578.
9. Picone, P., Ditta, L.A., Sabatino, M.A., Militello, V., San Biagio, P.L., Di Giacinto, M.L., Cristaldi, L., Nuzzo, D., Dispenza, C., and Giacomazza, D., *Ionizing radiation-engineered nanogels as insulin nanocarriers for the development of a new strategy for the treatment of Alzheimer's disease.* Biomaterials, **2016**. 80: p. 179-194.
10. Sadhasivam, L., Dey, N., Francis, A.P., and Devasena, T., *Transdermal patches of chitosan nanoparticles for insulin delivery.* Int J Pharm Pharm Sci, **2015**. 7(5): p. 84-88.
11. Carrillo-Conde, B.R., Brewer, E., Lowman, A., and Peppas, N.A., *Complexation Hydrogels as Oral Delivery Vehicles of Therapeutic Antibodies: An in Vitro and ex Vivo Evaluation of Antibody Stability and Bioactivity.* Ind Eng Chem Res, **2015**. 54(42): p. 10197-10205.
12. Yu, M., Wu, J., Shi, J., and Farokhzad, O.C., *Nanotechnology for protein delivery: Overview and perspectives.* J Control Release, **2016**. 240: p. 24-37.
13. Allen, T.M. and Cullis, P.R.J.S., *Drug delivery systems: entering the mainstream.* **2004**. 303(5665): p. 1818-1822.
14. Etheridge, M.L., Campbell, S.A., Erdman, A.G., Haynes, C.L., Wolf, S.M., and McCullough, J., *The big picture on nanomedicine: the state of investigational and approved nanomedicine products.* Nanomedicine : nanotechnology, biology, and medicine, **2013**. 9(1): p. 1-14.
15. Anselmo, A.C. and Mitragotri, S., *Nanoparticles in the clinic.* Bioeng Transl Med, **2016**. 1(1): p. 10-29.
16. Ventola, C.L., *Progress in nanomedicine: approved and investigational nanodrugs.* Pharmacy and Therapeutics, **2017**. 42(12): p. 742.
17. Bobo, D., Robinson, K.J., Islam, J., Thurecht, K.J., and Corrie, S.R., *Nanoparticle-Based Medicines: A Review of FDA-Approved Materials and Clinical Trials to Date.* Pharm Res, **2016**. 33(10): p. 2373-87.
18. Zhang, Y., Chan, H.F., and Leong, K.W., *Advanced materials and processing for drug delivery: the past and the future.* Adv Drug Deliv Rev, **2013**. 65(1): p. 104-20.
19. Milane, L. and Amiji, M., *Clinical approval of nanotechnology-based SARS-CoV-2 mRNA vaccines: impact on translational nanomedicine.* Drug Deliv Transl Res, **2021**. 10.1007/s13346-021-00911-y.
20. Kisby, T., Yilmazer, A., and Kostarelos, K., *Reasons for success and lessons learnt from nanoscale vaccines against COVID-19.* Nature Nanotechnology, **2021**. 16(8): p. 843-850.
21. FDA, *Moderna COVID-19 Vaccine EUA Letter of Authorization.pdf*. **2020**.
22. FDA, *Pfizer COVID-19 EUA Letter of Authorization reissued 122320.pdf*. **2020**.

23. Wolfram, J., Zhu, M., Yang, Y., Shen, J., Gentile, E., Paolino, D., Fresta, M., Nie, G., Chen, C., and Shen, H., *Safety of nanoparticles in medicine.* Current drug targets, **2015**. 16(14): p. 1671-1681.
24. Park, K., *Facing the truth about nanotechnology in drug delivery.* ACS Nano, **2013**. 7(9): p. 7442-7.
25. Pietroiusti, A., Campagnolo, L., and Fadeel, B., *Interactions of engineered nanoparticles with organs protected by internal biological barriers.* Small, **2013**. 9(9-10): p. 1557-1572.
26. Blanco, E., Shen, H., and Ferrari, M., *Principles of nanoparticle design for overcoming biological barriers to drug delivery.* Nature biotechnology, **2015**. 33(9): p. 941.
27. Anselmo, A.C. and Mitragotri, S., *Nanoparticles in the clinic: An update.* Bioeng Transl Med, **2019**. 4(3): p. e10143.
28. Cuggino, J.C., Blanco, E.R.O., Gugliotta, L.M., Alvarez Igarzabal, C.I., and Calderón, M., *Crossing biological barriers with nanogels to improve drug delivery performance.* Journal of Controlled Release, **2019**. 307: p. 221-246.
29. Metselaar, J.M. and Lammers, T., *Challenges in nanomedicine clinical translation.* Drug Deliv Transl Res, **2020**. 10(3): p. 721-725.
30. Hagens, W.I., Oomen, A.G., de Jong, W.H., Cassee, F.R., and Sips, A.J., *What do we (need to) know about the kinetic properties of nanoparticles in the body?* Regul Toxicol Pharmacol, **2007**. 49(3): p. 217-29.
31. Chacko, R.T., Ventura, J., Zhuang, J., and Thayumanavan, S., *Polymer nanogels: a versatile nanoscopic drug delivery platform.* Adv Drug Deliv Rev, **2012**. 64(9): p. 836-51.
32. Kabanov, A.V. and Vinogradov, S.V., *Nanogels as pharmaceutical carriers: finite networks of infinite capabilities.* Angew Chem Int Ed Engl, **2009**. 48(30): p. 5418-29.
33. Oh, J.K., Lee, D.I., and Park, J.M., *Biopolymer-based microgels/nanogels for drug delivery applications.* Progress in polymer science, **2009**. 34(12): p. 1261-1282.
34. Soni, K.S., Desale, S.S., and Bronich, T.K., *Nanogels: An overview of properties, biomedical applications and obstacles to clinical translation.* Journal of Controlled Release, **2016**. 240: p. 109-126.
35. Zhang, H., Zhai, Y., Wang, J., and Zhai, G., *New progress and prospects: The application of nanogel in drug delivery.* Materials Science and Engineering: C, **2016**. 60: p. 560-568.
36. Yin, Y., Hu, B., Yuan, X., Cai, L., Gao, H., and Yang, Q., *Nanogel: A Versatile Nano-Delivery System for Biomedical Applications.* Pharmaceutics, **2020**. 12(3).
37. Zha, L., Banik, B., and Alexis, F., *Stimulus responsive nanogels for drug delivery.* Soft Matter, **2011**. 7(13): p. 5908.
38. Molina, M., Asadian-Birjand, M., Balach, J., Bergueiro, J., Miceli, E., and Calderon, M., *Stimuli-responsive nanogel composites and their application in nanomedicine.* Chemical Society Reviews, **2015**. 44(17): p. 6161-6186.
39. Chan, M. and Almutairi, A., *Nanogels as imaging agents for modalities spanning the electromagnetic spectrum.* Materials horizons, **2016**. 3(1): p. 21-40.
40. Wu, H.Q. and Wang, C.C., *Biodegradable Smart Nanogels: A New Platform for Targeting Drug Delivery and Biomedical Diagnostics.* Langmuir, **2016**. 32(25): p. 6211-25.
41. Sivaram, A.J., Rajitha, P., Maya, S., Jayakumar, R., and Sabitha, M., *Nanogels for delivery, imaging and therapy.* Wiley Interdiscip Rev Nanomed Nanobiotechnol, **2015**. 7(4): p. 509-33.
42. Neamtu, I., Rusu, A.G., Diaconu, A., Nita, L.E., and Chiriac, A.P., *Basic concepts and recent advances in nanogels as carriers for medical applications.* Drug Deliv, **2017**. 24(1): p. 539-557.
43. Frey, H. and Haag, R., *Dendritic polyglycerol: a new versatile biocompatible material.* Reviews in Molecular Biotechnology, **2002**. 90(3): p. 257-267.
44. Tomalia, D.A., *Birth of a new macromolecular architecture: dendrimers as quantized building blocks for nanoscale synthetic polymer chemistry.* Progress in Polymer Science, **2005**. 30(3): p. 294-324.

45. Sisson, A.L. and Haag, R., *Polyglycerol nanogels: highly functional scaffolds for biomedical applications.* Soft Matter, **2010**. 6(20).
46. Calderon, M., Graeser, R., Kratz, F., and Haag, R., *Development of enzymatically cleavable prodrugs derived from dendritic polyglycerol.* Bioorg Med Chem Lett, **2009**. 19(14): p. 3725-8.
47. Sisson, A.L., Steinhilber, D., Rossow, T., Welker, P., Licha, K., and Haag, R., *Biocompatible functionalized polyglycerol microgels with cell penetrating properties.* Angewandte Chemie International Edition, **2009**. 48(41): p. 7540-7545.
48. Khandare, J., Mohr, A., Calderón, M., Welker, P., Licha, K., and Haag, R., *Structure-biocompatibility relationship of dendritic polyglycerol derivatives.* Biomaterials, **2010**. 31(15): p. 4268-4277.
49. Kainthan, R.K. and Brooks, D.E., *In vivo biological evaluation of high molecular weight hyperbranched polyglycerols*. Biomaterials. Vol. 28. **2007**. 4779-4787.
50. Steinhilber, D., Seiffert, S., Heyman, J.A., Paulus, F., Weitz, D.A., and Haag, R., *Hyperbranched polyglycerols on the nanometer and micrometer scale.* Biomaterials, **2011**. 32(5): p. 1311-1316.
51. Calderon, M., Quadir, M.A., Sharma, S.K., and Haag, R., *Dendritic polyglycerols for biomedical applications.* Adv Mater, **2010**. 22(2): p. 190-218.
52. Mura, S., Nicolas, J., and Couvreur, P., *Stimuli-responsive nanocarriers for drug delivery.* Nature materials, **2013**. 12(11): p. 991-1003.
53. Torchilin, V., *Multifunctional and stimuli-sensitive pharmaceutical nanocarriers.* European Journal of Pharmaceutics and Biopharmaceutics, **2009**. 71(3): p. 431-444.
54. Wei, M., Gao, Y., Li, X., and Serpe, M.J., *Stimuli-responsive polymers and their applications.* Polymer Chemistry, **2017**. 8(1): p. 127-143.
55. Cuggino, J.C., Molina, M., Wedepohl, S., Igarzabal, C.I.A., Calderón, M., and Gugliotta, L.M., *Responsive nanogels for application as smart carriers in endocytic pH-triggered drug delivery systems.* Eur Polym J, **2016**. 78: p. 14-24.
56. Oh, J.K., Siegwart, D.J., Lee, H.-i., Sherwood, G., Peteanu, L., Hollinger, J.O., Kataoka, K., and Matyjaszewski, K., *Biodegradable Nanogels Prepared by Atom Transfer Radical Polymerization as Potential Drug Delivery Carriers: Synthesis, Biodegradation, in Vitro Release, and Bioconjugation.* Journal of the American Chemical Society, **2007**. 129(18): p. 5939-5945.
57. Saito, G., Swanson, J.A., and Lee, K.-D., *Drug delivery strategy utilizing conjugation via reversible disulfide linkages: role and site of cellular reducing activities.* Advanced Drug Delivery Reviews, **2003**. 55(2): p. 199-215.
58. Forman, H.J., Zhang, H., and Rinna, A., *Glutathione: overview of its protective roles, measurement, and biosynthesis.* Mol Aspects Med, **2009**. 30(1-2): p. 1-12.
59. Lushchak, V.I., *Glutathione homeostasis and functions: potential targets for medical interventions.* J Amino Acids, **2012**. 2012: p. 736837.
60. Gamcsik, M.P., Kasibhatla, M.S., Teeter, S.D., and Colvin, O.M., *Glutathione levels in human tumors.* Biomarkers, **2012**. 17(8): p. 671-91.
61. Guo, X., Cheng, Y., Zhao, X., Luo, Y., Chen, J., and Yuan, W.E., *Advances in redox-responsive drug delivery systems of tumor microenvironment.* J Nanobiotechnology, **2018**. 16(1): p. 74.
62. Zhang, X., Malhotra, S., Molina, M., and Haag, R., *Micro- and nanogels with labile crosslinks - from synthesis to biomedical applications.* Chem Soc Rev, **2015**. 44(7): p. 1948-73.
63. Carvalho, A.M., Teixeira, R., Novoa-Carballal, R., Pires, R.A., Reis, R.L., and Pashkuleva, I., *Redox-Responsive Micellar Nanoparticles from Glycosaminoglycans for CD44 Targeted Drug Delivery.* Biomacromolecules, **2018**. 19(7): p. 2991-2999.
64. Steinhilber, D., Sisson, A.L., Mangoldt, D., Welker, P., Licha, K., and Haag, R., *Synthesis, Reductive Cleavage, and Cellular Interaction Studies of Biodegradable, Polyglycerol Nanogels.* Adv Funct Mater, **2010**. 20(23): p. 4133-4138.

65. Zhang, X., Achazi, K., Steinhilber, D., Kratz, F., Dernedde, J., and Haag, R., *A facile approach for dual-responsive prodrug nanogels based on dendritic polyglycerols with minimal leaching.* Journal of Controlled Release, **2014**. 174: p. 209-216.
66. Shatsberg, Z., Zhang, X., Ofek, P., Malhotra, S., Krivitsky, A., Scomparin, A., Tiram, G., Calderon, M., Haag, R., and Satchi-Fainaro, R., *Functionalized nanogels carrying an anticancer microRNA for glioblastoma therapy.* J Control Release, **2016**. 239: p. 159-68.
67. Fleige, E., Quadir, M.A., and Haag, R., *Stimuli-responsive polymeric nanocarriers for the controlled transport of active compounds: concepts and applications.* Advanced drug delivery reviews, **2012**. 64(9): p. 866-884.
68. Constantin, M., Cristea, M., Ascenzi, P., and Fundueanu, G., *Lower critical solution temperature versus volume phase transition temperature in thermoresponsive drug delivery systems.* Express Polym Lett, **2011**. 5(10): p. 839-848.
69. Djokpé, E. and Vogt, W., *N-Isopropylacrylamide and N-Isopropylmethacryl-amide: Cloud Points of Mixtures and Copolymers.* Macromol Chem Phys, **2001**. 202(5): p. 750-757.
70. Dybal, J., Trchová, M., and Schmidt, P., *The role of water in structural changes of poly(N-isopropylacrylamide) and poly(N-isopropylmethacrylamide) studied by FTIR, Raman spectroscopy and quantum chemical calculations.* Vibrational Spectroscopy, **2009**. 51(1): p. 44-51.
71. Fujishige, S., Kubota, K., and Ando, I., *Phase transition of aqueous solutions of poly(N-isopropylacrylamide) and poly(N-isopropylmethacrylamide).* The Journal of Physical Chemistry, **1989**. 93(8): p. 3311-3313.
72. Boer, M., Duchnik, E., Maleszka, R., and Marchlewicz, M., *Structural and biophysical characteristics of human skin in maintaining proper epidermal barrier function.* Postepy Dermatol Alergol, **2016**. 33(1): p. 1-5.
73. Ng, K.W. and Lau, W.M., *Skin Deep: The Basics of Human Skin Structure and Drug Penetration*, in *Percutaneous Penetration Enhancers Chemical Methods in Penetration Enhancement: Drug Manipulation Strategies and Vehicle Effects*, N. Dragicevic and H.I. Maibach, Editors. **2015**, Springer Berlin Heidelberg: Berlin, Heidelberg. p. 3-11.
74. Menon, G.K., Cleary, G.W., and Lane, M.E., *The structure and function of the stratum corneum.* Int J Pharm, **2012**. 435(1): p. 3-9.
75. Yousef, H., Alhajj, M., and Sharma, S., *Anatomy, Skin (Integument), Epidermis*. **2020**: StatPearls Publishing, Treasure Island (FL).
76. Bos, J.D. and Meinardi, M.M.H.M., *The 500 Dalton rule for the skin penetration of chemical compounds and drugs.* Exp Dermatol, **2000**. 9(3): p. 165-169.
77. Mbah, C., Uzor, P.F., and Omeje, E., *Perspectives on transdermal drug delivery.* J Chem Pharm Res, **2011**. 3(3): p. 680 -700.
78. Schneider, M., Stracke, F., Hansen, S., and Schaefer, U.F., *Nanoparticles and their interactions with the dermal barrier.* Dermatoendocrinol, **2009**. 1(4): p. 197-206.
79. Wertz, P.W., *Current understanding of skin biology pertinent to skin penetration: skin biochemistry.* Skin Pharmacol Physiol, **2013**. 26(4-6): p. 217-26.
80. Giulbudagian, M., Rancan, F., Klossek, A., Yamamoto, K., Jurisch, J., Neto, V.C., Schrade, P., Bachmann, S., Ruhl, E., Blume-Peytavi, U., Vogt, A., and Calderon, M., *Correlation between the chemical composition of thermoresponsive nanogels and their interaction with the skin barrier.* J Control Release, **2016**. 243: p. 323-332.
81. Bouwstra, J.A., Honeywell-Nguyen, P.L., Gooris, G.S., and Ponec, M., *Structure of the skin barrier and its modulation by vesicular formulations.* Progress in Lipid Research, **2003**. 42(1): p. 1-36.
82. Viano, M., Alotto, D., Aillon, A., Castagnoli, C., and Silvagno, F., *A thermal gradient modulates the oxidative metabolism and growth of human keratinocytes.* FEBS Open Bio, **2017**. 7(12): p. 1843-1853.

83. Chanmugam, A., Langemo, D., Thomason, K., Haan, J., Altenburger, E.A., Tippett, A., Henderson, L., and Zortman, T.A., *Relative Temperature Maximum in Wound Infection and Inflammation as Compared with a Control Subject Using Long-Wave Infrared Thermography.* Advances in Skin & Wound Care, **2017**. 30(9).
84. Cuggino, J.C., Strumia, M.C., Welker, P., Licha, K., Steinhilber, D., Mutihac, R.-C., and Calderón, M., *Thermosensitive nanogels based on dendritic polyglycerol and N-isopropylacrylamide for biomedical applications.* Soft Matter, **2011**. 7(23): p. 11259-11266.
85. Gerecke, C., Edlich, A., Giulbudagian, M., Schumacher, F., Zhang, N., Said, A., Yealland, G., Lohan, S.B., Neumann, F., Meinke, M.C., Ma, N., Calderon, M., Hedtrich, S., Schafer-Korting, M., and Kleuser, B., *Biocompatibility and characterization of polyglycerol-based thermoresponsive nanogels designed as novel drug-delivery systems and their intracellular localization in keratinocytes.* Nanotoxicology, **2017**. 11(2): p. 267-277.
86. Witting, M., Molina, M., Obst, K., Plank, R., Eckl, K.M., Hennies, H.C., Calderon, M., Friess, W., and Hedtrich, S., *Thermosensitive dendritic polyglycerol-based nanogels for cutaneous delivery of biomacromolecules.* Nanomedicine, **2015**. 11(5): p. 1179-87.
87. Plank, R., Yealland, G., Miceli, E., Lima Cunha, D., Graff, P., Thomforde, S., Gruber, R., Moosbrugger-Martinz, V., Eckl, K., Calderon, M., Hennies, H.C., and Hedtrich, S., *Transglutaminase 1 Replacement Therapy Successfully Mitigates the Autosomal Recessive Congenital Ichthyosis Phenotype in Full-Thickness Skin Disease Equivalents.* J Invest Dermatol, **2019**. 139(5): p. 1191-1195.
88. LaCount, T.D., Zhang, Q., Hao, J., Ghosh, P., Raney, S.G., Talattof, A., Kasting, G.B., and Li, S.K., *Modeling Temperature-Dependent Dermal Absorption and Clearance for Transdermal and Topical Drug Applications.* AAPS J, **2020**. 22(3): p. 70.
89. Jaque, D., Martinez Maestro, L., del Rosal, B., Haro-Gonzalez, P., Benayas, A., Plaza, J.L., Martin Rodriguez, E., and Garcia Sole, J., *Nanoparticles for photothermal therapies.* Nanoscale, **2014**. 6(16): p. 9494-530.
90. Fomina, N., McFearin, C.L., Sermsakdi, M., Morachis, J.M., and Almutairi, A., *Low Power, Biologically Benign NIR Light Triggers Polymer Disassembly.* Macromolecules, **2011**. 44(21): p. 8590-8597.
91. Rancan, F., Giulbudagian, M., Jurisch, J., Blume-Peytavi, U., Calderon, M., and Vogt, A., *Drug delivery across intact and disrupted skin barrier: Identification of cell populations interacting with penetrated thermoresponsive nanogels.* European Journal of Pharmaceutics and Biopharmaceutics, **2017**. 116: p. 4-11.
92. Asadian-Birjand, M., Bergueiro, J., Rancan, F., Cuggino, J.C., Mutihac, R.C., Achazi, K., Dernedde, J., Blume-Peytayi, U., Vogt, A., and Calderón, M., *Engineering thermoresponsive polyether-based nanogels for temperature dependent skin penetration.* Polymer Chemistry, **2015**. 6(32): p. 5827-5831.
93. Bergueiro, J. and Calderon, M., *Thermoresponsive nanodevices in biomedical applications.* Macromol Biosci, **2015**. 15(2): p. 183-99.
94. Dewhirst, M.W., Viglianti, B.L., Lora-Michiels, M., Hoopes, P.J., and Hanson, M., *Thermal Dose Requirement for Tissue Effect: Experimental and Clinical Findings.* Proc SPIE Int Soc Opt Eng, **2003**. 4954: p. 37.
95. Roti Roti, J.L., *Cellular responses to hyperthermia (40-46 degrees C): cell killing and molecular events.* Int J Hyperthermia, **2008**. 24(1): p. 3-15.
96. Pearson, J.P. and Brownlee, I.A., *Structure and Fucntion of Mucosal Surfaces*, in *Colonization of Mucosal Surfaces*. **2005**, American Society of Microbiology.
97. Araujo, F., Martins, C., Azevedo, C., and Sarmento, B., *Chemical modification of drug molecules as strategy to reduce interactions with mucus.* Adv Drug Deliv Rev, **2018**. 124: p. 98-106.
98. Boegh, M., Foged, C., Müllertz, A., and Mørck Nielsen, H., *Mucosal drug delivery: barriers, in vitro models and formulation strategies.* J Drug Deliv Scie Tech, **2013**. 23(4): p. 383-391.

99. Pearson, J.P., Chater, P.I., and Wilcox, M.D., *The properties of the mucus barrier, a unique gel – how can nanoparticles cross it?* Therapeutic Delivery, **2016**. 7(4): p. 229-244.
100. Cone, R.A., *Barrier properties of mucus.* Adv Drug Deliv Rev, **2009**. 61(2): p. 75-85.
101. Lai, S.K., Wang, Y.-Y., Wirtz, D., and Hanes, J., *Micro- and macrorheology of mucus.* Adv Drug Deliv Rev, **2009**. 61(2): p. 86-100.
102. Bansil, R. and Turner, B.S., *Mucin structure, aggregation, physiological functions and biomedical applications.* Current Opinion in Colloid & Interface Science, **2006**. 11(2): p. 164-170.
103. Perez-Vilar, J. and Mabolo, R., *Gel-forming mucins. Notions from in vitro studies.* Histol Histopathol, **2007**. 22(4): p. 455-64.
104. Thornton, D.J. and Sheehan, J.K., *From mucins to mucus: toward a more coherent understanding of this essential barrier.* Proc Am Thorac Soc, **2004**. 1(1): p. 54-61.
105. Perez-Vilar, J. and Hill, R.L., *The Structure and Assembly of Secreted Mucins * 210.* J Bio Chemi, **1999**. 274(45): p. 31751-31754.
106. Lai, S.K., Wang, Y.-Y., and Hanes, J., *Mucus-penetrating nanoparticles for drug and gene delivery to mucosal tissues.* Adv Drug Deliv Rev, **2009**. 61(2): p. 158-171.
107. Johansson, M.E., Sjovall, H., and Hansson, G.C., *The gastrointestinal mucus system in health and disease.* Nat Rev Gastroenterol Hepatol, **2013**. 10(6): p. 352-61.
108. Boegh, M. and Nielsen, H.M., *Mucus as a barrier to drug delivery - understanding and mimicking the barrier properties.* Basic Clin Pharmacol Toxicol, **2015**. 116(3): p. 179-86.
109. HUGO. *HUGO gene nomenclature committee* 2021 [cited 2021 Mar. 25]; Available from: http://www.genenames.org.
110. Hollingsworth, M.A. and Swanson, B.J., *Mucins in cancer: protection and control of the cell surface.* Nature Reviews Cancer, **2004**. 4(1): p. 45-60.
111. Bron, A.J., Tiffany, J.M., Gouveia, S.M., Yokoi, N., and Voon, L.W., *Functional aspects of the tear film lipid layer.* Experimental Eye Research, **2004**. 78(3): p. 347-360.
112. Atuma, C., Strugala, V., Allen, A., and Holm, L., *The adherent gastrointestinal mucus gel layer: thickness and physical state in vivo.* American Journal of Physiology-Gastrointestinal and Liver Physiology, **2001**. 280(5): p. G922-G929.
113. Witten, J., Samad, T., and Ribbeck, K., *Selective permeability of mucus barriers.* Curr Opin Biotechnol, **2018**. 52: p. 124-133.
114. García-Díaz, M., Birch, D., Wan, F., and Nielsen, H.M., *The role of mucus as an invisible cloak to transepithelial drug delivery by nanoparticles.* Advanced drug delivery reviews, **2018**. 124: p. 107-124.
115. Leal, J., Smyth, H.D.C., and Ghosh, D., *Physicochemical properties of mucus and their impact on transmucosal drug delivery.* Int J Pharm, **2017**. 532(1): p. 555-572.
116. Lieleg, O. and Ribbeck, K., *Biological hydrogels as selective diffusion barriers.* Trends Cell Biol, **2011**. 21(9): p. 543-51.
117. Yildiz, H.M., McKelvey, C.A., Marsac, P.J., and Carrier, R.L., *Size selectivity of intestinal mucus to diffusing particulates is dependent on surface chemistry and exposure to lipids.* J Drug Target, **2015**. 23(7-8): p. 768-74.
118. Witten, J., Samad, T., and Ribbeck, K., *Molecular Characterization of Mucus Binding.* Biomacromolecules, **2019**. 20(4): p. 1505-1513.
119. Chatterjee, B., Amalina, N., Sengupta, P., and Mandal, U.K., *Mucoadhesive polymers and their mode of action: A recent update.* J App Pharm Sci, **2017**. 7(5): p. 195-203.
120. Ostuni, E., Chapman, R.G., Holmlin, R.E., Takayama, S., and Whitesides, G.M., *A Survey of Structure–Property Relationships of Surfaces that Resist the Adsorption of Protein.* Langmuir, **2001**. 17(18): p. 5605-5620.
121. Wu, L., Shan, W., Zhang, Z., and Huang, Y., *Engineering nanomaterials to overcome the mucosal barrier by modulating surface properties.* Advanced Drug Delivery Reviews, **2018**. 124: p. 150-163.

122. Netsomboon, K. and Bernkop-Schnurch, A., *Mucoadhesive vs. mucopenetrating particulate drug delivery.* Eur J Pharm Biopharm, **2016**. 98: p. 76-89.
123. Boddupalli, B.M., Mohammed, Z.N., Nath, R.A., and Banji, D., *Mucoadhesive drug delivery system: An overview.* J Adv Pharm Technol Res, **2010**. 1(4): p. 381-7.
124. Sosnik, A., das Neves, J., and Sarmento, B., *Mucoadhesive polymers in the design of nano-drug delivery systems for administration by non-parenteral routes: A review.* Prog Polym Sci, **2014**. 39(12): p. 2030-2075.
125. Alhalaweh, A., Vilinska, A., Gavini, E., Rassu, G., and Velaga, S.P., *Surface Thermodynamics of Mucoadhesive Dry Powder Formulation of Zolmitriptan.* AAPS PharmSciTech, **2011**. 12(4): p. 1186-1192.
126. G. Sandri, S.R., Bonferoni, M.C., Ferrari, F., Mori, M., and Caramella, C., *The role of chitosan as a mucoadhesive agent in mucosal drug delivery.* Journal of Drug Delivery Science and Technology, **2012**. 22(4): p. 275-284.
127. He, P., Davis, S.S., and Illum, L., *In vitro evaluation of the mucoadhesive properties of chitosan microspheres.* International Journal of Pharmaceutics, **1998**. 166(1): p. 75-88.
128. Dekina, S., Romanovska, I., Ovsepyan, A., Tkach, V., and Muratov, E., *Gelatin/carboxymethyl cellulose mucoadhesive films with lysozyme: Development and characterization.* Carbohydrate Polymers, **2016**. 147: p. 208-215.
129. Luo, Y., Teng, Z., Li, Y., and Wang, Q., *Solid lipid nanoparticles for oral drug delivery: Chitosan coating improves stability, controlled delivery, mucoadhesion and cellular uptake.* Carbohydrate Polymers, **2015**. 122: p. 221-229.
130. Shaikh, R., Raj Singh, T.R., Garland, M.J., Woolfson, A.D., and Donnelly, R.F., *Mucoadhesive drug delivery systems.* Journal of pharmacy & bioallied sciences, **2011**. 3(1): p. 89-100.
131. Russo, E., Selmin, F., Baldassari, S., Gennari, C.G.M., Caviglioli, G., Cilurzo, F., Minghetti, P., and Parodi, B., *A focus on mucoadhesive polymers and their application in buccal dosage forms.* J Drug Deliv Scie Tech, **2016**. 32: p. 113-125.
132. Barthelmes, J., Dünnhaupt, S., Unterhofer, S., Perera, G., Schlocker, W., and Bernkop-Schnürch, A., *Thiolated particles as effective intravesical drug delivery systems for treatment of bladder-related diseases.* Nanomedicine, **2013**. 8(1): p. 65-75.
133. Maisel, K., Ensign, L., Reddy, M., Cone, R., and Hanes, J., *Effect of surface chemistry on nanoparticle interaction with gastrointestinal mucus and distribution in the gastrointestinal tract following oral and rectal administration in the mouse.* J Control Release, **2015**. 197: p. 48-57.
134. Feng, C., Li, J., Kong, M., Liu, Y., Cheng, X.J., Li, Y., Park, H.J., and Chen, X.G., *Surface charge effect on mucoadhesion of chitosan based nanogels for local anti-colorectal cancer drug delivery.* Colloids and Surfaces B: Biointerfaces, **2015**. 128: p. 439-447.
135. Mahmood, A., Laffleur, F., Leonaviciute, G., and Bernkop-Schnürch, A., *Protease-functionalized mucus penetrating microparticles: In-vivo evidence for their potential.* International Journal of Pharmaceutics, **2017**. 532(1): p. 177-184.
136. Efiana, N.A., Phan, T.N.Q., Wicaksono, A.J., and Bernkop- Schnürch, A., *Mucus permeating self-emulsifying drug delivery systems (SEDDS): About the impact of mucolytic enzymes.* Colloids and Surfaces B: Biointerfaces, **2018**. 161: p. 228-235.
137. Menzel, C. and Bernkop-Schnürch, A., *Enzyme decorated drug carriers: Targeted swords to cleave and overcome the mucus barrier.* Advanced Drug Delivery Reviews, **2018**. 124: p. 164-174.
138. Matsui, H., Wagner, V.E., Hill, D.B., Schwab, U.E., Rogers, T.D., Button, B., Taylor, R.M., Superfine, R., Rubinstein, M., Iglewski, B.H., and Boucher, R.C., *A physical linkage between cystic fibrosis airway surface dehydration and Pseudomonas aeruginosa biofilms.* Proceedings of the National Academy of Sciences, **2006**. 103(48): p. 18131.

139. Fahy, J.V. and Dickey, B.F., *Airway Mucus Function and Dysfunction.* New England Journal of Medicine, **2010**. 363(23): p. 2233-2247.
140. Mitchell, M.J., Billingsley, M.M., Haley, R.M., Wechsler, M.E., Peppas, N.A., and Langer, R., *Engineering precision nanoparticles for drug delivery.* Nat Rev Drug Discov, **2021**. 20(2): p. 101-124.
141. Olmsted, S.S., Padgett, J.L., Yudin, A.I., Whaley, K.J., Moench, T.R., and Cone, R.A., *Diffusion of macromolecules and virus-like particles in human cervical mucus.* Biophysical journal, **2001**. 81(4): p. 1930-1937.
142. Mrsny, R.J., *Lessons from nature: "Pathogen-Mimetic" systems for mucosal Nano-medicines.* Adv Drug Deliv Rev, **2009**. 61(2): p. 172-192.
143. Bourganis, V., Karamanidou, T., Samaridou, E., Karidi, K., Kammona, O., and Kiparissides, C., *On the synthesis of mucus permeating nanocarriers.* European Journal of Pharmaceutics and Biopharmaceutics, **2015**. 97: p. 239-249.
144. Laffleur, F., Hintzen, F., Shahnaz, G., Rahmat, D., Leithner, K., and Bernkop-Schnürch, A., *Development and in vitro evaluation of slippery nanoparticles for enhanced diffusion through native mucus.* Nanomedicine, **2014**. 9(3): p. 387-396.
145. Liu, M., Zhang, J., Shan, W., and Huang, Y., *Developments of mucus penetrating nanoparticles.* Asi J Pharm Sci, **2015**. 10(4): p. 275-282.
146. Lowe, S., O'Brien-Simpson, N.M., and Connal, L.A., *Antibiofouling polymer interfaces: poly (ethylene glycol) and other promising candidates.* Polymer Chemistry, **2015**. 6(2): p. 198-212.
147. Huckaby, J.T. and Lai, S.K., *PEGylation for enhancing nanoparticle diffusion in mucus.* Adv Drug Deliv Rev, **2018**. 124: p. 125-139.
148. Popov, A., *Mucus-Penetrating Particles and the Role of Ocular Mucus as a Barrier to Micro- and Nanosuspensions.* J Ocul Pharmacol Ther, **2020**. 36(6): p. 366-375.
149. Schneider, C.S., Xu, Q., Boylan, N.J., Chisholm, J., Tang, B.C., Schuster, B.S., Henning, A., Ensign, L.M., Lee, E., Adstamongkonkul, P., Simons, B.W., Wang, S.-Y.S., Gong, X., Yu, T., Boyle, M.P., Suk, J.S., and Hanes, J., *Nanoparticles that do not adhere to mucus provide uniform and long-lasting drug delivery to airways following inhalation.* Science Advances, **2017**. 3(4): p. e1601556.
150. Ensign, L.M., Tang, B.C., Wang, Y.-Y., Tse, T.A., Hoen, T., Cone, R., and Hanes, J., *Mucus-Penetrating Nanoparticles for Vaginal Drug Delivery Protect Against Herpes Simplex Virus.* Science Translational Medicine, **2012**. 4(138): p. 138ra79.
151. Schopf, L., Enlow, E., Popov, A., Bourassa, J., and Chen, H., *Ocular Pharmacokinetics of a Novel Loteprednol Etabonate 0.4% Ophthalmic Formulation.* Ophthalmology and Therapy, **2014**. 3(1): p. 63-72.
152. Shan, W., Zhu, X., Liu, M., Li, L., Zhong, J., Sun, W., Zhang, Z., and Huang, Y., *Overcoming the Diffusion Barrier of Mucus and Absorption Barrier of Epithelium by Self-Assembled Nanoparticles for Oral Delivery of Insulin.* ACS Nano, **2015**. 9(3): p. 2345-2356.
153. Shan, W., Zhu, X., Tao, W., Cui, Y., Liu, M., Wu, L., Li, L., Zheng, Y., and Huang, Y., *Enhanced Oral Delivery of Protein Drugs Using Zwitterion-Functionalized Nanoparticles to Overcome both the Diffusion and Absorption Barriers.* ACS Applied Materials & Interfaces, **2016**. 8(38): p. 25444-25453.
154. Morishita, M., Goto, T., Peppas, N.A., Joseph, J.I., Torjman, M.C., Munsick, C., Nakamura, K., Yamagata, T., Takayama, K., and Lowman, A.M., *Mucosal insulin delivery systems based on complexation polymer hydrogels: effect of particle size on insulin enteral absorption.* Journal of Controlled Release, **2004**. 97(1): p. 115-124.
155. Norris, D.A., Puri, N., and Sinko, P.J., *The effect of physical barriers and properties on the oral absorption of particulates.* Adv Drug Deliv Rev, **1998**. 34(2): p. 135-154.
156. Witten, J. and Ribbeck, K., *The particle in the spider's web: transport through biological hydrogels.* Nanoscale, **2017**. 9(24): p. 8080-8095.

157. Cui, Y., Shan, W., Liu, M., Wu, L., and Huang, Y., *A strategy for developing effective orally-delivered nanoparticles through modulation of the surface "hydrophilicity/hydrophobicity balance".* J Mater Chem B, **2017**. 5(6): p. 1302-1314.
158. Wu, L., Liu, M., Shan, W., Cui, Y., Zhang, Z., and Huang, Y., *Lipid nanovehicles with adjustable surface properties for overcoming multiple barriers simultaneously in oral administration.* International Journal of Pharmaceutics, **2017**. 520(1): p. 216-227.
159. Zhu, X., Wu, J., Shan, W., Zhou, Z., Liu, M., and Huang, Y., *Sub-50 nm Nanoparticles with Biomimetic Surfaces to Sequentially Overcome the Mucosal Diffusion Barrier and the Epithelial Absorption Barrier.* Advanced Functional Materials, **2016**. 26(16): p. 2728-2738.
160. Liu, M., Zhang, J., Zhu, X., Shan, W., Li, L., Zhong, J., Zhang, Z., and Huang, Y., *Efficient mucus permeation and tight junction opening by dissociable "mucus-inert" agent coated trimethyl chitosan nanoparticles for oral insulin delivery.* J Control Release, **2016**. 222: p. 67-77.
161. Perera, G., Zipser, M., Bonengel, S., Salvenmoser, W., and Bernkop-Schnürch, A., *Development of phosphorylated nanoparticles as zeta potential inverting systems.* European Journal of Pharmaceutics and Biopharmaceutics, **2015**. 97: p. 250-256.
162. Bonengel, S., Prüfert, F., Perera, G., Schauer, J., and Bernkop-Schnürch, A., *Polyethylene imine-6-phosphogluconic acid nanoparticles – a novel zeta potential changing system.* International Journal of Pharmaceutics, **2015**. 483(1): p. 19-25.
163. Griesser, J., Burtscher, S., Köllner, S., Nardin, I., Prüfert, F., and Bernkop-Schnürch, A., *Zeta potential changing self-emulsifying drug delivery systems containing phosphorylated polysaccharides.* European Journal of Pharmaceutics and Biopharmaceutics, **2017**. 119: p. 264-270.
164. Köllner, S., Dünnhaupt, S., Waldner, C., Hauptstein, S., Pereira de Sousa, I., and Bernkop-Schnürch, A., *Mucus permeating thiomer nanoparticles.* European Journal of Pharmaceutics and Biopharmaceutics, **2015**. 97: p. 265-272.
165. Anitha, A., Deepa, N., Chennazhi, K.P., Nair, S.V., Tamura, H., and Jayakumar, R., *Development of mucoadhesive thiolated chitosan nanoparticles for biomedical applications.* Carbohydrate Polymers, **2011**. 83(1): p. 66-73.
166. Yin, L., Ding, J., He, C., Cui, L., Tang, C., and Yin, C., *Drug permeability and mucoadhesion properties of thiolated trimethyl chitosan nanoparticles in oral insulin delivery.* Biomaterials, **2009**. 30(29): p. 5691-700.
167. Oh, S. and Borros, S., *Mucoadhesion vs mucus permeability of thiolated chitosan polymers and their resulting nanoparticles using a quartz crystal microbalance with dissipation (QCM-D).* Colloids Surf B Biointerfaces, **2016**. 147: p. 434-441.
168. Leichner, C., Jelkmann, M., and Bernkop-Schnurch, A., *Thiolated polymers: Bioinspired polymers utilizing one of the most important bridging structures in nature.* Adv Drug Deliv Rev, **2019**. 151-152: p. 191-221.
169. Puri, V., Sharma, A., Kumar, P., and Singh, I., *Thiolation of Biopolymers for Developing Drug Delivery Systems with Enhanced Mechanical and Mucoadhesive Properties: A Review.* Polymers, **2020**. 12(8).
170. Liu, S., Shen, Z., Wu, B., Yu, Y., Hou, H., Zhang, X.-X., and Ren, H.-q., *Cytotoxicity and Efflux Pump Inhibition Induced by Molybdenum Disulfide and Boron Nitride Nanomaterials with Sheetlike Structure.* Environmental Science & Technology, **2017**. 51(18): p. 10834-10842.
171. Danquah, C.A., Kakagianni, E., Khondkar, P., Maitra, A., Rahman, M., Evangelopoulos, D., McHugh, T.D., Stapleton, P., Malkinson, J., Bhakta, S., and Gibbons, S., *Analogues of Disulfides from Allium stipitatum Demonstrate Potent Anti-tubercular Activities through Drug Efflux Pump and Biofilm Inhibition.* Scientific Reports, **2018**. 8(1): p. 1150.
172. Bandi, S.P., Bhatnagar, S., and Venuganti, V.V.K., *Advanced materials for drug delivery across mucosal barriers.* Acta Biomaterialia, **2021**. 119: p. 13-29.

173. Mollazadeh, S., Mackiewicz, M., and Yazdimamaghani, M., *Recent advances in the redox-responsive drug delivery nanoplatforms: A chemical structure and physical property perspective.* Materials Science and Engineering: C, **2021**. 118: p. 111536.
174. Wen, H. and Li, Y., *Redox sensitive nanoparticles with disulfide bond linked sheddable shell for intracellular drug delivery.* Med. Chem, **2014**. 4(11): p. 748-755.
175. Yang, F., Wang, J., Peng, G., Fu, S., Zhang, S., and Liu, C., *PEG-based bioresponsive hydrogels with redox-mediated formation and degradation.* Journal of Materials Science: Materials in Medicine, **2012**. 23(3): p. 697-710.
176. Weinhart, M., Grunwald, I., Wyszogrodzka, M., Gaetjen, L., Hartwig, A., and Haag, R., *Linear poly(methyl glycerol) and linear polyglycerol as potent protein and cell resistant alternatives to poly(ethylene glycol).* Chem Asian J, **2010**. 5(9): p. 1992-2000.
177. Abbina, S., Vappala, S., Kumar, P., Siren, E.M.J., La, C.C., Abbasi, U., Brooks, D.E., and Kizhakkedathu, J.N., *Hyperbranched polyglycerols: recent advances in synthesis, biocompatibility and biomedical applications.* J Mater Chem B, **2017**. 5(47): p. 9249-9277.
178. Manzanares-Guevara, L.A., Licea-Claverie, A., Oroz-Parra, I., Bernaldez-Sarabia, J., Diaz-Castillo, F., and Licea-Navarro, A.F., *Smart Nanoformulation Based on Stimuli-Responsive Nanogels and Curcumin: Promising Therapy against Colon Cancer.* ACS Omega, **2020**. 5(16): p. 9171-9184.
179. Cuggino, J.C., Blanco, E.R.O., Gugliotta, L.M., Alvarez Igarzabal, C.I., and Calderon, M., *Crossing biological barriers with nanogels to improve drug delivery performance.* J Control Release, **2019**. 307: p. 221-246.
180. reports, F. *Advancing health through innovation 2020. In: New drug therapy approvals*. 2020 [cited 2021 Mar. 26]; Available from: https://www.fda.gov/drugs/new-drugs-fda-cders-new-molecular-entities-and-new-therapeutic-biological-products/novel-drug-approvals-2020.
181. reports, F. *Advancing health through innovation 2019. In: New drug therapy approvals*. 2019 [cited 2021 Mar.26]; Available from: https://www.fda.gov/drugs/new-drugs-fda-cders-new-molecular-entities-and-new-therapeutic-biological-products/novel-drug-approvals-2019.
182. Sachdeva, S., Lobo, S., and Goswami, T., *What is the future of noninvasive routes for protein- and peptide-based drugs?* Therapeutic Delivery, **2016**. 7(6): p. 355-357.
183. Chaudhary, R., Balhara, M., and Chhillar, A.K., *Protein Therapeutic: Production, Application, and Future Scenario*, in *Metabolic Engineering for Bioactive Compounds: Strategies and Processes*, V.C. Kalia and A.K. Saini, Editors. **2017**, Springer Singapore: Singapore. p. 73-88.
184. Dimitrov, D.S., *Therapeutic proteins.* Methods Mol Biol, **2012**. 899: p. 1-26.
185. Krejsa, C., Rogge, M., and Sadee, W., *Protein therapeutics: new applications for pharmacogenetics.* Nature Reviews Drug Discovery, **2006**. 5(6): p. 507-521.
186. Pisal, D.S., Kosloski, M.P., and Balu-Iyer, S.V., *Delivery of therapeutic proteins.* J Pharm Sci, **2010**. 99(6): p. 2557-75.
187. Ratanji, K.D., Derrick, J.P., Dearman, R.J., and Kimber, I., *Immunogenicity of therapeutic proteins: influence of aggregation.* J Immunotoxicol, **2014**. 11(2): p. 99-109.
188. Frokjaer, S. and Otzen, D.E., *Protein drug stability: a formulation challenge.* Nat Rev Drug Discov, **2005**. 4(4): p. 298-306.
189. Mitragotri, S., Burke, P.A., and Langer, R., *Overcoming the challenges in administering biopharmaceuticals: formulation and delivery strategies.* Nat Rev Drug Discov, **2014**. 13(9): p. 655-72.
190. Ichikawa, H., *Design of Nanoparticles for Oral Delivery of Peptide Drugs*, in *Nanoparticle Technology Handbook*. **2018**. p. 407-414.
191. Bajracharya, R., Song, J.G., Back, S.Y., and Han, H.-K., *Recent Advancements in Non-Invasive Formulations for Protein Drug Delivery.* Computational and Structural Biotechnology Journal, **2019**. 17: p. 1290-1308.
192. Pretorius, E. and Bouic, P.J.D., *Permeation of Four Oral Drugs Through Human Intestinal Mucosa.* AAPS PharmSciTech, **2009**. 10(1): p. 270-275.

193. Morishita, M. and Peppas, N.A., *Is the oral route possible for peptide and protein drug delivery?* Drug Discov Today, **2006**. 11(19-20): p. 905-10.
194. Turner, J.R., *Intestinal mucosal barrier function in health and disease.* Nat Rev Immunol, **2009**. 9(11): p. 799-809.
195. Vancamelbeke, M. and Vermeire, S., *The intestinal barrier: a fundamental role in health and disease.* Expert Rev Gastroenterol Hepatol, **2017**. 11(9): p. 821-834.
196. Tuma, P.L. and Hubbard, A.L., *Transcytosis: crossing cellular barriers.* Physiological reviews, **2003**. 83(3): p. 871-932.
197. Pelaseyed, T., Bergstrom, J.H., Gustafsson, J.K., Ermund, A., Birchenough, G.M., Schutte, A., van der Post, S., Svensson, F., Rodriguez-Pineiro, A.M., Nystrom, E.E., Wising, C., Johansson, M.E., and Hansson, G.C., *The mucus and mucins of the goblet cells and enterocytes provide the first defense line of the gastrointestinal tract and interact with the immune system.* Immunol Rev, **2014**. 260(1): p. 8-20.
198. König, J., Wells, J., Cani, P.D., García-Ródenas, C.L., MacDonald, T., Mercenier, A., Whyte, J., Troost, F., and Brummer, R.-J., *Human intestinal barrier function in health and disease.* Clinical and translational gastroenterology, **2016**. 7(10): p. e196.
199. Menard, S., Cerf-Bensussan, N., and Heyman, M., *Multiple facets of intestinal permeability and epithelial handling of dietary antigens.* Mucosal Immunol, **2010**. 3(3): p. 247-59.
200. Agarwal, V. and Khan, M.A., *Current status of the oral delivery of insulin.* Pharm. Technol, **2001**. 10: p. 76-90.
201. Cone, R.A., *Mucus*, in *Mucosal Immunology (Third Edition)*, J. Mestecky, et al., Editors. **2005**, Academic Press: Burlington. p. 49-72.
202. Griessinger, J., Dunnhaupt, S., Cattoz, B., Griffiths, P., Oh, S., Borros i Gomez, S., Wilcox, M., Pearson, J., Gumbleton, M., Abdulkarim, M., Pereira de Sousa, I., and Bernkop-Schnurch, A., *Methods to determine the interactions of micro- and nanoparticles with mucus.* Eur J Pharm Biopharm, **2015**. 96: p. 464-76.
203. Srinivasan, B., Kolli, A.R., Esch, M.B., Abaci, H.E., Shuler, M.L., and Hickman, J.J., *TEER measurement techniques for in vitro barrier model systems.* J Lab Autom, **2015**. 20(2): p. 107-26.
204. Clarke, L.L., *A guide to Ussing chamber studies of mouse intestine.* Am J Physiol Gastrointest Liver Physiol, **2009**. 296(6): p. G1151-66.
205. Dezani, A.B., Pereira, T.M., Caffaro, A.M., Reis, J.M., and Serra, C.H., *Determination of lamivudine and zidovudine permeability using a different ex vivo method in Franz cells.* J Pharmacol Toxicol Methods, **2013**. 67(3): p. 194-202.
206. Gonzalez, L.M., Moeser, A.J., and Blikslager, A.T., *Porcine models of digestive disease: the future of large animal translational research.* Translational Research, **2015**. 166(1): p. 12-27.
207. Ziegler, A., Gonzalez, L., and Blikslager, A., *Large Animal Models: The Key to Translational Discovery in Digestive Disease Research.* Cell Mol Gastroenterol Hepatol, **2016**. 2(6): p. 716-724.
208. Nagpal, R., Wang, S., Solberg Woods, L.C., Seshie, O., Chung, S.T., Shively, C.A., Register, T.C., Craft, S., McClain, D.A., and Yadav, H., *Comparative Microbiome Signatures and Short-Chain Fatty Acids in Mouse, Rat, Non-human Primate, and Human Feces.* Front Microbiol, **2018**. 9: p. 2897.
209. Treuting, P.M., Dintzis, S.M., Liggitt, D., and Frevert, C.W., *Comparative anatomy and histology: a mouse and human atlas (expert consult)*. **2011**: Academic Press.
210. Nejdfors, P., Ekelund, M., Jeppsson, B., and Westrom, B.R., *Mucosal in vitro permeability in the intestinal tract of the pig, the rat, and man: species- and region-related differences.* Scand J Gastroenterol, **2000**. 35(5): p. 501-7.
211. Krupa, L., Bajka, B., Staroń, R., Dupont, D., Singh, H., Gutkowski, K., and Macierzanka, A., *Comparing the permeability of human and porcine small intestinal mucus for particle transport studies.* Scientific Reports, **2020**. 10(1): p. 20290.

212. Haslam, I.S., O'Reilly, D.A., Sherlock, D.J., Kauser, A., Womack, C., and Coleman, T., *Pancreatoduodenectomy as a source of human small intestine for Ussing chamber investigations and comparative studies with rat tissue.* Biopharmaceutics & Drug Disposition, **2011**. 32(4): p. 210-221.
213. Pietzonka, P., Walter, E., Duda-Johner, S., Langguth, P., and Merkle, H.P., *Compromised integrity of excised porcine intestinal epithelium obtained from the abattoir affects the outcome of in vitro particle uptake studies.* Eur J Pharm Sci, **2002**. 15(1): p. 39-47.
214. Volpe, D.A., *Variability in Caco-2 and MDCK Cell-Based Intestinal Permeability Assays.* Journal of Pharmaceutical Sciences, **2008**. 97(2): p. 712-725.
215. Fleisher, D., *Biological transport phenomena in the gastrointestinal tract: cellular mechanisms.* Transport processes in pharmaceutical systems, **2000**: p. 147-184.
216. Hilgendorf, C., Spahn-Langguth, H., Regårdh, C.G., Lipka, E., Amidon, G.L., and Langguth, P., *Caco-2 versus Caco-2/HT29-MTX Co-cultured Cell Lines: Permeabilities Via Diffusion, Inside- and Outside-Directed Carrier-Mediated Transport.* Journal of Pharmaceutical Sciences, **2000**. 89(1): p. 63-75.
217. Béduneau, A., Tempesta, C., Fimbel, S., Pellequer, Y., Jannin, V., Demarne, F., and Lamprecht, A., *A tunable Caco-2/HT29-MTX co-culture model mimicking variable permeabilities of the human intestine obtained by an original seeding procedure.* European Journal of Pharmaceutics and Biopharmaceutics, **2014**. 87(2): p. 290-298.
218. Lesuffleur, T., Porchet, N., Aubert, J.P., Swallow, D., Gum, J.R., Kim, Y.S., Real, F.X., and Zweibaum, A., *Differential expression of the human mucin genes MUC1 to MUC5 in relation to growth and differentiation of different mucus-secreting HT-29 cell subpopulations.* Journal of Cell Science, **1993**. 106(3): p. 771.
219. Briske-Anderson, M.J., Finley, J.W., and Newman, S.M., *The Influence of Culture Time and Passage Number on the Morphological and Physiological Development of Caco-2 Cells.* Proceedings of the Society for Experimental Biology and Medicine, **1997**. 214(3): p. 248-257.
220. Spottl, T., Hausmann, M., Gunckel, M., Herfarth, H., Herlyn, M., Schoelmerich, J., and Rogler, G., *A new organotypic model to study cell interactions in the intestinal mucosa.* European Journal of Gastroenterology & Hepatology, **2006**. 18(8).
221. Capes-Davis, A., Bairoch, A., Barrett, T., Burnett, E.C., Dirks, W.G., Hall, E.M., Healy, L., Kniss, D.A., Korch, C., Liu, Y., Neve, R.M., Nims, R.W., Parodi, B., Schweppe, R.E., Storts, D.R., and Tian, F., *Cell Lines as Biological Models: Practical Steps for More Reliable Research.* Chemical Research in Toxicology, **2019**. 32(9): p. 1733-1736.
222. Kauffman, A., Gyurdieva, A., Mabus, J., Ferguson, C., Yan, Z., and Hornby, P., *Alternative functional in vitro models of human intestinal epithelia.* Frontiers in Pharmacology, **2013**. 4(79).
223. Almeqdadi, M., Mana, M.D., Roper, J., and Yilmaz, Ö.H., *Gut organoids: mini-tissues in culture to study intestinal physiology and disease.* American Journal of Physiology-Cell Physiology, **2019**. 317(3): p. C405-C419.
224. Wallach, T. and Bayrer, J.R., *Intestinal organoids: new frontiers in the study of intestinal disease and physiology.* Journal of pediatric gastroenterology and nutrition, **2017**. 64(2): p. 180.
225. Ayehunie, S., Stevens, Z., Landry, T., Taimi, M., Klausner, M., and Hayden, P., *Novel 3D Human Small Intestinal Tissue Model (EpiIntestinalTM) to Assess Drug Permeation & Inflammation.* **2014**.
226. Ayehunie, S., Landry, T., Stevens, Z., Armento, A., Hayden, P., and Klausner, M., *Human Primary Cell-Based Organotypic Microtissues for Modeling Small Intestinal Drug Absorption.* Pharmaceutical Research, **2018**. 35(4): p. 72.
227. Markus, J., Landry, T., Stevens, Z., Scott, H., Llanos, P., Debatis, M., Armento, A., Klausner, M., and Ayehunie, S., *Human small intestinal organotypic culture model for drug permeation,*

inflammation, and toxicity assays. In Vitro Cellular & Developmental Biology - Animal, **2021**. 57(2): p. 160-173.

228. Cui, Y., Claus, S., Schnell, D., Runge, F., and MacLean, C., *In-Depth Characterization of EpiIntestinal Microtissue as a Model for Intestinal Drug Absorption and Metabolism in Human.* Pharmaceutics, **2020**. 12(5).
229. Westerhout, J., Steeg, E.v.d., Grossouw, D., Zeijdner, E.E., Krul, C.A.M., Verwei, M., and Wortelboer, H.M., *A new approach to predict human intestinal absorption using porcine intestinal tissue and biorelevant matrices.* European Journal of Pharmaceutical Sciences, **2014**. 63: p. 167-177.
230. Dahan, A. and Hoffman, A., *The effect of different lipid based formulations on the oral absorption of lipophilic drugs: The ability of in vitro lipolysis and consecutive ex vivo intestinal permeability data to predict in vivo bioavailability in rats.* European Journal of Pharmaceutics and Biopharmaceutics, **2007**. 67(1): p. 96-105.
231. Karlsson, N.G., Herrmann, A., Karlsson, H., Johansson, M.E., Carlstedt, I., and Hansson, G.C., *The glycosylation of rat intestinal Muc2 mucin varies between rat strains and the small and large intestine: a study of O-linked oligosaccharides by a mass spectrometric approach.* Journal of Biological Chemistry, **1997**. 272(43): p. 27025-27034.
232. Takenaka, T., Harada, N., Kuze, J., Chiba, M., Iwao, T., and Matsunaga, T., *Human Small Intestinal Epithelial Cells Differentiated from Adult Intestinal Stem Cells as a Novel System for Predicting Oral Drug Absorption in Humans.* Drug Metabolism and Disposition, **2014**. 42(11): p. 1947.
233. Baumgart, D.C. and Carding, S.R., *Inflammatory bowel disease: cause and immunobiology.* The Lancet, **2007**. 369(9573): p. 1627-1640.
234. Xavier, R.J. and Podolsky, D.K., *Unravelling the pathogenesis of inflammatory bowel disease.* Nature, **2007**. 448(7152): p. 427-34.
235. Lee, M.J., Parker, C.E., Taylor, S.R., Guizzetti, L., Feagan, B.G., Lobo, A.J., and Jairath, V., *Efficacy of Medical Therapies for Fistulizing Crohn's Disease: Systematic Review and Meta-analysis.* Clinical Gastroenterology and Hepatology, **2018**. 16(12): p. 1879-1892.
236. Strober, W., Fuss, I., and Mannon, P., *The fundamental basis of inflammatory bowel disease.* J Clin Invest, **2007**. 117(3): p. 514-21.
237. Feagins, L.A., Souza, R.F., and Spechler, S.J., *Carcinogenesis in IBD: potential targets for the prevention of colorectal cancer.* Nat Rev Gastroenterol Hepatol, **2009**. 6(5): p. 297-305.
238. Molodecky, N.A., Soon, I.S., Rabi, D.M., Ghali, W.A., Ferris, M., Chernoff, G., Benchimol, E.I., Panaccione, R., Ghosh, S., Barkema, H.W., and Kaplan, G.G., *Increasing incidence and prevalence of the inflammatory bowel diseases with time, based on systematic review.* Gastroenterology, **2012**. 142(1): p. 46-54 e42; quiz e30.
239. Carter, M.J., Lobo, A.J., and Travis, S.P.L., *Guidelines for the management of inflammatory bowel disease in adults.* Gut, **2004**. 53(suppl 5): p. v1.
240. Targan, S.R., *Current limitations of IBD treatment: where do we go from here?* Ann N Y Acad Sci, **2006**. 1072: p. 1-8.
241. Lichtenstein, G.R., *Comprehensive review: antitumor necrosis factor agents in inflammatory bowel disease and factors implicated in treatment response.* Therap Adv Gastroenterol, **2013**. 6(4): p. 269-93.
242. Michielan, A. and D'Inca, R., *Intestinal Permeability in Inflammatory Bowel Disease: Pathogenesis, Clinical Evaluation, and Therapy of Leaky Gut.* Mediators Inflamm, **2015**. 2015: p. 628157.
243. Youshia, J. and Lamprecht, A., *Size-dependent nanoparticulate drug delivery in inflammatory bowel diseases.* Expert Opinion on Drug Delivery, **2016**. 13(2): p. 281-294.
244. Lamprecht, A., Yamamoto, H., Takeuchi, H., and Kawashima, Y., *Nanoparticles enhance therapeutic efficiency by selectively increased local drug dose in experimental colitis in rats.* J Pharmacol Exp Ther, **2005**. 315(1): p. 196-202.

245. Lautenschlager, C., Schmidt, C., Lehr, C.M., Fischer, D., and Stallmach, A., *PEG-functionalized microparticles selectively target inflamed mucosa in inflammatory bowel disease.* Eur J Pharm Biopharm, **2013**. 85(3 Pt A): p. 578-86.
246. Laroui, H., Ingersoll, S.A., Liu, H.C., Baker, M.T., Ayyadurai, S., Charania, M.A., Laroui, F., Yan, Y., Sitaraman, S.V., and Merlin, D., *Dextran sodium sulfate (DSS) induces colitis in mice by forming nano-lipocomplexes with medium-chain-length fatty acids in the colon.* PLoS One, **2012**. 7(3): p. e32084.
247. Chassaing, B., Aitken, J.D., Malleshappa, M., and Vijay-Kumar, M., *Dextran sulfate sodium (DSS)-induced colitis in mice.* Curr Protoc Immunol, **2014**. 104: p. 15 25 1-15 25 14.
248. Silva, I., Pinto, R., and Mateus, V., *Preclinical Study in Vivo for New Pharmacological Approaches in Inflammatory Bowel Disease: A Systematic Review of Chronic Model of TNBS-Induced Colitis.* J Clin Med, **2019**. 8(10).
249. Strober, W., Fuss, I.J., and Blumberg, R.S., *The Immunology of Mucosal Models of Inflammation.* Annual Review of Immunology, **2002**. 20(1): p. 495-549.
250. Barnett, M. and Fraser, A., *Animal models of colitis: lessons learned, and their relevance to the clinic.* Ulcerative Colitis–Treatments, Special Populations and the Future, **2011**. 2: p. 161-165.
251. Jiminez, J.A., Uwiera, T.C., Douglas Inglis, G., and Uwiera, R.R., *Animal models to study acute and chronic intestinal inflammation in mammals.* Gut Pathog, **2015**. 7: p. 29.
252. Langer, R. and Vacanti, J., *Advances in tissue engineering.* Journal of pediatric surgery, **2016**. 51(1): p. 8-12.
253. Kolios, G., *Animal models of inflammatory bowel disease: how useful are they really?* Current opinion in gastroenterology, **2016**. 32(4): p. 251-257.
254. DeVoss, J. and Diehl, L., *Murine models of inflammatory bowel disease (IBD): challenges of modeling human disease.* Toxicol Pathol, **2014**. 42(1): p. 99-110.
255. Fedorak, R.N., Gangl, A., Elson, C.O., Rutgeerts, P., Schreiber, S., Wild, G., Hanauer, S.B., Kilian, A., Cohard, M., LeBeaut, A., and Feagan, B., *Recombinant human interleukin 10 in the treatment of patients with mild to moderately active Crohn's disease.* Gastroenterology, **2000**. 119(6): p. 1473-1482.
256. Schreiber, S., Fedorak, R.N., Nielsen, O.H., Wild, G., Williams, C.N., Nikolaus, S., Jacyna, M., Lashner, B.A., Gangl, A., Rutgeerts, P., Isaacs, K., Van Deventer, S.J.H., Koningsberger, J.C., Cohard, M., LeBeaut, A., and Hanauer, S.B., *Safety and efficacy of recombinant human interleukin 10 in chronic active Crohn's disease.* Gastroenterology, **2000**. 119(6): p. 1461-1472.
257. Nguyen, T.L., Vieira-Silva, S., Liston, A., and Raes, J., *How informative is the mouse for human gut microbiota research?* Dis Model Mech, **2015**. 8(1): p. 1-16.
258. Gkouskou, K.K., Deligianni, C., Tsatsanis, C., and Eliopoulos, A.G., *The gut microbiota in mouse models of inflammatory bowel disease.* Front Cell Infect Microbiol, **2014**. 4: p. 28.
259. Chater, P.I., Wilcox, M.D., and Pearson, J.P., *Efficacy and safety concerns over the use of mucus modulating agents for drug delivery using nanoscale systems.* Adv Drug Deliv Rev, **2018**. 124: p. 184-192.
260. Murgia, X., Loretz, B., Hartwig, O., Hittinger, M., and Lehr, C.M., *The role of mucus on drug transport and its potential to affect therapeutic outcomes.* Adv Drug Deliv Rev, **2018**. 124: p. 82-97.
261. Mayrhofer, G., *Fixation and staining of granules in mucosal mast cells and intraepithelial lymphocytes in the rat jejunum, with special reference to the relationship between the acid glycosaminoglycans in the two cell types.* The Histochemical journal, **1980**. 12(5): p. 513-526.
262. Anselmo, A.C., Gokarn, Y., and Mitragotri, S., *Non-invasive delivery strategies for biologics.* Nat Rev Drug Discov, **2019**. 18(1): p. 19-40.
263. Vargason, A.M., Anselmo, A.C., and Mitragotri, S., *The evolution of commercial drug delivery technologies.* Nat Biomed Eng, **2021**. 10.1038/s41551-021-00698-w.

264. Patel, A., Patel, M., Yang, X., and Mitra, A.K., *Recent advances in protein and Peptide drug delivery: a special emphasis on polymeric nanoparticles.* Protein and peptide letters, **2014**. 21(11): p. 1102-1120.
265. Andus, K.L. and Raub, T.L., *Biological barriers to protein delivery*. Vol. 4. **2012**: Springer Science & Business Media.
266. Cao, S.-j., Xu, S., Wang, H.-m., Ling, Y., Dong, J., Xia, R.-d., and Sun, X.-h., *Nanoparticles: Oral Delivery for Protein and Peptide Drugs.* AAPS PharmSciTech, **2019**. 20(5): p. 190.
267. Tiwari, N., Sonzogni, A., and Calderón, M., *Can dermal delivery of therapeutics be improved using thermoresponsive nanogels?* Nanomedicine (London, England), **2019**. 14(22): p. 2891.
268. Freitas Jr, R., *Nanomedicine. volume I: Basic capabilities, Landes Bioscience,(8.4. 1.1 Thermography of the Human Body).* Texas: Georgetown, **1999**.
269. Chanmugam, A., Langemo, D., Thomason, K., Haan, J., Altenburger, E.A., Tippett, A., Henderson, L., and Zortman, T.A., *Relative Temperature Maximum in Wound Infection and Inflammation as Compared with a Control Subject Using Long-Wave Infrared Thermography.* ASW, **2017**. 30(9).
270. Wedel, B., Hertle, Y., Wrede, O., Bookhold, J., and Hellweg, T., *Smart Homopolymer Microgels: Influence of the Monomer Structure on the Particle Properties.* Polymers, **2016**. 8(4).
271. Borzova, V.A., Markossian, K.A., Chebotareva, N.A., Kleymenov, S.Y., Poliansky, N.B., Muranov, K.O., Stein-Margolina, V.A., Shubin, V.V., Markov, D.I., and Kurganov, B.I., *Kinetics of Thermal Denaturation and Aggregation of Bovine Serum Albumin.* PLoS One, **2016**. 11(4): p. e0153495.
272. Michnik, A., *Thermal stability of bovine serum albumin DSC study.* Journal of Thermal Analysis and Calorimetry, **2003**. 71(2): p. 509-519.
273. Green, R.J., Hopkinson, I., and Jones, R.A.L., *Unfolding and Intermolecular Association in Globular Proteins Adsorbed at Interfaces.* Langmuir, **1999**. 15(15): p. 5102-5110.
274. Michnik, A., Michalik, K., and Drzazga, Z., *Stability of bovine serum albumin at different pH.* Journal of Thermal Analysis and Calorimetry, **2005**. 80(2): p. 399-406.
275. *THERMAL GRADIENTS IN THE HUMAN SKIN.* Acta Physiologica Scandinavica, **1969**. 76(s323): p. 18-23.
276. Witting, M., Molina, M., Obst, K., Plank, R., Eckl, K.M., Hennies, H.C., Calderón, M., Frieß, W., and Hedtrich, S., *Thermosensitive dendritic polyglycerol-based nanogels for cutaneous delivery of biomacromolecules.* Nanomedicine: Nanotechnology, Biology and Medicine, **2015**. 11(5): p. 1179-1187.
277. Giulbudagian, M., Yealland, G., Honzke, S., Edlich, A., Geisendorfer, B., Kleuser, B., Hedtrich, S., and Calderon, M., *Breaking the Barrier - Potent Anti-Inflammatory Activity following Efficient Topical Delivery of Etanercept using Thermoresponsive Nanogels.* Theranostics, **2018**. 8(2): p. 450-463.
278. Giulbudagian, M., Honzke, S., Bergueiro, J., Isik, D., Schumacher, F., Saeidpour, S., Lohan, S.B., Meinke, M.C., Teutloff, C., Schafer-Korting, M., Yealland, G., Kleuser, B., Hedtrich, S., and Calderon, M., *Enhanced topical delivery of dexamethasone by beta-cyclodextrin decorated thermoresponsive nanogels.* Nanoscale, **2017**. 10(1): p. 469-479.
279. Abdel-Mottaleb, M.M., Moulari, B., Beduneau, A., Pellequer, Y., and Lamprecht, A., *Surface-charge-dependent nanoparticles accumulation in inflamed skin.* J Pharm Sci, **2012**. 101(11): p. 4231-9.
280. Venuganti, V.V.K. and Perumal, O.P., *Poly(amidoamine) dendrimers as skin penetration enhancers: Influence of charge, generation, and concentration.* Journal of Pharmaceutical Sciences, **2009**. 98(7): p. 2345-2356.
281. Alnasif, N., Zoschke, C., Fleige, E., Brodwolf, R., Boreham, A., Rühl, E., Eckl, K.-M., Merk, H.-F., Hennies, H.C., Alexiev, U., Haag, R., Küchler, S., and Schäfer-Korting, M., *Penetration of*

normal, damaged and diseased skin — An in vitro study on dendritic core–multishell nanotransporters. Journal of Controlled Release, **2014**. 185: p. 45-50.
282. Küchler, S., Radowski, M.R., Blaschke, T., Dathe, M., Plendl, J., Haag, R., Schäfer-Korting, M., and Kramer, K.D., *Nanoparticles for skin penetration enhancement – A comparison of a dendritic core-multishell-nanotransporter and solid lipid nanoparticles.* European Journal of Pharmaceutics and Biopharmaceutics, **2009**. 71(2): p. 243-250.
283. Miceli, E., Kuropka, B., Rosenauer, C., Osorio Blanco, E.R., Theune, L.E., Kar, M., Weise, C., Morsbach, S., Freund, C., and Calderón, M., *Understanding the elusive protein corona of thermoresponsive nanogels.* Nanomedicine, **2018**. 13(20): p. 2657-2668.
284. Clogston, J.D. and Patri, A.K., *Zeta potential measurement.* Methods Mol Biol, **2011**. 697: p. 63-70.
285. Nugent, S.G., Kumar, D., Rampton, D.S., and Evans, D.F., *Intestinal luminal pH in inflammatory bowel disease: possible determinants and implications for therapy with aminosalicylates and other drugs.* Gut, **2001**. 48(4): p. 571.
286. Fischer, H. and Widdicombe, J.H., *Mechanisms of acid and base secretion by the airway epithelium.* The Journal of membrane biology, **2006**. 211(3): p. 139-150.
287. Pérez-Vilar, J. and Mabolo, R., *Gel-forming mucins. Notions from in vitro studies.* Histology and histopathology, **2007**.
288. Samiec, P.S., Dahm, L.J., and Jones, D.P., *Glutathione S-Transferase in Mucus of Rat Small Intestine.* Toxicological Sciences, **2000**. 54(1): p. 52-59.
289. Hagen, T.M., Wierzbicka, G.T., Bowman, B.B., Aw, T., and Jones, D.P., *Fate of dietary glutathione: disposition in the gastrointestinal tract.* American Journal of Physiology-Gastrointestinal and Liver Physiology, **1990**. 259(4): p. G530-G535.
290. Shaik, I.H. and Mehvar, R., *Rapid determination of reduced and oxidized glutathione levels using a new thiol-masking reagent and the enzymatic recycling method: application to the rat liver and bile samples.* Analytical and bioanalytical chemistry, **2006**. 385(1): p. 105-113.
291. Aw, T.Y., *Intestinal glutathione: determinant of mucosal peroxide transport, metabolism, and oxidative susceptibility.* Toxicol Appl Pharmacol, **2005**. 204(3): p. 320-8.
292. Yang, G., Phua, S.Z.F., Bindra, A.K., and Zhao, Y., *Degradability and Clearance of Inorganic Nanoparticles for Biomedical Applications.* Advanced Materials, **2019**. 31(10): p. 1805730.
293. Circu, M.L. and Aw, T.Y., *Redox biology of the intestine.* Free Radic Res, **2011**. 45(11-12): p. 1245-66.
294. Callens, C., Ceulemans, J., Ludwig, A., Foreman, P., and Remon, J.P., *Rheological study on mucoadhesivity of some nasal powder formulations.* European Journal of Pharmaceutics and Biopharmaceutics, **2003**. 55(3): p. 323-328.
295. Carvalho, F.C., Bruschi, M.L., Evangelista, R.C., and Gremião, M.P.D., *Mucoadhesive drug delivery systems.* Brazilian Journal of Pharmaceutical Sciences, **2010**. 46(1): p. 1-17.
296. Barthelmes, J., Dünnhaupt, S., Unterhofer, S., Perera, G., Schlocker, W., and Bernkop-Schnürch, A.J.N., *Thiolated particles as effective intravesical drug delivery systems for treatment of bladder-related diseases.* **2013**. 8(1): p. 65-75.
297. Leitner, V.M., Walker, G.F., and Bernkop-Schnürch, A., *Thiolated polymers: evidence for the formation of disulphide bonds with mucus glycoproteins.* European Journal of Pharmaceutics and Biopharmaceutics, **2003**. 56(2): p. 207-214.
298. Dunnhaupt, S., Barthelmes, J., Hombach, J., Sakloetsakun, D., Arkhipova, V., and Bernkop-Schnurch, A., *Distribution of thiolated mucoadhesive nanoparticles on intestinal mucosa.* Int J Pharm, **2011**. 408(1-2): p. 191-9.
299. Ziegler, A., Gonzalez, L., Blikslager, A.J.C., gastroenterology, m., and hepatology, *Large animal models: the key to translational discovery in digestive disease research.* **2016**. 2(6): p. 716-724.

300. Nejdfors, P., Ekelund, M., Jeppsson, B., and Weström, B.J.S.j.o.g., *Mucosal in vitro permeability in the intestinal tract of the pig, the rat, and man: species-and region-related differences.* **2000**. 35(5): p. 501-507.
301. Nunes, R., Silva, C., and Chaves, L., *Tissue-based in vitro and ex vivo models for intestinal permeability studies*, in *Concepts and Models for Drug Permeability Studies*, B. Sarmento, Editor. **2016**, Woodhead Publishing. p. 203-236.
302. Yuan, S., Hollinger, M., Lachowicz-Scroggins, M.E., Kerr, S.C., Dunican, E.M., Daniel, B.M., Ghosh, S., Erzurum, S.C., Willard, B., Hazen, S.L., Huang, X., Carrington, S.D., Oscarson, S., and Fahy, J.V., *Oxidation increases mucin polymer cross-links to stiffen airway mucus gels.* Science Translational Medicine, **2015**. 7(276): p. 276ra27-276ra27.
303. Zscheppang, K., Berg, J., Hedtrich, S., Verheyen, L., Wagner, D.E., Suttorp, N., Hippenstiel, S., and Hocke, A.C., *Human Pulmonary 3D Models For Translational Research.* Biotechnology Journal, **2018**. 13(1): p. 1700341.
304. Obst, K., Yealland, G., Balzus, B., Miceli, E., Dimde, M., Weise, C., Eravci, M., Bodmeier, R., Haag, R., Calderón, M., Charbaji, N., and Hedtrich, S., *Protein Corona Formation on Colloidal Polymeric Nanoparticles and Polymeric Nanogels: Impact on Cellular Uptake, Toxicity, Immunogenicity, and Drug Release Properties.* Biomacromolecules, **2017**. 18(6): p. 1762-1771.
305. Lea, T., *Caco-2 Cell Line*, in *The Impact of Food Bioactives on Health: in vitro and ex vivo models*, K. Verhoeckx, et al., Editors. **2015**, Springer

Copyright 2015, The Author(s). Cham (CH). p. 103-11.
306. Yang, J., Duan, Y., Zhang, X., Wang, Y., and Yu, A., *Modulating the cellular microenvironment with disulfide-containing nanoparticles as an auxiliary cancer treatment strategy.* Journal of Materials Chemistry B, **2016**. 4(22): p. 3868-3873.
307. Wang, S., Ye, Q., Zeng, X., and Qiao, S., *Functions of Macrophages in the Maintenance of Intestinal Homeostasis.* J Immuno Research, **2019**. 2019: p. 1512969.
308. Hirota, K. and Terada, H., *Endocytosis of particle formulations by macrophages and its application to clinical treatment*, in *Molecular regulation of endocytosis*. **2012**, InTech: Croatia.
309. Peiser, L. and Gordon, S., *The function of scavenger receptorsexpressed by macrophages and their rolein the regulation of inflammation.* Microbes and Infection, **2001**. 3(2): p. 149-159.
310. Zani, I.A., Stephen, S.L., Mughal, N.A., Russell, D., Homer-Vanniasinkam, S., Wheatcroft, S.B., and Ponnambalam, S., *Scavenger receptor structure and function in health and disease.* Cells, **2015**. 4(2): p. 178-201.
311. Gustafson, H.H., Holt-Casper, D., Grainger, D.W., and Ghandehari, H., *Nanoparticle Uptake: The Phagocyte Problem.* Nano Today, **2015**. 10(4): p. 487-510.
312. Kuhn, D.A., Vanhecke, D., Michen, B., Blank, F., Gehr, P., Petri-Fink, A., and Rothen-Rutishauser, B., *Different endocytotic uptake mechanisms for nanoparticles in epithelial cells and macrophages.* Beilstein Journal of Nanotechnology, **2014**. 5: p. 1625-1636.
313. Saha, K., Kim, S.T., Yan, B., Miranda, O.R., Alfonso, F.S., Shlosman, D., and Rotello, V.M., *Surface Functionality of Nanoparticles Determines Cellular Uptake Mechanisms in Mammalian Cells.* Small, **2013**. 9(2): p. 300-305.
314. Murdaca, G., Colombo, B.M., and Puppo, F., *Anti-TNF-alpha inhibitors: a new therapeutic approach for inflammatory immune-mediated diseases: an update upon efficacy and adverse events.* Int J Immunopathol Pharmacol, **2009**. 22(3): p. 557-65.
315. Colombel, J.F., Sandborn, W.J., Rutgeerts, P., Enns, R., Hanauer, S.B., Panaccione, R., Schreiber, S., Byczkowski, D., Li, J., Kent, J.D., and Pollack, P.F., *Adalimumab for Maintenance of Clinical Response and Remission in Patients With Crohn's Disease: The CHARM Trial.* Gastroenterology, **2007**. 132(1): p. 52-65.

316. Hanauer, S.B., Feagan, B.G., Lichtenstein, G.R., Mayer, L.F., Schreiber, S., Colombel, J.F., Rachmilewitz, D., Wolf, D.C., Olson, A., Bao, W., and Rutgeerts, P., *Maintenance infliximab for Crohn's disease: the ACCENT I randomised trial.* The Lancet, **2002**. 359(9317): p. 1541-1549.
317. Lichtenstein, G.R., Yan, S., Bala, M., Blank, M., and Sands, B.E., *Infliximab maintenance treatment reduces hospitalizations, surgeries, and procedures in fistulizing Crohn's disease.* Gastroenterology, **2005**. 128(4): p. 862-869.
318. Qiu, Y., Chen, B.L., Mao, R., Zhang, S.H., He, Y., Zeng, Z.R., Ben-Horin, S., and Chen, M.H., *Systematic review with meta-analysis: loss of response and requirement of anti-TNFalpha dose intensification in Crohn's disease.* J Gastroenterol, **2017**. 52(5): p. 535-554.
319. Biancheri, P., Brezski, R.J., Di Sabatino, A., Greenplate, A.R., Soring, K.L., Corazza, G.R., Kok, K.B., Rovedatti, L., Vossenkämper, A., Ahmad, N., Snoek, S.A., Vermeire, S., Rutgeerts, P., Jordan, R.E., and MacDonald, T.T., *Proteolytic Cleavage and Loss of Function of Biologic Agents That Neutralize Tumor Necrosis Factor in the Mucosa of Patients With Inflammatory Bowel Disease.* Gastroenterology, **2015**. 149(6): p. 1564-1574.e3.
320. Koetting, M.C., Guido, J.F., Gupta, M., Zhang, A., and Peppas, N.A., *pH-responsive and enzymatically-responsive hydrogel microparticles for the oral delivery of therapeutic proteins: Effects of protein size, crosslinking density, and hydrogel degradation on protein delivery.* J Control Release, **2016**. 221: p. 18-25.
321. Koetting, M.C. and Peppas, N.A., *pH-Responsive poly(itaconic acid-co-N-vinylpyrrolidone) hydrogels with reduced ionic strength loading solutions offer improved oral delivery potential for high isoelectric point-exhibiting therapeutic proteins.* Int J Pharm, **2014**. 471(1-2): p. 83-91.
322. Circu, M.L. and Aw, T.Y., *Intestinal redox biology and oxidative stress.* Seminars in Cell & Developmental Biology, **2012**. 23(7): p. 729-737.
323. Barnett, M., Fraser, A.J.U.C.T., Special Populations, and Future, t., *Animal models of colitis: lessons learned, and their relevance to the clinic.* **2011**. 2: p. 161-165.
324. Kolios, G.J.C.o.i.g., *Animal models of inflammatory bowel disease: how useful are they really?* **2016**. 32(4): p. 251-257.
325. Wirtz, S. and Neurath, M.F., *Mouse models of inflammatory bowel disease.* Adv Drug Deliv Rev, **2007**. 59(11): p. 1073-83.
326. Mankertz, J. and Schulzke, J.-D.J.C.o.i.g., *Altered permeability in inflammatory bowel disease: pathophysiology and clinical implications.* **2007**. 23(4): p. 379-383.
327. Geremia, A., Biancheri, P., Allan, P., Corazza, G.R., and Di Sabatino, A.J.A.r., *Innate and adaptive immunity in inflammatory bowel disease.* **2014**. 13(1): p. 3-10.
328. Konig, J., Wells, J., Cani, P.D., Garcia-Rodenas, C.L., MacDonald, T., Mercenier, A., Whyte, J., Troost, F., and Brummer, R.J., *Human Intestinal Barrier Function in Health and Disease.* Clin Transl Gastroenterol, **2016**. 7(10): p. e196.
329. Lee, S.H., *Intestinal permeability regulation by tight junction: implication on inflammatory bowel diseases.* Intestinal research, **2015**. 13(1): p. 11.
330. Neurath, M.F., *Cytokines in inflammatory bowel disease.* Nat Rev Immunol, **2014**. 14(5): p. 329-42.
331. Leonard, F., Ali, H., Collnot, E.-M., Crielaard, B.J., Lammers, T., Storm, G., and Lehr, C.-M., *Screening of budesonide nanoformulations for treatment of inflammatory bowel disease in an inflamed 3D cell-culture model.* ALTEX-Alternatives to animal experimentation, **2012**. 29(3): p. 275-285.
332. Gustafsson, J.K., Ermund, A., Johansson, M.E., Schütte, A., Hansson, G.C., Sjövall, H.J.A.J.o.P.-G., and Physiology, L., *An ex vivo method for studying mucus formation, properties, and thickness in human colonic biopsies and mouse small and large intestinal explants.* **2011**. 302(4): p. G430-G438.

333. Chen, Y., Lin, Y., Davis, K.M., Wang, Q., Rnjak-Kovacina, J., Li, C., Isberg, R.R., Kumamoto, C.A., Mecsas, J., and Kaplan, D.L.J.S.r., *Robust bioengineered 3D functional human intestinal epithelium.* **2015**. 5: p. 13708.
334. Cornick, S., Tawiah, A., and Chadee, K., *Roles and regulation of the mucus barrier in the gut.* Tissue Barriers, **2015**. 3(1-2): p. e982426.
335. Lock, J.Y., Carlson, T.L., and Carrier, R.L., *Mucus models to evaluate the diffusion of drugs and particles.* Adv Drug Deliv Rev, **2018**. 124: p. 34-49.
336. Costa, J. and Ahluwalia, A., *Advances and Current Challenges in Intestinal in vitro Model Engineering: A Digest.* Front Bioeng Biotechnol, **2019**. 7: p. 144.
337. Nam, J., Son, S., Ochyl, L.J., Kuai, R., Schwendeman, A., and Moon, J.J., *Chemo-photothermal therapy combination elicits anti-tumor immunity against advanced metastatic cancer.* Nature Communications, **2018**. 9(1): p. 1074.
338. Wang, J., Zhang, Y., Liu, L., Cui, Z., Liu, X., Wang, L., Li, Y., and Li, Q., *Combined chemo/photothermal therapy based on mesoporous silica-Au core-shell nanoparticles for hepatocellular carcinoma treatment.* Drug Dev Ind Pharm, **2019**. 45(9): p. 1487-1495.
339. Yang, S., Palanikumar, L., Jeong, S., Kim, K., Lee, J., Jeoung, E., Kim, C., Ryu, J.-H., and Park, M.-H., *Synergistic Effect of Photothermal Therapy and Chemotherapy Using Camptothecin-Conjugated Gold Nanorods.* Particle & Particle Systems Characterization, **2018**. 35(2): p. 1700307.
340. Ensign, L.M., Schneider, C., Suk, J.S., Cone, R., and Hanes, J., *Mucus penetrating nanoparticles: biophysical tool and method of drug and gene delivery.* Advanced Materials, **2012**. 24(28): p. 3887-3894.
341. Ensign, L.M., Henning, A., Schneider, C.S., Maisel, K., Wang, Y.Y., Porosoff, M.D., Cone, R., and Hanes, J., *Ex vivo characterization of particle transport in mucus secretions coating freshly excised mucosal tissues.* Mol Pharm, **2013**. 10(6): p. 2176-82.
342. Jia, Z., Guo, Z., Yang, C.-T., Prestidge, C., and Thierry, B., *"Mucus-on-Chip": A new tool to study the dynamic penetration of nanoparticulate drug carriers into mucus.* IJPharm, **2021**. 598: p. 120391.
343. Boegh, M., Baldursdóttir, S.G., Müllertz, A., and Nielsen, H.M., *Property profiling of biosimilar mucus in a novel mucus-containing in vitro model for assessment of intestinal drug absorption.* European Journal of Pharmaceutics and Biopharmaceutics, **2014**. 87(2): p. 227-235.
344. Kocevar-Nared, J., Kristl, J., and Smid-Korbar, J., *Comparative rheological investigation of crude gastric mucin and natural gastric mucus.* Biomaterials, **1997**. 18(9): p. 677-81.
345. Huck, B.C., Hartwig, O., Biehl, A., Schwarzkopf, K., Wagner, C., Loretz, B., Murgia, X., and Lehr, C.-M., *Macro- and Microrheological Properties of Mucus Surrogates in Comparison to Native Intestinal and Pulmonary Mucus.* Biomac **2019**. 20(9): p. 3504-3512.
346. Van den Brande, J.M.H., Koehler, T.C., Zelinkova, Z., Bennink, R.J., te Velde, A.A., ten Cate, F.J.W., van Deventer, S.J.H., Peppelenbosch, M.P., and Hommes, D.W., *Prediction of antitumour necrosis factor clinical efficacy by real-time visualisation of apoptosis in patients with Crohn's disease.* Gut, **2007**. 56(4): p. 509-517.
347. Levin, A.D., Wildenberg, M.E., and van den Brink, G.R., *Mechanism of action of anti-TNF therapy in inflammatory bowel disease.* Journal of Crohn's and Colitis, **2016**. 10(8): p. 989-997.
348. Na, Y.R., Stakenborg, M., Seok, S.H., and Matteoli, G., *Macrophages in intestinal inflammation and resolution: a potential therapeutic target in IBD.* Nature Reviews Gastroenterology & Hepatology, **2019**. 16(9): p. 531-543.
349. Han, X., Ding, S., Jiang, H., and Liu, G., *Roles of Macrophages in the Development and Treatment of Gut Inflammation.* Frontiers in Cell and Developmental Biology, **2021**. 9: p. 385.
350. Biancheri, P., Di Sabatino, A., Corazza, G.R., and MacDonald, T.T., *Proteases and the gut barrier.* Cell and Tissue Research, **2013**. 351(2): p. 269-280.

351. Rahman, M.A. and Ali, J., *Development and in vitro Evaluation of Enteric Coated Multiparticulate System for Resistant Tuberculosis.* Indian journal of pharmaceutical sciences, **2008**. 70(4): p. 477-481.

8. ANNEX

AWARDS, PUBLICATIONS, AND CONFERENCES ASSOCIATED WITH THIS THESIS

Awards and grants

Doctoral scholarship by the German academic exchange service (DAAD), funding program 57129429, October 2015 – May 2020.

Travel grant by Women's representative for Female Promotion at the Freie Universität Berlin, department of biology, chemistry, and pharmacy (Frauenförderung) for attending the annual Meeting of the German Pharmaceutical Society (DPhG) in Hamburg, Germany 2018.

Research articles

Charbaji, R.*, Kar, M.*, Theune, L.E.*, Bergueiro, J., Eichhorst, A., Navarro, L., Graff, P., Stumpff, F., Calderón, M., and Hedtrich, S., Design and Testing of Efficient Mucus-Penetrating Nanogels—Pitfalls of Preclinical Testing and Lessons Learned. Small, 2021. n/a(n/a): p. 2007963.

(*) Authors contributed equally.

Peigneux, A., Glitscher, E.A., **Charbaji, R.**, Weise, C., Wedepohl, S., Calderon, M., Jimenez-Lopez, C., and Hedtrich, S., Protein corona formation and its influence on biomimetic magnetite nanoparticles. J Mater Chem B, 2020. 8(22): p. 4870-4882.

Theune, L.E., **Charbaji, R.**, Kar, M., Wedepohl, S., Hedtrich, S., and Calderon, M., Critical parameters for the controlled synthesis of nanogels suitable for temperature-triggered protein delivery. Mater Sci Eng C Mater Biol Appl, 2019. 100: p. 141-151.

Conference contributions

R. Charbaji, L. E. Fechner, J. Bergueiro, M. Kar, M. Calderón, S. Hedtrich; Redox-sensitive nanogels: A promising approach for efficient drug delivery in mucosal tissue?, the annual Meeting of the German Pharmaceutical Society (DPhG), Hamburg, Germany, October 02 - 05, 2018.